INSTITUTE OF ELECTRICAL ENGINEERING

SLOVAK ACADEMY OF SCIENCES

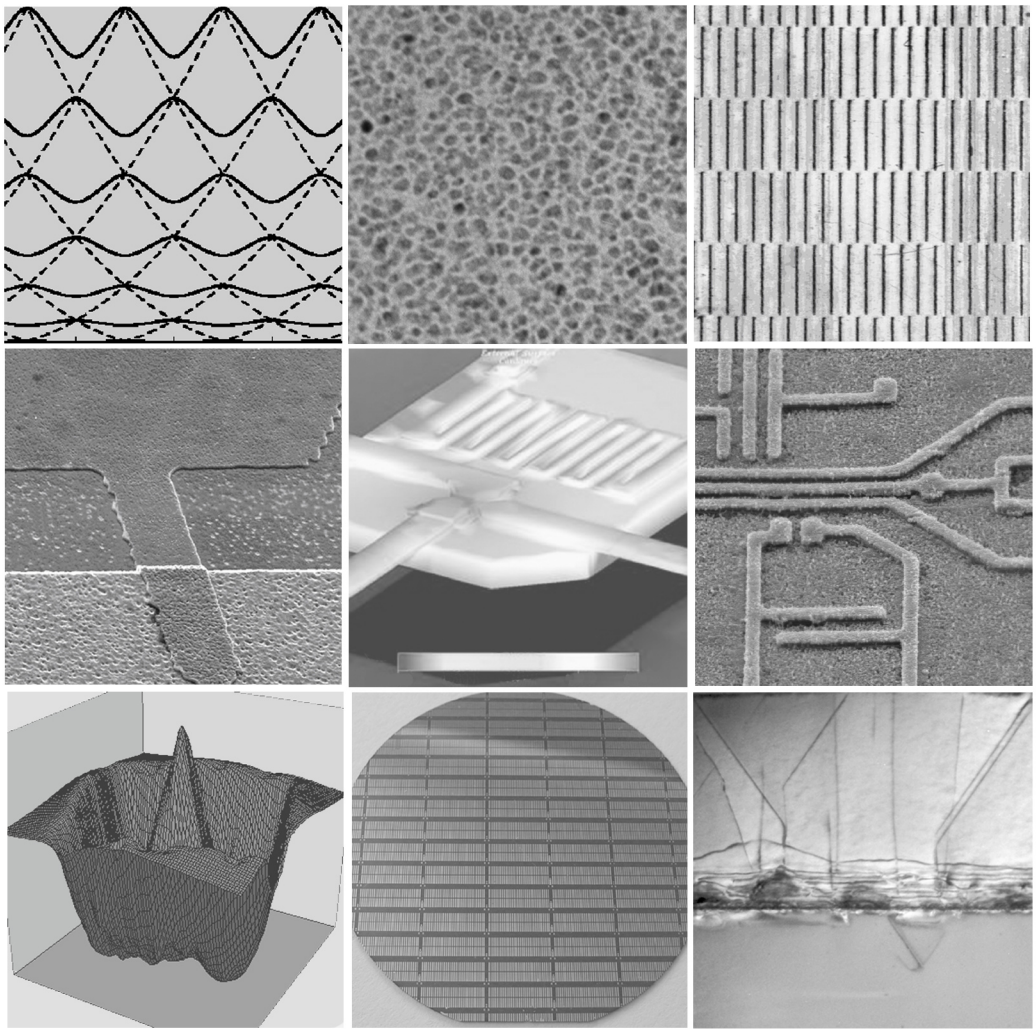

BIENNIAL REPORT 2003 - 2004

INSTITUTE OF ELECTRICAL ENGINEERING

SLOVAK ACADEMY OF SCIENCES

BIENNIAL REPORT

1. January 2003 – 31. December 2004

Institute of Electrical Engineering
Slovak Academy of Sciences
Dúbravská cesta
841 04 BRATISLAVA, SLOVAK REPUBLIC

Phone: (# 421-2) 54775806
Fax: (# 421-2) 54775816
Homepage: www.elu.sav.sk

Edited by:

Vladimír Cambel
Anton Pevala
Jozef Osvald
Marianna Španková
Peter Eliáš

Cover: Jakub Fröhlich Photo: Anton Sládek

Bratislava 2005

Preface

This Biennial Report gives an overview of the scientific activities of the Institute of Electrical Engineering in 2003 and 2004. The results of our research are summarised in nine sections, which correspond with the nine research departments of the Institute.

Our most important activities were linked with the 5th and 6th Framework Programmes. The Institute joined the programmes successfully from the beginning. Of note is the special support under the 5th Framework Programme the Institute received for its Centre of Excellence: Applied Superconducting Training Research Advanced Centre (ASTRA). We appreciate it as an acknowledgement of the scientific and technological excellence the Institute achieved in the field of applied superconductivity.

We also acknowledge increased support given to our research from national resources in 2003 and 2004. For the first time since the political changes in 1989, the funding of our research from national resources equalled the support received from the European Commission. A major role in this was played by the Slovak Science and Technology Assistance Agency (APVT) grant agency. Also important was national support under a governmental project entitled "New materials and devices in sub-micrometer technology". The Institute has been involved in this project along with other institutes of the Slovak Academy of Sciences since 2003.

During 2003 and 2004 we successfully continued with the training of PhD students. Usually 10 to 12 students work on PhD studies at the Institute. Some of our former PhD students are currently working in post-doc positions in European research laboratories.

I would like to express my gratitude to all staff members for their contributions to the prosperous development of the Institute in 2003 and 2004. I also want to express my wish and desire that the research groups of the Institute will continue their creative and successful work in the future.

Bratislava
March 2005

Dr. Karol Frőhlich
Director of the Institute

Contents

I General Overview

Organisation scheme of the Institute

Director
Dr. Karol Fröhlich

Administration

Technical Department

Vicedirector
Dr. Fedor Gömöry

Scientific secretary
Dr. Vladimír Cambel

Scientific Departments

- **Theory of Semiconductor Microstructures**
  Dr. Martin Moško
- **Microelectronic Structures**
  Dr. Tibor Lalinský
- **Semiconductor Technology and Diagnostics**
  Dr. František Dubecký
- **Optoelectronics**
  Dr. Jozef Novák
- **Superlattices**
  Dr. Ivo Vávra
- **Superconductor Physics**
  Dr. Fedor Gömöry
- **Electrodynamics of Superconductors**
  Dr. Milan Polák
- **Cryoelectronics**
  Dr. Štefan Chromik
- **Thin oxide films**
  Dr. Karol Fröhlich

Scientific Council

Head:
Dr. Martin Moško

Internal members:
Dr. Vladimír Cambel
Dr. Štefan Chromik
Dr. Tibor Lalinský
Dr. Pavol Kováč
Dr. Jozef Novák
Dr. Silvester Takács
Dr. Ivo Vávra

External members:
Prof. Štefan Bárta
Prof. Jaroslav Kováč
Dr. Eduard Dobročka

Thematic focus of the Institute

The Institute focuses on current problems in solid-state physics, microelectronics, information technology and electrical engineering. In 2003 and 2004, we concentrated on the following mutually interconnected research areas:

- Selected theoretical phenomena in solid-state physics applicable in modern microelectronic devices;
- New materials and technologies for use in information technologies, microelectronics, electrical power devices;
- Characterisation and application of new structures developed for sensors and advanced microelectronic devices;
- Applied superconductivity.

The quality of our research is reflected both in a number of publications and citations in international scientific journals and in quite a few domestic and international research and technology development (RTD) projects. The results achieved assure us that the Institute has embarked on a modern and promising research journey.

The Institute successfully participated in five RTD projects within the 5th Framework Programme. Within the 6th Programme, it is included in two RTD projects on superconductivity (Specific Targeted Research Projects) and in one Marie Curie RTD project.

Besides the RTD projects, the Institute was also involved in a network programme. It was granted Centre-of-Excellence status to work as of January 1, 2003 on an "Applied Superconductivity Training and Research Advanced Centre, ASTRA" programme under the umbrella of the European Commission. We view the acceptance of the project as an act of appreciation of the quality of research the Institute has performed on applied superconductivity in Europe.

Apart from international projects, in 2003 the Institute began work, along with other institutes of the Slovak Academy of Sciences, on a national governmental project entitled "New materials and devices in sub-micrometer technology".

In 2004 the Institute was awarded the title "Prestigious Research Organisation in Slovakia" by the Slovak Ministry of Education.

Selected theoretical problems of solid-state physics

As regards our activities in solid-state physics and the physics of advanced microelectronic devices, our researchers theoretically analysed electron transport in low-dimensional A^{III}-B^{V} semiconductor structures, such as quantum wells and quantum wires. The results were published in high-ranking, international journals (Physical Review Letters, Physical Review B), and they are being further used for research into new materials and technologies.

New materials and technologies

Our materials research concentrated on A^{III}-B^{V} semiconductors, advanced microelectronics materials (thin oxide films), superconducting materials (thin films, composite superconductors), and nano-structured materials.

As to our semiconductor-related activities, new A^{III}-B^{V} semiconductor structures and devices were prepared on planar and patterned substrates using metalorganic chemical vapour deposition (MOCVD). To prepare the patterned substrates, new wet-etch techniques were developed. The patterned substrates, which contained specific, three-dimensional objects, were used as templates for MOCVD overgrowth to form structures appropriate for specialised A^{III}-B^{V}-based micro-electro-mechanical systems (MEMS). Such devices were produced using non-planar device processing techniques developed at the same time. In addition, electronic properties and phase separation of MOCVD-grown $In_xGa_{1-x}P$ alloys were analysed.

Thin oxide films are investigated because of their potential application in new sub-100 nm complementary metal-oxide-semiconductor (CMOS) devices. Along with a LMGP laboratory (Grenoble, France) and with German AIXTRON A.G., we modified a metalorganic chemical vapour deposition technique to allow for the preparation of a wide variety of thin oxide films via a computer-controlled delivery of solutions rich in metal-organic precursors.

We also studied a great deal the preparation and properties of superconducting films and composite conductors. Our researchers successfully prepared thin MgB_2 films very soon after the discovery of superconductivity in MgB_2. After that they made progress in the application of MgB_2 films in Josephson junctions. Also, composite MgB_2/Fe superconductors were developed. Efforts are currently being made to increase critical current densities in MgB_2 composite superconductors by introducing effective pinning centres. Parameters of MgB_2 composite superconductors prepared at the Institute are comparable with those of the best samples prepared in Europe. The results paved the way for a participation of the MgB_2 group in a 6th Framework Programme project.

Nano-composite materials were produced within our efforts to control material properties at the nano-scale. The materials contain nano-sized metallic grains that are embedded in an insulating matrix. Such composites are expected to exhibit new properties, e.g. enhanced room-temperature magnetoresistivity.

Advanced microelectronic structures and devices

Results obtained in our A^{III}-B^{V} semiconductor materials research were used for the preparation of new devices that were further optimised for use in electronic systems.

The design of new devices is exemplified in the micromachined thermal converter. This unique device, whose operation is based on electro-thermal conversion, can be incorporated in a number of various MEMS devices, such as power sensors, gas sensors, pressure sensors, and microactuators.

The design of new electronic systems is represented by the scanning Hall probe microscope (SHPM) that was manufactured to perform detailed studies of superconductors. The core of the microscope is an advanced low-noise Hall sensor fabricated at the Institute. The microscope can be used for basic research as well as for industrial material characterisation. We use it to study losses, current distributions, and grain boundary effects in superconductors.

Another low-temperature SHPM was specifically manufactured to allow for the large-scale imaging of magnetic fields in close proximity to magnetic and superconducting samples at 4.2 – 300 K. The microscope combines large-area scanning with high spatial and magnetic field resolution. It can be inserted in standard, helium-flowing cryostats.

We used the microscope to characterise MgB_2 filaments. It was demonstrated that such measurements can be used to estimate local critical currents in MgB_2 samples as well as to estimate the superconductor microstructure and space homogeneity in superconductor samples.

In 2004, a research group was assembled at the Institute to study properties of GaN-based structures designed for high-power, microwave applications. The group made progress in the processing of GaN-based structures and devices, such as high electron mobility transistors. The transistors were passivated to study the effect of passivation on their performance.

Our research into physical properties of semi-insulating A^{III}-B^{V} semiconductors led to the development of a monolithic, strip-line X-ray detector being used as a sensor in a digital X-ray scanner, which was developed in collaboration with a small Slovak company, T&N System, s.r.o., based in Banská Bystrica. The digital X-ray scanner was awarded a Gold Incheba award at the international trade fair Incheba, Bratislava, in 2004.

The above-mentioned devices and equipment were developed within the material- and technology-related research activities of the Institute. They were supported within international and national funding schemes under NATO Science for Peace, the Slovak Academy of Sciences, and the APVT grant agency.

Applied superconductivity

Our research into superconductivity was focused on the application of high-T_c superconductors for energy transmission. Models of superconducting cables were constructed from Bi-2223/Ag tapes (Pb-Bi-Sr-Ca-Cu-O superconductor) within experiments carried out under a 5^{th} Framework Programme project entitled "Quality monitoring of Superconductors for the production of Efficient, Compact and reliable Energy Transmission Systems". An understanding of the behaviour of a superconducting cable in conditions exceeding critical current was one of the main outputs of the project.

Another important activity in the field of applied superconductivity was our participation in the European Fusion Programme in experiments focused on current redistribution in superconducting cables. Within an activity coordinated by the Max Planck Institute for Plasma Physics in Garching (Germany), we developed a multi-sensor system allowing for the deduction of current distribution in a large cable for plasma fusion equipment. The system significantly improved the early detection of cable current quench.

Summary of scientific outputs

The most important results of our research were published in international scientific journals. Figure 1 shows the number of publications per year published since 2000, including the number of publications with the first author from the Institute. In recent years, the Institute has published about 80 publications a year, which seems to be at saturation level, with the exception of 2003. The statistics shows that we published on average nearly two publications per research scientist a year.

The scientific significance of the publications is expressed by their citation impact. Figure 2 depicts the number of citations from the Web of Science (WoS) database since 1999. Note that the citation statistics are

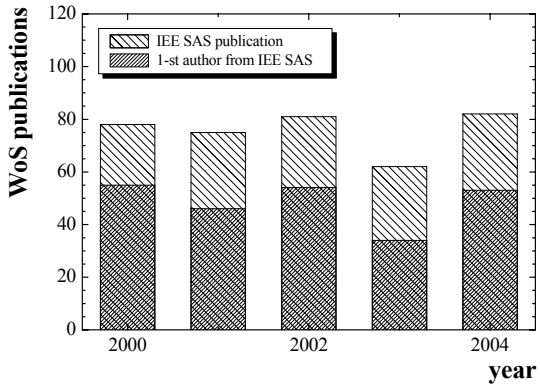

Fig. 1. Number of publications of the Institute in international journals according to the Web of Science database.

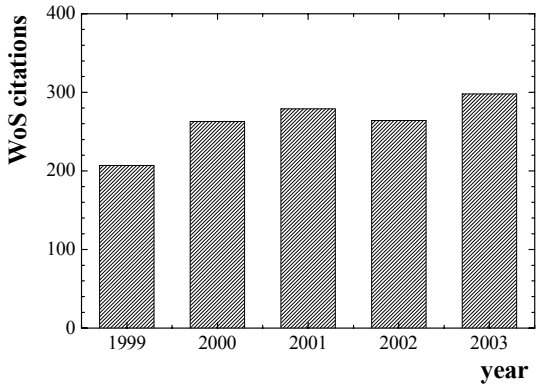

Fig. 2. Number of citations of the Institute according to the Web of Science database.

issued with a one-year-long delay. It also includes responses to papers published over the whole period before a given year. The number of citations increased annually even though the annual publication rate is saturated. We hope that this trend may reflect the increasing quality and recognition of the scientific output of the Institute.

Our research activities in 2003 and 2004 resulted in several important achievements in solid-state physics, materials science, and application outputs. The following list introduces the most important ones:

The strong localization theory shows that a disordered, one-dimensional wire with coherent electronic conduction is an insulator whose mean resistance and resistance dispersion increase exponentially with the wire length / localization length ratio. We showed theoretically that thermal smearing and resonant tunnelling make such a one-dimensional insulator undergo a crossover to a one-dimensional "metal" at full coherence. As a result, the resistance dispersion becomes wire length independent and smaller than unity. Concurrently, the mean resistance increases with the wire length / localization length ratio linearly and eventually polynomially, which manifests the so-called medium localization. The results were compared with an experiment and were published in Physical Review Letters **91** (2003) 136803.

We designed and developed special modular power opto-couplers in co-operation with NES Nová Dubnica as an industrial partner. The power opto-couplers were manufactured to serve as an isolated power supply for small, special electronic systems (communications units, safety systems or starting units). The basic module was designed for an output power of 100 mW and isolation voltages up to 22 kV. To allow for direct loading from high voltage sources, the light emitting devices on the input side of the module are in serial connection.

Under a Euratom/EFDA FU06-CT-2003-00041 international project, we developed and prepared measuring systems equipped with low-temperature Hall Probes for current distribution measurements in superconducting cables with nominal currents of 80 kA. The systems were developed for fusion research. The distribution and orientation of the Hall Probes in the systems were designed in co-operation with the Second University, Naples, Italy. The systems were calibrated, tested and installed in experimental facilities in Karlsruhe (TOSKA) and in a measuring device developed at Tesla Engineering, UK, for SULTAN (PSI Villigen, Switzerland).

We studied a series of samples that contained MgB_2 superconductor in direct contact with other metals, oxides and inter-metallic compounds. The influence of interfaces on the current carrying capability of MgB_2 was established. This allowed us to prepare reproducibly high-quality MgB_2 films on various substrates, such as poly-crystalline Si, single-crystalline SiC, amorphous buffer SiC layer on Si (100). We also improved properties of composites containing MgB_2 filament in an iron matrix. Additionally, thin MgB_2 layers were patterned by a focused Ga-ion beam into strips several tens of nanometres wide and 100 nm long.

We found that the critical current density can be substantially increased (3.6 times in magnetic field of 5T at the temperature of 4.2K) if fine metallic particles with good electrical and thermal conductivity (W, Hf, etc.) are inserted in the superconducting core. Along with the expected gettering effect on impurities (at first oxygen), the stability of the current transport was improved as well. This result is significant for the further development of MgB_2 composite wires in the 6^{th} Framework Programme NMP3-CT-2004-505724 project with the acronym HIPERMAG.

We realized a portable digital modular X-ray scanner based on an array of monolithic X-ray GaAs detectors. This unique radiographic equipment yields high quality X-ray images. The device realises X-ray imaging in quantum mode (“single photon counting”), which substantially improves the contrast. To the best of our knowledge, the instrument is the first of its kind in the world. The X-ray sensor has original topology, and it was

produced using original technology. The scanner is based on GaAs substrates produced by a Slovak company (CMK s.r.o., Žarnovica, Slovakia). The readout and control electronics, automatic positioning, control and imaging software were developed and fabricated in collaboration with the end-user. The scanner consists of 480 readout channels covering a scanned area of 12x15 cm^2. This provides a large number of data points at the highest resolution (250 μm in the line direction and 80 μm in direction of the line movement). The control and imaging software allows for the setting of the step length, exposure duration, and scanning trace length.

We prepared thin, conducting films of Ru and Ru-based oxides ($SrRuO_3$) using metal-organic chemical vapour deposition (MOCVD). Ru and R-based oxides are possible candidates as new gate electrode materials to be used in a new generation of CMOS (complementary metal-oxide-semiconductor) transistors. We found out that the work function of Ru and $SrRuO_3$ electrodes is approximately 5 eV, which is appropriate for pMOS transistors. We demonstrated that MOS structures with upper Ru and $SrRuO_3$ electrodes and with an HfO_2 oxide layer as thin as 2 nm exhibited suitable capacitance-voltage characteristics and low leakage currents densities. We were among the first to show that thin conducting Ru and $SrRuO_3$ films are promising materials for a new generation of CMOS transistors with the characteristic dimension below 90 nm. The results were achieved under a project within the 5th Framework Programme INVEST (project IST-2000-28495-INVEST), Deliverable New D2: Selection of suitable metal oxides as potential electrodes in high-k CMOS devices. The results were presented at the European Material Research Society (E-MRS) conference in Strasbourg, May 2004, and they were published in the Material Science in Semiconductor Processing journal.

PhD study at the Institute

Besides the research work described above, the researchers of the Institute were involved in the training of PhD students. The Institute was commissioned as an external educational institution to educate PhD students in the following areas:

- Electronics
- Physics of condensed matter and acoustics
- Electro technology and materials
- Theory of electrical engineering

In 2003 and 2004, seventeen PhD students studied at the Institute. Three of them finished their PhD studies successfully in the period. The other students are currently still working on their PhD studies. A PhD should officially be completed within three years. However, most PhD theses worked on at the Institute are experimental works, which typically require more than four years for completion.

Three PhD students from aboard visited the Institute for a long-term stay during their PhD work. This form of co-operation with EU countries is promising. Their work was supported by the "Applied Superconductivity Training and Research Advanced Centre" (ASTRA). One PhD study is being realised "en co-tutelle" within the framework of collaboration with the French CNRS laboratory in Grenoble.

Funding of research

The Institute of Electrical Engineering is a research-oriented governmental organisation. Governmental contributions to the budget of the Institute are mostly spent on personnel costs. A smaller part of the support is distributed among research groups and on a project – grant basis. Fig. 3 shows the development of both budget components from 2000 to 2004. The governmental contribution to the budget increased relatively to the total budget especially in 2003 and 2004. The increase played a crucial role in pay rises being able to be given out at the Institute.

Our research work was mostly funded by national and international grant agencies, namely VEGA, the Science and Technology Assistance Agency (APVT), the European Commission, and NATO. Fig. 4 shows the composition of the 2003 and 2004 budgets. It is noteworthy that the role of domestic funding agencies in the budgets, namely that of APVT, increased in contrast with their contribution in previous years. As regards funding from international projects, the largest support came from the 5th (5 RTD projects, 3 networks) and 6th (3 RTD projects) Framework Programmes. Hence, our involvement in European research activities is crucial for us. As is shown in the figure, funding from industrial contracts remained quite low in the period. To gain industrial-sector funding is the challenge for the future. Although the governmental funding gradually increased, still only a very small part can be used to renew equipment (~ 6%).

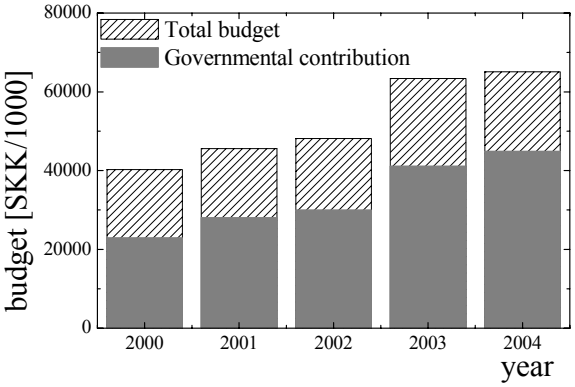

Fig. 3. Budget development from 2000 to 2004.

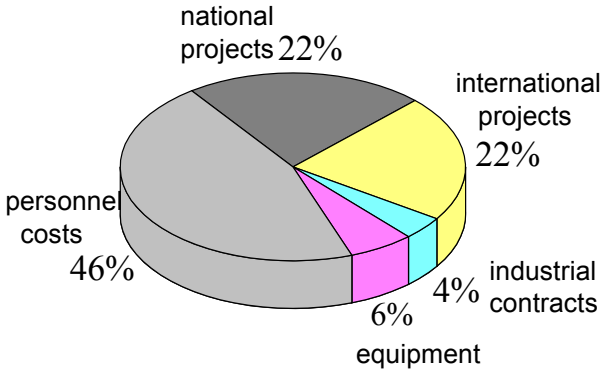

Fig. 4. Approximative budget composition in 2003 and 2004.

Conferences

From 17 to 21 October 2004, the Institute organized the Fifth International Conference on Advanced Semiconductor Devices and Microsystems – ASDAM '04. The conference, held biannually in Smolenice, Slovakia, since 1996, has acquired a reputation of being one of the most attractive semiconductor meetings in Central Europe. 82 participants took part in the ASDAM '04 conference. The conference topics traditionally range from semiconductor nanodevices to microsystems. ASDAM '04 concentrated on the following areas:

Materials and nanotechnologies;
Nanostructures and nanodevices;
Modelling and characterization;
Micro-(nano)-electro-mechanical systems.

A number of contributions were related to the technology, characterisation and modelling of nanostructures and nanodevices. Also covered were multifunctional materials, new production processes and devices, and microsystem technologies. Several invited lectures and many contributed papers reported on new materials, such as SiC, GaN and AlGaN. Additionally, the conference was of a multidisciplinary character, which catered for cross-field scientific discussions. The Conference Proceedings were published by the Institute of Electrical and Electronics Engineers, Inc. - IEEE.

II Research activities

Department of Theory of Semiconductor Microstructures

Martin Moško

Research scientists
Pavel Vagner
Andrej Gendiar

Phd students
Radoslav Németh

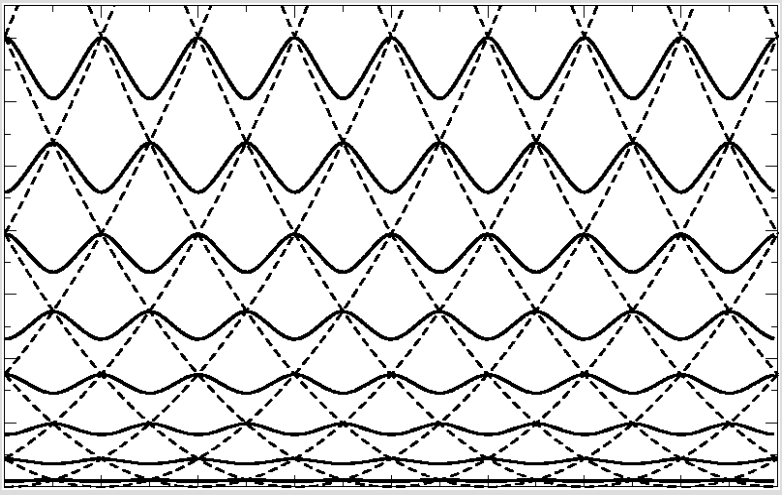

In 2003-2004 the activities of the group were focused on two topics: 1) Theoretical investigation of electronic transport in mesoscopic wires and rings; 2) Numerical simulation of statistical properties of various spin lattice models. These activities were performed within the project "Effect of many-particle Coulomb interaction on the carrier transport in one- and two-dimensional semiconductors", supported by the Slovak Grant agency VEGA, within the project "Strongly correlated and disordered electronic systems", supported by the Science and Technology Assistance Agency, and within the project "Quantum transport in mesoscopic conductors: many-body theory and experimental studies", supported by Deutsche Forschungsgemeinschaft. Moreover, starting by November 1, 2004, we solve the Marie-Curie RTD project called "Conductance of disordered mesoscopic conductor obtained from many-body calculation of electronic structure", which is supported by the European Commission within the 6th-Framework Programme.

Our results can be summarised as follows:

1. Using the self-consistent Hartree-Fock approximation for spinless electrons at zero temperature, we have simulated tunneling of a weakly interacting one-dimensional electron gas through a single delta barrier in a finite one-dimensional wire biased by macroscopic contacts. We have calculated the electron transmission as a function of the electron energy and system length. We have compared our results with the results of correlated many-body models. A good agreement has been found. In particular, as the system length (L) becomes large, the transmission at the Fermi level decays as $L^{-2\alpha}$, where the power α depends only on the e-e interaction. It has so far been believed that this universal power law can only be obtained within the correlated many-body model. Its existence within the Hartree-Fock model is a surprising new result.
2. Using the self-consistent Hartree-Fock approximation at zero temperature, we have also studied the persistent current of the interacting spinless electron gas in a continuous 1D ring with a single delta barrier. We have compared our results with the results of correlated models, with the Luttinger liquid model and microscopic Hubbard model. We have again recovered the universal power laws already known from the correlated model studies. In particular, we have found that the persistent current decays faster than L^{-1} and eventually as $L^{-1-\alpha}$, where $\alpha > 0$ is a universal power.
3. We have shown theoretically that the disordered 1D Andersor insulator undergoes at full coherence the crossover to a 1D "metal", caused by thermal smearing and resonant tunneling. As a result, the resistance dispersion becomes wire length independent and smaller than unity, while the mean resistance grows with the wire length – localization length ratio linearly and eventually polynomially, manifesting the so-called medium localization.
4. Finally, we have developed the numerical algorithm called „Tensor Product Variational Approach (TPVA)". The TVPA is a variational self-consistent method that evaluates the ground state of a 3D-transfer matrix and/or 2D-quantum Hamiltonian. We have succesfully applied the algorithm to a variety of statistical spin systems in 2D and 3D.

Collaboration:

We have co-operated with Thomas Schäpers from the Institute of Thin Films and Interfaces (ISG), Forschungszentrum Jülich, Germany, with Peter Markoš from the Institute of Physics of the Slovak Academy of Sciences, and with Michal Bajdich from the Department of Physics of the North Carolina State University.

Martin Moško

Tunneling of weakly interacting one-dimensional Fermions through a delta barrier: Universal power law from Hartree-Fock model

M. Moško, A. Gendiar, and P. Vagner

Electron gas in a quantum wire is a realistic one-dimensional (1D) electron system. If the wire is biased by two macrospcopic contacts and the wire length is shorter than the electron mean free path, ballistic electron transport takes place. Then each energy subband occupied by electrons contributes to the wire conductance by an amount $2e^2/h$, i.e., the ballistic conductance is universally quantized. This quantization is understood within the Fermi liquid model of noninteracting quasi-particles [1].

If a localized scatterer is introduced into the 1D wire, quantization of conductance breaks down due to the electron backscattering from the scatterer. For non-interacting electrons, the conductance is given by the electron transmission coefficient at the Fermi level, as staded by the Landauer formula [1]. However, the electron-electron (e-e) interaction alters the electron properties of the system qualitatively. In the Luttinger liquid model [2], the conductance of an infinite wire containing a single scatterer varies with temperature as $\sim T^{2\alpha}$ for $T\rightarrow 0$, where the power α depends only on the e-e interaction. For repulsive interaction α is positive and reflection at zero temperature is perfect, no matter how strong or weak the scatterer is.

The same result was found by Matveev *et al.* [3] in a non-Luttinger liquid model. They studied the Landauer conductance of the interacting 1D electron gas through a delta barrier in a wire with contacts. They replaced the many-body wave function by the Slater determinant of single-electron wave functions and analyzed the effect of the Hartree-Fock potential on the tunneling transmission. Assuming a weak e-e interaction of finite range, they derived the transmission by using the renormalization group (RG). They confirmed the universal power law $T^{2\alpha}$. In the model the delta barrier is impenetrable since it induces the Friedel oscillations of the Hartree-Fock potential which reflects the electrons at the Fermi level perfectly (as long the wire is infinite and $T\rightarrow 0$).

Is it possible to reproduce this result by means of the self-consistent Hartree-Fock solution? According to Ref.4 it holds for any e-e interaction strength, that the self-consistent Hartree-Fock solution drives the 1D system with a localized scatterer into the charge-density-wave groundstate with a finite single-particle gap at the Fermi level. This statement was not supported by any explicit self-consistent Hartree-Fock result, nevertheless, the self-consistent Hartree-Fock approach was identified as qualitatively incorrect because a single scatterer cannot change the bulk properties.

The authors of Ref. 4 therefore developed a non-self-consistent Hartree-Fock approximation. In this approximation they found similar power laws as in the correlated models [2,3], but with a non-universal (barrier-strength-dependent) power α. Their own correlated models [4], based on advanced RG techniques, confirmed the universal power law [2,3]. It thus seems, that the universal power-law behavior cannot be obtained in the Hartree-Fock model.

In our work [5] we have studied the Landauer conductance of the weakly interacting 1D electron gas through a single delta barrier in a finite wire connected to contacts, with the e-e interaction described by the Hartree and Fock potentials. In this sense we have considered the non-Luttinger liquid model of Matveev et al. [3], but instead of the RG approach we have applied the self-consistent Hartree-Fock solution. We have evaluated the tunneling transmission at zero temperature and we have compared it with the analytical theory of Matveev et al. A good agreement has been found. In particular, we have reproduced the universal power law behavior in terms of the length dependence: As the system length (L) becomes large, the transmission at the Fermi level decays as $L^{-2\alpha}$, where α depends only on the e-e interaction. We have also found that the Friedel oscillations decay with distance, i.e., that the self-consistent Hartree-Fock soulution does not drive our system into the charge-density-wave groundstate. The fact that the universal power law behavior can be reproduced on the Hartree-Fock level is a surprising result.

[1] *Davies, J. H., The Physics of Low-Dimensional Semiconductors: An introduction (Cambridge University Press, Cambridge, UK, 1998).*

[2] *Kane C. L. and Fisher, M. P. A.: Phys. Rev. Lett.* ***68****, (1992) 1220.*

[3] *Matveev, K. A., Yue, D., and Glazman, L. I.: Phys. Rev. Lett.* ***71*** *(1993) 3351.*

[4] *Meden, V., Metzner, W., Schollwock,U., and Schonhammer, K., Phys. Rev.* ***B65*** *(2002) 045318.*

[5] *Moško, M., Gendiar, A., Vagner, P., and Schapers, T.: unpublished.*

Spinless Hartree-Fock model of persistent currents in rings with single scatterer: Comparison with correlated models

R. Németh and M. Moško

Electrons confined in a very narrow wire form the one-dimensional (1D) electron gas. By tying the wire ends to each other one creates a 1D ring with the electron motion along the ring circumference. If the ring circumference is shorter than the electron coherence length, one speaks about the mesoscopic ring. An external magnetic flux applied through the opening of such ring gives rise, in analogy with the atomic diamagnetic current, to a persistent equlibrium current circulating around the ring [1].

Observations of persistent currents in metallic [2,3] and semiconducting rings [4] stimulated many theoretical papers focused on the electron-electron (e-e) interaction and disorder in such systems [1,5]. A quantitative understanding of the observed amplitude of the currents is so far not satisfactory and the role of the e-e interaction and disorder need further research. In this work we focus on the persistent current of interacting spinless electrons in a 1D ring with a single scatterer. Let us review recent results for this simplified problem.

If the e-e interaction is ignored, the leading behavior of the persistent current (I) as a function of the magnetic flux (Φ) and ring circumference (L) can be derived analytically for an arbitrary scatterer . It is a periodic function of Φ with period $\Phi_0=h/e$, it decays as $1/L$, and its shape is determined by the absolute value of the transmission ampliture t_{kF} of the scatterer at the Fermi wave vector k_F. In the limit of small t_{kF} it reads $I\sim L^{-1}\sin(2\pi\Phi/\Phi_0)$. These results were derived for a continuous ring [6] and hold also for the ring-shaped tight-binding lattice at half filling [7].

For a repulsive e-e interaction in the continuous ring, the spinless persistent current can still be derived analytically in the Luttinger liquid model [6]. For $L\to\infty$ and for an arbitrary strength of the scatterer, the current can be expressed as $I\sim L^{-1-\alpha}\sin(2\pi\Phi/\Phi_0)$, where the power $\alpha>0$ is universal, depending only on the e-e interaction.

The authors of Ref. 7 obtained the persistent current microscopically by solving the Hubbard chain with nearest-neighbor hopping and interaction. Using the renormalization group, they indeed found for a 1D ring with a single scatterer the current which decays faster than $1/L$ and is a sine-like function of Φ. The shape $I\sim\sin(2\pi\Phi/\Phi_0)$I and the universal scaling $I\sim L^{-1-\alpha}$ were confirmed for long chains and/or strong scatterers.

In addition, they concluded that the sine-like shape and the $L^{-1-\alpha}$ scaling can only be obtained in the correlated many-body model, not in the Hartree-Fock approximation ignoring the correlation effects. They used a non-self-consistent Hartree-Fock approximation and, indeed, found the qualitatively wrong results. The self-consistent Hartree-Fock approximation, according to these authors, drives the model with a single scatterer into the charge-density-wave groundstate with a finite single-particle gap, which is wrong because a single scatterer cannot change the bulk properties of the system. Hence, no attempt has been done to test the dependence $I\sim L^{-1-\alpha}\sin(2\pi\Phi/\Phi_0)$ in the self-consistent Hartree-Fock approximation. However, there is a motivation to do so.

Indeed, recently [8] the self-consistent Hartree-Fock approximation was used to study tunneling of the weakly-interacting electron gas through a single scatterer in a 1D wire with leads. It has been found that there is no charge-density-wave groundstate in such model, moreover, the tunneling probability has been found to decay with the wire length as $L^{-2\alpha}$, in accord with correlated models [9,10]. This suggests that an attempt to obtain the persistent current $I\sim L^{-1-\alpha}\sin(2\pi\Phi/\Phi_0)$ in the self-consistent Hartree-Fock approximation might be meaningful.

We have attempted to do so in our work [11]. Using the self-consistent Hartree-Fock approximation at zero temperature, we have studied the persistent current of the interacting spinless electron gas in a continuous 1D ring with a single delta barrier. We have compared our results with the results of correlated models, with the Luttinger liquid model [6] and microscopic Hubbard model [7]. A good agreement has been found. First, the persistent current has been found to decay faster than L^{-1} and eventually as $L^{-1-\alpha}$, where $\alpha > 0$ is universal. Second, the persistent current has been found to be a sine-like function of magnetic flux.

[1] *Imry, Y., Introduction to Mesoscopic Physics (Oxford University Press, Oxford, UK, 2002).*

[2] *Levy, L. P., Dolan, G., Dunsmuir,J., and Bouchiat,H.: Phys. Rev. Lett.* ***64*** *(1990) 2074.*

[3] *Chandrasekar, V., Webb, R. A., Brady M. J., Ketchen, M. B., Gallagher,W. J., and Kleinsasser, A.: Phys. Rev. Lett.* ***67*** *(1991) 3578.*

[4] *Mailly, D., Chapelier, C., and Benoit A.: Phys. Rev. Lett.* ***70*** *(1993) 2020.*

[5] *Eckern, U. and Schwab, P.: J. Low Temp. Phys.* ***126*** *(2002) 1291.*

[6] *Gogolin, A., and Prokof'ev, N.: Phys.Rev. B****50*** *(1994) 4921.*

[7] *Meden, V. and Schollwock, U.: Phys. Rev. B****67*** *(2003) 035106.*

[8] *Moško, M., Gendiar, A., Vagner, P., and Schappers, T.: unpublished.*

[9] *Kane, C. L. and Fisher, M. P. A.: Phys. Rev. Lett.****68*** *(1992) 1220.*

[10] *Matveev, K. A., Yue, D., and Glazman, L. I.: Phys. Rev. Lett.* ***71*** *(1993) 335.*

[11] *Németh, R. and Moško M.: unpublished.*

Coherent electron transport in a disoredered one-dimensional wire

M. Moško and P. Vagner

Theory of coherent electron transport at zero temperature teaches us [1,2], that any coherent one-dimensional (1D) wire is insulating whenever the wire length L exceeds the electron localization length ξ. Specifically, the mean resistance $<\rho>$, the typical resistance ρ_t, and the resistance dispersion $\Delta\rho$ exhibit the exponential rise (in units $2e^2/h$)

$$<\rho>=\frac{1}{2}(e^{2L/\xi}-1)\,,\quad \rho_t=e^{L/\xi}-1\,,\quad \Delta\rho\approx e^{L/\xi}\,. \qquad (1)$$

The disordered 1D insulator described by equations (1) is believed to exist also at low enough nonzero temperatures (without hopping and at full coherence) and the crossover to the 1D "metal" is expect to occur only if inelastic collisions are present [1,2]. In our work [3] we report a surprising finding, that the crossover to a different 1D "metal" occurs at full coherence due to the thermal averaging at a certain very low temperature. The resulting 1D "metal" exhibits the wire resistance which grows with L/ξ linearly and eventually polynomially owing to the medium localization. In addition, dispersion $\Delta\rho$ becomes L/ξ-independent and smaller than unity. Below we briefly discuss the most important results.

The coherent tunneling across the disordered wire is described by the electron transmission amplitude t_k and electron transmission probability $T = |t_k|^2$, which we evaluate microscopically by mean of the transfer-matrix method. Once the transmission is known, we evaluate the two-terminal conductance from the Landauer formula

$$G=\int_0^\infty d\varepsilon\left[-\frac{df(\varepsilon)}{d\varepsilon}\right]T(\varepsilon)\,, \qquad (2)$$

where $f(\varepsilon)$ is the Fermi distribution. Then we obtain the wire resistance as

$$\rho=1/G-1/f(0)\,, \quad (3)$$

where $1/f(0)$ is the contact resistance (~1 at low T). We perform this calculation for the ensemble of macroscopically identical wires with various randomness of disorder. We obtain the mean resistance, typical resistance, resistance dispersion, etc. Since we consider the weak low-density disorder, our final results depend solely on the universal dimensionless parameters L/ξ and T/T_ξ, independently on microscopic details of disorder. Here $k_B T_\xi = 1 / [\, g(\varepsilon_F)\, \xi\,]$, where $g(\varepsilon_F)=1/(\pi\hbar v_F)$ is the density of the energy levels. For the weak low-density disorder the localization length coincides with the classical elastic mean free path [3]. In the GaAs quantum wires one typically finds ξ = 10 μm and $T_\xi \sim 1$ K.

In the figure we show the mean and typical resistances of the 1D wire as a function of universal parameters L/ξ and T/T_ξ. In the top panel we reproduce at

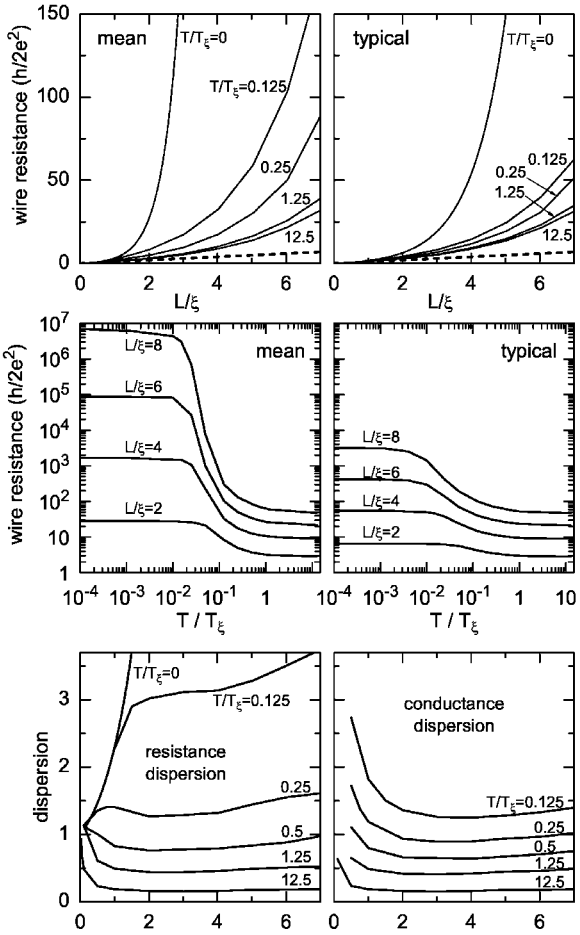

$T/T_\xi = 0$ the exponential rise (1). However, at $T/T_\xi>0$ both $<\rho>$ and ρ_t clearly rise with L/ξ slower than exponentially. Eventually, at $T/T_\xi>1$ the metallic behavior $<\rho> = \rho_t \approx L/\xi$ can be observed up to $L/\xi \approx 2$, while for larger L/ξ the growth is faster than linear but far much slower than $\exp(L/\xi)$. If we plot these results in a logarithmic scale (Fig.3 in Ref. 3), it is clearly visible that for $T/T_\xi>1$ both $<\rho>$ and ρ_t grow with L/ξ polynomially. The bottom panel shows the resistance dispersion $\Delta\rho$ and conductance dispersion Δg, where $g = 1/\rho$. At T=0 K, $\Delta\rho$ follows exponential dependence (1) and Δg diverges. For $T/T_\xi >0$ both $\Delta\rho$ and Δg are strongly modified, for $T/T_\xi>1$ and $L/\xi >1$ they are smaller than unity and independent on L. If measured experimentally, the L-independent Δg would distinguish this transport regime from others in which Δg always varies with L in a certain typical way [1].

[1] *Datta, S., Electron Transport in Mesoscopic Systems (Cambridge Univ. Press, UK, 1995).*
[2] *Imry, Y., Introduction to Mesoscopic Physics (Oxford University Press, Oxford, UK, 2002).*
[3] *Moško, M., Vagner, P., Bajdich, M., and Schäpers, T.: Phys. Rev. Lett.* ***9*** *(2003) 136803.*

Critical properties of two- and three-dimensional spin lattice models in the thermodynamic limit

A. Gendiar

It is known that spin interactions are responsible for origin of the ferromagnetism and antiferromagnetism in solids. Therefore, a variety of spin models have been proposed to mimic real magnets. We study the ground state properties of the models where the individual spins are coupled by ferromagnetic and/or antiferromagnetic interactions in the presence of an external magnetic field and temperature.

In order to study critical properties of the lattice models in thermodynamic limit (size of the spin model goes to infinity), we need to define an appropriate mathematical algorithm. Since majority of these lattice models cannot be solved analytically, several numerical approximative methods must be used. In the last decades, a powerful numerical technique, called the density matrix renormalization group (DMRG) [1], was developed and applied to various one-dimensional (1D) quantum and/or 2D classical lattice models, e.g., fermionic and bosonic systems, the transfer matrix DMRG and systems out of equilibrium. Moreover, it has also been successfully applied to the other research fields, for instance, to quantum chemistry, quantum information theory, small grains and nuclear physics [2]. The current research is focused on the extension of DMRG to higher dimensions, particularly, to propose a new DMRG algorithm for 2D quantum and/or 3D classical systems.

We derived an efficient numerical algorithm based on DMRG ideas that can be thought of as an extension of the method to 3D. The algorithm is called the tensor product variational approach (TPVA) [3]. An unknown variational trial state Ψ is written in the product form of local weights $V_{i,j}$ so as to maximize variational partition function

$$\lambda_{\mathrm{var}} = \frac{\langle \Psi | W_B^N | \Psi \rangle}{\langle \Psi | \Psi \rangle} = \frac{\sum_{\{\sigma\}} \prod_{i,j} V_{i,j} W_B^{i,j} \overline{V}_{i,j}}{\sum_{\{\sigma\}} \prod_{i,j} V_{i,j} \overline{V}_{i,j}}.$$

The trial state Ψ is decomposed into the tensor product state form. The Boltzmann weight $W_{\mathrm{B}} = \exp(-H/k_{\mathrm{B}}T)$ involves thermal fluctuations to a given Hamiltonian H. The TPVA is a variational method which self-consistently improves the free degrees of freedom in the local weight $V_{\mathrm{i,j}}$. Its advantage is that it reaches the correct ground state regardless the initial choice of the local weights [3,4].

We have suggested further improvements of the tensor product state by increasing the number of degrees of freedom in the local weights $V_{\mathrm{i,j}}$. Particularly, either we enlarge the size of each local weight or we implement auxiliary variables in $V_{\mathrm{i,j}}$ [5].

We found that the TPVA yields highly reliable results for the spin models studied out of the second-order phase transitions if compared to the standard Monte Carlo simulations. The high accuracy persists also at the transition points for the models exhibiting the first-order phase transitions (such as Potts model) [4]. In a vicinity of the second-order phase transition, the TPVA tends to behave as a mean-field approximation with the classical (mean-field) critical exponents. Despite it, we are able to calculate the correct (non-mean-field) critical exponent β by extrapolating the effective exponent β_{eff} within the temperature region where the data are obtained in a high precision [6].

We applied the TPVA to a more complex problem where a frustration is caused by mutually competing ferromagnetic and antiferromagnetic interactions leading to spin wave modulations as experimentally observed, for instance, in cerium antimonide (CeSb). The 3D S = 1/2 ANNNI model mimics such a behavior including the so-called devil's stairs. Our purpose was to clarify the phase structure of this ANNNI model by calculating its non-trivial global phase diagram [7].

We reformulated the TPVA to study 2D quantum spin models (the Heisenberg model) and estimated the ground state energy in the lowest approximation of the tensor product state [8].

Furthermore, we studied various 2D classical spin models. We calculated snapshots [9] (known from Monte Carlo simulations), we found the critical exponent in the vertex model with 10 vertex configurations that belongs to the Ising universality class [10], and derived a method for stochastic diffusion-annihilation processes [11].

[1] *White, S. R.: Phys. Rev. Lett.* ***69*** *(1992) 2863.*

[2] *Schollwöck, U.: accepted to Rev. Mod. Phys. 77 (2005), cond-mat/0409292.*

[3] *Nishino, T., Okunishi, K., Hieida, Y., Maeshima, N., and Akutsu, Y.: Nucl. Phys.* ***B575*** *(2000) 504; Nishino, T. Okunishi, K., Hieida, Y., Maeshima, N., Akutsu, Y., and Gendiar, A.: Prog. Theor. Phys.* ***105*** *(2001) 409.*

[4] *Gendiar, A. and Nishino, T.: Phys. Rev.* ***E65*** *(2002) 046702.*

[5] *Gendiar, A., Maeshima, N., and Nishino, T.: Prog. Theor. Phys.* ***110*** *(2003) 691.*

[6] *Gendiar, A., Nishino, T., and Derian, R.: Acta Phys. Slov.* ***55*** *(2005) 141.*

[7] *Gendiar, A., and Nishino, T.: Phys. Rev.* ***B71*** *(2005) 024404.*

[8] *Nishio, Y., Maeshima, M., Gendiar, A., and Nishino, T.: unpublished.*

[9] *Ueda, K., Otani, R., Nishio, Y., Gendiar, A., and Nishino, T.: accepted for publication in J. Phys. Soc. Jpn., cond-mat/0409445.*

[10] *Ueda, K., Otani, R., Nishio, Y., Gendiar, A., and Nishino, T.: submitted to J. Phys. Soc. Jpn., cond-mat/0501277.*

[11] *Kemper, A., Gendiar, A., Nishino, T., Schadschneider, A. Zittartz, J.: J. Phys. A: Math. Gen.* ***36*** *(2003) 29.*

Department of Microelectronics Structures

Tibor Lalinský

Research scientists
Jozef Osvald
Ján Kuzmík

Research Engineers
Štefan Haščík
Želmíra Mozolová

Technical staff
Martin Grujbár
Ivan Benkovič

PhD Students
Martin Krnáč

Students
Gabriel Vanko

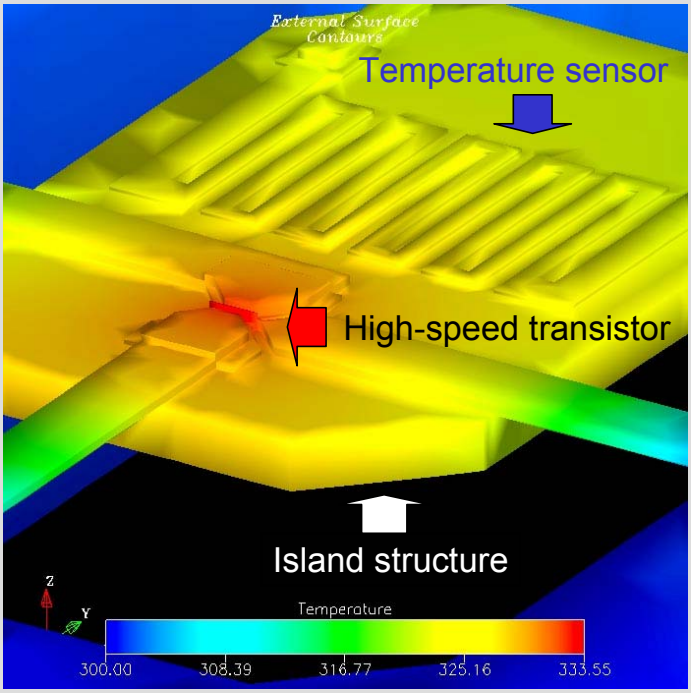

Our research work in 2003-2004 was focused on these two main topics: 1) Design and development of GaAs heterostructure based MEMS devices capable to sense the transmitted power given by the product of its electromagnetic field vector components practically up to millimetre-wave band range; 2) Quantum heterostructures based on III –V and III-N semiconductor materials.

The first topic was solved within the NATO SfP project No.: SfP-974172. The project finished on November 30, 2004. It covered R&D fields from semiconductor high-technology of sophisticated MEMS devices through design of new high-frequency precise power measuring methods up to production of new power measuring equipment.

Within this project, new GaAs micromachining approaches compatible with GaAs heterostructure based device fabrication techniques were introduced. Efforts were made to cover the basic fabrication technologies, techniques, processes, and materials. One of the main goals was to show how to integrate GaAs HEMTs with GaAs micromechanical structures and controlled circuits in fully monolithic integrated approach in order to produce the "single-chip" power sensor of a high electro-thermal performance.

This project introduced the fabricated "single-chip" sensor in all its complexity and multidisciplinary basis. Therefore, besides fabrication methods, non-conventional optical methods were developed to analyze the basic thermo-mechanical properties of the sensor device. They permitted (in situ) to study three-dimensional (3D) device nano-deformations induced by temperature changes in both stationary and non-stationary dynamic process conditions.

Various approaches and design concepts in the field of 3D thermo-mechanical modeling and simulation were also introduced and directly compared with comprehensive experimental electro-thermo-mechanical characterization of the sensor device. In general, these model approaches demonstrated a great potential for studying the thermo-mechanical phenomena and effects observed in MEMS devices on the required micro- and nano-scale. They are considered to be indispensable for the design of any novel 3D GaAs thermally based MEMS devices.

The results obtained in the field of MEMS design and development highlight new prospects for design of new generation of millimetre-wave circuits, gas sensors, micro-bolometers and detectors of spin-polarized electrons based on GaAs micro(nano)machining technology. The benefit from the new research topics appeared is expected in near future.

Another topic of research was the technology and analysis of the parameters of AlGaN/GaN HEMT transistor. MOS gate contacts are an alternative for the Schottky gate contacts. The main advantages of such contacts are lower leakage currents at high temperatures together with lower noise. Another advantages are higher power and higher breakdown voltages of the transistors. We have prepared the structures on the base of $Al/ZrO_2/(Al)GaN$. This type of contact has a very high permittivity of the dielectrics and its future we see mainly in high power structures with the gate length in the nanometer range. The interface state density for this material is also acceptable.

The research staff of our department have organized in order of the fifth International Conference on **A**dvanced **S**emiconductor **D**evices and **M**icrosystems – **ASDAM** 2004. It was held at Smolenice Castle, Slovakia, on October 17-21, 2004. The conference was devoted to the latest results of research and development in the field of high technology devices and microsystems.

A lot of research work at our department has been done in collaboration with local and other institutes and universities. This included co-operation with the Electron Beam Lithography Department at the Institute of Informatics (Bratislava), the Department of Microelectronics, Slovak University of Technology (Bratislava), the International Laser Center (Bratislava), the Institute of Electronic Structures & Lasers, FORTH, Crete (Heraklion), the Department of Microelectronics, Czech Technical University in Prague, and the Institute for Solid-State Electronics, Technical University of Vienna. I would like to express gratitude to all our partners.

The contributions in this booklet are short reports on our research performed within the two main topics introduced above. Most of them were partly published in numerous journals and conferences.

Tibor Lalinský

Micromachined thermal converter device based on polyimide-fixed island structure

T. Lalinský, Š. Haščík, Ž. Mozolová, M. Krnáč, and M. Grujbár

Micromachined Thermal Converter (MTC) device integrates microelectronic devices such as high-speed transistors or resistors, and temperature sensors on thermally isolated micromechanical structures, such as membranes, cantilevers and bridges. The microelectronic devices are designed to serve as micro-heaters, and the temperature sensors are proposed "in situ" to sense the temperature of the micromechanical structures. The device as described above should be capable to perfom an electro-thermal conversion as required for many thermally based MEMS devices such as power sensors, gas sensors, pressure sensors and microactuators.

The main design criterions, such as high electro-thermal conversion efficiency, linearity, short response time, thermal stability, micromechanical integrity and integration device simplicity should be taken into account in the MTC design [1,2].

Due to a higher thermal resistance and operation at high temperatures, MTC based on GaAs should be able to perform electro-thermal conversion with a higher conversion efficiency than Si. Likewise, the high-speed performance of GaAs heterostructure based field-effect transistors (HFET, pHEMT) creates conditions for design of the MTC devices fully compatible with monolithic microwave and millimetre-wave integrated circuits. Therefore, the GaAs based MTC devices could be considered to be a "heart" of power sensors in both microwave and millimetre-wave band range.

Recently, we have introduced a novel approach in design of MTC device [1-3]. It is based on so called a suspended island structure. It consists of GaAs pHEMT (as a microwave heater) and thin film meander-like resistor (as a temperature sensor) monolithically integrated on 1 μm thick GaAs/AlGaAs island structure fixed by 1 μm thick polyimide membrane.

Fig. 1 shows a schematic cross-section through the island based MTC device.

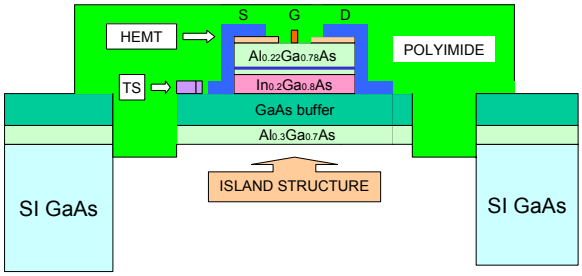

Fig. 1. Schematic cross-section through island based MTC device.

To fabricate the MTC device a front-side surface processing and micromachining are combined with a back-side bulk GaAs micromachining. Basically, the process flow is divided into two steps involving a front-side processing of the pHEMT heater and temperature sensor, followed by a surface micromachining of the island structure, and a back-side bulk micromachining of the GaAs substrate as a last processing step [3]. A real view of the MTC device is shown in Fig. 2.

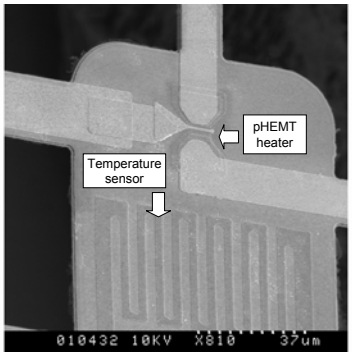

Fig. 2. A real view of fabricated MTC device.

An comprehensive electro-thermal conversion efficiency of the fabricated island based MTC device (Fig. 2) was investigated [1,2]. A 0.8 μm gate length GaAs pHEMT was used for the controlled thermal heating.

The temperature changes induced in the island structure by the electrical power dissipated in the pHEMT were sensed using the temperature sensor. The temperature sensor was operated under constant current bias of 0.8 mA, so the corresponded sensor voltage as a function of the power dissipation was sensed in real time.

An excellent linearity in the measured power to voltage (*P-V*) and power to temperature (*P-T*) conversion characteristics was observed, especially if the device was tested in air atmosphere. The device voltage sensitivity and thermal resistance value were determined to be as high as 10 V/W and 10 K/mW, respectively.

[1] *Lalinský, T., Krnáč, M., Haščík, Š., Mozolová, Ž., Matay, L., Kostič, I., Hrkút, P., Andok, R., Držík, M., and Chlpík, J.: Proceedings of the 14th MicroMechanics Europe Workshop, Delft, 2003, 45.*

[2] *Lalinský, T., Krnáč, M., Haščík, Š., Mozolová, Ž., Matay, L., Kostič, I., Hrkút, P., Jakovenko, J., and Husák, M.: Proceedings of the MEMS Symposium, ICMAT 2003, Singapoure, 2003, 543.*

[3] *Haščík, Š., Lalinský, T., Krnáč, M., Mozolová, Ž., Matay, L., Hrkút, P.: J. Phys.* ***54*** *(2004) C100.*

Thermo-mechanical characterization of micromachined GaAs Based thermal converter using contact-less optical methods

T. Lalinský, M. Krnáč, Š. Haščík, and Ž. Mozolová

The GaAs based micromachined thermal converters (MTCs) seem to be very attractive for design of various thermally based MEMS devices such as power sensors, pressure sensors or gas sensors. Their attractivity reflects some intrinsic material properties of GaAs as are especially lower thermal conductivity, high-temperature electronics and heterostructure based quantum effects. MTC based on GaAs should be capable to perform an electro-thermal conversion of higher conversion efficiency, so the maximum value of the thermal resistance should be much higher than in case of Si.

The multiplayer heterostructure based design of MTC is often very complicated [1]. It contains various materials of each other different thermo-mechanical properties. To study the thermally induced thermo-mechanical effects in the MTC devices a novel contactless optical methods are strongly desired.

In this contribution non-conventional optical methods are introduced to analyze the basic thermo-mechanical properties of the island based thermal converter device developed. They permit (in situ) to study the device 3D nano-deformations induced by the temperature changes in both stationary and non-stationary dynamic process conditions on the required micro- and nano-scale.

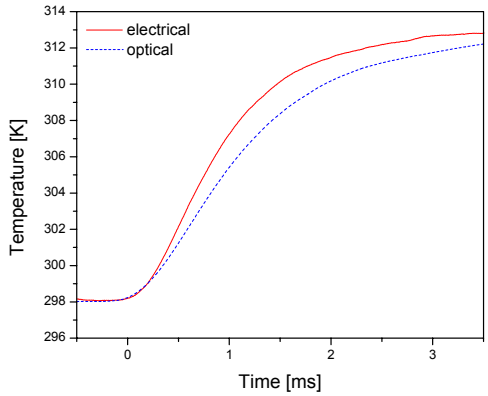

Fig. 1. Thermal time response characteristics of island based MTC device.

In order to evaluate the temperature time constant of the MTC a new optical method was applied. It is based on measurement of deformation changes of the island structure induced by the temperature changes. Temperature changes in most of such micromechanical structures can induce structure deformations due to different thermo-mechanical properties of the multiplayer material system. The non-stationary dynamic process of transient heat flow creates also time dependent mechanical movements. To observe these deformation changes the optical methods can be applied. We have used the Laser Doppler Vibrometer (LDV). The heterodyne interferometrical system of Polytec OFV-303 vibrometer is capable to detect the vibrational amplitudes in units of some nanometers.

Fig. 1 shows the temperature time response characteristic of the device obtained by the optical measurement. For comparison, time response characteristic obtained by the electrical measurement is also shown. A good agreement can be observed. The time constant value about 1.32 ms is determined from the exponential fit.

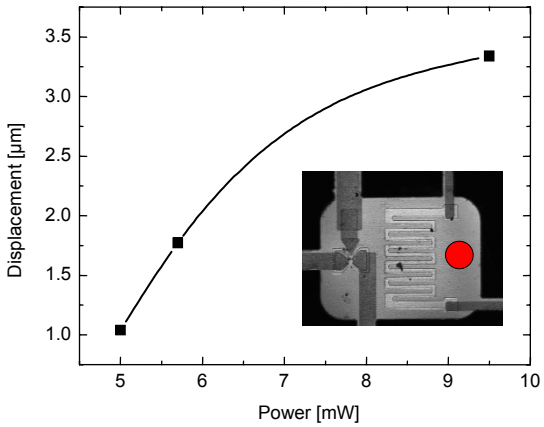

Fig. 2. Deformation changes induced in island based MTC device by power dissipation.

LDV method was also used to analyze deformation changes in any point of the device. Fig. 2 shows the deformation changes induced in the place of the temperature sensor (see measuring point in the included picture) by the power dissipation in the pHEMT heater. It can be seen that the deformation at the measuring point has tendency to increase with the power dissipation (temperature increase). It achieves the value about 3.3 µm at the power dissipation of 9.5 mW, what corresponds to the temperature increase of 395 K. The deformation changes observed can be considered to be negligible with respect to the dimensions of the polyimide fixed island structure (160x120 μm^2).

In order to visualize the 3D static deformation of the micromachined device a confocal microscope was also used [1].

[1] *Lalinský, T., Držík, M., Chlpík, J., Krnáč, M., Haščík, Š., and Mozolová, Ž.: Proceedings of EUROSENSORS XIII Conference, Rome, 2004, 239.*

Temperature dependence of current in inhomogeneous Schottky diodes

J. Osvald

Chand [1] described an interesting effect which should appear in inhomogeneous Schottky diodes at low temperatures. He simulated forward parts of *I-V* curves of non-interactive inhomogeneous Schottky diodes using approximation of an apparent barrier height. It was assumed that the diodes have a common series resistance, The calculations showed that the current at lower temperatures may exceed the current at high temperatures.

Since the approach of apparent barrier heights is relatively widely used in the literature we want to direct attention to the fact, that it could lead to unphysical values at certain circumstances. Very important property of the substitution of the barrier height distribution by the apparent barrier height is that for a given mean barrier height and for increasing standard deviation and lowering

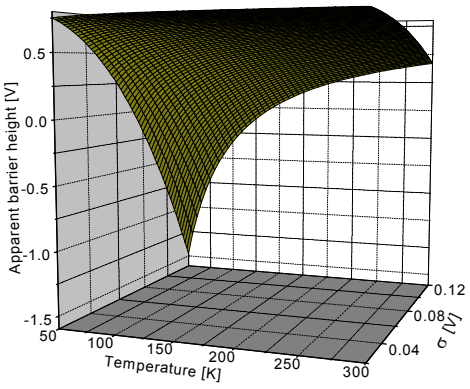

Fig. 1. The apparent barrier height for the mean barrier heigt φ_0= 0.8 V as a function of temperature and standard deviation of the Gaussian barrier height distribution σ.

the temperature the apparent barrier height starts to be negative (Fig. 1). For extreme values of standard deviations and temperatures the value of apparent barrier height may be even sufficiently large in negative region. For lower barrier heights from the apparent barrier height is negative even for less extreme values of these quantities. Negative value of apparent barrier height does not enable to generate *I-V* curves for higher reverse voltages and are evidently also the source of peculiarities with saturation current density discussed in.

We recalculated *I-V* curves of [1] in a different manner. Instead of using apparent barrier height defined by (1) or modified by approximation by Chand [1] we simulated the diode current from its definition according to the expression

$$I = \int_0^{2\varphi_0} SA^{**}T^2 \rho(\varphi) \exp(-q\varphi / kT \{\exp[q(V - RI)/kT - 1\} d\varphi,$$

where $\rho(\varphi)$ is Gaussian barrier height distribution. We used the same barrier height interval as in [1] – from 0 to 1.6 V. Then we compared our results with ones calculated in [1] with apparent barrier height approximation. As it is seen in Fig. 2 our results confirmed Chand's approach and

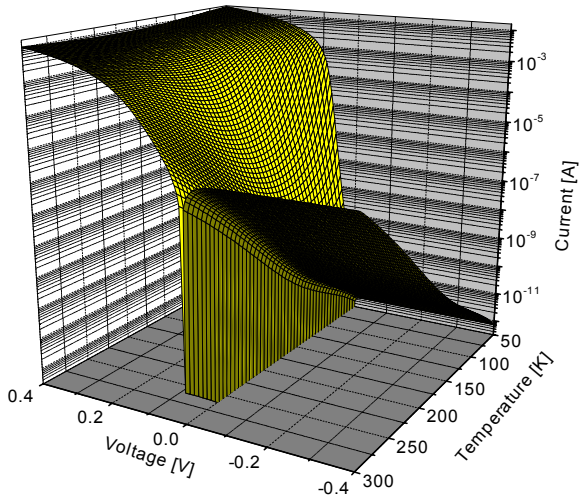

Fig. 2. I-V curves of n-Si inhomogeneous Schottky diodes with area S = 7.87x10^{-7} m2 φ_0 = 0.8 V, σ = 0.1 V, R = 20 Ω as a function of temperature.

did not show the effect of saturation current increase for decreasing temperature. The apparent barrier height is not constant with the temperature but the apparent barrier height itself which drives the current is temperature dependent. This fact is clear already from the Fig. 1.

Usage of negative barrier heights in integration interval may lead even to unphysical negative barrier heights at low temperatures. For higher temperatures barrier heights calculated analytically are practically the same as apparent barriers derived only from positive barriers in the distribution. Intersection of *I-V* curves for different temperatures is not caused by higher ideality factors of the curves – the ideality factor of inhomogeneous diodes remains unity when the constituting single diodes have ideality factor unity, too.

This intersection is caused by the temperature dependence of the apparent barrier height itself [2].

[1] *Chand, S.: Semicond. Sci. Technol.* ***17*** *(2003) L36.*
[2] *Osvald, J.: Semicond. Sci.Technol .* ***18*** *(2004) L24.*

Self-consistent analysis of Si δ-doped layer placed in a non-central position in GaAs structure

J. Osvald

Planar doping (δ-doped layers) attracted attention in recent years because of the possibility to attain greater mobilities of charge carriers in semiconductors which is a result of a space separation of electrons and holes from their parent ions. Charge carriers are confined into a thin sheet by V-shaped potential in such structures.

We have theoretically studied the influence of a position of a δ-doped layer relative to the semiconductor surface on its electronic structure and a free charge carrier profile. The semiconductor material was GaAs and δ-doping was assumed to be formed by Si atoms with uniform distribution in the δ-layer. The electronic structure was calculated by solving Poisson and Schrödinger equations self-consistently. We have studied the influence of the δ-doped position on eigenvalues and eigenfuctions of electrons in two-dimensional structure. The structure studied consisted of GaAs with a single Si δ-doped layer. The effective mass approximation has been used for the description of the system. Using LDA for including many-body exchange and correlation effects reduces the problem to the one-electron one. The effective confining potential has been calculated by solving simultaneously the Schrödinger and Poisson equations. As a result of calculations the confining potential, subband energy levels, their occupation probabilities and the total free carrier density were obtained. In the study it

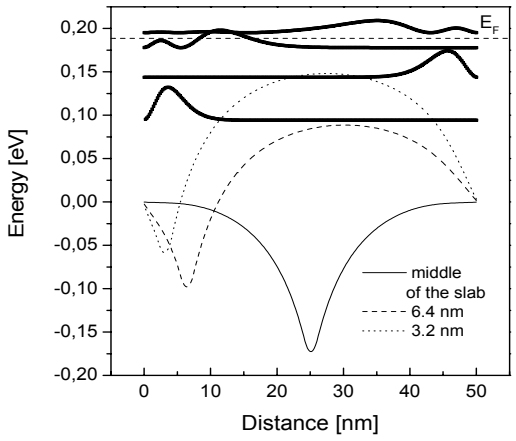

Fig. 1. Confining potential together with squares of electron eigenfunctions for the δ-doped layer with concentration N_d = $5x10^{12}$ cm^{-2} placed in GaAs 3.2 nm from the surface.

was assumed that the Fermi level is not pinned at the semiconductor surface, there is no charge transfer from the semiconductor to the surface and charge neutrality is valid in the semiconductor as a whole. It was found that shifting the δ-doped layer from the centre toward the semiconductor surface causes a creation of another potential well with electron concentration peak at the other surface of the sample. Similar effect of the side peak

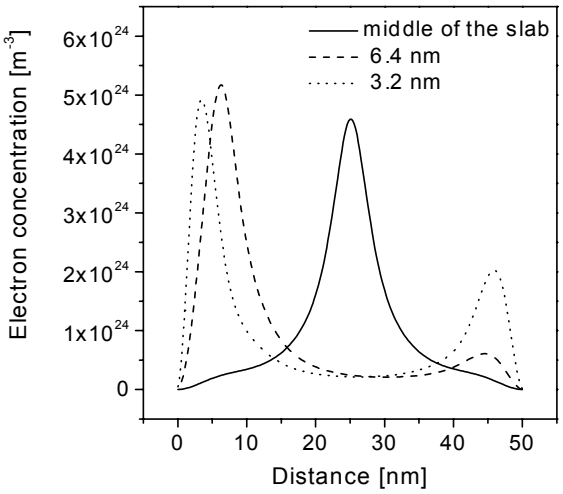

Fig. 2. Electron concentration in the semiconductor for sheet doping concentrations N_d = $5x10^{12}$ cm^{-3} and various δ-doped layer positions - in the middle of the slab, 6.4 nm from the surface, and 3.2 nm from the surface. The δ-doped layer is placed at the position of the left peak of every curve.

creation was observed by applying external electric field to the structure. Further approaching of the semiconductor surface leads to alternating population of the energy levels between the two potential wells (Fig. 1 and 2).

We have shown that non-symmetric placement of the δ-doped layer into the semiconductor slab causes appearance of the second potential well and redistribution of free electrons also into this well. In this new well the energy levels are occupied starting with the second lowest one. The occupation number of the second lowest level increases with decreasing distance of the δ-doped layer from the surface of the semiconductor and electrons are concentrated only in the new formed well. On the other hand the occupation number of the lowest energy level decreases with δ-doped layer approaching the semiconductor surface. This division of electrons into two two-dimensional gases should lead to enhanced mobility of electrons as a result of their space separation.

[1] *Osvald, J.: Physica E* ***23*** *(2004) 147.*
[2] *Osvald, J.: J. Phys. D: Appl. Phys.* ***37*** *(2004) 2655.*

ZrO_2 /GaN metal oxide semiconductor structures characterization

J. Kuzmík and Š. Haščík

The RF power [1], linearity [2] and noise [3] performance of group III-nitrides transistors can be improved if the gate leakage is reduced. Low leakage, minimal density of interface states (D_{it}) in semiconductor/insulator junction, together with the high insulator electrical strength and permittivity are required in MOS structures. Usage of the high permittivity (or high k) dielectric material may enable to design MOS GaN FETs with sufficient gate insulation while obtaining minimal transconductance (g_m) deterioration and a small threshold voltage shift ΔV_T. Moreover, the increased permittivity leads to a proportional decrease of the electric field in the insulator. This softens the insulator electrical strength requirement. Till now, ZrO_2 (permittivity of 15-20) has exclusively been reported as a perspective dielectric material for Si CMOS.

In our work commercial Ga-polarity GaN films grown by metal-organic chemical vapour-phase deposition (MOCVD) on sapphire substrate were used. Zr(tfacac)4 was selected as a precursor substance for 22 nm thick ZrO_2 deposition by MOCVD [4]. GaN/ZrO_2/Al MOS structures were processed with a layout of 50 μm diameter circular dots. Reference GaN/Ni/Au Schottky barrier contacts were also prepared. To characterize the oxide interface charge and dielectric performance, capacitance measurements using Terman [5] and light assisted *C-V* methods [6] were used.

Typical *I-V* curves of MOS and Schottky barrier diodes are shown in Fig. 1. Measurements of MOS leakage currents at different temperatures (from room temperature to 170 °C, not shown) revealed a weak temperature dependency as expected for the Frenkel-Poole trap-assisted conduction mechanism. The maximal capacitance value (65 pF) of the MOS structures indicated

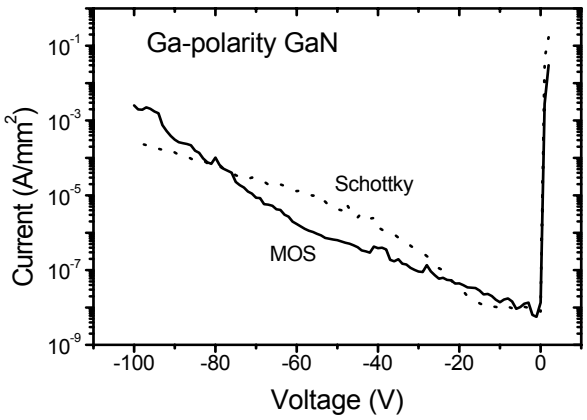

Fig. 1. GaN/ ZrO_2 MOS and Schottky diode I-V characteristics.

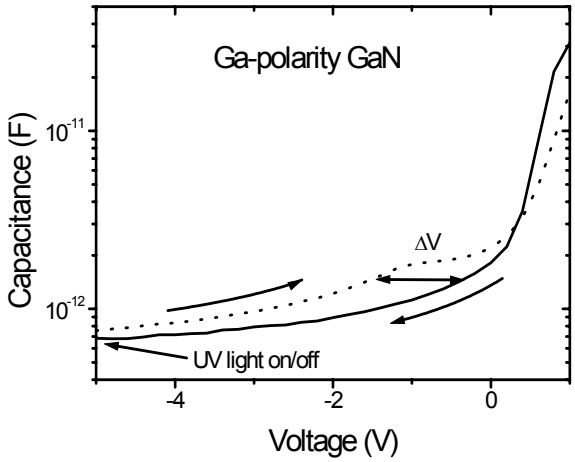

Fig. 2. GaN/ ZrO_2 MOS ligh-assited C-V.

an oxide permittivity $\varepsilon_r \sim 20$. Terman method was not applicable in our case as the low free carrier concentration in the sample (5-7 x 10^{15} cm^{-3}) imposed inappropriate conditions for the measurement precision. Light-assisted *C-V* characteristic is shown in Fig. 2. $D_{it} \sim 1x10^{12}$ cm^{-2} eV^{-1} was calculated as $D_{it} = C_{ox}\,\Delta V/qE_G$ [6], where C_{ox} is the oxide capacitance, ΔV is the voltage shift, q is the electron charge and E_G the GaN band gap. Finally we demonstrated the ZrO_2 feasibility by processing ZrO_2/AlGaN/GaN MOS HEMTs with a minimal g_m deterioration and ΔV_T corresponding to $\varepsilon_r > 20$ not shown.

In conclusion, electrical performance of ZrO_2 oxide insulator on GaN has been investigated. It was shown that $D_{it} \sim 1x10^{12}$ cm^{-2} eV^{-1} and a high ZrO_2 permittivity $\varepsilon_r \sim 20$ can be obtained. ZrO_2 deposition optimization may lower the leakage.

This work has been performed in frame of the Greece-Slovakia project, co-authors G. Konstantinidis, A. Georgakilas from FORTH Greece, and in collaboration with FKE TU Vienna, Austria, co-authors S. Harasek, E. Bertagnolli and D. Pogany.

[1] *Adivarahan, V., et al.: IEEE Electron Dev. Letters* ***24*** *(2003) 541.*
[2] *Khan Asif, M., et al.: phys. stat. sol. (a)* ***200*** *(2003) 155.*
[3] *Rumyantsev, S. L., et al.: Journal of Applied Physics* ***88*** *(2000) 6726.*
[4] *Gehring, A., et al.: Proc. 33rd European Solid-State Device Research Conference, 16-18 September 2003, Estoril, Portugal, 473.*
[5] *Schroder, D. K.: Semiconductor Material and Device Characterization, John Wiley & Sons, Inc., New York, Chichester, Wienheim, Brisbane, Singapore, Toronto 1998, second edition, 377.*
[6] *Tan, J., et al.: Appl. Phys. Letters* ***70*** *(1997) 2280.*

Department of Semiconductor Technology and Diagnostics

František Dubecký

Research scientists
Pavel Boháček
Jozef Huran
Dušan Korytár
Bohumír Zaťko

Research engineers
Mária Sekáčová

Technical staff
Miloslav Ruček
Viktor Štefanec

PhD Students
Andrea Perďochová
Patrik Vagovič

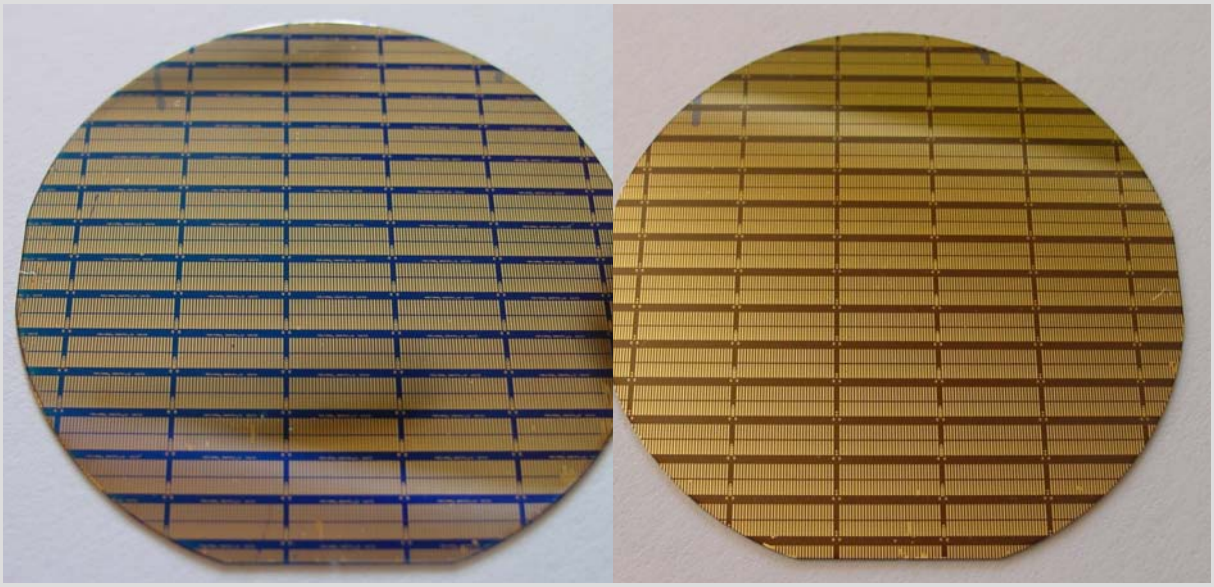

Research activities of the Department have interdisciplinary character, covering semiconductor materials science, technology, applied physics and applications:

(i) Characterisation and diagnostics of basic physical parameters of semiconductor materials - mainly GaAs and InP along with measurement techniques to evaluate conductivity, Hall mobility, magnetoresistance, *I-V* and *C-V* characteristics, the Department also uses e.g. DLTS, Admittance Transient Spectroscopy, High Resolution X-ray Diffraction and Topography, EBIC, SEM, AFM, etc.;

(ii) Study of physical problems related to the development of III-V radiation and particle detectors, such as the transport of charge carriers, deep-level (radiation) defects, electric field distribution, etc.;

(iii) Investigation of the technology of III-V particle, X-ray detectors and fast photo- and opto- devices. The technology includes preparation of contacts (Schottky, injecting, ohmic), optimization of device topology, treat-ment of interface and surface passivation. The detection properties of fabricated devices are tested using sources of α-particles, X- and gamma-ray photons;

(iv) In part, X-ray diffraction and devices for X-ray optics are investigated and developed;

(v) Finally, the Department also studies special plasma technologies and related phenomena. The technologies are developed for sensors based, e.g. on SiC.

The main goal of the Department (staff of 8 people) is to develop semiconductor devices suitable for small-scale fabrication, utilising unique III-V technology facilities of the Institute based in the town of Piešťany, 80 km north of Bratislava.

The Department activities included:

Basic research projects

(1) *Study of electro-physical and technological tasks of InP and GaAs based ionization radiation detectors preparation*, Grant No. 2/1167/22, principal investigator F. Dubecký;

(2) *Micromachined metal oxide gas microsensors, Grant No.* 1/0170/03, principal investigator I. Hotový

(3) *Investigation of technology, physical and detection performances of X- and gamma ray InP-based detectors*, Grant No. 2/4151/04, principal investigator F. Dubecký;

Grants of the Slovak Grant Agency for Science (SGAS)

Application research project

(4) *Modular imaging X-ray system utilizing radiation de-tectors based on GaAs semiconductor compound,* principal investigator F. Dubecký, Grant of the Slovak Ministry of Privatization, No. 2/9015/21.

International research project:

(5) *Monolithic X-ray optics based on multiple successive diffraction,* principal investigator D. Korytár. Financial support: COST No. P7 (X-ray and Neutron Optics).

Activities of the Department within the 6 FWP EC programme are in progress.

The technology equipment, used for fabrication of devices as small as 1 μm, is placed in a 100&1000 clean room 225 m^2-large. It consists of an automatic contact lithography aligner, a projection lithography system with, a wet-chemical treatment line, a BALZERS UMS 500 UHV evaporation system, a BALZERS BAS 450 magnetron and reactive sputtering apparatus, an annealing furnace, a SECON XPD200 dry plasma equipment for the deposition of dielectric layers, and a SECON XPL 200P reactive ion etching system.

The key electronic testing equipment includes: HP 4192A PC-controlled low-frequency impedance analyzer, DLS 82 PC-controlled deep-level spectrometer, automatic test system (AVT 110) with 50 controlled needle probes, X-ray diffractometer with a monolithic fourfold monochromator and attachments for the Lang and double crystal topography, automatic *I-V* measurement system (D/S Lab, Ltd.) up to 1 kV, and HP 54600 A two-channel digital oscilloscope.

The Department organized the 6th International Autumn School on X-Ray Scattering from Surfaces and Thin Layers, Smolenice 2003. It also participated at the program preparation of the 5th ASDAM'04 International Conference (Advanced Semiconductor Devices and Microsystems), Smolenice, October 2004.

Our research is based on a long-term fruitful collaboration with many groups in Slovakia and research groups abroad (e.g. University of Florence, IMEM CNR, Parma, both in Italy, Institute of Radio Engineering and Electronics and Institute of Physics, Czech Academy of Sciences, Prague, Czech Republic, Institute of Plasma Physics and Laser Microfussion, Warsaw, Poland).

František Dubecký

Monolithic strip line X-ray detector based on semi-insulating GaAs mounted onto flexible PCB holder

F. Dubecký, B. Zaťko, M. Sekáčová, P. Boháček, and J. Huran

The GaAs substrates used for X-ray detector fabrication were grown by the CMK Ltd. (Žarnovica, Slovakia) using LEC method. The monolithic strip line configuration is based on an improved SAMO topology [1, 2] with strip pitch 0.25 mm and overall dimensions of 0.18×2.5 mm^2. A monolithic line detector with 32 strips is edge irradiated, giving geometrical spatial resolution in the direction of the line of 0.25 mm, corresponding to a digital spatial resolution of less than 0.1 mm. Higher spatial resolution in the direction of line movement is achievable by tuning of the operating bias voltage, with a value of 1 μm/V, but to the detriment of time scanning, detection efficiency and energy resolution. Real values achieved ranged from about 30 μm (@ 50 V) up to 220 μm at full depletion (given by the detector thickness), which is optimal.

Collecting Schottky contacts placed on the top side of the chip were formed by Ti/Pt/Au while backside metallization was deposited by evaporation of AuGeNi eutectic alloy (200 nm) onto a 500 nm thick, nonstoichiometric (As-rich) defective buffer, thus creating a non-injecting contact. The sample surface was

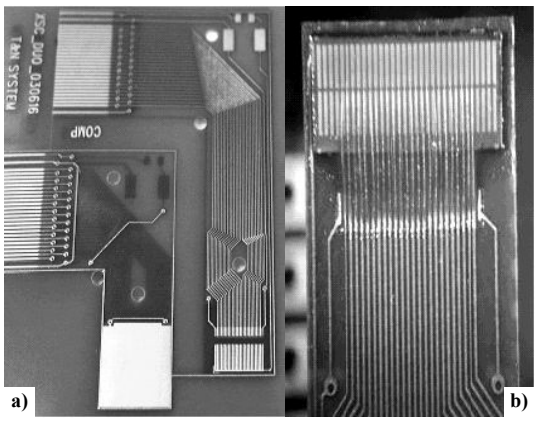

Fig. 1. Developed flexible PCB supports (a) and detail of mounted/bonded line chip (b).

passivated with 100 nm of silicon nitride PECVD deposited at 350 °C. The fabricated chips were stabilized by annealing at 100 °C for 10 hours prior to mounting Chips were glued by a silver paste directly onto a 0.25 mm thick PCB (Fig. 1a) contacted by Al wire and covered by highly insulating epoxy (Fig. 2b).

Typical RT reverse *I-V* characteristics of fabricated detectors, for various combinations of parallel connection of the strips, are shown in Fig. 2a. The characteristics have a blocking behaviour, with gradually increasing saturation current in the range of 10 nA, and a threshold voltage above 300 V. The linear increase of current with increasing number of strips connected in parallel confirms that there is negligible electrical charge diffusion between neighbouring strips up to a bias voltage of 200 V. Typical pulse height spectra from an ^{241}Am gamma-ray source (59.5 keV) measured by the same set of strips connected in parallel are illustrated in Fig. 2b. A partial decrease of the charge collection efficiency (CCE) and energy resolution is observed with increasing number of connected strips. The calculated detection efficiency of

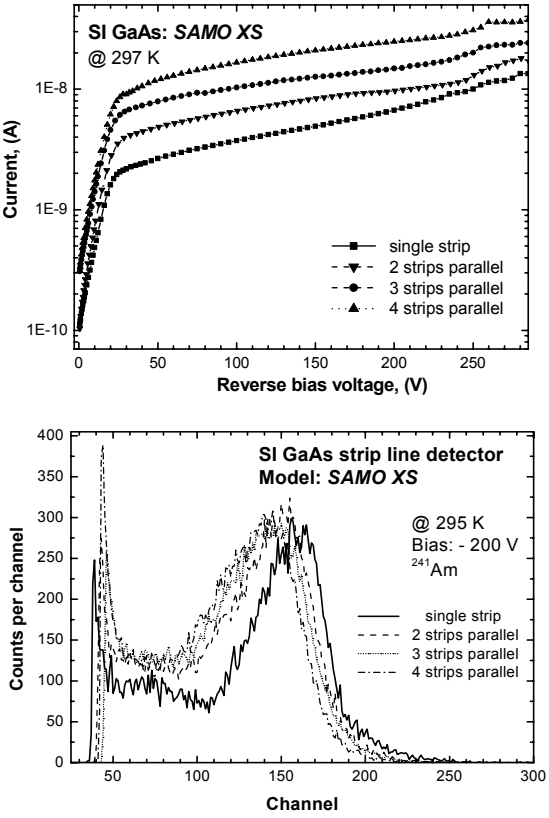

Fig. 2. I-V characteristics (a) and ^{241}Am pulse-height spectra (b) observed with GaAs single strip and strips connected in parallel.

the strip shows that the volume of the GaAs strip is fully active at a bias voltage of (200 ± 25) V. This was evaluated using a reference CdTe detector 1.5 mm thick (almost 100 % absorption efficiency of 59.5 keV photons) taking into account GaAs strip detector geometry and attenuation for given thickness. We used for control calculation also the known activity of the ^{241}Am gamma-ray source. The developed SI GaAs line strip detectors were tested in a high photon flux from an X-ray tube, showing acceptable performance in imaging applications (see following contribution).

[1] *Dubecký F., et al.: Nucl. Instr. Meth.* ***A458*** *(2001) 152.*
[2] *Dubecký F., et al.: Nucl. Instr. Meth.* ***A531*** *(2004) 314.*

Simulation of the reverse *I-V* characteristics of the Schottky barrier radiation detector structures prepared on semi-insulating GaAs

P. Boháček, F. Dubecký, and M. Sekáčová

In our contribution, we apply a simple model based on the thermionic field emission (TFE) theory [1], taking into account Schottky barrier lowering and tunnelling effects [2] on the reverse current-voltage (*I-V*) characteristics of semi-insulating (SI) GaAs radiation detector structures. The useful parameters, Schottky barrier height and electrical resistivity of the substrate material, were calculated. Calculated resistivity values were compared to values obtained from conductivity measurements on the substrates.

The samples were prepared using undoped liquid encapsulated Czochralski (LEC) SI GaAs 2" wafers with crystallographic orientation (100) from manufacturer – Wacker Chemitronic (Germany). The wafer thickness was reduced by lapping and chemo-mechanically polishing to 250 μm (#°WA). Original wafer thickness was about 400 μm. The symmetrical back-to-back Schottky sandwich structures with semitransparent Au contacts were prepared by electron beam evaporation of Au in a high-vacuum deposition system without passivation layers. Samples of square shape with an area 7.3 mm^2 were cleaved from the wafer and contacted by silver paste on standard metallic transistor holder (TO 5).

The reverse *I-V* characteristics of the radiation detector structures were measured in a dark, electrically shielded probe station in a temperature range from 300 to 360 K in step of 20 K. The conductivity measurements were used for determination of the resistivity by the van der Pauw method in the same temperature range.

In our simulation the equation for the reverse current I_r of the detector structure from [1] after transformation can be rewritten:

$$V_r = I_r^2 B_k \exp\left(\frac{2q(\Phi_{b0} - \Delta\Phi)}{k}\right) + R_b I_r + E_C - E_F - \Phi_{b0} + \Delta\Phi \cdot$$

V_r is reverse voltage on the structure terminals, Φ_{b0} is the Schottky energy barrier height, $\Delta\Phi$ is the lowering of the barrier due to the electric field (the Schottky effect), T is the absolute temperature, k_B is the Boltzmann constant, E_F is the Fermi level, E_C is the lower edge of the conduction band, R_b is the bulk resistance, q is the electronic charge, and B_k is a constant.

The values of the measured resistivities and the resistivities and barrier heights calculated from our modified TFE model are presented in Table 1. The values obtained for the Schottky barrier height for the sample #°WA are Φ_{b0} = (0.89 ± 0.01) eV. These values are slightly higher than published data for Au on N type GaAs (0.79 eV from *I-V* measurements) [1].

The values of measured and calculated current were re-counted to the current density. The current density-voltage (*J-V*) curves are reported on a log-log scale in Fig.°1 (sample #°WA), as a function of the temperature in the range 300 - 360 K, in step of 20 K. The simulated curves are marked by the broken lines and measured values by the solid ones. The *J-V* characteristics in Fig. 1 are practically linear and the transport is bulk limited. It can be seen from the Fig. 1 that the experimental results are in good agreement with the simulated values.

Table 1. Calculated and measured results for variable temperatures obtained with sample # WA. T is the absolute temperature and ρ is the specific electrical resistivity.

T (K)	Φ_{b0} (eV)	ρ (meas.) (Ω m)	ρ (sim.) (Ω m)
300	0.894	4.20 x 10^5	6.08 x 10^5
320	0.890	6.42 x 10^4	6.86 x 10^4
340	0.890	1.22 x 10^4	1.47 x 10^4
360	0.883	2.81 x 10^3	2.96 x 10^3

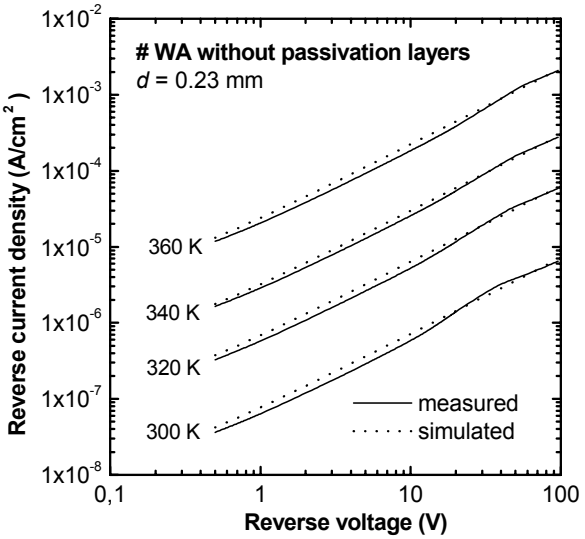

Fig. 1. Measured (solid line) and simulated (broken line) reverse J-V characteristics (in the log-log scale) of radiation detector structure (# WA) without passivation layers in the temperature range from 300 to 360 K.

We are thankful to I. Bešše, M. Krempaský, J. Betko, and R. Senderák for the contribution to this work.

[1] *Rhoderick, E.H. and Williams, R.H.: Metal-Semiconductor Contacts, Clarendon, Oxford (1988).*

[2] *Lee, T.C., Au, H.L., Chen, T.P., Ling, C.C., Fung, S., and Beling, C.D.: Semicond. Sci. Technol.* ***8*** *(1993) 70.*

Study of monolithic radiation line detector based on semi-insulating GaAs using X-ray source

B. Zaťko and F. Dubecký

Digital X–ray imaging is the most perspective field of application of RT semiconductor radiation detectors [1]. The main advantages include: i) higher sensitivity in comparison to photographic film due to much better absorption, ii) suppression of low–frequency noise by pulse–processing front–end electronics, iii) linear behaviour over entire dynamic range, which can be chosen arbitrarily according to the application, iv) setting of a threshold allows to discriminate (not only) noise from signal, and also photon energies, v) multiple thresholds can be implemented, which open completely new perspectives for X–ray imaging application [2, 3].

Great effort is concentrating for the development of radiation detectors based on bulk semi–insulating (SI) GaAs due to its low cost coupled with good properties in detection of X– and γ–radiation [4, 5]. In our previous paper we study the spectrometric performance at RT of SI GaAs radiation detectors and coupled read-out electronics, mainly charge sensitive preamplifiers [6].

Strip detectors were fabricated from SI GaAs bulk crystals grown by VGF method produced by CMK Ltd. Basic material parameters were determined from galvanomagnetic measurement give resistivity 5.2 x 10^7 Ωcm and the Hall mobility 5200 – 5800 cm^2/Vs measured at RT. Collecting Schottky contacts (Au/Zn metallization of 120 nm) are placed on the top side using a simple one side or sophisticated double–sided optical photolithography and lift–off process. Backside metallization was deposited onto a defective As–implanted buffer layer by evaporation of AuGeNi eutectic (thickness 200 nm), creating a quasi–ohmic non–injecting contact. Sample surface is passivated by PE CVD silicon nitride 100 nm thick.

Schematic view of several strips of line detector is depicted in Fig. 1. The sizes of strips are listed in millimeters. Each strip detector consists of two parts, which are connected parallel into the preamplifier input. The X–rays impinge from the edge of detector, which ensures the total absorption length of 2.5 mm. The shape of the each strip is trapezoidal to minimize the influence of photon scattering.

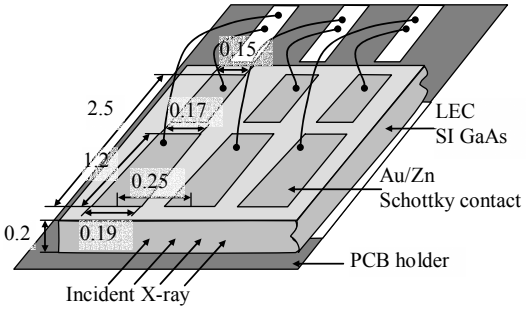

Fig. 1. Schematic view of several SI GaAs strips.

The current-voltage characteristic of SI GaAs single strip has a blocking behaviour with gradually increasing current in saturation region. More details are presented in our previous paper [7]. The strip line detector is glued by silver paste directly onto a 0.25 mm thick PCB holder with ultrasonic bonding made by Al wire and covered by highly insulating epoxy. Individual strips are dc coupled to our developed analog read–out card, which consists of 24 charge sensitive preamplifiers, linear amplifiers, discriminators with one adjustable common level through the software and counter for each channel. The discriminator level determines the minimum energy of X-ray which can be detected. Analog read–out card is connected with a digital card which provides the read-out of individual channel and communication with a PC.

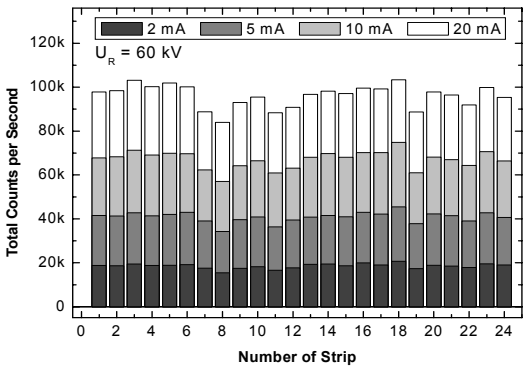

Fig. 2. Response of each strip to X-ray beam.

The response of radiation detection system to X–ray beam is shown in Fig. 2. An aluminum filter was placed between the line detectors and X–ray tube to reduce the number of generated X–ray photons. Measured dispersion of total counts in each channel is too high as corresponds to the value of photon noise. This is explainable with dispersion of strip detectors performance and analog electronic read–out system. Several repeated measurements with X–ray beam showed that differences in total counts in each channel in not worse than 1 %.

This work was done in collaboration with IZFP EADQ Dresden, Germany (M. Herms, L. Haupt, I. Bešše).

[1] *Revolution in medical imaging, Science and Technology, Business Week, 1997, July 7, p. 134.*
[2] *Da Via C., et al.: Nucl. Instr. Meth.* ***A395*** *(1997) 148.*
[3] *Mikulec B.: Nucl. Instr. Meth.* ***A510*** *(2003) 1.*
[4] *Schlessinger T.E. and James R.B.: Semiconductor for Room Temperature Nuclear Detector Application, Semiconductors and semimetals. Vol. 43, Academic Press, San Diego (1995).*
[5] *McGregor D. S. and Hermon H.: Nucl. Instr. Meth.* ***A395*** *(1997) 101.*
[6] *Zaťko B., et al.: Nucl. Instr. Meth.* ***A531*** *(2004) 111.*
[7] *Dubecký F., et al.: Nucl. Instr. Meth.* ***A531*** *(2004) 314.*

Digital X-ray scanner based on semi-insulating GaAs monolithic line detectors working in quantum imaging regime

F. Dubecký, B. Zaťko, M. Sekáčová, P. Boháček, and J. Huran

The result presents successful realization of the portable digital modular X-ray scanner based on application of monolithic X-ray GaAs strip line detectors. This is a unique radiographic equipment where X-ray imaging is realised in quantum mode („single photon counting“) allowing substantiall improvement of the digital image in contrast. Following our knowledge, this instrument is the first over the word using GaAs X-ray detectors. Monolithic strip line GaAs X-ray sensor uses an original topology and technology developed. Base semi-insulating GaAs substrate has domestic origin (producer: CMK sro., Žarnovica, Slovakia). Monolithic chips of detectors are directly mounted onto flexible PCB carriers using exchangable coupling via input microconnectors (see previous contributions). Readout and control electronics, automatic positionning, control and imaging software were developed and fabricated in collaboration with the end-user of the result.

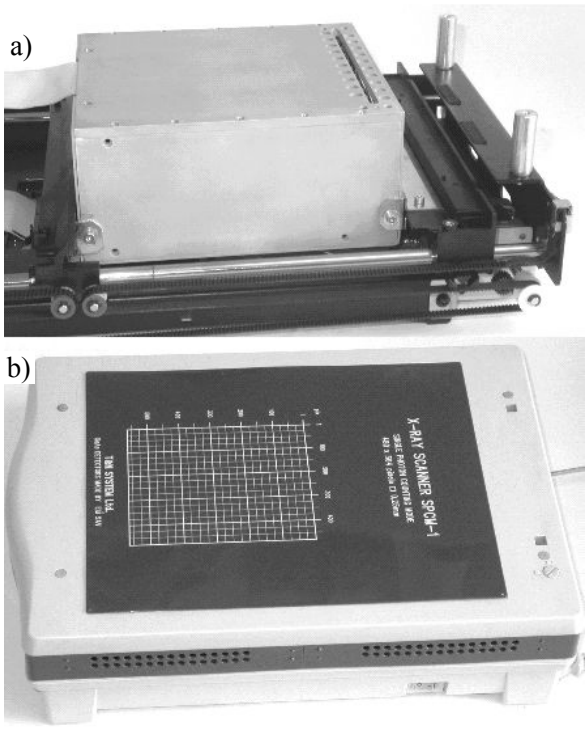

Fig. 1. Detection unit with SI GaAs detectors (a) and view of the closed X-ray digital scanner (b).

Fabricated digital scanner (Fig. 1) consits of 480 readout channels with the scanned area of 12 x 15 cm^2, created by 843 x 750 points at the highest position resolution (250 μm in the line direction and 80 μm in direction of the line movement). Control and imaging softwares allow to set length of the step, exposition duration and scanning trace length. Photograph and observed „quantum“ digital X-ray images of selected objects are shown in Fig. 2. Observed test digital X-ray images show high quality.

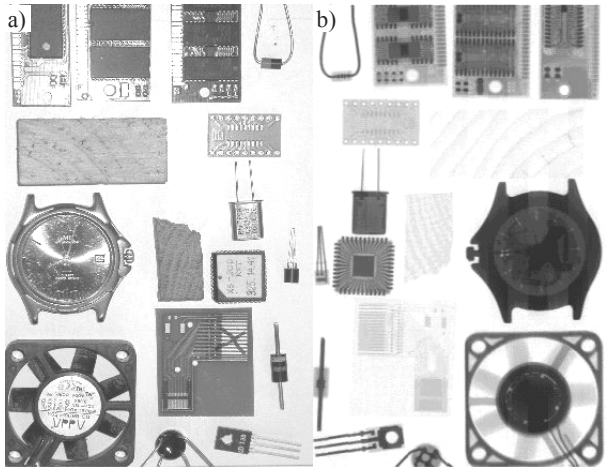

Fig. 2. Photograph of various scanned objects (a) and their X-ray images (b) obtained using developed quantum scanner (@ 70 kV, 8 mA, 50 ms) using step of 0.25 mm.

The digital X-ray scanner was presented at the international trade fair INCHEBA, Bratislava 2004 within the exposition of the Slovak Academy of Sciences. The scanner was awarded by *GOLD INCHEBA*. This applied research result was obtained within the framework of domestic scientific-technical research project. Result was presented at four international conferences and workshops [1-4], 2 foreigner research institutes (IMEM CNR, Parma, IPP and LM, Warsaw) and university (UF and INFN, Florence).

Co-operating partner and result end-user: T&N System, sro., Severná 5, Banská Bystrica, Slovakia.

The work was done in collaboration with Faculty of Nuclear Physics and Technique, Slovak Technical University, Bratislava, Slovakia (V. Nečas, A. Perďochová).

[1] *Dubecký F., et al.: APCOM 2004 - Proc. of the 10th Int. Workshop on Applied Physics of Condensed Matter. Eds.: D. Barančok et al. Bratislava: FEI STU, 2004. ISBN: 80-227-2073-9, p. 46.*

[2] *Dubecký F., et al.: Proc. of the 13th Semi-Conducting and Insulating Materials Conference, SIMC-XIII-2004. Beijing 2004, in press.*

[3] *Dubecký F., et al.: Nuclear Instr. and Meth. in Phys. Res.* ***A531*** *(2004) 314.*

[4] *Dubecký F., et al.: Nuclear Instr. and Meth. in Phys. Res. A (2005), in press.*

[5] *Dubecký F., et al.: XVIth Int. Workshop on Room Temperature Semiconductor X- and Gamma-Ray Detectors, ROME, October 2004, http://www.nss-mic.org/2004.*

Testing of a monolithic 2D beam compressor for hard X-ray beams

D. Korytár

In technology of microelectronic devices there is a need to measure locally various structural parameters of microelectronic structures, such as composition and strains, on the scale of the smallest microelectronic elements, i.e. on the (sub)micrometer level. The X-ray microbeams produced by glass capillary, by a pinhole and by a phase zone plate, Kirkpatrick-Baez (K-B) mirror system, waveguides, or refractive lenses have rather high angular divergence and thus their use for high resolution measurements is limited.

In our previous ESRF experiments a silicon monolithic 2D X-ray magnifier was tested at the beam energies around 10 keV. In its version with two noncoplanar asymmetric {311} diffractors about 15 times magnification was obtained [1].

The same monolithic silicon crystal with (113) + (-311) + (2-2-4) asymmetric diffractors was repolished and used as the X-ray beam compressor. For this purpose, the beam directions had to be reversed compared to the beam magnifier (see Figure 1).

Testing of the beam compressor was done at BM05 at ESRF Grenoble [2]. The X-ray beam monochromatized by an Si(111), Si(-1-1-1) vertical monochromator to the energy of 9.5 keV was used. The crystal block was adjusted into the first diffraction in such a way that the

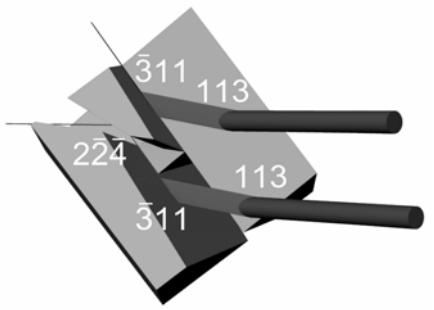

Fig. 1. Three dimensional model of a silicon monolithic beam expander/compressor for about 10 keV X-ray radiation. In its version with three diffractors (bottom part of the crystal block) the incoming and outgoing beams are mutually parallel. Beam expansion takes place for the beams from the left to the right, beam compression for the reverse beam directions.

reciprocal lattice vector of the first diffractor lies in the horizontal axis of the goniometer.

Rotating the crystal about the horizontal axis (Renninger scan) further multiple diffractions (both simultaneous and successive) can be obtained. A scintillation detector and an X-ray eye were used to find desired diffractions; rectangular metal grids in the incident beam were employed to form a structured incident beam (transferred into a system of microbeams in the output beam) and a high resolution X-ray film and FreLoN CCD camera were used to record the X-ray images at the output side of beam compressor. Because of a strong decrease of the spatial resolution in the case of three diffraction the experiment was performed with (113) and (-311) asymmetric diffractors only, which has the drawback that the incident and outgoing beams are not parallel and that the outgoing beam does not lie in the horizontal plane of synchrotron facility.

Fig. 2 shows one window (a) of a larger rectangular wire grid, which was put into the incident beam, and the demagnified image of this grid at the output of the X-ray beam compressor (b). The demagnification at the output side is about 10 and 13 times in vertical and horizontal direction, respectively.

Here we would like to stress about two orders of

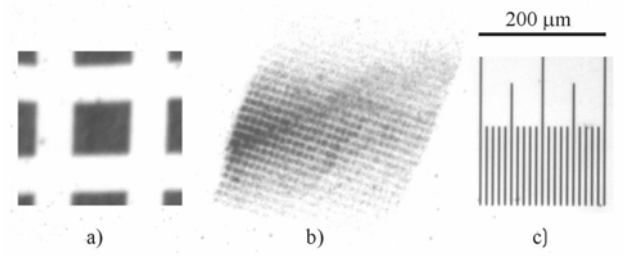

Fig. 2. More than 400 parallel X-ray microbeams (b) formed by a monolithic X-ray beam compressor at 9.5 keV by a wire mesh with 100 μm windows and 48 μm wires (a) put into the incident beam. Microbeams size is 7.6 x 9.9 μm^2 (H x W), their separation 3.3 μm horizontally and 4.3 μm vertically. Exposition time 2 min., film resolution not better than 2 μm. Fine scale lines in the inlet (c) are 10 μm apart.

magnitude decrease of the needed exposition time compared to the X-ray magnifier described in [1]. This demonstrates a real 2D beam compression, which can open the way to broader utilization of the 2D beam compressor as beam conditioning optics.

This work was done in close collaboration with Fraunhofer IZFP Dresden (T. Baumbach), IMEM CNR Parma (C. Ferrari, N. Verdi), ESRF Grenoble (L. Helfen) and Masaryk University Brno (P. Mikulík, A. Kuběna).

[1] *Korytár, D., Mikulík, P., Ferrari, C., Hrdý, J., Baumbach, T., Freund, A., and Kuběna, A.: J. Phys. D: Appl. Phys.* ***36*** *(2003) A65.*

[2] *Korytár, D., Baumbach, T., Ferrari, C., Helfen, L., Verdi, N., Mikulík, P., Kuběna, A., and Vagovič, P.: accepted in J. Phys. D: Appl. Phys.*

Evaluation of spatial resolution in X-ray beam compressors

D. Korytár and P. Vagovič

A 2D X-ray beam compressor based on Si (113) + (-311) asymmetric diffractors was successfully tested at BM05 at ESRF Grenoble. Microbeams sized below 10 μm have been obtained by means of 2D compression of the X-ray beams structured by wire grids [1] (see also previous page). The smallest obtainable beam is in terms of image formation related to spatial resolution for this kind of imaging. It is thus desirable to evaluate the spatial resolution and Figure 1 illustrates an indirect procedure for this. A beam of 0.1 x 0.1 mm^2 was formed by the beamline slits. Microscopic #200 mesh grid was positioned to the entrance window of a scintillation counter attached to the detector arm of goniometer.

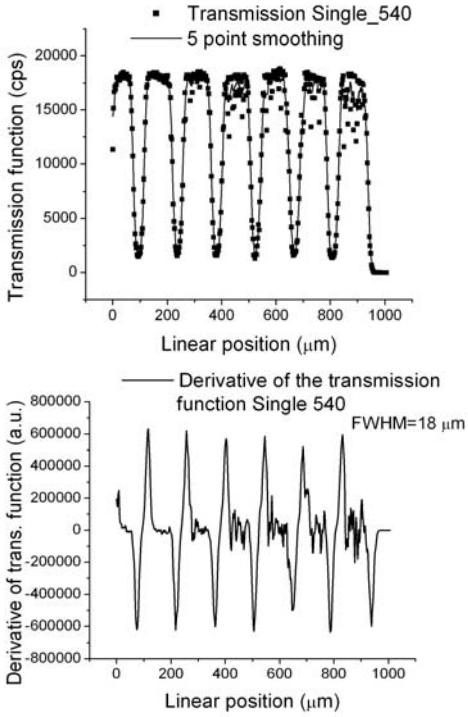

Fig. 1. Transmission function measured by scanning a microscopic mesh #200 (100 μm windows, 33 μm wires) across the compressed beam (a) and calculated derivative function (b) giving resolution represented by the FWHM.

Transmission function was measured scanning the grid across the outgoing microbeam. Derivative of the transmission function is sensitive to the sharpness of the edges and because of that the full width at half maximum (FWHM) is sometimes used to characterize resolution in imaging techniques [2]. We consider the value of 18 μm unexpectedly high. The same analysis was done for simulated image in [1]. From the derivative of the transmission intensity profile function we determined the FWHM = 5 μm.

In the next step we tried to analyse the microbeams formed by the demagnifier and exposed onto an X-ray film while a larger rectangular wire grid (100 μm windows and 48 μm wires) was put into the incident beam. The demagnification at the output side is about 10 and 13 times in vertical and horizontal direction, respectively [1]. Horizontal and vertical intensity profiles were performed in rectangles according to the inlet to Fig. 2a. Fig. 2b shows the absolute value of derivative of the absorption function as well as the calculated FWHM of the vertical profile, which is 4 μm. In the horizontal direction, the FWHM was established as 3 μm.

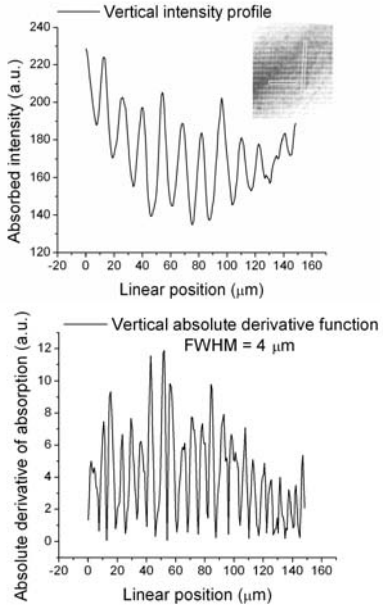

Fig. 2. Vertical absorbed intensity profile performed in the rectangle according to the inlet (a). The absolute value of the derivative of the absorption function (b) with the calculated FWHM of the vertical profile being 4 μm. In horizontal direction the FWHM was established as 3 μm.

In view of these results and considering also results of beam tracing simulation we reevaluated results in Fig. 1. We considered that the applied smoothing of transmission function by means of 5 neighbouring points is not adequate for the density of measured points used. We then tried 3 points for smoothing transmission functionand re-calculated derivative and obtained a new value for FWHM of 5 μm. This value is now consistent with the values obtained by the image analyses.

[1] *Korytár, D., Baumbach, T., Ferrari, C., Helfen, L., Verdi, N., Mikulík, P., Kuběna, A., and Vagovič, P.: accepted in J. Phys. D: Appl. Phys.*

[2] *Kagoshima, Y., Ibuki, T., Yokoyama, Y., Takai, K., Tsusaka, Y., Matsui, J.: Jpn. J. Appl. Phys.* ***41*** *(2002) 412.*

Progress in amorphous silicon carbide technology

J. Huran

Most of traditional integrated circuit technologies using silicon devices are not able to operate at temperatures above 250 ^{0}C, especially when high operating temperatures are combined with high power, high frequency and high radiation environments. In addition to high-temperature applications, SiC has potencial for use in high-power, high-frequency, and radiation-resistant applications [1]. Silicon carbide (SiC), aluminum nitride (AlN), gallium nitride (GaN), boron nitride (BN), diamond, and zinc selenium (ZnSe) are just some of the premier wide-bandgap semiconductors now being developed for use in the aforementioned applications. However, SiC has several advantages over other wide-bandgap semiconductors at the present time including commercial availability of substrates [2], known device processing techniques, and the ability to grow a thermal oxide for use as masks in processing, device passivation layers, and gate dielectrics. Furthermore, SiC can also be used as a thin buffer layer for the growth of diamond films on silicon substrates [3]. For example, a-$Si_{1-x}C_x$:H was used as a wide window material to enhance the conversion efficiency of amorphous solar cell [4]. Nitrogen-doped amorphous SiC films were grown by plasma enhanced chemical vapour deposition (PE CVD) technique.

All films were prepared on lightly doped n-type Si substrates (111). The films were deposited in a high frequency parallel-plate plasma reactor in which the frequency, the RF power and the substrate temperature were maintained at 13.56 MHz, 0.06 Wcm^{-2}, and 350 ^{o}C, respectively.

A typical RBS spectrum of as deposited samples is shown in Fig. 1. The films were silicon rich with a C/Si ratio from 0.7 to 0.8. The nitrogen concentration was 10 at.% in sample D2 and 14 at.% in sample D3.

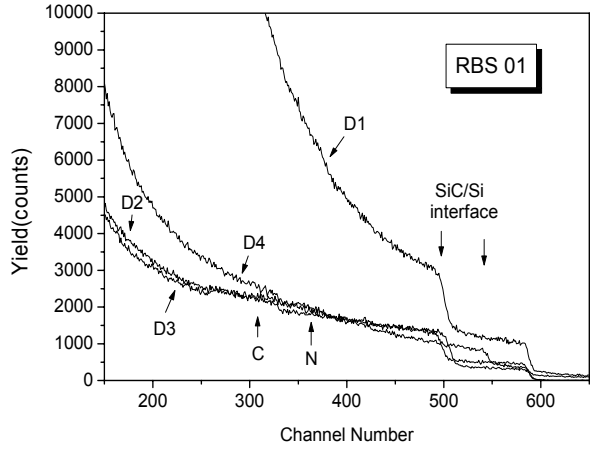

Fig. 1. A typical RBS spectrum of as deposited amorphous SiC films on Si substrate.

The electron beam irradiation experiments were carried out as follows: samples D2 and D3 (with different nitrogen concentrations) were irradiated by 20 pulses (indicated as D2e20, D3e20). The *I-V* characteristics of diodes from samples with different nitrogen-doped SiC films are compared in Figure 2.

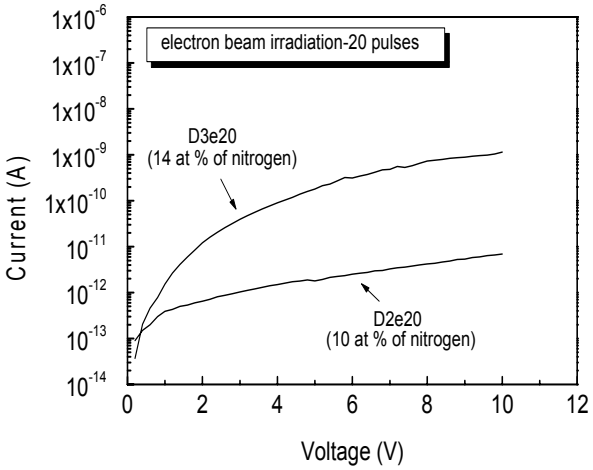

Fig. 2. I-V characteristics of diodes prepared from samples with nitrogen-doped SiC films irradiated by 20 pulses of electron beam (sample D2e20 - 10 at. % of nitrogen, sample D3e20 - 14 at. % of nitrogen).

Both samples D2 and D3 were exposed to the same pulse electron beam irradiation conditions (20 pulses). The diode currents at applied bias of 5 V were about 2 pA and 200 pA for samples D2e20 and D3e20, respectively. These results confirm the fact that samples D3e20 with higher nitrogen doping (i. e. with nitrogen content of 14 at. %) exhibit about two orders of magnitude higher conductivity (i. e. lower resistivity) as compared to lightly doped samples D2e20 (with nitrogen content of 10 at. %).

[1] *Trew, R.J., Yan, J.B., and Mock, P.M.: Proc. IEEE 79 (1991) 598.*
[2] *Advanced Technology Materials, Inc., 7 Commerce Drive, Danbury, CT 06810-4169.*
[3] *Wang, E.G.: Physica B**185** (1993) 85.*
[4] *Nahano, S., Kishi, Y., Ohnishi, M., Tsuda, S., Shibuya, H., Nakamura, N., Hishikawa, Y., Tarui, H., Takahawa, T., and Kuwano, Y.: Mat. Res. Soc. Symp. Proc. **49** (1985) 275.*

Recent progress in development of monolithic strip line X-ray detectors based on semi-insulating InP

F. Dubecký, B. Zaťko, M. Sekáčová, P. Boháček, J. Huran, and V. Šmatko

In the last decade, X-ray digital imaging systems in medicine, security, as well as in on-line control for non-destructive testing of materials and processes, initiated an interest in wide band-gap semiconductor radiation detectors with a high atomic number, *Z* [1]. InP based particle detectors may offer an attractive alternative to detectors made of GaAs and CdTe for the detection of high energy photons. An appropriate combination of the band-gap value (1.35 eV) and the high atomic numbers Z (49/15) of the constituents favour InP, for the fabrication of highly efficient photon detectors. InP exhibits an absorption efficiency about three times higher than GaAs regarding the photons with energy up to 150 keV. Semi-insulating (SI) InP also outperforms CdTe and ternary alloy CdZnTe in terms of cost and offers potentially the fastest operation rate due to its 2-3 times higher electron drift velocity in the electric field region mostly used for detector operation [2]. Moreover, SI InP material is already more homogeneous than CdTe and shows indications of a negligible level of polarization effects, in contrast to CdTe. Our paper [3] is the first devoted to the fabrication of monolithic InP detector arrays required for their introduction into X-ray imaging applications.

The key problem in the case of SI InP based detector is related to its operation in a quasi-ohmic regime [3, 4]. In such a case pixel detectors in monolithic array must be divided by trenches formed between neighbouring detectors by mechanical means, using, e.g., a thin diamond saw, or etching (wet or dry – reactive ion etching, RIE) after additional photolithographic masking.

Example of double line array of SI InP detectors mounted and bonded onto PCB support with trenches done by sawing is shown in Fig. 1. Diamond saw of 30 μm width was used in this case. Pixel pitch is 1 mm.

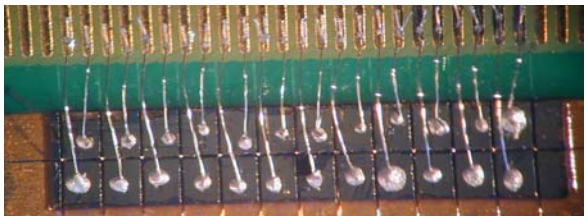

Fig. 1. Double line array of SI InP detectors with trenches formed by mechanical sawing (saw width was 30 μm).

Much more effective is formation of trenches by etching. Example of developed wet etching using solution based on HBr acid is shown in Fig. 2. Before etching additional photolithographic masking for opening thin gaps (8 μm) between neighbouring strip detectors was applied. Trench depth and width is about 20 μm and 43 μm, respectively. Observed SEM images (Fig. 2) show that etching process is dependent on the

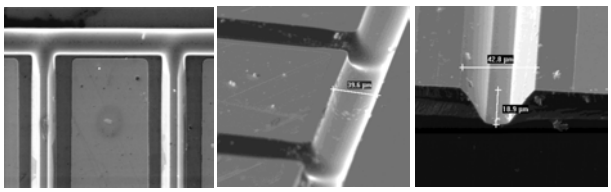

Fig. 2. SEM Iimages of trenches around strips formed by wet etching using HBr acid-based solution.

crystalographic orientation. As follows from *I-V* measurements of the single strip and strips connected in parallel (Fig. 3), we can deduce that even a trench depth of about 20 μm developed on one chip side, (the etched depth occupies less than 10 % of the whole wafer thickness), is efficient in suppressing the electrical charge intermixing. The estimated supression reached an acceptable level of about 80 % what was confirmed

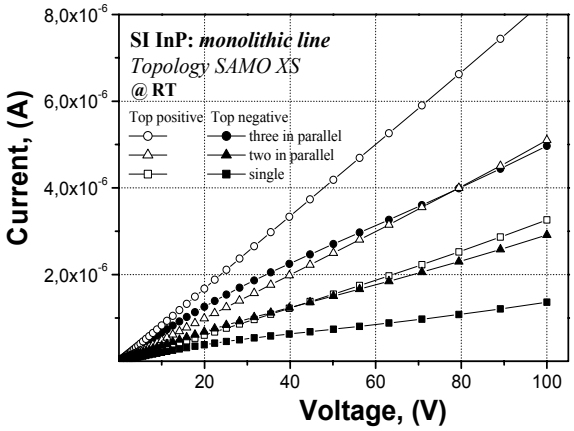

Fig. 3. I-V characteristics measured with the single strip and strips connected in parallel.

also by the *I-V* measurement between the two neighbouring strips in *planar* configuration. A future possibility for improving this value is to form trenches symmetrically on both sides of the chip or to develop anisotropic etching process.

[1] *Schlesinger, T.E.and James, R.B.: Semiconductors for Room Temperature Nuclear Detector Applications, Semiconduc-tors and Semimetals, Vol. 43, Eds. R.K. Willardson, A.C. Beer, and E.R. Weber, Academic Press, San Diego 1995.*

[2] *Handbook Series on Semiconductor Parameters, Vol. I, Eds. M. Levinshtein, S. Rumyantsev, and M. Shur, World Scientific Publ. Co., Singapore 1996.*

[3] *Dubecký, F., et al.: Nucl. Instr. Meth.* ***A531*** *(2004) 181.*

[4] *Boháček, P., et al.: Materials Sci & Engn.* ***B91-92*** *(2002) 516.*

First results observed with mini-tomograph system based on GaAs detector

B. Zaťko and F. Dubecký

The study of inner structure of objects has a beginning in discovery of X-ray. Nondestructive testing of investigated objects is the most perspective in many fields of applications [1]. First medicine computer tomograph was invented in 1971.

Computer tomography is organized by principle of working: X-ray (X-CT), emission (E-CT), ultrasound (US-CT) and nuclear magnetic resonance (NMR-CT).

Using X-CT the tested object is outshined by X-ray in all directions. In our case we used a passive γ-radiation source ^{241}Am with photons energy of 60 keV.

Schematic view of X-CT is depicted in Fig. 1. The beam of X-ray or γ-ray impinges to the investigated sample. The radiation is partially absorbed and detected by semi-insulating GaAs detector, where occurs its transformation to electric signal. The number of registered pulses is recorded by computer for every point of x axis. Minimum step is 0.22 mm. After measuring all points corresponding to the sample we get projective data for one angle. Then the sample is rotated and another projective data are collected. The minimum rotation step is 1.8 degree. Investigated object is rotated from 0 to 360 degree. The shifting and rotating of the object ensure two stepping motors controlled by computer.

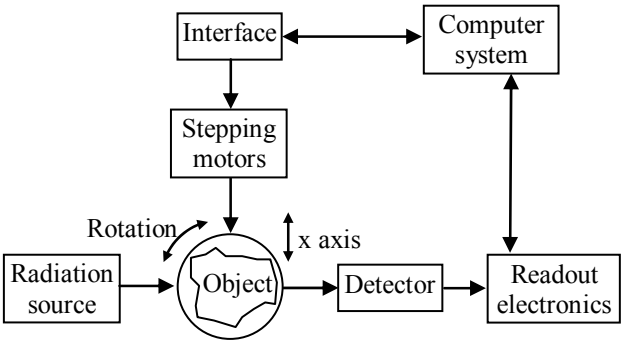

Fig. 1. Schematic view of X-CT.

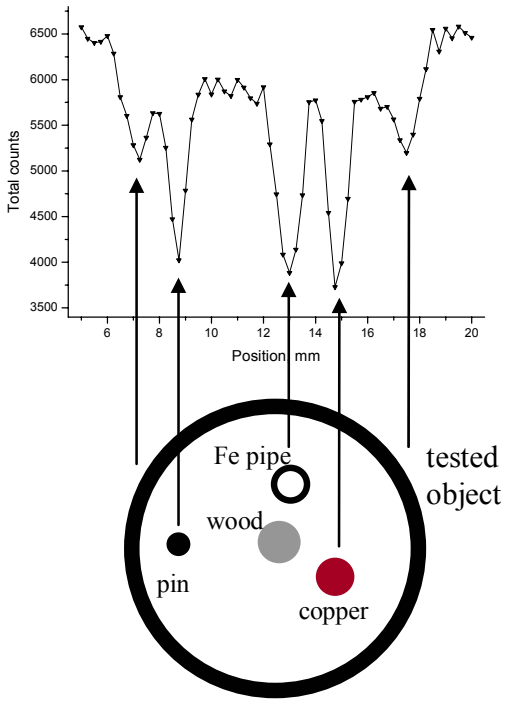

Fig. 2. The tested sample and the corresponding projected graph.

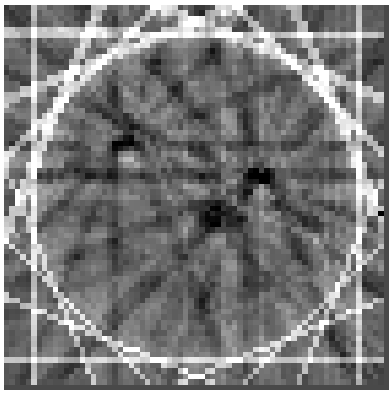

Fig. 3. First tomograph image of tested object.

The Fig. 2 shows a data of one projection of tested sample, which consist of the teflon ring wherein pin, wood, Fe pipe and copper were covered. The dependence of total counts vs. position represents the absorption of γ–ray in each point. Five peaks in graph correspond to teflon ring, pin, wood, Fe pipe, copper and teflon ring. The measurement was done with 8 projections from 0 to 180 degree and the step of rotation was 22.5 degree. The collected data was processed by image reconstruction software [2]. Fig. 3 depicts final image of tested sample. We can see only three of four objects; pin, copper, wood and Fe pipe are joined to one. This is due to the wood and Fe pipe are too closely. If we want to distinguish these two objects the rotation step need to be smaller. In all measured projections were only five peaks instead of six which is necessary for right image reconstruction.

This work was supported in a part by the grant of Slovak Grant Agency for Science No.2/4151/24. We thank to Professor I. Frollo, Institute of Measurement, SAS Bratislava, for the image reconstruction.

[1] *Pham, Van Tinh: Výpočtová technika v hardwarovej a softwarovej realizácii počítačového romografu pre tomografické zobrazenie vnútornej štruktúry materálu. PhD thesis. Technical University in Zvolen 2002.*

[2] *Image reconstruction from projection. HET408 Biomedical Imaging. http://marr.bsee.swin.edu.au/~dtl/het408.html.*

Department of Optoelectronics

Jozef Novák

Research scientists
Július Betko (up to January 2004)
Vladimír Cambel
Ján Fedor (since November 2004)
Dagmar Gregušová
Peter Kordoš (since June 2004)
Michal Kučera
Róbert Kúdela
Marián Morvic

Technical staff
Pavol Mužík
Peter Martiš
Ivan Sabo

Research Engineers
Peter Eliáš
Stanislav Hasenöhrl
Ján Šoltýs
Pavel Štrichovanec

PhD Student
Jozef Martaus

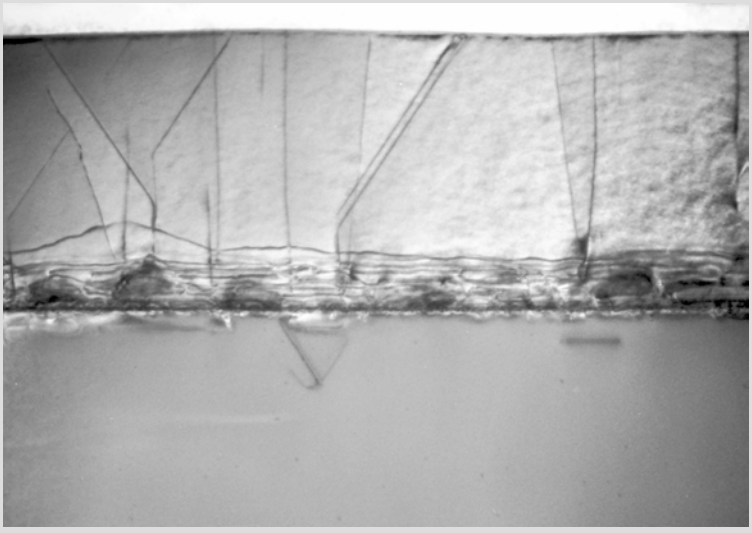

In 2003 and 2004 researchers at the Department of Optoelectronics continued work on the epitaxial growth, characterization and application of III-V semiconductor layers and structures. Apart from work on InP/InGaAs and GaAs/InGaP, our traditional material systems, we turned our attention to a new material: gallium nitride.

We prepared and investigated epitaxial structures grown on both planar substrates and non-planar (patterned) substrates. Growth on patterned substrates is more complex compared with growth on planar substrates, and it requires an interdisciplinary approach that encompasses crystallography, chemistry and the physics of epitaxial growth.

We performed our growth experiments using an Aixtron AIX 200 R&D MOVPE apparatus. Structures were grown for our research work, but we also provided structures for other departments of the Institute.

In 2003 and 2004 we mainly focused on two research projects. One project, supported within the 5th Framework programme, was entitled "New gallium phosphide grown by vertical gradient freeze method for light emitting diodes". It started under identification number IST-2001-32793 on 1 March 2002. Our role in it was twofold: (i) We provided assistance in the development of the epi-ready finalization of gallium phosphide substrates produced by Phostec; (ii) We used MOVPE technology for the development of high-brightness LED structures based on GaP substrates. Participation in this project was pretentious and very exciting: We achieved a number of interesting results related to graded InGaP buffers grown on GaP substrates, strain relaxation, and the development of high brightness LED structures.

The other project, funded by the Science and Technology Assistance Agency (APVT), was entitled "Submicron vector Hall probe microscope". It was centered on the development of a magnetic field vector sensor based on submicron-sized Hall probes on pyramidal-shaped objects. To produce such a device, the technologist needs to master difficult processing techniques, such as those based on conformal resist deposition and submicron lithography with an atomic force microscope.

The APVT agency has recently funded four of our projects: We are happy to see that national resources play an increasing role in project funding. The project resources were partly used to support our PhD students. Two PhD students finished successfully their work in 2003 or 2004. Four other PhD theses are currently close to completion.

The Department of Optoelectronics has enjoyed broad international co-operation. Most of the activities mentioned above were part of broader international efforts. In 2003 and 2004 we co-operated with the following institutions: the Institute for Thin Films and Ion Technology Research Centre Jülich (Germany), the Institute of Materials Research CSIC, Barcelona (Spain), University of Parma and MASPEC Parma (Italy), the Institute of Physics ASCR Prague, and the Institute of Radiotechnique and Electronics Prague (Czech Republic). Also vital for our work was close co-operation among members of the Department. I would like to express my gratitude to all of them for their fruitful work and enthusiasm in 2003 and 2004.

Jozef Novák

Crossover from direct to indirect band gap structure in epitaxial $In_xGa_{1-x}P$ alloy

J. Novák, S. Hasenöhrl, R. Kúdela, and M. Kučera

The InGaP alloy exhibits some of the largest direct gaps among the non-nitride III-V semiconductors, which makes it an attractive material for the preparation of optoelectronic devices. In addition, by changing its composition this alloy can serve as transparent substrate for highly-effective light emitting diodes prepared on GaAs or GaP substrate. However, a decrease in the InP mole fraction in this alloy makes the material change its band gap structure from direct to indirect. It is very difficult to determine the composition at which the crossover from a direct to indirect structure occurs. It is because of its proximity and because of the presence of the long range ordering effect in $In_xGa_{1-x}P$. As follows from a theoretical and experimental study published by Bugajski et al. [1], the situation around the crossover point is slightly complicated by the existence of two crossover points very close to one another. The Γ-L crossover point most likely occurs at x slightly higher than that of the Γ-X crossover point, which makes the L the lowest conduction band valley for x lower as x =0.33. A photoluminescence study of bulk $In_xGa_{1-x}P$ crystals prepared by a modified Bridgman method showed that an alloy with an InP mole fraction x higher than 0.32 exhibited InP-like PL spectra unlike materials with x value lower than 0.26 that showed GaP-like spectra. The position of the direct-indirect crossover was located at x=0.36, E_g = 2.33 eV at a temperature of 2 K [2].

Photoluminescence spectra of InGaP epitaxial layers grown at a low InP mole fraction are dominated by the main transition, which is ascribed to the recombination of an exciton bound to a neutral donor. This transition is somewhat broader (full width at half maximum is about of 15 meV in comparison to 9 meV in GaP) than a similar transition, which can be observed in a GaP epitaxial layer. At lower energies two phonon assisted replicas shifted by 48 meV. There was not a significant difference in these phonon energies from those observed in GaP epitaxial layer.The intensity of PL signal decreased with increase in the InP mole fraction, and a decrease of band gap energy resulted in the vanishing of transitions at highest energies. Small part of photoluminescence signal may have been caused also by the GaP substrate or by the GaP buffer layer. As the InP molar fraction in the InGaP layer increased, absorption increased as well, and consequently, a main part of the PL signal was absorbed in this layer. The last sample showing GaP-like photoluminescence in this series was grown at x=0.254. Further increase in the InP mole fraction to a value of x=0.276 led not only to the drastic increase of photoluminescence intensity but also to a change in the appearance of the PL spectra (see Fig. 4). It consists of one broad peak that is very similar to the photoluminescence of the InGaP layers with a direct band gap structure grown on GaAs substrates. We suppose that this increase of intensity together with the change of type of spectra from GaP-like to InGaP-like (or InP-like) indicates a crossover point from an indirect to a direct band gap structure. This crossover lies close to x = 0.27 and E_g = 2.215 eV.

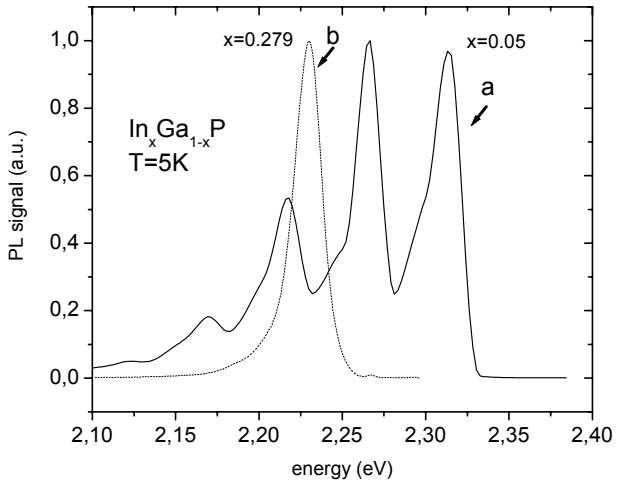

Fig. 1. Photoluminescence spectra of two InGaP layers with a different band gap structure. Sample (a) presents a typical PL signal from indirect band gap with dominant transition at 2.314 eV and its phonon replicas shifted by 48 meV.

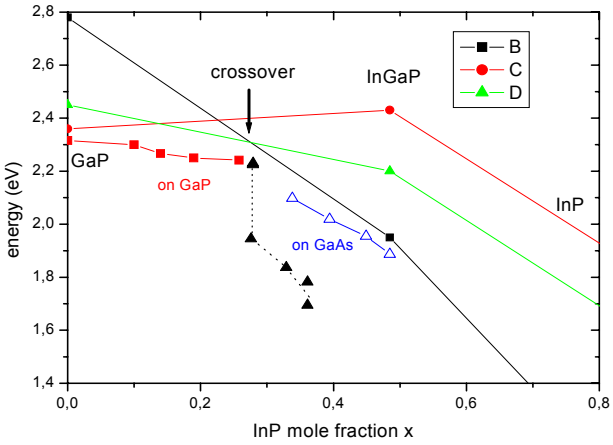

Fig. 2. Dependence of InGaP band gap energy on the InP mole fraction x. Arrow indicates position of direct – indirect crossover.

[1] *Bugajski M., Kontkiewicz A.M., and Mariette H.: Phys. Rev.* ***B28****,(1983) 7105.*

[2] *Onton . and, and Chicotka J.R.,: Phys. Rev.* ***B4*** *(1971) 1847.*

Spinodal-like decomposition of InGaP epitaxial layers grown by MOVPE on GaP substrates

J. Novák, S. Hasenöhrl, I. Vávra, and M. Kučera

Phase separation on the surface of an epitaxial layer during growth is quite different from conventional spinodal decomposition observed in alloys. The free energy of an alloy is lowered by compositional fluctuations in the bulk of its crystal, which is separated into phases at a certain critical temperature. By metalorganic chemical vapour phase epitaxy (MOVPE) it is possible to prepare nearly metastable alloys with composition within the miscibility gap. Spinodal decomposition does not proceed into the bulk of a material because of low diffusion coefficients in III-V semiconductors and relatively high growth rates, but its influence is often observable on the surface of a layer grown. The separation on the surface of an epitaxial layer requires that the surface free energy be lowered by elemental segregation. The term "spinodal-like" decomposition is usually used to distinguish the surface localized spinodal decomposition during epitaxial growth from alloy decomposition occurring during equilibrium crystal growth. Phase separation is not understood as well as ordering, but it similarly needs to be controlled since compositional variations can influence PL emission spectra or other parameters.

The spinodal-like decomposition of InGaP epitaxial layers grown at 740 °C by MOVPE was studied by means of photoluminescence and TEM. A series of samples with increasing molar ratio of indium phosphide x_{In} was prepared in order to study the properties of $In_xGa_{1-x}P$ layers grown on (001) oriented GaP substrates as a function of x_{In}. Compressively strained layers with a thickness of 1.2 μm were deposited directly on GaP substrate. Growth parameters were initially optimized to avoid the tendency to 3D growth (creation of hexagonal hillocks) in GaP and $In_xGa_{1-x}P$ with low x_{In}. Based on a growth optimization process described in [1], we chose for the present experiment the growth temperature (T_g) of 740 °C, growth rate of 0.8 μm/hr, and the reactor pressure of 20 hPa. For the growth of GaP and a low x_{In} content $In_xGa_{1-x}P$ the optimum V/III ratio was 74. For the last sample investigated, the V/III ratio was changed to 348 for the reasons explained below.

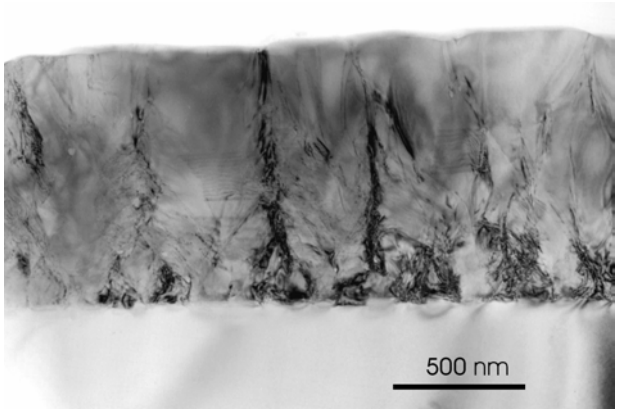

Fig. 1. TEM cross-sectional images of spinodal-like contrast in the InGaP layer. sample MO664 with spinodal-like decomposition(black areas) through whole layer width from interface up to surface.

Both methods revealed that for the epitaxial growth of InGaP up to x = 0.2, the V/III ratio value close to 75 can deliver a sufficient amount of phosphorus to grow uniform layers. Further increase in the InP mole fraction x (at the same value of V/III ratio) led to the growth instability connected with spinodal-like decomposition and compositional fluctuations. Both effects are reflected in TEM views as contrast modulations parallel and vertical to the growth direction. The spinodal domains are parallel with the growth direction and they start from the interface between epitaxial layer and substrate usually. We suppose that high lattice mismatch can cause a surface roughness sufficiently high to start a partial elastic relaxation and to allow spinodal like decomposition at the grown surface. This effect may be suppressed by additional presence of phosphorus atoms at the grown surface. The low temperature photo-luminescence spectra showed that in partialy decomposed samples a characteristic broad peak occurred close to 1.945 eV. An increase in the V/III ratio up to a value of 350 suppressed the decomposition, and PL signal with only one narrow transition was obtained.

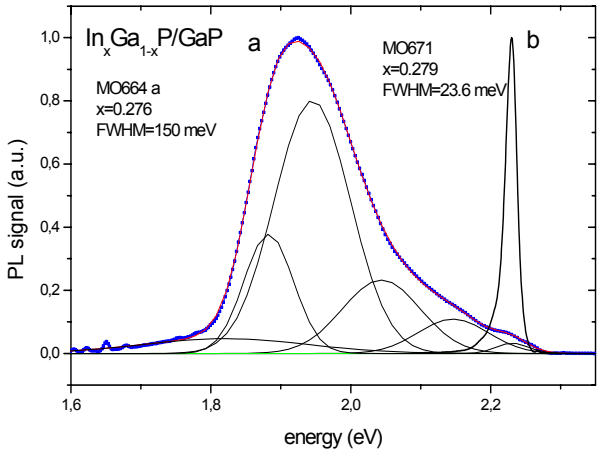

Fig. 2. Photoluminescence spectra of two InGaP layers grown at different V/III ratios (a = 75, b = 350).

[1] *Novák J, Hasenöhrl S. .Kúdela R., Kučera M.: J. of Crystal Growth* ***275*** *(2005) 1287.*

Relaxed graded GaP/$In_xGa_{1-x}P$ buffer layers – growth and characterization

S. Hasenöhrl, J. Novák, M. Kučera, I. Vávra, and R. Kúdela

The encompassment of technology for preparing blue light emitting semiconductor sources in the last years enabled the subsequent developments in solid state lighting. The low efficiency of green sources that are necessary for white and full color applications remains the significant problem. The highest efficiency LEDs are based on $(Al_xGa_{1-x})_{0.5}In_{0.5}P$ material lattice matched to GaAs and joined to the optically transparent GaP substrate by wafer bonding technique. For green emission the content of Al has to be higher than 0.3. Increasing the Al content leads to significant decrease in internal radiative recombination efficiency and causes problems with p-type doping.

Green emission can be obtained from Al free ternary compound $In_xGa_{1-x}P$. At $x_{In} = 0.27$ it exhibits direct band gap structure with energy gap of 2.24 eV with corresponding emission at 554 nm. However, for this composition there is not available substrate with similar lattice parameter. The way how to overcome this limitation is the preparation of virtual substrate based on GaP/$In_xGa_{1-x}P$ system with final composition of $x_{In} \geq 0.27$. This kind of substrate will allow matching of lattice parameters between substrate and top LED structure. Moreover, it will be optically transparent for light emitted from LED.

Concept of epitaxial graded composition buffers is well known from GaAs/InGaAs and Si/SiGe systems but much less often it is used for GaP/InGaP. There are several problems which have to be solved in order to prepare buffer with properties that make it suitable for use as a virtual substrate.

The first problem which we solved was the optimization of growth conditions for GaP and $In_xGa_{1-x}P$ with x_{In} varying from 0 to 0.33. Optimized parameters were: growth rate, reactor pressure, growth temperature and V/III ratio. Layers were characterized by optical microscopy, scanning electron microscopy, atomic force microscopy, transmission electron microscopy and X-ray diffractometry.

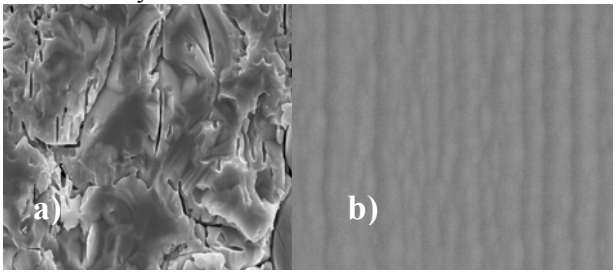

Fig. 1. Top view SEM micrographs of buffer systems. a) belongs to structure MO670 and it shows, that structure grown at non-optimized conditions exhibits the tendency for layer degradation, b) shows the surface of structure MO 689 grown at optimized conditions.

The next problem solved was the design of graded buffer structure. We investigated the following parameters that influenced the buffer crystalline structure: number of InGaP layers in the buffer N_i, thickness of individual layers D, compositional difference between two adjacent $In_xGa_{1-x}P$ layers Δx_{In} and average grading rate of the structure R_{grad}. Composition of individual layers expressed as $In_{Ni\cdot\Delta x}Ga_{(1-Ni\cdot\Delta x)}P$ (where $N_i = 1 \div N$) was changed linearly. Each buffer was finished by 1000 nm thick cap layer of composition $In_{(N+1)\cdot\Delta x}Ga_{(1-(N+1)\cdot\Delta x)}P$. Results from GaP/InGaP growth optimization and basic ideas for buffer structure design are published in [1].

As seen on SEM and TEM micrographs on Figures 1 and 2 $In_xGa_{1-x}P$ with $x_{In} > 0.26$ exhibits tendency to material degradation. At this time we are trying to explain the mechanism responsible for this degradation. Two possible reasons can be supposed. The first one is the degradation due to formation of dislocation pileups which are created as a result of dislocation immobilization on branch defects. In this case the degradation process should depend on the growth temperature and on the grading rate. In our samples these parameters had only small effect on the crystalline quality. The second possible mechanism is the surface-directed spinodal decomposition. Our results indicate that in our samples spinodal-like decomposition is the process responsible for material degradation. This conclusion is supported by our investigation that degradation is strongly affected by the V/III ratio. By increasing the surface coverage with phosphorus atoms it is possible to suppress layer degradation.

[1] *Hasenöhrl, S., Novák, J., Vávra, I., and Šatka, A.: J. Crystal Growth* ***272*** *(2004) 633.*

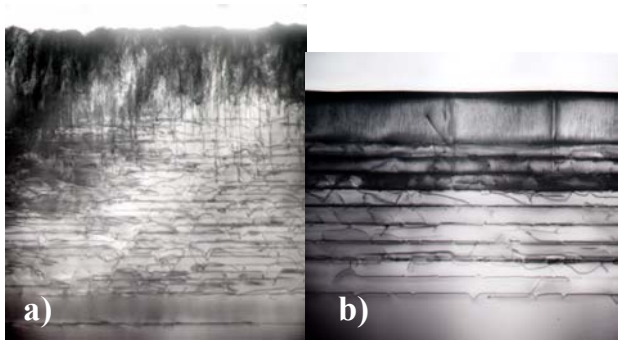

Fig .2. Cross-sectional TEM micrographs of buffer systems. a) of structure MO670 shows vertical features typical for material degraded due to surface-directed spinodal decomposition, b) of structure MO 689 shows good crystalline quality of top layer suitable for use as a virtual substrate for LED structures.

Optical Characterisation of Graded $Ga_{1-x}In_xP$ Buffer Multilayers Grown on GaP Substrates

M. Kučera, S. Hasenöhrl, D. Gregušová, and J. Novák

The growth of a LED structure on a GaP substrate is the alternative to a standard InGaAlP LED's technology. The advantage of such approach should be the absence of the light absorption in the substrate and no need for the wafer bonding process. Main problem of such concept is the strain present in the grown layers. Rather sophisticated and properly tailored buffer structures could carry out the role of a filter minimizing the propagation of dislocations into the active device structure [1].

In the study, we have grown $Ga_{1-x}In_xP$ multilayer buffer structures on GaP substrates by LP MOCVD [2] with x ranging from 0.03 for the first layer to 0.27 - 0.33 for the topmost one. The grading rate was Δx = 0.01-0.03 in one buffer step, the step width was varied from 100 to 300 nm, except of the topmost layer with the width of 1000 nm. Evaluation of the buffer quality was made by the optical microscopy, SEM, TEM, and PL techniques. Growth temperature of 740 °C, pressure of 20 mbar, and V/III ratio equal to 80 were the basic growth parameters [2].

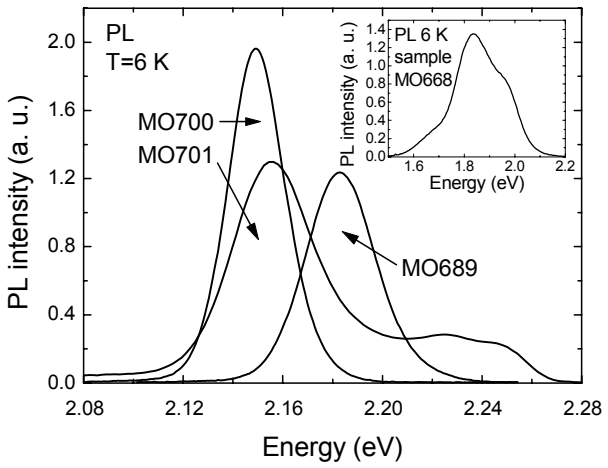

Fig. 1. PL spectra of selected InGaP buffer structures.

In Fig. 1 PL spectra of typical structures are presented. The inset shows PL spectrum of the buffer with the uppermost layer with x = 0.33. We see the spectrum is very broad and also the PL intensity was weak. It indicates a poor crystalline quality, which was confirmed also by the investigation of the sample structure and morphology by SEM, TEM and AFM techniques [2]. In further experiments, the composition of the uppermost layer was changed to x = 0.27 and V/III of the topmost layer was enhanced to 350. It crucially improved luminescence properties of samples MO689 and MO700, with high radiation intensity. PL of sample MO700 exhibited the best halfwidth (27 meV, compared to 33 meV for sample MO689). The sample consists of 27 buffer layers with Δx = 0.1 (MO689: 9 layers with Δx = 0.3) and T_{gr} of $Ga_{1-x}In_xP$ was lowered to 710 °C (better strain relaxation). Indeed, finer grading and temperature tuning improved the crystalline quality of the buffer. Sample MO701 exhibited poorer PL intensity and the spectrum consisted of two separate PL peaks. This structure was grown with $Ga_{1-x}In_xP$ layers alternating with 5 nm wide InP layers. This modification did not improve PL properties.

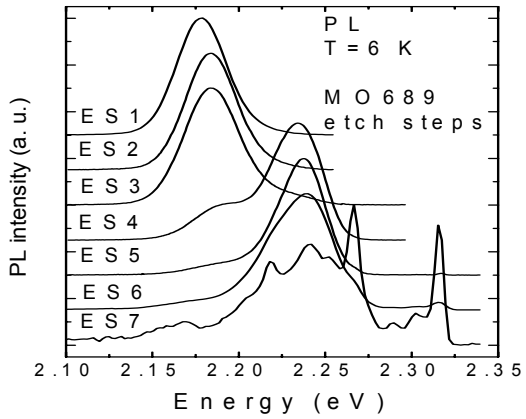

Fig. 2. PL spectra of sample MO 689 after sequential etching-off with a step of 40 to 100 nm. Symbol ESn designates the PL spectrum after nth etch step.

We investigated sample MO689 for in-depth PL properties. Fine gradual etch-off of the surface with etching step 40-100 nm was made. The PL spectra after seven etch steps are shown in Fig. 2. We see the shifts of PL peaks pointing to some composition change across the topmost $Ga_{1-x}In_xP$ layer. When calculating Δx corresponding to the shifts, the change in the composition of about 1% was obtained on the overall etch depth of 800 nm. The spectrum after 7th etch-off shows GaP-like spectral features, indeed the radiation comes from an indirect-gap material. This can be (1) the bottom part of the topmost buffer layer or (2) buffer layer(s) underlying the topmost one. We see that x = 0.27 chosen for the topmost layer is very close to the optimum: it gives the direct band-gap for efficient luminescence and at the same time the mismatch of the layer is minimized.

[1] *Kim, T. P., McCulough, W. S., and Fitzgerald, E. A.: J. Vac. Sci. Technol.* ***B 17*** *(1999) 1485.*

[2] *Hasenöhrl, S., Novák, J., Vávra, I., and Šatka, A.: J. Cryst. Growth* ***272*** *(2004) 633.*

Photoluminescence Characterisation of LP MOCVD-Grown Quaternary $(Al_yGa_{1-y})_{1-x}In_xP$ and Ternary $Ga_{1-x}In_xP$ Layers

M. Kučera, R. Kúdela, and J. Novák

$(Al_yGa_{1-y})_{1-x}In_xP$ with a high content of Al and lattice-matched to GaAs should be grown in order to obtain a wide band-gap material for LED's lighting at 540 nm. It is well-known that Al atoms form deep levels connected with nonradiative centres. Therefore, we have chosen another possible solution: to prepare mismatched layers with rather low Al content ($y \cong 0.1$). To reduce the density of defects to a reasonable value, a buffer structure consisting of $Ga_{1-x}In_xP$ layers with a gradual change of x was grown as the first step. Structures consisted of four interlayers (x ranging from 0.485 to 0.32) and final quaternary or ternary layer. Samples were characterized by X-ray measurement (lattice mismatch), optical microscopy, AFM, and PL spectroscopy. The growth temperature, the composition of the layers, the layer width, and the In/Ga ratio were crucial tuning parameters. The following technological problems were studied: (1) Minimizing the lattice and surface defect density connected with strain relaxation, (2) optimizing the thickness of individual layers, (3) comparing the results on different substrates (better results were obtained on the n-doped ones) (4) optimizing the growth temperature (growth at 770 °C resulted in the best crystalline quality).

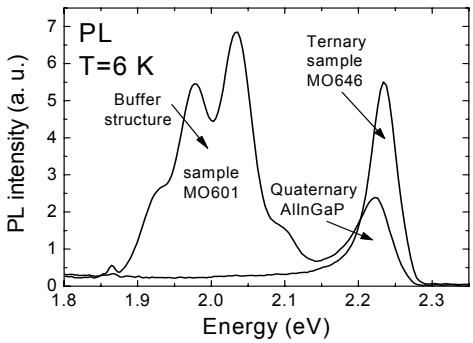

Fig. 1. PL spectra of typical quaternary and ternary layers grown o the graded buffer structure.

In Fig. 1 the example of a typical quaternary and ternary PL spectrum is presented. PL maximum at about 2.25 eV was the highest achievable radiation energy in the frame of the study. If we take the residual strain and some shift of PL maximum relative to material band-gap into account, it corresponds to the gap of about 2.3 eV. In the spectrum of the quaternary, we see four peaks from the graded interlayer structure and a separate quaternary-related peak. PL intensity from the fourth buffer layer and from the quaternary is lowered as a consequence of defects created by the strain relaxation. PL spectrum of the ternary exhibits only the peak corresponding to the uppermost layer. It indicates a good quality of the layer. The maximum energy is about 2.235 eV with half width of 42 meV, and the PL intensity was high. These PL properties were the best in the framework of the study.

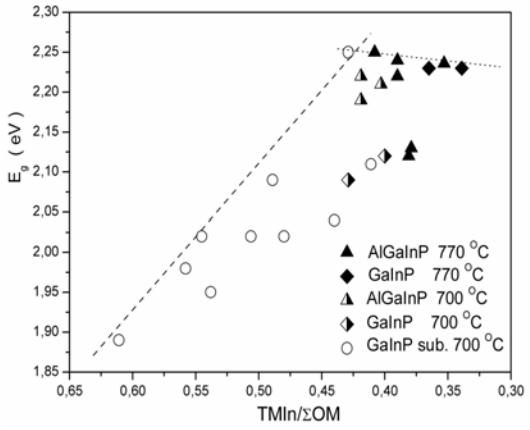

Fig. 2. Energies of PL maxima obtained for the studied set of samples vs. molar fraction of TMIn.

In Fig. 2 the PL maximum energy vs. TMIn/ΣOM during the sample growth is depicted. We see: (1) In general higher gaps were obtained for T_{gr} = 770 °C, (2) the dependence on T_{gr} is not so clear for quaternaries, and (3) maximum achievable PL energy is around 2.25 eV for quaternaries as well as for ternaries.

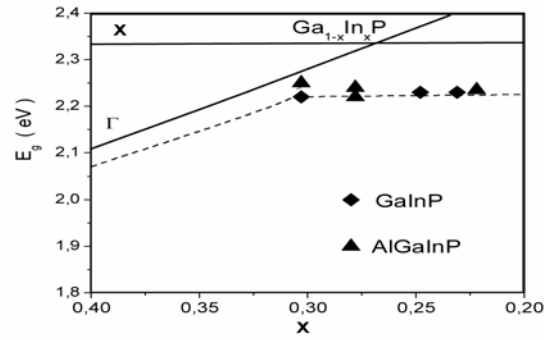

Fig. 3. Comparison of band-gap energies obtained in our study (points) with the theory (full lines) and unstrained monocrystal materials (dashed line) [1].

In Fig. 3 the comparison of the results with published data [1] and theoretical band gaps of $Ga_{1-x}In_xP$ is presented. In the work of Onton [1] monocrystals without strain were prepared. We see that PL maxima both in our study and that in [1] are very close.

This study was done in the frame of EC project VGF-GaP LED's; No: IST-2001-32 793.

[1] *Onton, A. and Chicotka, R. J: J. Phys. Rev.* ***4*** *(1971) 1847.*

MOVPE growth of 2DEG AlGaAs/GaAs structures for tip-induced LAO

R. Kúdela, V. Cambel, J. Šoltýs, J. Fedor, and M. Morvic

The tip-induced local anodic oxidation (LAO) is an effective tool for fabrication of nanometer devices with two-dimensional electron gas (2DEG). It is based on the oxidation of the semiconductor surface by the atomic force microscope (AFM) tip. The principle of the method lies in the formation of additional deep electron levels near the surface and consequent trapping of the electrons from the layer with 2DEG. Typical lateral dimensions of such oxidized area can be lowered down to ~ 40 nm. To use this method effectively, one has to fill two important conditions: first, the layer with the 2DEG must be placed near the surface, typically less than 50 nm. Second, the difference between density of surface states oxidized and un-oxidized surface has to be as high as possible. The last condition is important for creation of high barriers for electrons in the layer with 2DEG.

Optimal layer configuration is given by necessary electron sheet concentrations and band gap differences between GaAs and AlGaAs. Important layer is thin GaAs cap which prevents spontaneous oxidation of AlGaAs surface and creation of electron traps in AlGaAs. On the other hand, GaAs layer has high density of surface states (in the order of 10^{12} cm^{-2}), and its energy gap smaller than that of underlying AlGaAs re-distributes the mobile electrons from the 2DEG-layer in a uncontrollable way.

The aim of this work was to prepare proper MOVPE structures for LAO and to avoid complications with charge redistribution mentioned above. We have prepared 2DEG structures by MOVPE method in horizontal Aixtron AIX 200 reactor in hydrogen atmosphere. Arsine, trimethylgallium, trimethyl-aluminium, and silane were used as basic precursors. Total pressure in reactor was 20 mbar, growth temperature was 700 ^{O}C. Special attention has been payed to optimizing of growth process in order to supress the background concentration, especially in AlGaAs. Structures were grown with various growth rates and V/III ratios.

Table 1.

growth rate GaAs (nm/min)	V/III ratio GaAs	growth rate AlGaAs (nm/min)	V/III ratio AlGaAs
20	191	27.5	*167*
10	575	13.8	*502*
5	1150	6.8	*1005*

They consisted from GaAs buffer, AlGaAs spacer, Si delta-doped plane, AlGaAs top, and GaAs cap. Thickness of AlGaAs spacer varied from 5 to 25 nm as well as thickness of the top layer. Temperature dependencies of Hall concentrations and mobilities were measured down to helium temperature. Results in Fig 1. show correlation between growth conditions and maximum measured Hall mobilities. The best values were measured on samples with sheet concentration ~ 5×10^{11} cm^2.

Strong dependence of the Hall mobility on the sheet concentration was observed. It can be caused by re-distribution of electrons between GaAs/AlGaAs interface, delta-doping plane and the surface. Because the thickness of spacer is 20 nm, we suppose that we measure transport in two paralell layers simultaneously in the samples with sheet concentration ~ 10^{12} cm^{-2}. The first one is 2DEG at the GaAs/AlGaAs interface and the second one carriers in delta-plane. Strong dependence on the thickness of GaAs buffer layer was observed. Standard thickness was 200 nm for samples shown in the Fig. 1. When the thickness was reduced to 100 nm the mobility was reduced to about 50 000 $cm^2V^{-1}s^{-1}$. Because the surface passivation plays a key role in re-distribution of the carriers, several types of cap layers has been examinated and evaluated.

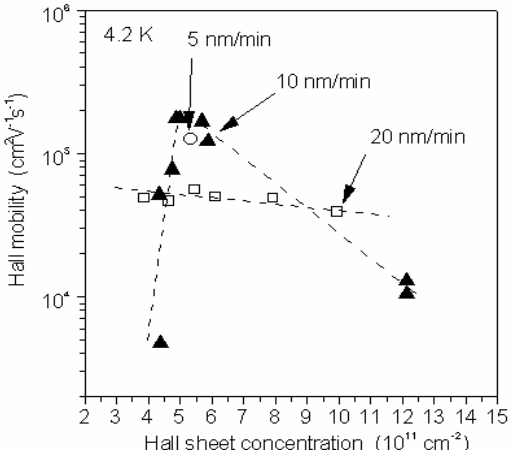

Fig. 1. Dependence of Hall mobilities on sheet concentrations for various growth conditions

Samples were oxidized by means of an AFM Topometrix Explorer using commertial tips. Voltage of 10-15 V was applied at ambient humidity close to 50 %. Effective barrier height of 45 meV was achieved at our samples. Line widths from 150 to 450 nm were prepared in non-contact and contact modes. Our MC simulations showed that the measured current-voltage characteristics are in agreement with the theoretical ones. We can conclude that the standard MOVPE technology is usable for preparation AlGaAs/GaAs 2DEG structures and further processimg with LAO technique.

Two-dimensional electron transport through a barrier prepared by tip-induced oxidation

V. Cambel, J. Šoltýs, M. Moško, and R. Kúdela

We have studied transport of a two-dimensional electron gas in shallow heterostructure prepared by metalorganic chemical vapour deposition. Using atomic force microscopy we have locally oxidized the surface of a two terminal device. The oxidation depletes the area with the two-dimensional electron gas below the oxide line, and divides the device into two regions isolated by an energy barrier. We have found that the logarithm of the transport current between these two regions depends linearly on the root of the applied voltage, which shows that the current is controlled by the Pool-Frenkel effect. The experimental results are supported by computer simulations of current-voltage characteristics using ensemble Monte Carlo method with molecular dynamics included to encounter for the electron-electron and electron-donor interactions.

The local anodic oxidation (LAO) induced by the tip of the atomic force microscope (AFM) is an effective tool for fabrication of nanometer-scaled structures and devices. The advantage of the method is its universality. It can be applied to metals, semiconductors, and semiconductor heterostructures, and allows fabrication of the quantum point contacts, quantum wires, and room temperature single-electron transistors [1].

Consider the GaAs/AlGaAs heterostructure with a two-dimensional electron gas (2DEG) at the GaAs/AlGaAs heterointerface placed close to the sample surface. When LAO is applied to the surface, the GaAs layer is oxidized and the 2DEG below the oxidized area is depleted. The depleted region acts on the 2DEG as an insulating energy barrier and the 2DEG is thus effectively divided into two regions (see Fig. 1). We have studied electron transport between these two regions.

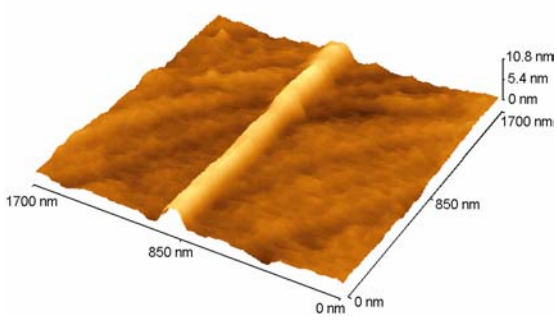

Fig. 1. Typical line prepared by LAO on the top of shallow GaAs/AlGaAs heterostructure.

We have studied experimentally as well as theoretically transport of the 2DEG in structures described above.

We have found from the temperature-dependence of the current-voltage (*I-V*) experimental characteristics, that the height of LAO barrier depends on the writing characteristics (writing voltage or current, AFM mode - contact or non-contact). In all cases, however, the logarithm of the transport current rises nearly linearly with the square root of the applied voltage. This suggests that the *I-V* characteristics are controlled by the Pool-Frenkel effect – by a decrease of the effective barrier resulting from superposition of the applied voltage and remote donor potentials.

We support this physical picture by a microscopic simulation that combines Monte Carlo and molecular dynamics simulations. The Monte Carlo simulation is the exact semi-classical simulation of non-equilibrium single-electron transport. The molecular dynamics simulation is the exact simulation of classical many-body dynamics of the Coulomb carriers interacting with each other and with fixed Coulomb charges. It incorporates in a unified manner such many-body effects like the space charge effect, carrier-carrier scattering, dynamic screening, and multiple-ion scattering. The effect of the individual remote donors on the barrier height is automatically included on the same (classical) level.

The summary of our results at 143 K is shown in Fig. 2. Squares are for experiment and circles for simulation with donors present in the system. Both curves show linear dependence of *ln (I)* versus $U^{1/2}$, and reproducible jumps, which can be explained by Coulomb blockade. When ionized donors are removed from the simulation, the current is lowered, the character of the curve changes to $ln(I) \sim U$, and the jumps disappear, which can be explained by the absence of Poole-Frenkel effect in the system without ionized donors [2].

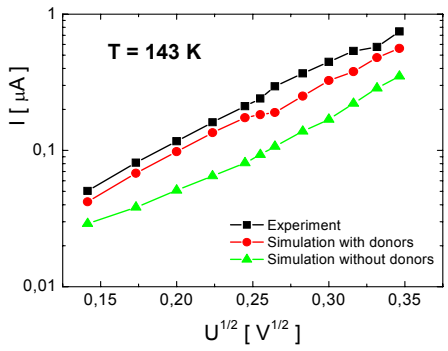

Fig. 2. I-V characteristics of the 2DEG transport.

[1] *Lüscher, S., Fuhrer, A., Held, R., Heinzel, T., Ensslin, K., Bichler, M., and Wegscheider, W.,: Microelectronics Journal* ***33*** *(2002) 319.*

[2] *Cambel, V., Šoltýs, J., Moško, M., and Kúdela, R.: Superlattices and Microstructures* ***36*** *(2004) 359.*

Conductivity and Hall effect on free-standing highly resistive GaN:Fe substrates

P. Kordoš, M. Morvic, J. Betko, and J. Novák

One key issue at the preparation of GaN-based devices is the lack of native substrates. Recently it has been shown that large area free-standing GaN layers with the thickness of 0.3–0.5 mm and their resistivity up to ~ 10^9 Ω cm can be prepared by hydride vapor phase epitaxy [1]. However, little is known about their conduction mechanism. From temperature dependent resistivity measurements an activation energy of 0.51 eV [1] and 0.34 eV [2] has been found, but Hall effect data are not presented yet.

The GaN:Fe samples, obtained from Cree-GaN Inc., were grown by HVPE technique in the thickness of 300 to 450 μm. The layers were separated from the sapphire template before characterization. Samples of about 5 × 5 mm^2 were cut from each wafer and In-contacts were alloyed. Temperature dependent conductivity and low magnetic field (B = 0.8 T) Hall effect measurements were carried out using a high-impedance system. Four typical GaN:Fe samples were selected for this study [3]. Their 300 K resistivity, apparent Hall concentration and Hall mobility are given in Table I. The first two samples show high mobility ($\mu_{H,300} \cong$ 330 $cm^2 V^{-1} s^{-1}$) and the other two have very low mobility (4 and 10 $cm^2 V^{-1} s^{-1}$).

The activation energy E_ρ evaluated from the temperature dependent resistivity data, as commonly used in literature, is found to be 0.605 and 0.58 eV for "high-mobility" samples 1 and 2, but only 0.40 and 0.36 eV for "low-mobility" samples 3 and 4, respectively (Tab. I). In fact, the true thermal activation energy can be evaluated from the proportionality $n_H/T^{3/2} \sim \exp(-E_n/kT)$, supposing the value of a Hall scattering factor close to one. Note that the carriers are electrons deduced from the negative Hall coefficient. The same activation energy as from resistivity data results for samples 1 and 2, $E_n = E_\rho$ = 0.60 and 0.58 eV, respectively. However, for "low-mobility" samples much lower E_n values of 0.195 and 0.14 eV than E_ρ ones are found for samples 3 and 4, respectively (Tab. I). This indicates that simple band conduction behavior might be not applied in general.

The Hall mobility of samples 1 and 2 decreases with increasing temperature but for "low-mobility" samples 3 and 4 a remarkable increase of μ_H with T is obtained (Fig. 1). Temperature dependence of the Hall mobility can be described by simple equation $\mu_H = C_\mu T^x$. For "high-mobility" samples 1 and 2, the mobility scattering power $x = -1.5$ is found. This value is typical for scattering on phonons. However, the mobility power $x > 4$ results for samples 3 and 4. Due to high lattice mismatch between GaN:Fe layer and sapphire substrate a polycrystalline growth might occur. In that case both the concentration of carriers and their mobility are thermally activated, i.e. $n = n_0 \exp(-E_{nb}/kT)$ and $\mu = \mu_0 \exp(-\Phi_b/kT)$, where E_{nb} is the activation energy of the carrier concentration and Φ_b is the barrier height at the grain boundaries. Our experimen-tal mobility data on samples 3 and 4 can be fitted according these equations, as shown in Fig. 1 - dashed lines. Resulting activation energy is $E_{nb} \cong$ 0.21 eV for both samples and the barrier height is Φ_b = 0.18 and 0.14 eV for samples 3 and 4, respectively. The values obtained can be good compared with activation energies of 0.29 – 0.41 eV and barrier heights of 0.09 – 0.11 eV reported before for various MBE grown high resistive GaN layers with grain boundary controlled conduction [3]. The activation energy of traps at the boundaries $E_t = E_{nb} + \Phi_b$ actually equals to the activation energy E_ρ = 0.36 and 0.40 eV evaluated from the resistivity data. Thus, energies of 0.51 and 0.34 eV reported before for Fe-doped GaN [1,2] might be also referred to the activation energy of defect related traps with different concentration.

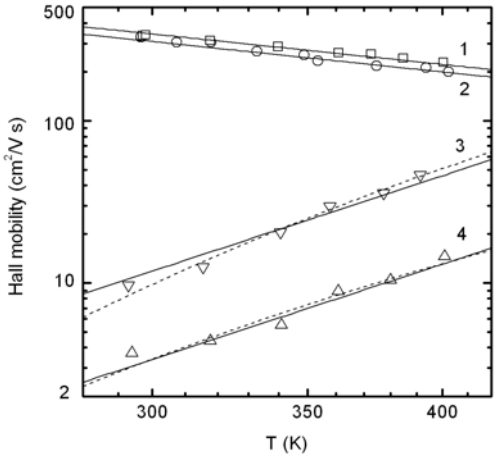

Fig. 1. Temperature dependence of Hall mobility (log-log scale) for GaN:Fe layers. The solid and dashed lines are theoretical fits assuming $\mu \sim T^x$ and $\mu \sim \exp(-\Phi_b/kT)$, respectively.

Tab. I. The layer thickness, resistivity, Hall concentration,Hall mobility, and activation energies E_ρ, E_n for GaN:Fe samples.

#	d (μm)	ρ_{300} (Ω cm)	$n_{H,300}$ (cm^{-3})	$\mu_{H,300}$ ($cm^2 V^{-1} s^{-1}$)	E_ρ (eV)	E_n (eV)
1	447	5.7×10^8	3.2×10^7	337	0.605	0.60
2	340	1.6×10^7	1.2×10^9	329	0.58	0.58
3	347	2.3×10^5	7.4×10^{12}	4	0.40	0.195
4	309	5.5×10^4	1.2×10^{13}	10	0.36	0.14

[1] *Vaudo, R. P., Xu, X., Salant, Malcarne, A., J., and Brandes, G. R. : phys. stat. sol. (a)* ***200*** *(2003) 18.*

[2] *Heitz, R., Maxim, P., Eckey, L., Thurian, P., Hoffmann, Broser, A., I., Pressel, K., and Meyer, B. K.: Phys. Rev.* ***B55*** *(1997) 4382.*

[3] *Kordoš, P., Morvic, M., Betko, J., Novák, J., Flynn, J., and Brandes, G. R:, Appl. Phys. Lett.* ***85*** *(2004) 5616.*

Influence of passivation induced stress on the performance of AlGaN/GaN HEMTs

D. Gregušová, P. Kordoš, and J. Novák

The AlGaN/GaN high electron mobility transistor has become a key electronic device for high-power application in microwave frequencies. However, there are still some problems that concern the production of GaN-based HEMTs, namely DC/RF dispersion, current slump or even collapse [1]. In this study the effect of stress in passivation layer on the properties of AlGaN/GaN heterostructure and HEMTs is investigated.

The HEMTs used in this study were based on an AlGaN/GaN heterostructure, which was grown on sapphire substrate using LP MOVPE. The heterostructure was intentionally undoped (i.e. polarization doped). It consisted of a 20 nm $Al_xGa_{1-x}N$ layer (x = 0.20) and a 10 nm GaN cap layer grown on top of a GaN buffer. AlN was used as the nucleation layer.

The HEMTs were processed using conventional fabrication steps [2]. Two-finger devices with gate lengths of 0.3 – 0.7 μm and a gate width of 100 or 200 μm were prepared. Van der Pauw patterns (0.3 × 0.3 mm^2 active area) were processed simultaneously for the Hall effect measurements at room temperature. PECVD was used to deposit SiO_2 or Si_3N_4 on the processed wafers at a frequency of 13.6 MHz and power of 30 W or 15 W, respectively. The passivation layers studied were of four types differing by deposition temperature (T_{dep}) and thickness (d): A SiO_2 layer with T_{dep} = 300° C and d = 172 nm (type A) and Si_3N_4 layers with 300° C and 133 nm (B), 300°C and 27 nm (C), and 150° C and 164 nm (D), respectively. The thickness of the layers was measured by ellipsometry. Stress induced in the structures by the passivation layers was evaluated by an optical autocollimation method. The unpassivated layer structure can be characterized by a sheet carrier density of 5.6 × 10^{12} cm^{-2} and a carrier mobility of 1390 cm^2/Vs (average values). The Hall effect as well as DC and RF properties of HEMTs were measured before and after passivation.

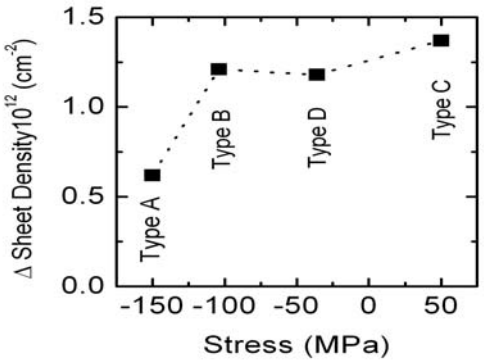

Fig. 1. Passivation induced sheet carrier density in dependence on the stress of passivation layer.

It has been found that used passivation layers and deposition conditions suffer following values of an additional stress: – 150 MPa (A), – 104 MPa (B), – 36 MPa (D), and 50 MPa (C). Hall effect measurements on van der Pauw patterns have shown an increase of the sheet carrier density and slight decrease of the carrier mobility in all passivated samples. The passivation induced sheet density increased from 0.62 × 10^{12} cm^{-2} to 1.37 ×10^{12} cm^{-2} with increased stress from compressive (– 150 MPa) to tensile (50 MPa), as it is shown in Fig.1. The lowering in the passivation effectiveness of SiO_2 compared with that of Si_3N_4 can be explained not only by more compressive stress but also by higher density of SiO_2/GaN interface states [3].

DC characterization of prepared HEMTs has shown partial improvement in the drain currents and extrinsic transconductances after applying all four types of passivation. From our results it can be shown that the Si_3N_4 passivation is more effective. It corresponds to the influence of passivation inducing of sheet carrier density. The dependences of $\Delta I_{DS}/I_{DS}$ and the density of current source-drain on the stress of passivation layer are displayed in Fig.2. The more detailed analysis of HEMTs properties after passivation is given in [4].

This work was done in cooperation with the Institute of Thin Films and Interfaces, Research Centre Jülich, Germany and International Laser Center, Bratislava.

[1] *Binary, C., Kruppa, W., Dietrich, H. B., Kelner, G., Wickenden, A. E.,and Freitas, J. A.: Solid State Electron.* ***41*** *(1997) 1549.*

[2] *Bernát, J., Javorka, P., Fox, A., Marso, M., Lüth, H., and Kordoš, P.: Solid State Electron.* ***47*** *(2003) 2097.*

[3] *Hashizume, T., Ootomo, S., Oyama, S. ,Konishi, M., and Hasegawa, H.: J.Vac. Sci. Ttechnol.* ***B19*** *(2001) 1675.*

[4] *Gregušová, D., Bernát, J., Držík, M., Marso, M., Novák, J.,Uherek, and F., Kordoš, P.: published on line in phys. status solidi (c),* ***2****, February, 01.2005.*

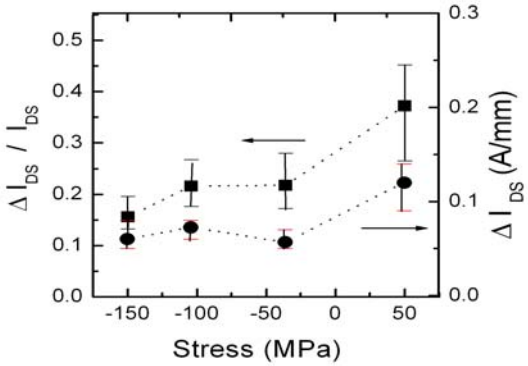

Fig. 2. The dependence of $\Delta I_{DS}/I_{DS}$ and ΔI_{DS} on the stress.

Smooth GaN recess by wet photoelectrochemical etching

D. Gregušová, J. Novák, P. Kordoš

The GaN-based material system has gained much attention for its electrical properties. The development of effective low-damage etching for GaN device fabrication remains an outstanding problem, especially in recessing technology [1]. Photo-enhanced wet etching techniques are promising for the low-damage processing of GaN-based devices [2]. If the semiconductor surface is illuminated during etching with short-wavelength radiation, it generates electron-hole pairs that enhance surface oxidation processes In this work we present a photo-enhanced chemical etching technique that yielded smooth GaN surfaces Samples *A(460)* with a free carrier concentration of 9.5 x 10^{16} cm^{-3} and *B(648)* with a concentration of 1 x 10^{18} cm^{-3}. used in this experiment were grown by metalorganic chemical vapour deposition on (0001) sapphire substrates. Non-alloyed 40 nm-thick Ti metal contact topology, patterned by a standard lift-off process, provided electrical contact to the samples and was also used as the etching mask pattern. To etch the samples, we used 0.02, 0.2, and 2 M KOH etching solutions at room temperature. Etching was carried out in an electrochemical cell. A standard 320 – 480 nm EXFO lite lamp system (50 Watt miniature arc lamp) with filters at 365 nm was used to illuminate the samples, approximately 5 x 5 mm^2 whose size was. Figure 1 shows a plot of the photocurrent flowing between the sample and the Pt electrode during etching at the maximum possible illumination intensity (the lamp iris was fully opened).

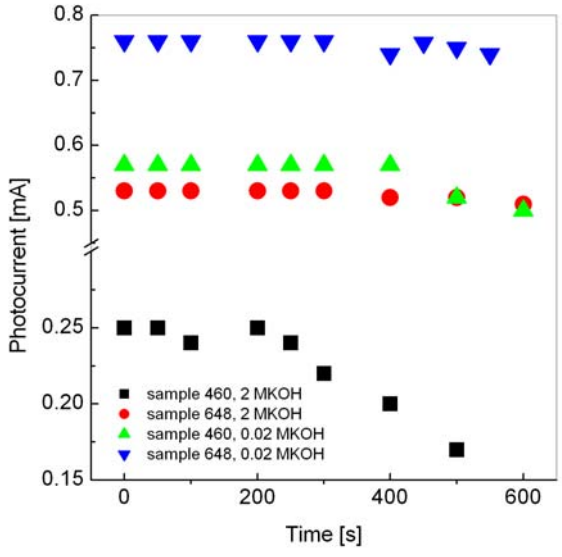

Fig. 1. Variation of the photocurrent versus etching time with KOH concentration in etching solution and doping concentration as the parameters.

It is shown that the photocurrent became saturated at a certain value of etching time (depending on the etching solution concentration and on the sample doping concentration). In this region the etching depth depended linearly on etching time. The saturation suggests that at high illumination intensity the etching process is limited by the rate at which the reactants in the solution diffuse to and react with the semiconductor surface The etching at lower intensities than the maximum intensity proceeded slower, yielding surface with rms as high as 50 nm. The etching rate at the maximum illumination intensity was higher yielding rms roughness values as low as 5 nm (see Fig. 2) for shallow etching (tens of nanometre). If the etching was performed under illumination without the filter, the etching rate was lower however the surface roughness worsened, which leads to an assumption that the etching was more efficient at 365 nm. The etching rate is also markedly dependent on the layer doping. A quality recess technology should be capable of shallow etching yielding smooth surfaces under well depth control. The work shows that such requirements can be met by the photeelectrochemical etching of GaN in 0.2 or 0.02 M KOH solutions at etching rates of 70 - 90 nm/min under maximum illumination intensity using a 365 nm filter.

This work was done in cooperation with the Institute of Thin Films and Interfaces, Research Centre Jülich, Germany.

[1] *Youtsey, C., Adesida, I., Romano, L. T., and Bulman, G:, Appl. Phys. Let.* ***72*** *(1998) 560.*
[2] *Minsky, M. S., White, M., and Hu, E. L:. Appl. Phys. Let .* ***68*** *(1996) 1531.*

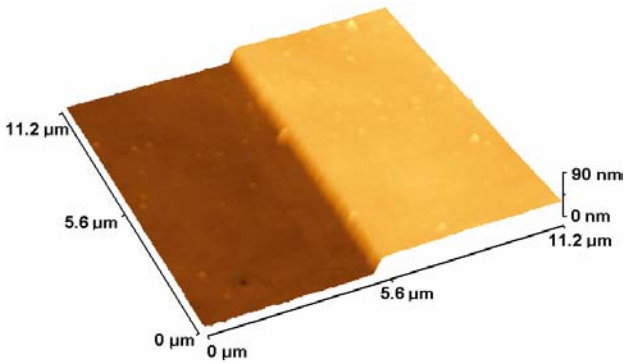

Fig. 2. AFM picture of a GaN (648) layer etched in a 0.2 MKOH solution at an etching rate of 92 nm/min. The etching to a depth of 40 nm produced an rms value of 5 nm.

Conformal AZ5214-E resist deposition on patterned (100) III-V substrates

P. Eliáš and D. Gregušová

Electronic devices traditionally manufactured in planar substrates, such as (100) or (110), have topographies that do not extend very much in the vertical dimension. However, using the vertical dimension for the design of electronic devices brings new benefits and design possibilities. To name just a few: The so-called vertical transistor is expected to increase device density per unit area. Epitaxial heterostructures grown on patterned substrates impart one-dimensional or zero-dimensional quantum confinement to electronic devices. Sensors formed on three-dimensional micromachined substrates exhibit extended functionality.

In the development of such "three-dimensional" devices the technologist needs to tackle the problem of conformal deposition of resist films on non-planar substrates. Planar substrates are traditionally coated with resist films on spinners spun between 2000 and 10000 revolutions per minute, which reliably provides films of uniform thickness, although the thickness is a complex function of spinner speed, resist viscosity, polymer molecular weight, solvent evaporation rate, temperature, etc. However, if resist is spun on a patterned substrate with vertical topography, it is very difficult or even impossible to achieve films of uniform thickness. It is because three-dimensional features obstruct the flow of resist during spinning – and the higher the features and the denser over the substrate the worse. The resist film may be very thin or even non-existent on tops and around convex edges of the three-dimensional objects. Conversely, it is usually considerably thicker close to the bottom areas and concave edges of the objects. These effects are caused by phenomena related to liquids, such as surface tension and non-uniform rapid drying.

To deposit resist films on non-planar substrates, various methods have been in use: (a) Programmable speed spin coating; (b) Spraying; (c) Meniscus coating; (d) Roller coating; (e) Plasma deposition; and (f) Electrodeposition.

We have been developing an alternative method based on resist deposition from water surface [1]. It basically involves the deposition of a small volume of resist by letting go a drop of resist off a syringe needle onto distilled water surface. The process parameters that need strict control include: the water temperature, the volume deposited down to a 0.1 μl precision, and the size of water surface area to which the drop is spread.

Upon the impact on water surface, the drop is "blown out" radially over the surface as the result of a difference in surface tension between the two liquids. As the drop is spread a thin considerably flexible floating film is formed via a rapid solidification process. The film is then draped over the three-dimensional features of patterned substrates by lowering the level of water in the tank.

The method, although simple and inexpensive, provides strikingly good results. They are exemplified in Figure 1. It shows SEM images of a profile, projected on a $(0\,\bar{1}\,1)$-related cleavage, of a 61 μm-high mesa ridge formed by wet etching in (100) semi-insulating InP substrate. The mesa is confined at sides by facets related to (211)A crystallographic planes inclined at 35.26° to (100).

The mesa object was conformally coated with a 1.6 μm-thick AZ5214-E resist layer using the present method. It is critical to cover convex and concave edges of three-dimensional objects conformally. In the figure the edges are indicated by the black and white fork-tailed arrows. Close-ups of the convex and concave edges (top right and bottom right, respectively) show that both edges are indeed conformally wrapped in the resist layer.

The present method is capable of forming conformal resist layers even on more severe topologies than the one shown in the figure. For example, similar quality layers can be formed over high-aspect-ratio mesa objects confined by steeper even vertical side facets.

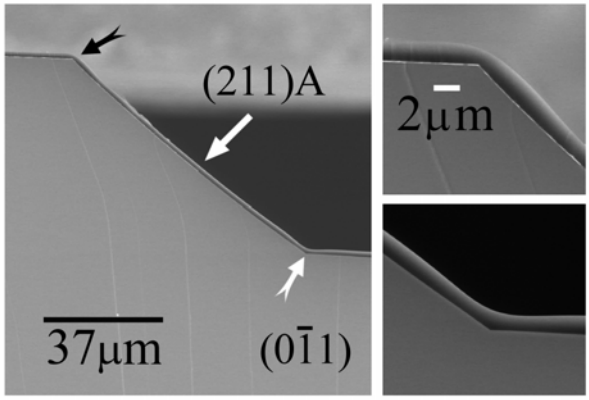

Fig. 1. Conformal layer of AZ 5214-E resist deposited by draping from water surface on a 61 μm-high mesa ridge formed by wet etching in (100) semi-insulating InP substrate. The SEM images show a profile of the mesa projected on a (011)-related cleavage. The mesa is confined at sides by facets related to (211)A crystallographic planes inclined at 35.26° to (100). The close-ups confirm uniform deposition in the most severe areas around the convex and concave edges (fork-tailed arrows).

[1] *Zhou, H., Chong, B. K., Stopford, P., Mills, G., Midha, A., Donaldson, L., and Weaver, J. M. R.: J. Vac. Sci. Technol.* ***B18*** *(2000) 3594.*

Large-scale high resolution scanning Hall probe microscope used for MgB_2 characterization

V. Cambel, J. Fedor, D. Gregušová, P. Kováč, and I. Hušek

Scanning Hall probe microscope (SHPM) is an important imaging tool used for detailed studies of superconductors in basic science as well as in industrial sector. It can be used for the studies of losses, current distribution, and effects at grain boundaries.

Only few SHPM for magnetic field imaging at temperatures below 77 K has been proposed up to now, most of them designed for small area (~ 10 x 10 μm^2) scanning. We have developed a large-scale low temperature SHPM for imaging the entire magnetic field in close proximity to magnetic and superconducting samples at 4.2 – 300 K. The microscope combines a large scanned area and high spatial and magnetic field resolution. The instrument is designed as an insert of standard helium flowing cryostats, contrary to the previous one [1]. The Hall sensor scans an area up to 7 x 25 mm^2 with a spatial resolution better than 5 μm.

Presented system was used for study of *ex-situ* prepared MgB_2 filaments. We have shown that external magnetic field induces local supercurrents in the MgB_2, from which global phenomena like critical current can be estimated. Moreover, it indicates also local microstructure and space homogeneity of the superconductor.

Single-core MgB_2 composite wire using commercial powder from Alfa Aesar has been made by *ex-situ* process using FeNiCo tube, heat treating, and rolling [2]. Then, FeNiCo sheath was carefully mechanically removed from the short wire pieces to avoid magnetic shielding of MgB_2 core during Hall probe scanning. The dimension of the MgB_2 core was 0.9 x 0.9 mm^2.

We have explored the local magnetic field close to the transverse section of such MgB_2 core. We have applied magnetic field parallel to the sample and scanned area 1.2 mm x 1.2 mm. The distance of the Hall probe from the sample surface was 20 μm $\pm$ 5 μm.

First, the sample was cooled to 25, 29, or 33 K in zero field, and then we have applied an external magnetic field of -350 mT, and scanned the sample. The local magnetic field in each point is composed of the external field applied to the sample, and the field from supercurrents that are induced in the sample by the external magnetic field. At 25 K the supercurrent J_C flows in a large part of the sample volume and fully compensates for the external field in the central part of the sample. Applying Bean model for hard superconductors, we have estimated the mean value of the critical current in the sample (~ 80 000 A/cm^2), which agrees with transport measurements. Similarly, we have evaluated the critical current at 29 K (~ 55 000 A/cm^2) and at 33 K (~ 10 000 A/cm^2).

We have extracted also local properties of the MgB_2 wire in the external magnetic field. In detailed scans local supercurrents fluctuate - they are more pronounced above large MgB_2 grains and one can distinguish several spots on the images. We assume that the grains represent localities of high-quality superconductor. They are visible due to the presence of additional local currents (vortexes) circulating within the grains [3].

[1] *Fedor, J., Cambel, V., Gregušová, D., Hanzelka, P., Dérer, J., and Volko, J.: Rev. Sci Instruments* ***74*** *(2003) 510.*
[2] *Kováč, P., Hušek, I., Melišek, T., Grovenor, C. R. M., and Haigh, S.: Supercond. Sci. Technol.* ***17****, 1225 (2004).*
[3] *Cambel, V.,. Fedor, J., Gregušová, D., Kováč, P. and Hušek, I.: Supecond. Sci. Technol.* ***18*** *(2005) 417.*

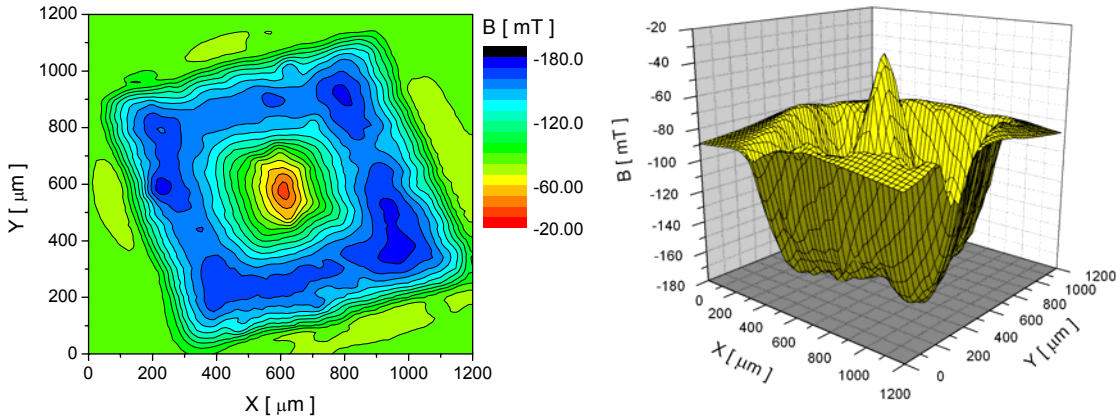

Fig. 1. Magnetic field distribution over the MgB_2 sample after zero field cooling, applying -350 mT and increasing the field to -100 mT at 29 K. Figure (a) is a contour plot, (b) is a surface plot of the field distribution.

QWIP structures prepared on patterned (001) GaAs substrate

P. Štrichovanec , R. Kúdela, I. Vávra, J. Šoltýs. M. Kučera, and J. Novák

The overgrowth of patterned surfaces of (001) GaAs substrates prepared by optical lithography and wet-chemical etching is very interesting as it can be used to improve the performance of some optoelectronic devices [1-3]. The aim of our work is to investigate the possibility to make quantum well (QW) heterostructures with good quality interfaces on various crystallographic planes of non-planar objects. This contribution presents the epitaxial overgrowth of patterned (100) GaAs semi-insulating substrates. [0-11]-oriented 20 μm-high mesa ridges with (111A) quasi-facets were prepared by wet-chemical etching in a H_3PO_4:H_2O_2:H_2O solution through a 100 nm-thick Ti mask layer.

The multiquantum well heterostructures (MQW) were based on GaAs/AlGaAs material system. Low pressure MOVPE (Metalorganic Chemical Vapour Deposition) was used for the overgrowth of the mesa ridges. The source materials were trimethylgallium (TMGa), trimethylindium (TMIn), trimethylaluminum (TMAl) and arsine (AsH3). The growth temperature was optimized to 700 °C.

The MQW heterostructures contain 6 nm-thick GaAs well layers (center Si doped $N_D = 1x10^{18}$ cm^{-3}) and 30 nm-thick $Al_{0,3}Ga_{0,7}As$ barrier layers (undoped). The number of periods was varied from 10 to 20. The MQW heterostructure was clad in the 300 nm-thick bottom

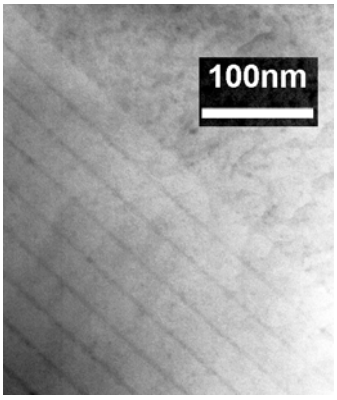

Fig. 1. TEM pictures of the AlGaAs/GaAs MQW structure on the mesa sidewall.

GaAs (Si doped N_D = 1 x 10^{18} cm^{-3}) and 500 nm-thick upper GaAs (Si doped N_D = 1 x 10^{18} cm^{-3}) layers.

In our contribution we concentrated on the development of patterning techniques using wet chemical etching to obtain different types of non-planar surface with optimal surface morphology. This was achieved by lowering the etching temperature and by a variation of the H_2O_2 content in the solution. The role of technological parameters, such as the growth temperature, molar ratios of organometalic and hydride sources in the reactor, was studied. The selectivity in the growth rate versus facet orientation was determined. The layer morphology and the occurrence of the facets at the top and bottom edges of the ridges were analyzed using SEM, TEM and AFM. The optical properties of various MQW heterostructures were analyzed by low temperature PL and FTIR measurements.

The optical properties and morphology of interfaces of the MQW heterostructure depend mainly on sidewall

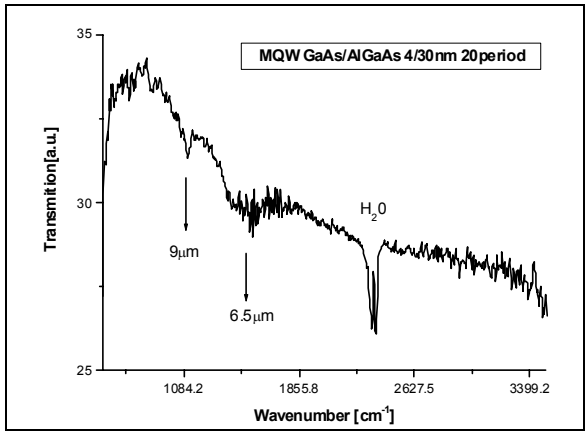

Fig. 2. FTIR spectrum of the MO711 MQW heterostructure.

surface roughness and stoichiometry. Wet chemical etching can produce mesa ridges with sidewall facets, related to the (111A) crystallographic plane. This is the slowest-etching crystallographic plane for most etching solution [1]. The stoichiometry of this surface determines the growth process, for which we employed the kinetically limited regime. However, also in this regime, due to the diffusion of reactants along the ridges, the Al content in AlGaAs layer can vary from bottom to top of the sidewall [2]. TEM cross-section analysis was used to define the (111)/(100) growth rate ratio: It was 1.5 for GaAs and 1.8 for AlGaAs. The lattice misfit in the GaAs/AlGaAs heterostructure was not observed. Low temperature PL measurements from sidewall structures determined the optical transition E_{E0} - E_{HH0} at an energy of 1.65eV with a full width half maximum of about 60 meV, which showed lower interface quality. FTIR measurements of the transmition spectrum confirmed an intersubband transition in the conduction band QW at a 9 μm wavelength.

[1] *Tsukamoto, S., Nagamune, Y., Nishioka, M., and Arakawa, Y.: J. Appl Phys.* ***71*** *(1992) 533.*

[2] *Bhat, R., Kapon, Simhony, E., S., Colas, E., Hwang, D. M., Stoffel, N. G., and Koza, M. A.: J. Crystal Growth* ***107*** *(1991) 716.*

[3] *Štrichovanec, P., Novák, J., Vávra, I., Kúdela, R., Kučera, M., and Šoltýs, J.: phys. stat. sol. (c), in press.*

Department of Thin Oxide Films

Karol Frőhlich

Research scientists
Daniel Machajdík
Alica Rosová
Milan Rosina

Technical staff
Alena Seifertová
Miroslav Pokorný

Research Engineers
Kristína Hušeková

PhD Students
Roman Lupták
Karol Čičo
Milan Ťapajna
Pavol Písečný

Students
Marek Franta
Michal Režňák
Michal Fajta

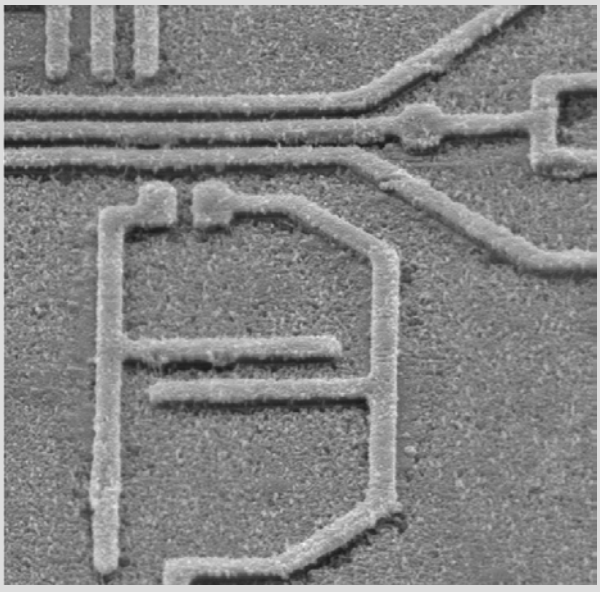

The main research activities of the Department of Thin Oxide Films are growth and characterization of thin oxide films and heterostructures. Liquid source delivery (liquid injection) and standard "thermal evaporation" metal-organic chemical vapour deposition (MOCVD) techniques are employed for the preparation of the films. Various type of oxide films were already prepared by this technique in the Department. Recent activities of the Department are focused on preparation of conducting and insulating films for integration of high permittivity (high-κ) dielectric oxide films with silicon CMOS technology.

During the period 2003-2004 the Department was involved in the following international research projects:

- Research and technology project "Integration of very high-κ dielectrics with silicon CMOS technology", INVEST, (IST-2001-39094), project of the 5th Framework Programme, since July 1, 2002,
- COST Action 528 "Chemical Solution Deposition of Thin Films", project "Growth of barriers, electrodes and functional oxide layers for integration in microelectronics".

Our effort during last two years was focused on the preparation and characterization of conducting thin films for application as gate electrodes for advanced complementary metal-oxide-semiconductor (CMOS) technology. We have shown that conducting Ru and $SrRuO_3$ thin films are promising candidates for gate electrodes for sub-90 nm pMOS field effect transistors.

Recently we have started also preparation of thin alternative dielectric films for advanced CMOS technology. We succeeded in preparation of La_2O_3 films, with dielectric constant ~ 17.

Growth of oxide layers is carried out in MOCVD reactors constructed in our Department. Actually there are three horizontal MOCVD reactors operated in the Department. The reactors use TriJet^{TM} liquid precursor delivery technology of AIXTRON AG.

Structural characterization of prepared films was carried out by means of X-ray diffraction and transmission electron microscopy. X-ray reflectivity measurements (Institute of Physics, SAS) was used for thickness determination of the films with the thickness below 50 nm. Atomic force microscopy (Department of Optoelectronics) was employed for the surface investigation of thin films.

Electrical characterisation of MOS structures was performed using an HP 4248A precision LCR meter and KEITHLEY 6517A Electrometer/high resistance meter.

In the recent years the Department had intensive contacts with the AIXTRON Company AG. The collaboration is focused on development of MOCVD process of thin film for microelectronic applications.

Department of thin oxide films has in the frame of international projects contacts with institutes, laboratories and companies from nearly all European countries. Let us mention long term and intensive collaboration on preparation of thin oxide films by MOCVD technique with the Laboratoire des Materiaux et du Genie Physique, INPG, Grenoble, France. Interface quality and composition of thin films were investigated by Rutherford backscattering analysis in the frame of cooperation with the LNP, Joint Institute for Nuclear Research, Russia. Composition analysis of the films prepared within the Department were carried out also by X-ray photon induced spectroscopy in the frame of collaboration with the Instituto de Ciencia de Materiales de Sevilla, Spain. Participation in the INVEST project within the 5th Framework Programme gave rise to cooperation with the Philips Research Leuven, IMEC, Leuven, Belgium, MDM Laboratory, Agrata Brianza, Italy, and with the IBM Research Laboratories, Zurich, Switzerland.

Karol Frőhlich

Growth of Ru, RuO_2, $SrRuO_3$ and $LaSrCoO_3$ conducting films by MOCVD

K. Hušeková, K. Frőhlich, and D. Machajdík

Ru-based compounds (Ru, RuO_2, $SrRuO_3$) and lanthanum strontium cobaltate ($LaSrCoO_3$) are promising materials for MOSFET gate electrodes due to their low resistivity. Metal-organic chemical vapour deposition (MOCVD) was chosen for the growth of conductive films because it is widely used in microelectronic industry, avoids surface damage by energetic particle bombardment and it provides uniform coverage over complicated device topography.

In this contribution we present our recent results of preparation and properties of thin Ru, RuO_2, $SrRuO_3$ and $LaSrCoO_3$ conductive oxide films grown by liquid precursor delivery MOCVD. The films were prepared by the AIXTRON TriJet^{TM} technology in a low-pressure hot-wall quartz reactor at the pressure 133 Pa.

$Ru(thd)_2$ (cod) dissolved in octane and isooctane was used as a precursor for growth of Ru and RuO_2 films, respectively [1]. Ru films prepared at 300 - 350 °C on Si/SiO_2 substrate had polycrystalline structure and exhibited room temperature resistivity $\rho_{300} \cong 20$ μΩcm. RuO_2 films were grown at 250 - 300 °C with a room temperature resistivity of 150 μΩcm.

$SrRuO_3$ films were deposited at temperatures between 400 and 800 °C using $Ru(thd)_2$ (cod) and $Sr(thd)_2$triglyme precursors dissolved in isooctane. Polycrystalline orthorhombic $SrRuO_3$ phase was identified by grazing incidence X-ray diffraction in the range of deposition temperatures between 500 and 800 °C. Transmission electron microscopy revealed that below 500 °C the films were composed of amorphous matrix containing $SrRuO_3$, Ru and RuO_2 grains.

Resistivity of $SrRuO_3$ films was found to be strongly depended on the molar ratio Sr/Ru in the solution [2]. At low deposition temperature (T_D = 500 °C), the films prepared at Sr/Ru = 1 exhibited low room temperature resistivity, while the films grown at Sr/Ru = 2 showed enhanced resistivity. At temperatures above 600 °C the films prepared at Sr/Ru = 2 exhibited low resistivity. The lowest resistivity was obtained for the films grown at 600 °C. The results show that the $SrRuO_3$ films with resistivity lower than 1 mΩcm can be prepared in a wide temperature range between 500 and 700 °C (Fig. 1).

Epitaxial $SrRuO_3$ were prepared at temperatures above 700 °C on single crystal $SrTiO_3$ and $LaAlO_3$ substrates. Analysis of preferred orientation by X-ray diffraction revealed epitaxial growth of $SrRuO_3$ film on both substrates.

Thin films of $LaSrCoO_3$ were prepared by MOCVD using $La(thd)_3$, $Sr(thd)_2$triglyme and $Co(thd)_3$ precursors dissolved in isooctane. The layers were grown at low pressure (133 Pa) and temperature range from 600 to 800 °C. The properties of $LaSrCoO_3$ were depending on the molar ratio of La/Sr and (La+Sr)/Co in the solution. Using appropriate molar ratio of precursors, we succeeded in the preparation of epitaxial $LaSrCoO_3$ films with resistivity of 1 mΩcm at temperatures above 750 °C.

In conclusion, we have shown that liquid precursor delivery MOCVD technology is suitable for the growth of conductive oxide layers. Using this technology, we have prepared thin films of Ru, RuO_2, $SrRuO_3$ and $LaSrCoO_3$ with required electrical properties.

This work was partially supported by the AIXTRON A. G. and by the VEGA agency (project 2/2068/24).

[1] *Frőhlich, K., Hušeková, K., Machajdík, D., Šoltýs, J., Patoprstý,V., Baumann, P., Lindner, J., and Schumacher, M.: Proceedings of the CVD XVI, 203rd Meeting of the Electrochemical Society, Paris, France, April 27, 2003.*

[2] *Frőhlich, K., Hušeková, K., Rosina, M., Rosová, A., Machajdík, D., Baumann, P.K.., Lindner, J., and Schumacher, M.: 10th European Meeting of Ferroelectricity, Cambridge, 2003.*

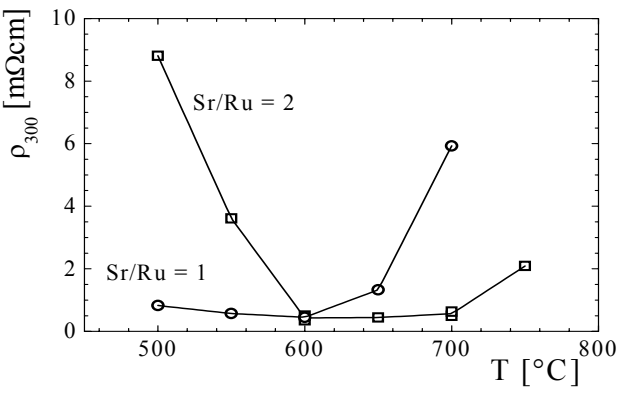

Fig. 1. Room temperature resistivity of $SrRuO_3$ films as a function of deposition temperature.

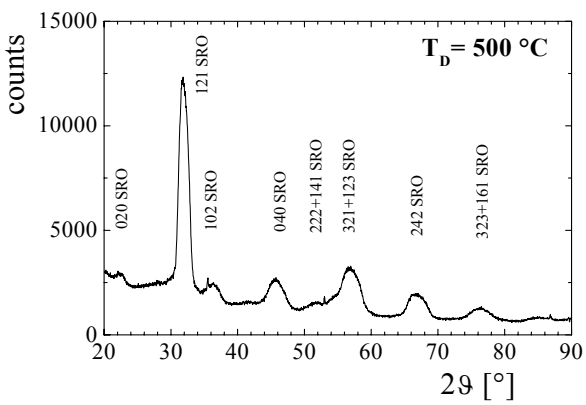

Fig. 2. Grazing incidence X-ray diffraction pattern of $SrRuO_3$ film grown at 500 °C on SiO_2/Si substrate.

Transmission electron microscopy of conducting thin films

A. Rosová, A. Seifertová, and M. Franta

To prepare good conducting thin layers suitable for new advanced CMOS technology using high-κ dielectrics one should know also their microstructural quality. Here we present a review of microstructure of Ru, RuO_2, $SrRuO_3$ and $La_{0.5}Sr_{0.5}CoO_3$ (LSCO) thin films [1, 2].

Ruthenium grows on SiO_2/Si substrate at 350 ºC as single-phase polycrystalline film with a grain size between 10 and 50 nm. TEM contrast reveals a presence of mechanical strain in the film probably due to different coefficient of thermal expansion (Fig. 1).

Grain size and morphology of RuO_2 depend strongly on deposition temperature. While the grain size of RuO_2 layer deposited at 500 ºC was about several hundred nm and grains were equiaxial, the deposition temperature decreasing to 250 ºC caused decreasing of grain size to several tens of nm and columnar character of the layer.

On the Figure 2 there is a TEM image of $SrRuO_3$ deposited at 500 ºC with the molar ratio in the injected solution Sr/Ru = 1 (see Husekova et al. in this Biennial report). The film consists of $SrRuO_3$ elongated grains with grain size of about tens of nm. Strips visible in grains on Figure 3 show abundant presence of planar defects, probably stacking faults, which are characteristic for slightly increased molar ratio Sr/Ru in the film [3]. Relatively slight decreasing of deposition temperature to 450 ºC caused appearance of secondary phases – RuO_2 and Ru in the $SrRuO_3$ film.

Polycrystalline LSCO films growth on SiO_2/Si substrates with clear columnar character of grains (Fig. 3). Lateral grain size of LSCO grains varies from 20 to 50 nm. On their grain boundaries there are located by one order smaller grains of secondary phase. The secondary phase is probably Co_3O_4, but we cannot completely eliminate a possible presence of Co_2SiO_4, which has very similar structure and lattice parameters to Co_3O_4.

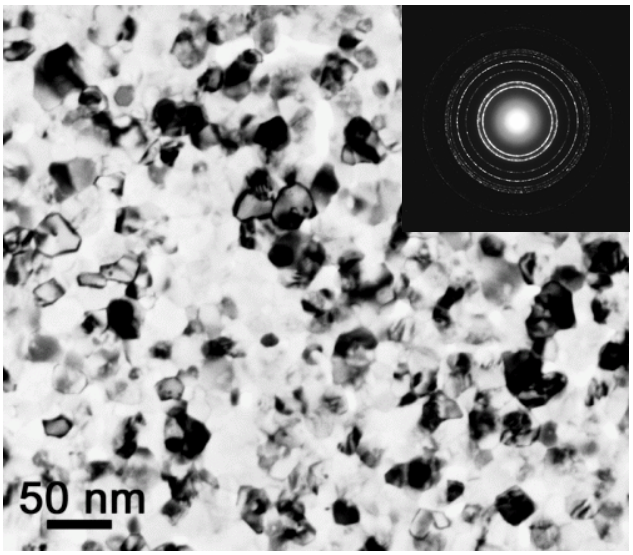

Fig. 1. Plane-view TEM image of Ru thin layer.

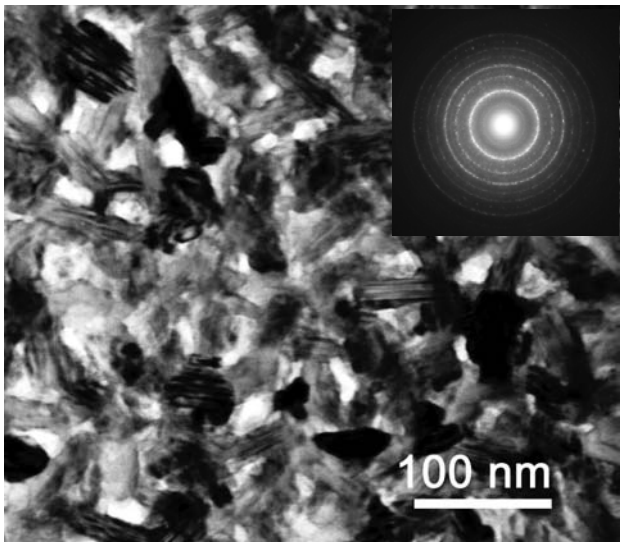

Fig. 2. Plane-view TEM image of $SrRuO_3$ layer.

[1] *Fröhlich, K., Husekova, K., Machajdik, D., Hooker, J.C., Perez, N., Fanciulli, M., Ferrari, S., Wiemer, C., Dimoulas, A., Vellianitis, G., and Roozeboom, F.: Mat. Sci. Eng.* ***B109*** *(2004) 117.*

[2] *Fröhlich, K., Husekova, K., Machajdik, D., Luptak, R., Tapajna, M., Hooker, J.C., Roozeboom, F., Kobzev, A.P., Wiemer, C., Ferrari, Fanciulli, M., Rossel, C., and Cabral Jr, C.: Mat. Sci. Sem. Proc. 7 (2004) 265.*

[3] *Xin, Y., Cao, G., and Crow, J.E.: J. Cryst. Growth* ***252*** *(2003) 372.*

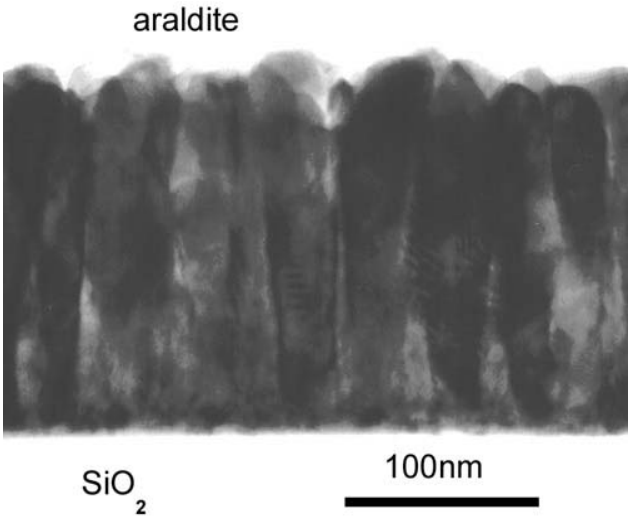

Fig. 3. Cross-section TEM of LSCO film.

Complementarity of X-ray diffraction and RBS in thin film characterization

D. Machajdík and K. Fröhlich

The properties of thin films are directly determined by structure, microstructure and composition. Diverse and in some cases very sophisticated analytical methods have been developed to characterize these properties. In this work complementarity of X-ray diffraction and RBS/channeling in structure study of textured thin films is discussed [1].

The texture of the two samples of the $SrTiO_3$ films deposited on MgO singlecrystal substrate was examined by Bragg-Brentano scan, ω and ϕ scans and pole figures. Bragg-Brentano diffraction patterns with strong reflections of the 00l family confirmed the presence of a $SrTiO_3$ phase with the preferred orientation of the grains in both samples. FWHM values of the ω scans measured on 002 $SrTiO_3$ reflection were 0.8° and 1.1°, respectively for both films. In spite of a small difference between the values, they indicate high degree of preferred orientation of the crystallites. In-plane epitaxy was confirmed by measurement of the ϕ scans on reflection 111 for the films and also on the MgO substrate. Based on all X-ray diffraction texture tests, we concluded that a high quality epitaxy of [100]$SrTiO_3$ || [100]MgO , [010]$SrTiO_3$ || [010]MgO type was present in both samples.

However, the investigation of the same films by RBS/channeling led to a significant modification of this concept. RBS spectra analysis by computer simulation [2,3] ascertained variations in elements concentrations within a range of ±4 % compared with the ideal stoichiometry. The presence of diffusion was found at the interface of the second sample. The diffusion of Ti atoms was slightly more intensive compared with those of Sr atoms.

A significant difference we found out by channeling. Angular scans across the [001] crystallographic channel showed very clearly the difference between both samples. While minimum of the angular scan in the first sample reaches 22% , the channeling effect did not occur at all in the second sample. An analysis of all the data for both samples led to the conclusion that the film in second sample was composed of parts that were textured, amorphous, and also polycrystalline with the crystallites oriented at random. Also backward analysis of the diffraction spectra revealed symptoms which indicate presence of such parts of the film. These symptoms were omitted at first due to the very weak intensity of respective signal in comparison with very strong dominant reflections created by the textured part of the film. This fact clarifies the unexpected contradiction by taking into account that while X-ray diffraction is highly sensitive to the textured part of the film, it is much less sensitive to amorphous and polycrystalline parts of the film if they are present. The difference in sensitivity can reach two and in some cases three orders of magnitude. However, the channeling of ions does not exhibit such selectivity. It works like an integral method sensitive to all parts of the film with varied degree of crystallinity. Therefore, the presence of amorphous and polycrystalline parts in a film with randomly orientated crystallites will effectively destroy the channeling of ions. Fig.1 schematically illustrates the difference in sensitivity of both methods when applied for the characterization of epitaxial thin films.

Experimental part of this work has been performed in cooperation with A. P. Kobzev from LNP SUJV Dubna, Russia and F. Weiss from LMGP INPG, Grenoble, France.

[1] *Machajdik, D., Fröhlich, K., and Kobzev, A.P. accepted to Vacuum.*
[2] *Shirokov, D.M. and Boháč, V.: Nucl. Instr. Meth.* ***B84*** *(1993) 497.*
[3] *Mayer M.: Technical report IPP 9/113 Max-Planck-Institut für Plasmaphysik, Garching, Germany, 1997.*

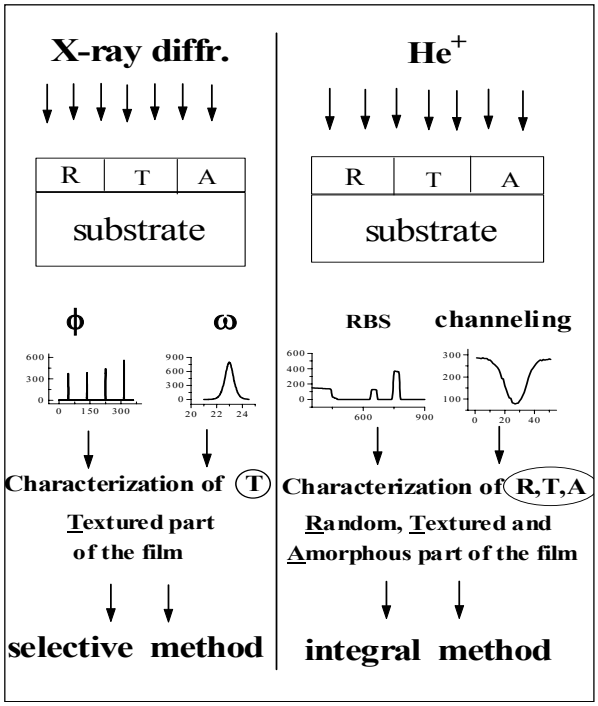

Fig. 1. Comparison of properties of X-ray diffraction and ion channeling method, applied for texture analysis in thin film; R -random part; T -textured part; A -amorphous part of the film.

Growth of lanthanum oxide films for application as a gate dielectric in CMOS technology

P. Písečný, K. Hušeková, K. Fröhlich, and D. Machajdík

We have investigated properties of insulating lanthanum oxide (La_2O_3) films in connection with the replacement of silicon oxide (SiO_2) gate dielectrics in new generation of CMOS devices. La_2O_3 could be considered as a candidate for CMOS gate application, since it has high dielectric constant close to 30 and enough large band gap equal to 4.3 eV [1].

La_2O_3 layers were grown on (100) n-type silicon using metal organic chemical vapour deposition (MOCVD) at 500 °C. A powder precursor, $La(thd)_3$ triglyme was used as a source of lanthanum. Samples for electrical measurements were prepared by evaporating of Al dots and backside contact at room temperature to form $Al/La_2O_3/Si$ metal-oxide-semiconductor (MOS) structure.

X-ray diffraction measurement showed that La_2O_3 films were polycrystalline with slightly distorted cubic structure. Thickness of deposited films was determined from X-ray reflectivity. Composition of the as-grown films was analyzed by X-ray photoelectron spectroscopy (XPS). Fig. 1 shows depth profile of photoemission O(1s) spectra. Composition of the film calculated from the area of the La(4d), O(1s) and C(1s) peaks gives 33 at % of La, 63 at % of O and 4 at % of C. Assuming formula $La_2(CO_3)_3$, we estimate that about 9 at % of lanthanum is bounded to the carbonate. Depth profiling show constant composition during the whole film thickness. After exposure to the air (50 h) we can observe, that the surface transforms completely to lanthanum carbonate (Fig. 1, curve b). Subsequent UHV annealing results in complete transformation lanthanum carbonates to lanthanum oxide at the surface. Spectra at the interface with silicon revealed presence of lanthanum silicate (La_ySiO_x), (Fig. 1, curve d). At the same time, carbon content decreases to about 27 % of its mean value in the film.

For electrical characterization we used MOS structures with various La_2O_3 film thickness. Dielectric constant and thickness of interface layer (t_{it}) of the as deposited samples with thickness from 5.8 to 14 nm were determined from *C-V* measurements. Dielectric constant (κ) of the film is ~ 11.2 and equivalent oxide thickness (EOT) of the La_xSiO_y interface layer is ~ 2.6 nm. The 70 nm thick as grown film has large flat band voltage V_{FB} ~ - 1.45 V and dielectric constant κ was about 10.5. We observed large hysteresis of *C-V* curve (ΔV_{FB} ~ 0.95 V for as grown film) in depletion region after double bias sweep, i.e. sweep voltage from accumulation to inversion and back to accumulation (Fig. 2). The flat band voltage decreased after O_2 annealing to about -0.96 V, ΔV_{FB} shrinks to ~ 0.3 V and dielectric constant increased to ~ 17. Possible mechanisms accounting for the increase of κ are discussed in Ref. [2].

In conclusion, we have prepared La_2O_3 dielectric films using MOCVD method. The La_2O_3 film has dielectric constant ~ 17 after oxygen annealing. XPS analysis confirmed presence of lanthanum silicate at the interface with silicon.

The authors would like to thank to L. Harmatha, M. Jergel, J.P. Espinos and J. Jakabovič for collaboration. This work was partially supported by the Slovak Republic governmental project (2003 SO 51/03R 06 00) and by the VEGA agency (project 2/2068/24).

[1] *Wilk, G.D., Wallace, R. M. and Anthony, J. M.: J. Appl. Phys.,* ***89*** *(2001) 5243.*

[2] *Písečný, P., Hušeková, K., Fröhlich, K., Harmatha, L., Šoltýs, J., Machajdík, D., Espinos, J.P., Jergel M., and Jakabovič, J. : Mater. Sci Semicond. Process.* ***7*** *(2004) 231.*

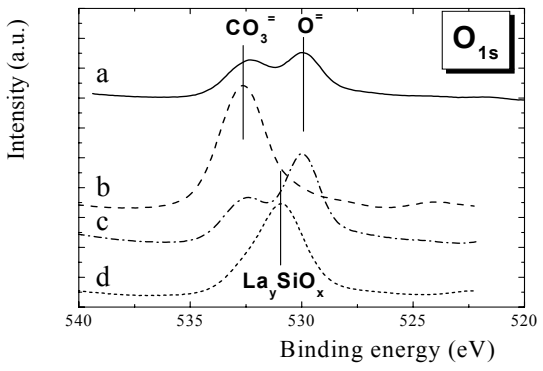

Fig. 1. XPS spectra of La_2O_3 a) at the surface (as-grown), b) at the surface after air exposure (50h), c) in the film volume d) at the interface with silicon.

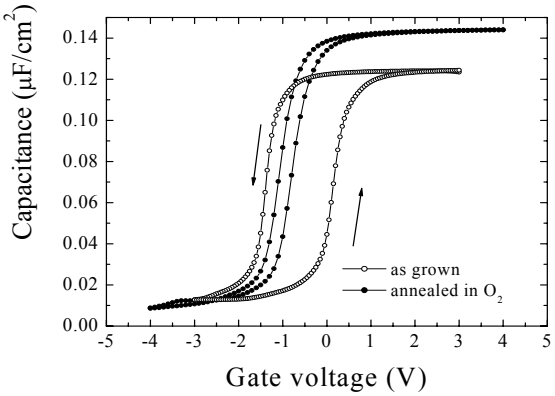

Fig. 2. High frequency (1MHz) C-V measurement for as- grown and oxygen-annealed 70 nm thin La_2O_3 film.

Stability of Ru metal gates for advanced CMOS technology

M. Ťapajna, K. Hušeková, R. Lupták, K. Frőhlich, and K. Čičo

As the thickness of SiO_2 film used in complementary metal-oxide-semiconductor (CMOS) technology reaches sub-100 nm dimensions, significant leakage current (above 1 A/cm^2) appears due to direct tunneling and reliability become major issue. Therefore, thicker dielectric films with higher dielectric constant, κ, should replace conventional SiO_2. This 'electrical thickness' is called equivalent oxide thickness, EOT. Up to date, HfO_2 and $HfSiO_x$ are widely accepted as the potential dielectrics for SiO_2 replacement.

Another scaling issue arises from polycrystalline Si (poly-Si) used as the gate electrode, since it reveals depletion effect. In addition, boron penetration markedly reduces channel mobility of pMOS transistor. Utilisation of metal gate in new CMOS technology can suppress these effects. Furthermore, usage of dual metal gates with work function, Φ_m, of 5.2 and 4.1 eV for pMOS and nMOS transistors, respectively, facilitates tuning of transistors' threshold voltage. The aim of this work is to investigate stability and electrical properties of Ru gate electrode grown on various dielectrics. In addition, thermal stability of $Ru/HfO_2/Si$ stack is examined.

The Ru films were grown using liquid precursor technology in a low-pressure hot-wall quartz MOCVD reactor at 350 °C. As substrates we have used p-doped Si with thermal SiO_2 and Al_2O_3 prepared by atomic-layer CVD (ALD), HfO_2 films were grown using ALD on the n-doped Si. The last structure was subjected to a forming gas annealing (FGA, 90% N_2 + 10% H_2) in temperature range 430 – 590 °C.

The Ru work function was extracted from the sets of capacitance vs. gate voltage (*C-V*) curves measured on MOS structures with different dielectric film thicknesses. From the curves, flat-band voltage, V_{FB}, can be determined. The V_{FB} is the measure of oxide quality (V_{FB}=0 for an ideal structure) and V_{FB} shift includes fixed oxide charge, N_{ox}, which depends on EOT and work function difference, Φ_{ms}, which is independent on EOT. Hence, knowing work function of Si, one can determines Φ_m from the intercept of linear fit to V_{FB} vs. EOT data, Fig. 1(a). Using this procedure we have obtained the Ru work function of 5.1, 5.0 and 5.3 eV for SiO_2, Al_2O_3 and HfO_2 dielectrics, respectively. According to requirement mentioned above, Ru is suitable material for pMOS technology [1].

We have examined properties of the gate $Ru/HfO_2/Si$ stack submitted to various FGA annealings. The *C-V* and *G-V* (*G* is the conductance) curves recorded after particular FGA are depicted in Fig. 1(b). Quality of the Si-oxide interface is frequently assessed by density of interface states, D_{it}, evaluated from the peak maximum of the *G-V* curve. As can be seen from inset of Fig. 1(b), D_{it} generally decreases with FGA temperature increasing. However, the *C-V* curves are shifted across the voltage axis toward the negative values after FGA at temperatures above 550 °C, probably due to Φ_m decreasing. Moreover, we have observed abrupt leakage current increasing upon FGA performed above this temperature. Nevertheless, this trade-off leads to an optimal FGA temperature at 510 °C for the Ru/HfO_2 gate stacks [2].

This work was supported by the EC project IST-2000-28495 INVEST.

[1] *Ťapajna, M., Písečný, P., Lupták, R., Hušeková, K., Frőhlich, K., Harmatha, L., Hooker, J.C., Roozeboom, F., and Jergel, M.: Mat. Sci. Semicond. Process. 7 (2004) 271.*

[2] *Ťapajna, M., Čičo, K., Lupták, R., Hušeková, K., Frőhlich, K., Harmatha, L., Hooker, J.C., and Roozeboom, F.: Proceedings ASDAM 2004 Conference, Smolenice, Slovakia, 2004, 167.*

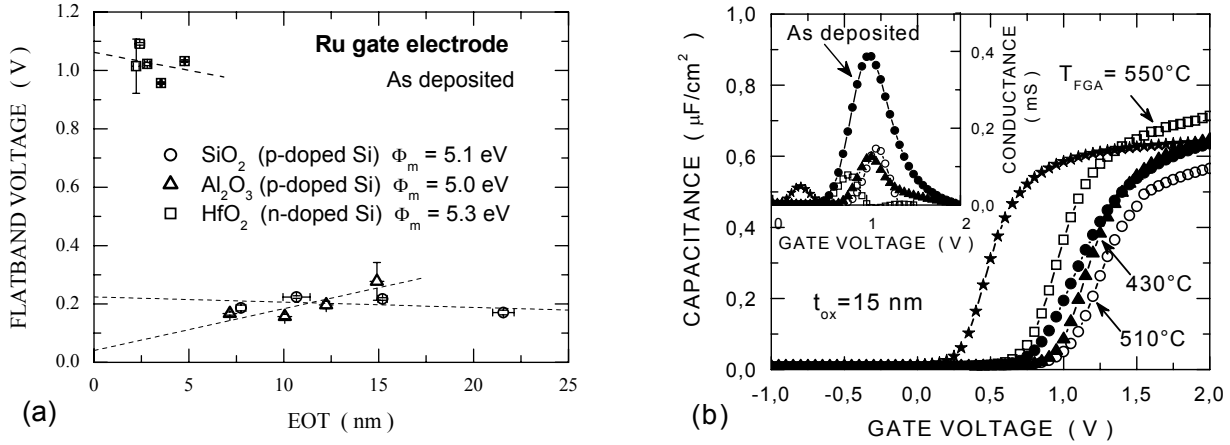

Fig. 1 (a) Extraction of work function of Ru grown on various dielectrics, (b) C-V and G-V (inset) curves measured on the $Ru/HfO_2/Si$ gate stack after FGA at different temperatures.

$SrRuO_3$ – promising material for advanced CMOS metal gates

K. Frőhlich, K. Hušeková, D. Machajdík, M. Ťapajna, and R. Lupták

Scaling down of complementary metal-oxide-semiconductor (CMOS) devices leads to introduction of dielectric constant (high-κ) films and metal gate electrodes. $SrRuO_3$, one of the Ru-based conductive oxides, was selected as a potential candidate for the gate electrode [1] because it exhibits low resistivity and good chemical stability.

Thin $SrRuO_3$ films were prepared by MOCVD using AIXTRON TriJet^{TM} liquid precursor delivery technology. $Sr(thd)_2$ triglyme and $Ru(thd)_2(cod)$ dissolved in iso-octane were used as starting materials. The films were grown at the deposition temperature 500 °C. As substrates we have used p- and n-doped silicon, covered by different dielectric layers: thermal SiO_2, Al_2O_3 and HfO_2. The Al_2O_3 and HfO_2 films were grown by ASM International using atomic layer chemical vapour deposition. The nominal thickness of the SiO_2 and Al_2O_3 dielectric films varied between 6 nm and 25 nm and between 2 and 15 nm for HfO_2. The films received forming gas annealing (430 °C / 30 min) prior gate electrode deposition. Electrodes for the capacitance-voltage (*C-V*) measurement were patterned by standard optical lithography followed by wet or Ar on beam etching.

Rutherford backscattering (RBS) technique was employed to analyse interface diffusion on as-deposited and rapid thermal annealed $SrRuO_3$/dielectric films. After rapid thermal annealing at 800 °C in nitrogen atmosphere RBS analysis indicated partial diffusion at the $SrRuO_3/SiO_2$, enhanced diffusion at the $SrRuO_3/Al_2O_3$ and no diffusion at the $SrRuO_3/HfO_2$ interfaces.

$SrRuO_3$ films exhibited fairly good stability in forming gas; they are stable up to 500 °C. Adding small amount of oxygen into the forming gas can increase their stability. We have observed, that after bubbling the forming gas through a $H_2O + H_2O_2$ mixture, the resistivity of polycrystalline $SrRuO_3$ films increased by only ~ 30 %.

Fig. 1 shows *C-V* characteristics of the $SrRuO_3/HfO_2/Si$ MOS structures measured at 1 MHz for the HfO_2 films thickness ranged from 2 to 15 nm. Even MOS structures with very thin HfO_2 films (2 nm) exhibited standard *C-V* behaviour.

The work function of the gate electrode can be extrapolated from the flat band voltage shift of the capacitance voltage characteristics for a set of MOS structures with various dielectric film thickness, assuming that the fixed oxide charge is located near the dielectric-Si interface. Extrapolation of the flat band voltage shift versus equivalent oxide thickness (EOT) for the set of the $SrRuO_3/HfO_2/Si$ structures yields work function value of 5.0 eV. This value is well adapted for pMOS application.

Fig. 2 shows the leakage current density for the MOS structures with $SrRuO_3$ gate electrode and various dielectrics as a function of dielectric film thickness, expressed through the equivalent oxide thickness, EOT. Leakage current density for the low EOT structures with HfO_2 films is already below the value typical for standard MOS structures with SiO_2 dielectric.

The results of the study show, that $SrRuO_3$ is promising gate electrode material for pMOS applications.

This work was supported in part by the EC (project IST-2000-28495-INVEST) and by the VEGA agency (project 2/2068/24).

[1] *Frőhlich, K., Hušeková,K., Machajdík, D., Lupták,R., Ťapajna, M., Hooker,J. C., Roozeboom, F., Kobzev, A. P., Wiemer, C., Ferrari, S., Fanciulli, M., Rossel, C., and Cabral, C.,: Mat. Science in Semicon. Processing 7 (2004) 265.*

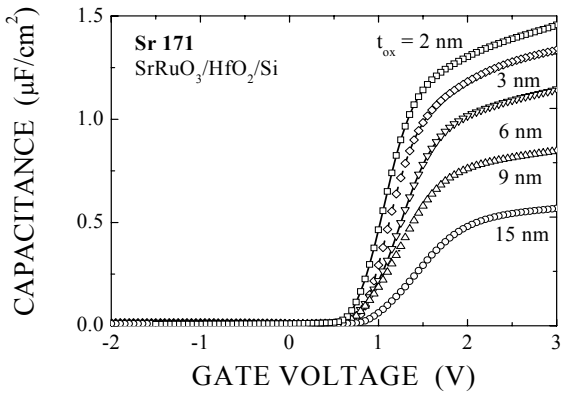

Fig. 1. Capacitance-voltage curves for $SrRuO_3/HfO_2/Si$ capacitors with various HfO_2 film thickness.

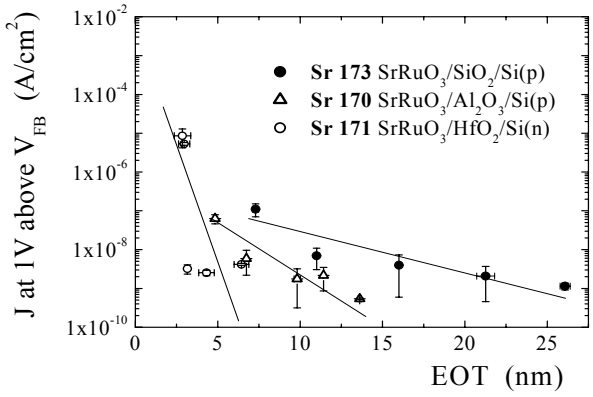

Fig. 2. Leakage currents for $SrRuO_3$ gate electrode and various dielectric gate stacks.

Department of Superlattices

Ivo Vávra

Research scientists
Peter Lobotka

Research Engineers
Eva Kováčová
Vasilij Šmatko

Technical staff
Ján Dérer

PhD Students
Peter Majchrák
Katarína Sedláčková

Students
Jozef Mihálov
Michal Minárik
Peter Prno

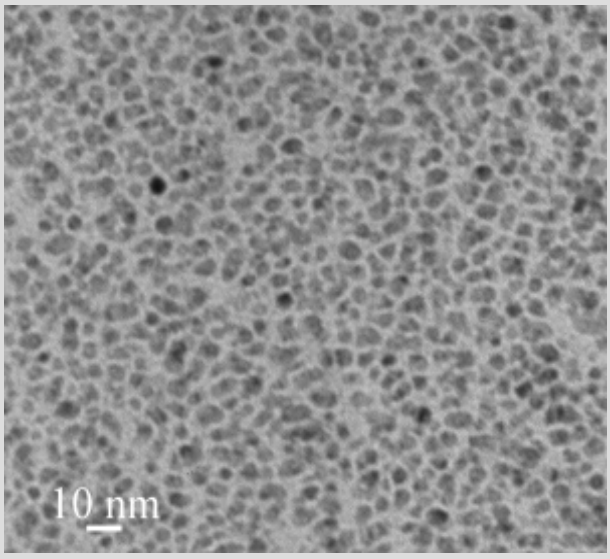

The main research activity of the Department in the years 2003 - 2004 was focused on the complex study of nanocomposite thin films. We developed our own preparation technology of nanocomposite thin films by modification of previously developed magnetron sputtering system for preparation of metallic superlattices. The form of our nanocomposite films is a periodic multilayer with non-continuous metallic and continuous insulating sublayers. The metallic sublayers are composed of crystalline nucleation islands (in-plane dimension of few nanometers) separated by an amorphous insulating sublayers. The advantages of our method are crystalline perfection of metallic particles and possibility to easily control a distance between particles in normal direction to the film plane. The quality of our nanocomposite layers was confirmed by electrical characterization, e.g. by Coulomb blockade observed at low temperature.

The Department was involved in the project entitled "Nanocrystalline thin films" supported by Slovak Grant Agency VEGA. The goal of this project is to develop a technology of nanocomposite films and their structural and electrical characterization. We were also active in COST 523 Action "Nanostructured materials". The Department participates in two APVT project: "Integrated MEMS sensors of electromagnetic radiation based on magnetoresistive thin films" and „Non-traditional multiphase nanostructured materials with extraordinary physical properties". The main contribution of the Department to the governmental project „New materials and devices in submicrometer technology" is the application of nanomaterials in electronics. We finished our theoretical simulation of 2D arrays of magnetic dots containing the magnetic point deffects and the experiment is prepared.

Besides of studying the nanocomposite films prepared at our Institute we are also involved in investigation of samples prepared by other techniques in collaborating organizations in the framework of bi-lateral cooperation.

Very effective, in last two year, was the work on the project **„**Thin film nanocomposites containing fulleren-like structures" (the collaboration with MFA Budapest). We have shown that it is possible to use the electrical characterization of nanocomposite Ni-C as a non-destructive method of detection of fullerene-like structures on the boundaries of Ni nanoparticles.

Two of our bilateral projects are focused on the superconducting nanocomposites: „Study of the transport properties of superconducting nanograins in dielectric matrix "(the collaboration with CNR Padova) and „Study of nanogranular superconductors" (the collaboration with JINR Dubna).

The Department has organized the first national conference on nanotechnology „Nanoved 2003", where most of the research teams from Slovakia and neighboring countries presented their activity in nanoscience and nanotechnology. During the conference the effective collaboration of Department with several domestic teams was established. It was decided to continue in organising of „Nanoved" conferences every one-and-a-half year.

Basic experimental equipment and methods available at the Department are:

- cryopumped vacuum apparatus for deposition of periodic multilayers by magnetron sputtering
- transmission electron microscope JEOL1200EX, technology of cross-sectional TEM specimens,
- scanning electron microscope BS340 adapted for a simple direct electron lithography
- electro- and magnetotransport measurements in the range of 300 – 4 K, and magnetic fields up to 1.5 T.

For the successful research in the field of nano-materials there are necessary "thin" vacuum technology, detailed nano-structural analysis, special lithographic techniques and sophisticated electrical measurements. The most important request is the intensive collaboration of all the staff members. I would like to express my gratitude for the work they have done within this two-year period.

Ivo Vávra

Fe/AlN and Fe/ SiO_2 nanocomposite thin films

I. Vávra, P. Lobotka, K. Sedláčková, V. Šmatko, E. Kováčová, and J. Dérer

The multilayer technology was used for the preparation of nanocomposite thin films consisting of iron nanoparticles embedded in an insulating matrix. The iron layers were prepared in the form of non-continuous films composed of Fe nuclei. The mean size of Fe nuclei is several nm. The distance between adjacent Fe particles is about 2 nm, which is a distance favorable for tunneling (Fig.1). The insulating layers (thickness of 2 nm) were sputtered at deposition parameters, which activate the planarization of the Fe layer surface. The TEM structural investigation revealed the amorphous structure of the insulating matrix. The Fe nanocrystallites in SiO_2 matrix have bcc structure, and surprisingly, fcc structure in AlN matrix. The electric transport mechanism in both types of nanocomposite films is a tunneling. Coulomb blockade effect of the transport was observed in both nanocomposite films (Fig. 2). Because of Fe bcc phase in Fe/SiO_2 nanocomposite the layer is magnetic. The magnetic properties were confirmed by longitudinal MOKE (Fig. 3). Consequently we observed the tunneling magnetoresistance effect (Fig. 4).

The applications of developed nanocomposite layers in sensorics are prepared.

Collaborators: J. Pištora *at Technical University, Ostrava, Czech Republic and* G. Radnóczi *at the Research Institute for Technical Physics and Material Sciencies, HAS, Budapest, Hungary.*

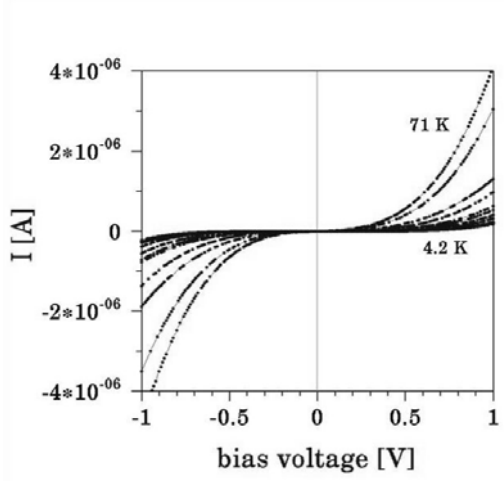

Fig. 2. I(V) characteristics of AlN/NbN nanocomposite film. The Coulomb blockade is observed at cryogenic temperatures.

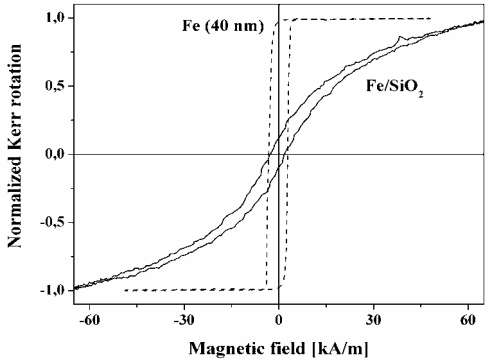

Fig. 3. Comparision of hysteresis loops of continuous Fe(40 nm) film and nanocomposite Fe/SiO_2 thin film. The loops were taken by longitudinal MOKE method.

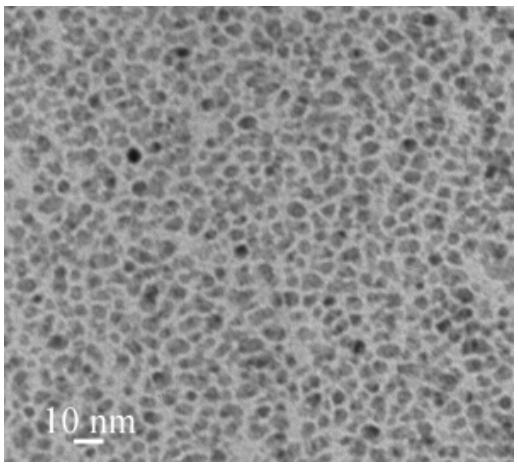

Fig. 1. TEM in plane micrograph of Fe/AlN nanocomposite layer. The fcc Fe nanocrystallites are separated by 2 nm of AlN.

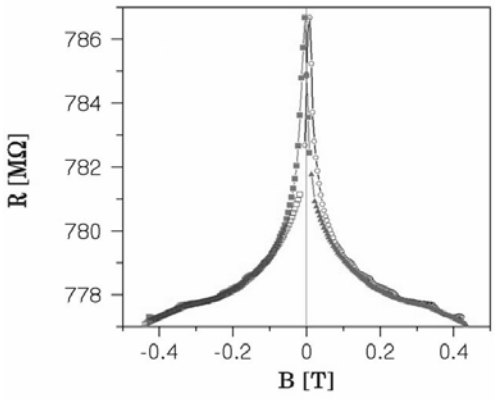

Fig. 4. R(B) dependence of Fe/SiO2 nanocomposite film measured in parallel to the film plane direction.

Superconductivity in NbN-AlN multilayered nanogranular thin-film composite

P. Lobotka, Š. Gaži, I. Vávra, and K. Sedláčková

Nanogranular superconductors are interesting objects from the point of view of basic and applied research.

Here we report on composite film consisting of nanoparticles made of superconductor embedded in an insulating matrix. In order to obtain a composite with T_c > 4.2 K, we have chosen material with a high bulk value of transition temperature – NbN. For the reason of chemical compatibility the proper insulating material is AlN. The thin films were deposited by sequential reactive sputtering of non-continuous NbN and continuous AlN sublayers on oxidized Si wafers. The average size of NbN nanoparticles was about 6 nm and the thickness of AlN

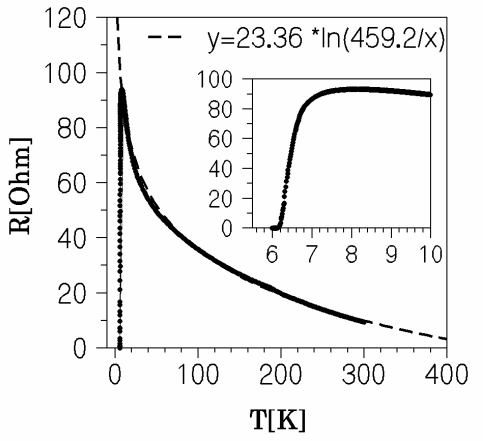

Fig. 1. Temperature dependence of the resistance of NbN - AlN composite is logarithmic. The superconducting transition temperature is 6.08 K.

was tailored so to allow for tunneling of single electrons.

On cooling, R(T) curve shows a steep logarithmic increase of the resistance [1] and then the transition to the superconducting state at T_c = 6.08 K (Fig. 1). This behavior is due to interplay between the Coulomb blockade of tunneling and the Josephson coupling. The ratio between E_c : E_J can be tuned by varying the temperature. Based on TEM micrographs, it is assumed that Josephson coupling is more probable in a direction normal to the substrate due to the shape of NbN nanoparticles. This indicates 2-D transport behavior of the film.

The *I-V* curve measured at 6.15 K (at the bottom of the superconducting transition shown in Fig. 1) and plotted in log-log scale (Fig. 2) shows three linear parts (only two of them are shown). At low current values the dependence $V \sim I^3$ was found, which can be attributed to Kosterlitz-Thouless mechanism in two-dimensional superconductors [2].

At higher currents the *I-V* curve shows several peaks in normal state of the composite, separated equidistantly with a period of 0.12 mA. This effect can be explained by occurrence of the phase slips in the layered composite. For better clarity, in Fig. 3 the differential resistivity dV/dI is plotted.

The measurements of transport properties in magnetic field are foreseen.

[1] *Simon R. W., et al., Phys. Rev B* ***36*** *(1987)1962.*
[2] *Tang L. H.,et al., Phys. Rev. B* ***67*** *(2003) 024508.*

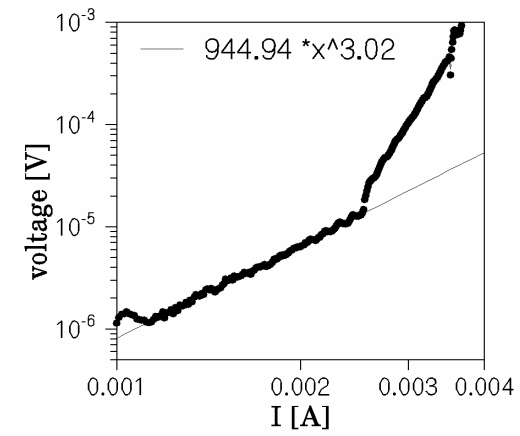

Fig. 2. At low currents the I-V dependence reveals Kosterlitz-Thouless mechanism ($V \sim I^3$) valid for 2-D superconductors.

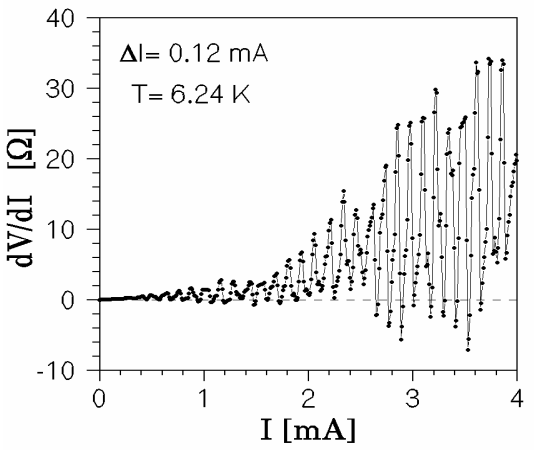

Fig. 3. Differentiated I-V curve shows at higher currents the peaks in dynamic resistance which is related to the regular occurrence of phase slips.

Structural, electrical and mechanical properties of C-Ni composite thin films

K. Sedláčková, P. Lobotka, and I. Vávra

Carbon-based composite thin films have large application potential because they possess unique mechanical properties, especially high hardness, high elasticity, and low friction coefficient [1]. A combination of pure carbon-based films with metallic nanoparticles, e.g. Ni [2] can enhance certain physical, electrical and mechanical properties of composite films.

C-Ni composite thin films were prepared by simultaneous dc magnetron sputtering of C and Ni from two sources in argon at 2.5 x 10^{-1} Pa. The films were deposited onto oxidised Si wafer (the SiO_2 thickness was 300 nm) at various substrate temperatures in the range from 25 to 800 ˚C. The nominal thickness of the films was 600 nm. The films deposited below 400 ˚C showed a columnar structure of hexagonal Ni_3C type crystalline grains embedded in a matrix consisting of an amorphous and/or graphite-like carbon (GLC) (Fig. 1). Above 400 ˚C the composite consists of globular fcc Ni grains sized between 50 and 100 nm that were separated by the fullerene-like carbon phase.

A correlation was found between the structure and electrical properties of the C-Ni composites. Two samples (25 and 400 ˚C), in which the prevailing matrix material is the disordered carbon, exhibited the tunneling effect (Fig. 2). They can be considered to be an insulator-metal composite with a 2D random network of tunnel junctions consisting of metallic Ni_3C nanoparticles separated by thin a-C barriers. In the films grown at 600 and 800 ˚C, in which fcc Ni globular crystallites were separated by well-conductive GLC, no tunneling effect was revealed by differential conductance measurements. The composites showed metallic behavior with temperature coefficient of resistivity TCR > 0.

The crystallographic phase of the crystallites in the C-Ni composites can be inferred from the magnetoresistivity measurements: composites, containing only hcp Ni_3C type structure give zero magnetoresistivity, while C-Ni nanocomposites containing fcc Ni in the composite showed a small anisotropic magnetoresistance ~ 0.1%.

Nano-mechanical properties (hardness 2 ÷ 11 GPa, elasticity 40 ÷ 120 GPa) of C-Ni films showed a distinct variation on the deposition temperature. Film deposited at 200 ˚C (Fig. 1) had the highest hardness 11 GPa and the highest modulus of elasticity 120 GPa. This observed behavior can be interpreted on the basis of the structure of the film: the high value of hardness is related to the presence of columnar structure of the Ni_3C phase and GLC phase.

Once the correlation between the structural, electrical, and mechanical properties was found for a particular film composition, it seemed that even without TEM study the basic features of the structure could be inferred from fast electro- and magnetotransport studies. This could be of some importance for the development of technology.

[1] *Yang, S. and Teer, D.G.: Surface and Coating Technology* ***131*** *(2000) S 412.*

[2] *Radnóczi, G., Kovács, G.J., Pécz, B., Geszti, O., and Sáfrán, G.: Vacuum* ***71*** *(2003) S 185.*

Collaborators: G. Radnóczi, G. Kovács *at the Research Institute for Technical Physics and Material Sciencies, HAS, Budapest, Hungary,* I. Bertóti, T. Ujvári *at the Institute of Materials and Enviromental Chemistry, Chemical Research Center, HAS, Budapest, Hungary.*

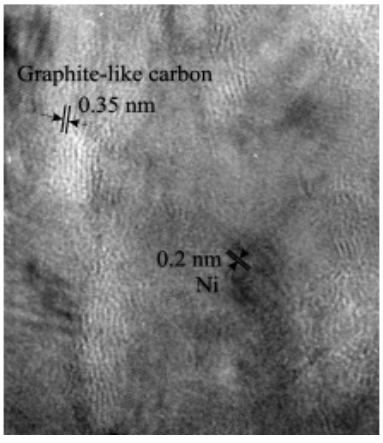

Fig. 1. HREM image cross-section of C-Ni composite film prepared at 200˚C shows graphene layers of GLC between hcp Ni_3C columnar crystalline grains.

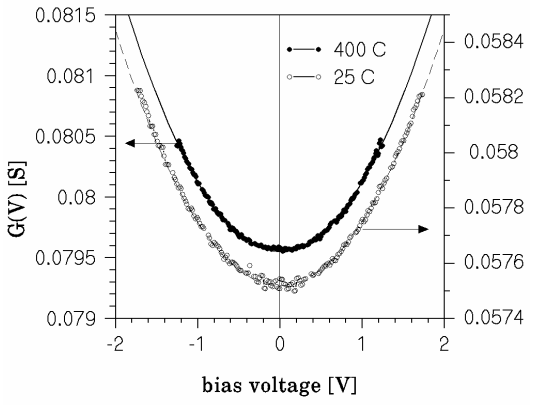

Fig. 2. G(V) dependence obtained at 77 K (88 K) for C-Ni composite prepared at 400˚C (25˚C) is a shallow parabola, providing the evidence for tunneling across amorphous thin carbon barriers.

Relationship of a magnetic defects and magnetic dot array properties

P. Majchrák and Ivo Vávra

For the application of magnetic dot arrays as the magneto-optical sensors it is necessary to understand the influence of finite size of magnetic dot array and individual magnetic defects on the overall magnetic properties of the dot array [1]. The study of the second effect has also practical reason - the magnetic point defect (e.g. the absence of one or more dots) appears relatively often as a consequence of imperfection in the patterning technology.

In the magnetic dot systems long-range magnetostatic interaction takes place. It might be interesting to understand an impact of defects to the magnetic properties of the finite arrays [2]. This motivation leads us to perform the computer simulations of arrays with magnetic defects. Our study concerns with: (i) correlation between defects positions and magnetic properties; (ii) disturbances of original anisotropy on macroscopic scales; (iii) hysteretic loops, saturation and coercive fields.

A study of the impact of the magnetic dot-vacancy and biasing field on the basic magnetic properties of magnetic dot array is reported. Magnetic bias is a constant magnetic field applied simultaneously with the remagnetization field, which is oriented perpendicularly to the magnetic reversal field. Simulations, which are presented, deal with the magnetic dot arrays in rotating magnetic field and in-line reversal field with the dot-vacancies in various positions. The results led us to conclude, that amplitude of two-fold magnetization contribution increases with asymmetry of the dot-vacancy position regarding to the center of array. The non-zero bias and the presence of magnetic defect are resulting in asymmetric behavior of magnetization response. For the characterization of asymmetrical hysteretic loops the specific coefficient of asymmetry was defined [3]. This quantitative characterization of asymmetry allows determining the range of relevant biases leading to maximal two-fold contributions to magnetic anisotropy of array.

The square-shaped sample of a square lattice array is studied in the quasistatic regime. The first step towards solution represents dipolar approximation justified for small single domain dots separated by distances highly exceeding dot diameter.

Magnetic dot-vacancy induces two-fold contribution to normally four-fold anisotropic array. It was found out, that applying of bias on magnetic dot array with magnetic dot defect can, in some cases, induce asymmetry of the hysteretic behavior. The quantitative characterization of asymmetry facilitates to find the region of the bias leading to maximal two-fold contribution of dot-vacancy, which means that simulation could be beneficial in determination of working point of the devices for defectoscopy. In future, we would like to clarify relations between properties of the set of coupled dot-vacancies and changes in behavior of the magnetic response.

[1] *Cowburn, R. P.: J. Magn. Magn. Mater.* ***242-245*** *(2002) 505.*
[2] *Russier, V., Petit, C., Legrand, J., and Pileni, M. P.: Appl. Surf. Science* ***164*** *(2000) 193.*
[3] *Majchrák, P., Horváth, D., Gmitra, M., and Vávra, I.: SPIE proceedings* ***5445*** *(2004) 262.*

Collaborators: D. Horváth and M. Gmitra, Department of Theoretical Physics and Astrophysics University of P. J. Šafárik, Moyzesova 16, 040 01 Košice.

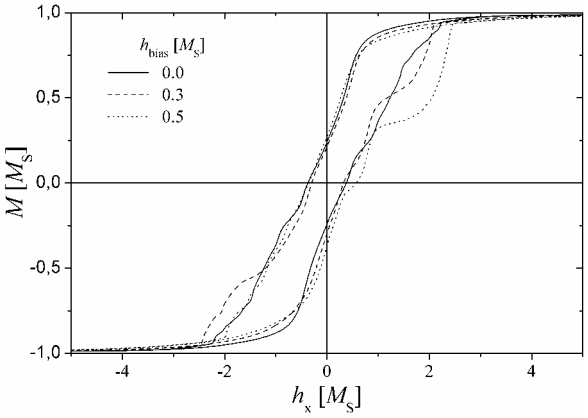

Fig. 1. Symmetry of the hysteretic magnetic response as the function of h_x for array with dot-vacancy at position i = 3 and j = 3 (abbreviated here by [3,3]) depending on various values of the biasing field.

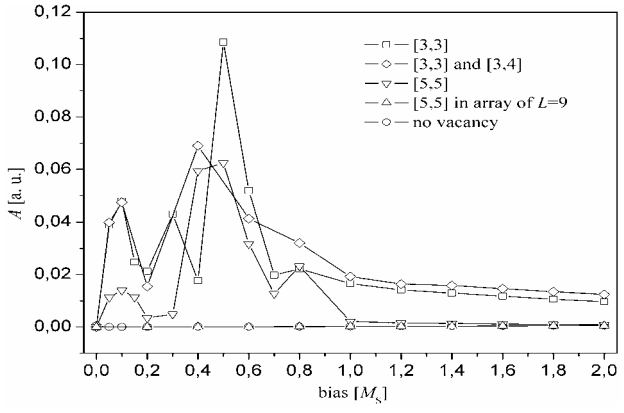

Fig. 2. The h_{bias} dependence of the coefficient of the asymmetry A simulated for various dot-vacancy positions.

Department of Superconductor Physics

Fedor Gömöry

Research scientists
Pavol Kováč
Jozef Pitel
Ján Šouc
Silvester Takács

Technical staff
Ľubomír Kopera
Ján Šlesár
Juraj Tančár

Research Engineers
Lubomír Frolek
Imrich Hušek
Tibor Melišek

PhD Students
Tomáš Holúbek
Boris Klinčok
Eugen Seiler
František Strýček

Students
Jakub Cambel
Edita Janíková
Michal Kopera
Miloslav Kulich
Lucia Noskovičová
Michal Vojenčiak

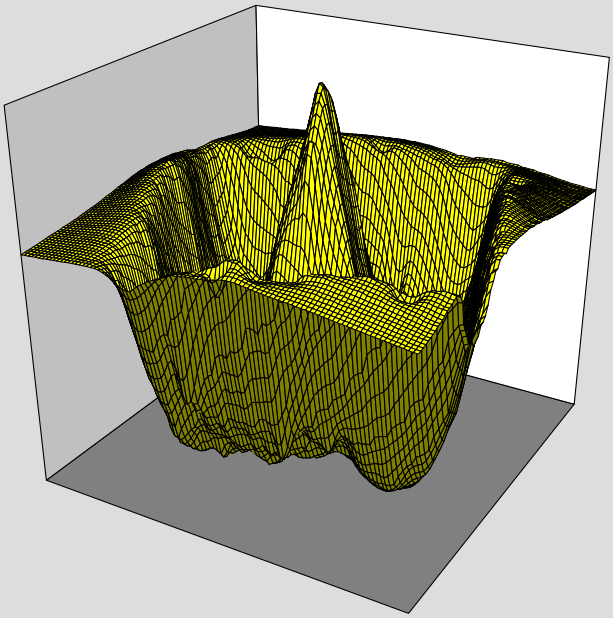

Research activities of the Department are dedicated to the study and development of materials and systems for high-current applications of superconductors.

Several classes of superconductors are known, without a general agreement on predicting the critical temperature for all of them. This represents a motivation for our theoretical work on the basic understanding of the topic.

Regarding the applications, our department has facilities for the entire range of fabrication steps to produce a composite wire from low- or high-temperature superconductor. Both usual and unconventional deforming techniques have been used in the past to prepare Nb_3Sn and Bi-2223/Ag wires, the current focus is on MgB_2/Fe,Cu composites. Chemical reactivity of the starting elements and the hardness of the compound itself makes it difficult to insert other elements in a controllable manner. Nevertheless, this is crucial for improving its properties, in the first row the current-carrying capability and its dependence on magnetic field. Also, the response to mechanical stress is important when considering a winding from MgB_2/Fe,Cu wire.

The composite containing superconducting filaments in metallic/ferromagnetic matrix represents an object whose features could be influenced by both the qualities of the used materials as well as the arrangement of filaments. We have studied the electromagnetic properties theoretically and experimentally, on a set of MgB_2/Fe,Cu and Bi-2223/Ag composites with well defined filament architecture, sometimes quite unconventional. Fair progress has been achieved in theoretical simulations. On top of finite element simulations with commercial codes, we adopted numerical techniques adequate to simulate the critical state as well as the flux creep in superconductor. Such studies are essential for the future use of composite superconductors in electric power devices.

When the electrical currents to be transported are in the range of kiloamperes, inevitably the superconducting wires should be cabled. We dedicate systematic effort to the understanding of the distribution of current, magnetic field, and the resulting energy loss in the flat cables used in the nuclear fusion technology. Concerning the cables for power transmission, we have designed, manufactured and tested short laboratory models to investigate some peculiarities in the current distribution, AC transport capacity and AC loss.

On the national level, the activities of our department have been financially supported by the academic grant agency VEGA within the projects "Flux penetration into superconductors of various shapes and configurations" and "Mechanically reinforced composite Bi-2223 superconductors with optimised filament architecture", and the grant agency APVT in the projects "Electromagnetic properties of superconducting composite conductors" and "Composite superconductors for cryogen-free devices".

International collaboration with the Imperial College in London, UK, „AC losses in AC fields in high temperature superconductors" has been supported by the Royal Society, while NATO financed our collaboration with INFN Genua, Italy, „AC losses in Bi-based multifilamentary superconducting tapes". Austrian Ost-West Fund supported our collaboration with the Technical University Vienna, Austria, and Unipress Warszawa, Poland, on „High temperature Bi-2223/Ag composite superconductors for coil windings".

Significant involvement in the international collaboration was for us the participation in multilateral projects of the 5th Framework Program of the EC „Quality monitoring of Superconductors for the production of Efficient, Compact and reliable Energy Transmission Systems", „The European network for superconductivity SCENET-2", and running of the Centre of Excellence „Applied Superconductivity Training and Research Advanced Centre". In the 6th Framework Program, we are involved in two RTD projects "Superconducting coated conductor cable" and „Nano- and micro-scale engineering of higher-performance MgB_2 composite superconductors for macro-scale applications".

Fedor Gömöry

Superconductors with singularities in the density of states: (s + d) model

S. Takács

Among many other effects, the increased density of states (DOS) near the Fermi energy is assumed to be the reason for the deviations of high T_c superconducting and normal parameters from the BCS model (assuming constant DOS near the Fermi surface). The form of such increased DOS can be of different type, the most known is the logarithmic type of the van Hove singularity. However, many experiments support the existence of even stronger singularities. Therefore, we calculated some parameters of superconductors with δ-function type singularities to show that they can be very different from the BCS model. These calculations have the advantage to be simple and are very illustrative, as the results give some limiting cases without need for any further assumptions and approximations in the calculation procedure [1]. The model was extended by including even some strong-coupling effects [2]. Analogous calculations can be made by taking into account the d-wave pairing interaction and the combination of (s+d)-wave symmetry of the order parameter [3].

The DOS is taken in the form $N(\varepsilon) = A_s\delta(\varepsilon)+A_d\delta(\varepsilon)$, where A_s and A_d are arbitrary constants. We consider both peaks to be at the Fermi energy, recognizing that the presence of the peaks in the off-symmetric position weakens the effects caused by the singularity [1,4].

The interaction pairing potential between two particles with the momentums k, k' is for mixed s+d pairing interaction of the form [3]

$$V(k,k')=V_s(k,k')+\eta(\phi)V_d(k,k')\eta(\phi')+V_i(k,k')[\eta(\phi)+\eta(\phi')]$$

where V_s, V_d are the interaction potentials of the individual channels, $\eta(\phi) = \cos(2\phi)$ is the basis function representing the symmetry of the crystal, and the "mixing" channel V_i depends on the relative distortion of the crystal lattice caused by the orthorhombic transition .

The energy gap in the weak coupling limit is then of the type $\Delta(T) = \Delta_s(T) + \Delta_d(T)\cos(2\phi)$. All important parameters of the superconductor can be determined from the properties of the energy gap, which can be calculated from the BCS type equation

$$\Delta(k,T) = \int d\varepsilon'\ V(k,k')N(\varepsilon')\Delta(k',T)W(k,k') / f_{k'},$$

$$f_k = \sqrt{\varepsilon_k^2 + \left|\Delta(k,T)\right|^2},\quad W(k,k') = \tanh\frac{f_{k'}}{2k_BT},$$

with k_B being the Boltzmann's constant.

The even and odd parts of the gap equation lead to two coupled non-linear equations, which can be linearized and decoupled in two cases: (1) $\Delta \to 0$, giving the critical temperature T_c and (2) $T \to 0$, giving the zero temperature energy gap Δ_0.

The critical temperature is changed only slightly with mixing the d-wave pair interaction weaker or comparable with that of the s-wave. However, for d-wave interactions much stronger than the s-wave interaction, T_c is given mainly by the d-wave interaction potential:

$$T_c = d\ T_0/2 = V_d\ A_d/4k_B,$$

where $T_0 = V_s\ A_s/2k_B$ is the critical temperature for the pure s-wave interaction potential and $d = V_d\ A_d/V_s\ A_s$.

The ratio of the zero temperature energy gap to the critical temperature, $R = 2\Delta_0/k_BT_c$, can be much higher by the mixing and it depends also on the mixing term. This ratio has a maximum at medium values of d ($\approx 2\div4$), and the obtained results for this maximum (about 20) may explain the very high measured values of R. Another striking feature of the results is that the effects connected with the d-wave interaction are weakened by the mixing term (the effects are stronger at low mixing).

Further characteristic parameter of superconductors is the relative jump in the specific heat at the critical temperature. The singular DOS changes this much more than the strong coupling between the electrons. This is true mostly for the pure s-wave interaction (by the factor 2.4), where the value of 3.64 (compared with 1.43 for the BCS model) is close to the highest measured experimental values (4.8). We would like to add that the calculations with power-law like singularities [5] (due to the extended saddle point in the DOS) lead to the values about 3.38, very close to our simple model. For pure s-wave interaction potential of the logarithmic van Hove type [6], the value of the jump decreased with increasing T_c. This behaviour is also present in our model.

The obtained results for the superconducting parameters should be seen as limiting values in the weak-coupling limit only. Mainly the extension to the strong-coupling for the pairing potential, including the singularities in the DOS for the coupling bosons, would be desirable. The combination with more sophisticated models, like the odd-pairing around the Fermi level, or higher angular momentum in the d-way gap, or even some non-Fermi-liquid behaviour, could also be interesting.

[1] *Takács, S.: Critical Temperature and Energy Gap in Superconductors with Singularities in the Density of States (DOS,) in: J.K. Srivastava and S.M. Rao (Eds.), Models and Methods of High-T_c Superconductivity: Some Frontal Aspects, Nova Science, New York, 2003,Chpt. 9, p. 289.*
[2] *Takács, S.: Phys. Rev.* ***B48*** *(1993) 13127.*
[3] *Takács, S.: Solid State Commun.* ***128*** *(2003) 455.*
[4] *Takács, S.: Phys. Rev.* ***B46*** *(1992) 3145.*
[5] *Sarkar, S. and Das, A.N.: Phys. Rev.* ***B54*** *(1996) 14974.*
[6] *Szczesniak, R. and Grabinski, S.: Acta Phys. Polonica* ***A 102*** *(2002) 401.*

Improvement of the current carrying capability of *ex-situ* MgB_2 wires by normal particle additions

P. Kováč, I. Hušek, and T. Melišek

A wide variety of powders, including Nb, Ti, Zr, Hf and W, metal oxides like Nb_2O_5, Ti_2O_5, V_2O_5 and other compounds like SiC, $SrCO_3$ and boron nitride, have all been used at the 10 wt% level as additions into commercial MgB_2 powder. For the fabrication of single-core *ex-situ* wires groove and two-axial rolling deformation were used with the final heat treatment at 950°C/0.5h in Ar [1]. Transport current measurements have shown that metal particle addition leads to an especially significant improvement in current carrying capacity. The presence of normal particles influences both the resistivity and also the thermal conductivity of the MgB_2 core [2,3], and the improved internal stability may be responsible for the increased critical current values. This observation may be very important for future development of practical MgB_2 composite superconducting wires.

Figure 1 shows $I_c(B)$ characteristics of all the wires with variable additions (MgB_2+10%X) compared to data from an MgB_2 wire sample without doping. Because all the wires have the same cross-sectional area, the corresponding current densities can be estimated by $J_c = 100\ I_c$ [Acm^{-2}]. As is apparent, the addition of all the metallic additions has a positive effect on I_c values. The greatest increase in I_c compared to the pure MgB_2 control sample is a factor of 3.26 times in an applied field of 5 T for Hf addition and a factor of 3.57 and 3.78 in 10T for W and SiC addition, respectively. The metal oxide additions do not give as positive an effect as the reactive metals, apart from doping with Nb_2O_5 particles, which results in a similar improvement as for Ti. SiC additions also improve the I_c values substantially. Only the compounds Ti_2O_3, $SrCO_3$, V_2O_5 and BN resulted in decreased I_c and J_c values, the lowest measured for $SrCO_3$, see Fig. 1.

Figure 2 gives the resistive transitions of three wires and clearly demonstrates the decreased normal state resistivity of wires with additions of metallic particles (W, Ti). The critical temperatures are also slightly affected ($T_{c\text{-mid}}$ = 38.2 K for pure MgB_2, 37.36 K for W addition and 36.4 K for Ti). Because the cross sectional area and length of each wire is very similar, the decreased wire resisitivity must be a result of improved conductivity in the MgB_2 core containing W or Ti particles.

Optical microscopy and SEM studies were used to study the distribution of these particles. Ti and W particles in the longitudinal section of the MgB_2 cores, and while the Ti particles are elongated along the wire axis and distributed reasonably homogeneously, the W particles seem to be both more uniform in shape and less uniformly distributed [4]. In fact, the Ti particles look hollow, as discussed below, and very different microhardness values were measured in the Ti grain centre (HV ≈ 530) in comparison to its outer area (HV ≈ 280).

Doping with metallic powders seems a very promising way to improve the properties of MgB_2 wires towards those required for practical applications, and to provide a basis for the development of future highly stable conductors.

[1] *Kováč P, Hušek I, and Melišek T: Superconductor Sci and Technology* ***15*** *(2002) 1340.*

[2] *Grovenor C. R. M, Goodsir L, Salter C. J, Kováč P., and Hušek I: Superconductor Science and Technology* ***17*** *(2004) 479.*

[3] *Kováč P, Hušek I, Grovenor C. R. M., and Salter C. J: Superconductor Science and Technology* ***16*** *(2003) 292.*

[4] *Kováč P., Hušek I., Melišek T., Grovenor C. R. M., Haigh S., and Jones H: Superconductor Science and Technology* ***17*** *(2004) 1225.*

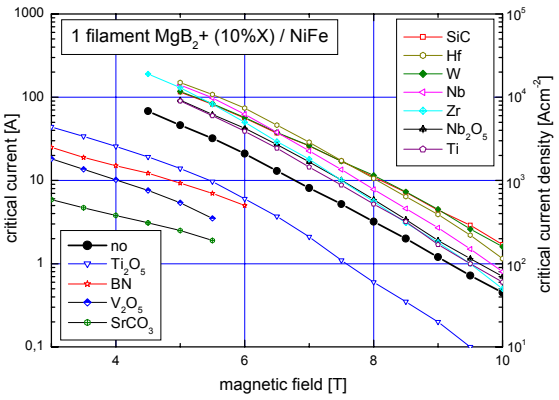

Fig. 1. $I_c(B)$ dependences for wires containing metallic powders, metal oxides and non- metallic powders.

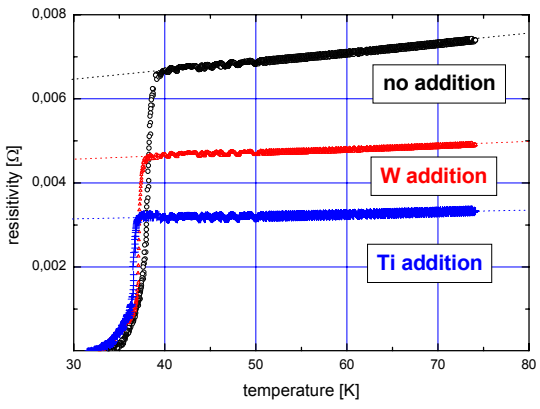

Fig. 2. Resistive transitions of MgB_2 samples with Ti and W additions compared to the reference (no addition) sample.

The role of MgO content in *ex-situ* MgB_2 wires

P. Kováč, I. Hušek, T. Melišek, and V. Štrbík

An experimental study of the effect of MgO content in the MgB_2 powder used for *ex-situ* made composite wires was carried out. Two single-core MgB_2/Fe/Cu wires were made using commercial MgB_2 powders from Alfa Aesar containing different fraction of MgO. Critical temperature and critical currents of as-deformed and heat-treated wires were measured. The differences between the wires are discussed and correlated with the MgO content. It was found that by increasing the amount of MgO the inter-grain connectivity worsens, but well distributed and low size MgO particles improve flux pinning [1].

Fig. 1 shows the results of resistive measurements for AD and HT wires. As it is apparent, the transitions are approximately 1 K higher in the wire made of A-II than wire WA-I. This correlates well with lower MgO content and so higher purity of powder A-II in comparison to A-I. It is supposed that the variation in T_c may result from a difference in stoichiometry. The T_c of $Mg_{1-x}B_2$ depends slightly on x. If the starting composition of the 2 batches was the same, different amounts of Mg-rich impurities may result in different Mg deficiencies in MgB_2. The slightly higher temperature difference for HT samples (1.1 K) than for as deformed (0.8 K) can be probably attributed to the larger amount of Mg phase in powder A-II, which yields a better stochiometry of the MgB_2 phase after heat treatment in WA-II. This figure demonstrates clearly the effect of core recrystalization, which shifts the middle of the resistive transition by 6.5 K. The improvement in MgB_2 crystals bonding by recrystalization have lead also to much narrow transitions for HT wires (≈ 1.0 K) in comparison to only packed powder in AD wires with the transition width of ≈ 4.0 K.

Fig. 2 shows the Kramer's plots of both as-deformed and heat-treated wires. A typical behavior of Kramer's plot ($I_c^{1/2}B^{1/4}$ versus B) is linear for the most low temperature superconductors above the field of maximal pinning force and is usually used for the upper critical field (B_{c2}) estimation. Presented plots are only partially linear and show an expressive curvature in low fields for AD wires and in high fields for HT ones. It was shown previously that the presence of iron in MgB_2 composite wire makes the $I_c^{1/2}B^{1/4}$ versus B characteristics below iron saturation non-liner [3].

It is attributed to the effect of iron shielding and lower magnetic flux density inside the iron in comparison to the external one. Therefore, B_{c2} extrapolation by $I_c^{1/2}B^{1/4} = 0$ cannot be used correctly for magnetically shielded superconductors. Nevertheless, two dotted lines and/or curves in Fig 2 show clearly ≈ 2 T difference in B_{c2} for WA-I-HT and WA-II-HT, while smaller and opposite B_{c2} difference ≈ 0.5 T for AD wires. The changed B_{c2} would correlates with the normal state resistivity (ρ) and T_c, $B_{c2} \approx \rho T_c$ [3]. After heat treatment MgO particles are included into MgB_2 [4], which reflects in an increased ρ_{WA-I}. Taking into account measured T_c and estimated B_{c2} difference for WA-I-HT and WA-I-HT, ρ_{WA-I} has to be by 26 % higher than ρ_{WA-II}. Apparent increase of upper critical field was already demonstrated by an increase of the normal state resisitivity, while the critical temperature decreased by 1 - 2 K. In conclusion, increased MgO content in WA-I-HT improves pinning and increases upper critical field.

[1] *Kováč, P., Hušek, I., Melišek, T., Grivel, J.C., Pachla W., Štrbík V., Diduszko R., Homeyer J., and Andersen N. H: Superconductor Science and Technology* ***17*** *(2004) L41.*
[2] *Kováč P., Ahoranta M., Lehtonen J., and Hušek I.: Physica C* ***397*** *(2003) 14.*
[3] *Goodman B. B.: Phys. Rev. Letters* ***6*** *(1961) 597.*
[4] *Zhu Y., Wu L., Volkov V., Li Q., Gu G., Moodenbaugh A. R., Malac M., Suenaga M., and Tranquada J.: Physica C* ***356*** *(2000) 239.*

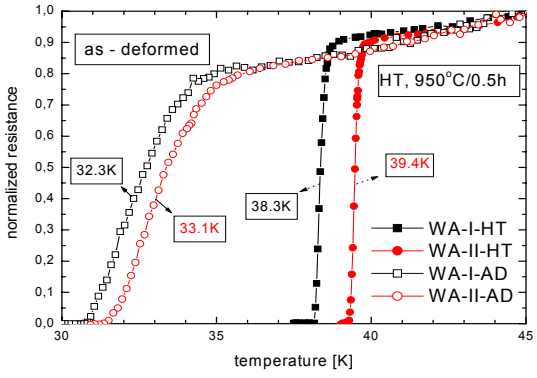

Fig. 1. Normalized R(T) for AD and HT wires.

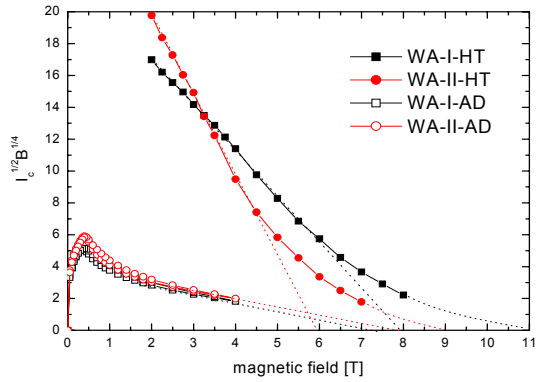

Fig. 2. Kramer's plots for AD and HT wires.

Dependence of the critical current in *ex-situ* multi- and mono-filamentary MgB_2/Fe wires on axial tension and compression

P. Kováč, T. Melišek, and I. Hušek

The transport critical current I_c of single- and four-core MgB_2/Fe wires under tensile and compressive axial strain ε was measured with a U-shaped spring set up. In all wires, I_c increases linearly and reversibly with applied tensile strain, up to a sample-dependent reversible strain limit ε_{irr}. The same reversible and linear $I_c(\varepsilon)$ relation is found when applying compressive strain. This shows how the $I_c(\varepsilon)$ increase with tension can be understood as a gradual release of the thermal pre-compression strain induced in the MgB_2 filaments of the composite. The value of the reversible strain limit ε_{irr} depends mainly on the degree of pre-compression, but also on the shape of the composite wire. It is highest in a square wire and lowest in the flattest tape. Tensile strain levels above ε_{irr} cause an irreversible degradation of I_c. This $I_c(\varepsilon)$ degradation, due to filament cracking, is significantly steeper in heat-treated wires than in as-deformed ones. The different $I_c(\varepsilon)$ regimes are analysed and the mechanical behaviour of the MgB_2/Fe composite is compared with that of typical Nb_3Sn wires and Bi,Pb(2223) tapes.

The MgB_2/Fe composites made by TIRT technique [1] were strained with a spring set-up, which can apply a tensile as well as a compressive force to the sample [2, 3]. The wires were Sn-Ag soldered to the base of a U-shaped spring made from brass or titanium. Two strain gauges, glued to the inner and outer face of the U's base, allow to extrapolate the strain state ε at the centre of the wire. Note that we use the standard definition of strain, $\varepsilon \equiv (l-l_0) / l_0$, with l_0 and l the length of the unstrained and strained sample, respectively. A negative value of ε thus indicates compressive strain, a positive one tensile strain.

Figure 1 shows normalized critical currents versus the applied strain. The critical current I_c increases linearly with the applied tensile strain up to $\varepsilon = 0.35$ % and then decreases sharply to become negligibly small at $\varepsilon \approx 0.5$ %. In contrast to BSCCO/Ag composites, where a multi-filamentary structure generally leads to a better mechanical performance, our mono- and multi-core MgB_2/Fe wires behave essentially the same. The only significant difference between both curves is in the slope K of the initial linear $I_c(\varepsilon)$ increase, $I_c(\varepsilon) \equiv (1+K\varepsilon)\, I_c(0)$. A similar $I_c(\varepsilon)$ dependences were measured by Kitaguchi and Goldacker [4,5].

Figure 2 compares the strain dependence of the critical current I_c with that of the power-law exponent n of the current-voltage characteristics, at $T = 4.2$ K and $\mu_0 H = 4$ T, for the four-core tape with aspect ration b/a =2. The similarities between both curves are striking. As long as the applied tensile strain ε remains lower than the reversible strain limit $\varepsilon_{irr} = 0.25$ %, the n-factor varies only little around the value $n \approx 20$. In this regime, the n-factor is determined by intra-granular magnetic flux pinning. As soon as ε_{irr} is exceeded, however, n decreases rapidly and irreversibly. This irreversible degradation of the n-factor closely mimics the degradation of I_c (note for instance the small 'plateau' in both curves at $\varepsilon \approx 0.3$ %).

[1] *Kováč, P., Hušek, I., and Melišek, T.: Superconductor Sci and Technology* ***15*** *(2002) 1340.*

[2] *ten Haken, B., Godeke, A., Schuver, H., and ten Kate, H.: IEEE Trans. Magn.* ***32*** *(1996) 2720.*

[3] *Kováč, P. and Bukva, P.: Superconductor Sci and Technology (2001)* ***14****.*

[4] *Kitaguchi, H., Kumakura, H., and Togano, K.: Physica C* ***363*** *(2001) 198.*

[5] *Goldacker, W.and Schlachter, S.: Physica C* ***378-381*** *(2002) 889.*

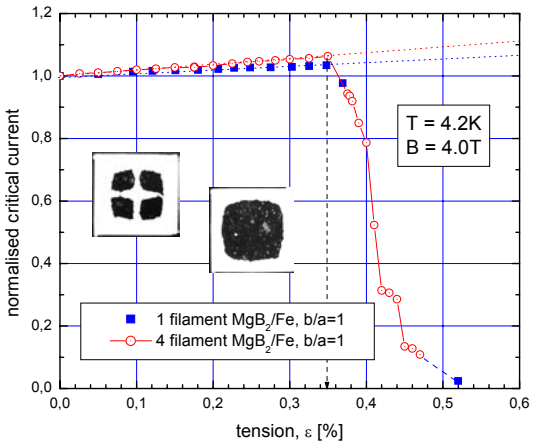

Fig. 1. Measured tensile $I_c(\varepsilon)$ dependence of symmetrical wires.

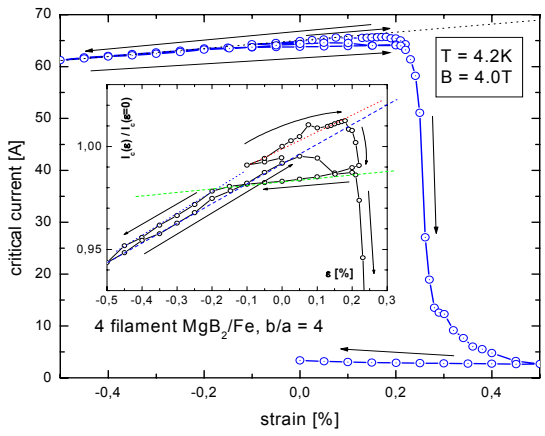

Fig. 2. $I_c(\varepsilon)$ dependence of flattened four core wire.

The effect of Fe-magnetization on $I_c(B)$ and $I_c(\alpha)$ characteristics of iron sheathed MgB_2 composite wires

P. Kováč, T. Melišek, and I. Hušek

Single- and four- core MgB_2 composites have been made by powder-in-tube (PIT) method using commercial MgB_2 powder in Fe sheath [1,3]. Transport currents of as-deformed wires were measured at 4.2 K and external magnetic fields B = 0 – 4T. Different $I_c(B)$ curves were observed for single- and four-core wires depending on the value of self-field current [4,5]. The behavior $I_c(B)$ and $I_c(\alpha)$ is influenced by Fe sheath magnetization by self-field and external field. Field distribution and $I_c(B)$ curves were calculated using finite element method (FEM) and they are used for explanation of experimental characteristics.

The field distribution in the cross sections of mono- and four-filament wires was modeled with FEMLAB software. The critical current versus external magnetic field dependence of conductors was simulated by FEM and compared to experimental data. The superconductor is close to the resistive transition and thus its permeability was assumed to be the same as for vacuum. The permeability of iron was obtained from the direct measurement of $B(H)$-curve for used iron sheath and the virgin curve was used in computations. The current density in the MgB_2 superconductor was assumed to be homogeneous. This was done to speed up the calculations. The shape of $I_c(B)$ was calculated by taking into account the real geometry of the iron sheathed MgB_2 core and the $I_c(B)$ dependence measured for a non magnetic copper-sheathed MgB_2 conductor [6]. Computation procedure was done as following: Firstly, the current density of the superconductor was set to be J_s. Then, the magnetic flux density distribution in MgB_2 superconductor was computed and corresponding J_c value evaluated. Finally, the J_c of the conductor was obtained by minimizing the error between $J_c(J_s)$ and J_s.

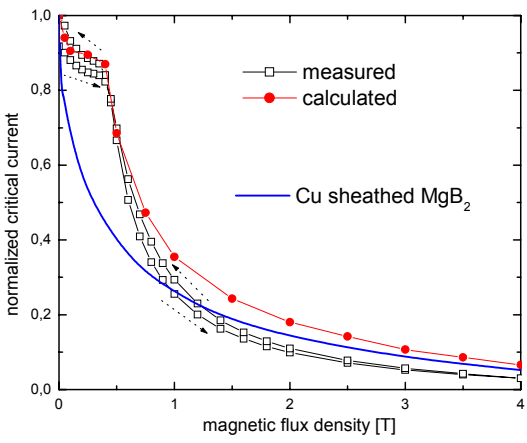

Fig. 1. Measured and calculated normalized critical currents.

Figure 1 shows the normalized critical currents versus the external magnetic field of copper sheath (non magnetic) wire, iron sheathed (magnetically) sheathed wire and calculated curve taking into account the real geometry of the iron and the $I_c(B)$ dependence measured for a non magnetic conductor. The $I_c(B)$-curves of iron sheathed wires measured in low external fields are highly deformed due to the magnetic shielding of used sheath. The iron sheath is magnetized by the self-field and as well by the external field. The $I_c(B)$-curve of iron sheathed MgB_2 can be divided into three parts due to variation on the shielding properties of iron. This variation is caused by the interaction of external field and self-field. The geometry of the wire cross section influences the critical current because the shielding depends on the shape and arrangement of the filaments against the applied field [6].

The shielding effect is also dependent on the external field orientations. Though the estimated difference in B_{ave} are very small (e.g. 0.086 T), by 15% larger I_c is measured when external field is parallel with the composite diagonal in comparison to parallel orientation with the wire side.

Figure 2 compares the field distribution around four-filament wire obtained by FEM analysis for external field is parallel with the composite diagonal in comparison to parallel orientation with the wire side.

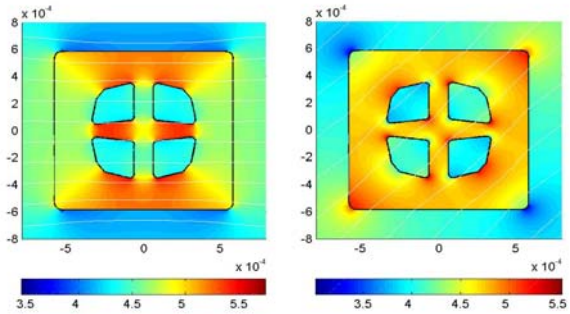

Fig. 2. Modeled magnetic field distribution for two external field orientations: B_{ex} is perpendicular to the wire side (left), B_{ex} is parallel with the wire diagonal (right).

[1] *Kováč, P., Hušek, I., and Melišek, T.: Superconductor Sci. Technol.* ***15*** *(2002) 1340.*
[2] *Grasso, G., Malagoli, A., Ferdeghini, C., Roncallo, S., Braccini, V., Cimberle, M. R., and Siri A. S.: Appl. Phys. Lett.* ***79*** *(2001) 230.*
[3] *Goldacker, W., Schlachter, S. .I, Zimmer, S. and Reiner, H.: Supercond. Sci. Technol.* ***14*** *(2001) 787.*
[4] *Horvath, J., Wang, X. L., Soltanian, S., and Dou, S. X.: Appl. Phys. Lett.* ***80*** *(2002) 829.*
[5] *Kováč, P., Hense, K., Melišek, T., Hušek, I., and Kirchmayr, H.: Superconductor Sci. and Technology* ***15*** *(2002)1037.*
[6] *Kováč, .P., Melišek, T., Ahoranta, M., Lehtonen, J., and Hušek, I.: Superconductor Sci. Technol.* ***16*** *(2003)793*

Shape effects linked with the flux penetration into superconducting filaments

E. Seiler and F. Gömöry

The current-carrying capability of the superconducting BSCCO-2223 tape is particularly determined by the pinning of magnetic flux, leading to hysteretic properties, and to energy loss in AC regimes. By optimizing the geometrical arrangement of the superconducting filaments the AC energy losses can be significantly reduced. Thus, the understanding of the behaviour of an array of flat superconducting filaments in the magnetic field is very important.

We studied experimentally the behaviour of two BSCCO-2223/Ag superconducting tapes with different filament architecture in homogenous AC magnetic field, applied perpendicularly to the tapes wide face [1]. In one tape, the filaments formed two columns, where their flat faces were parallel to each other and perpendicular to the applied field. In the other tape, the filaments were arranged in an overlapping brick-wall-like pattern. Our conclusion was, that the two filamentary geometries behave in the same way in the diamagnetic state, while in the critical state the behaviour is different for one and the other geometry.

In the diamagnetic state, the geometrical effects connected with the shape and arrangement of the filaments, are naturally characterized by the constant χ_0 – the real part of the complex AC susceptibility under these conditions. It can be both measured and numerically calculated for the filamentary distributions met in practice [2]. The calculations treat the filaments as being ideally diamagnetic. The result of such calculation for the

Fig. 1. Magnetic field distribution in the diamagnetic state.

geometry of a real 19 filament tape is shown in the Fig.1.

To investigate theoretically the behaviour of the tapes in the critical state, we developed a numerical method that allows us to simulate the flux penetration into various geometrical arrangements of filaments, also with very low symmetry [3]. The method employs the critical state model, and is based on minimizing the energy of the magnetic field inside and around the superconductor. The field distribution is calculated using the finite-element method, and the superconductor is divided into small current channels that are gradually filled with the critical current density. The superconductor is assumed to be infinitely long in the *z* direction, while the homogenous magnetic field is applied in the *y* direction. This makes the problem effectively 2D. The agreement between our method and similar MMEV method is discussed in [4].

In the Figure 2, the distribution of magnetic field lines around two superconducting filaments is shown at medium flux penetration level. The distribution of the current in the current channels is shown in the inset – the lighter shade of gray marks the current in the +*z* direction.

Our numerical method permits to simulate also the situation when the media surrounding the superconductor has not linear magnetic properties. In the Figure 3 the field lines distribution is shown, for a superconducting strip, whose wide faces are in contact with ferromagnetic strips having nonlinear $\mu_r(B)$ dependence.

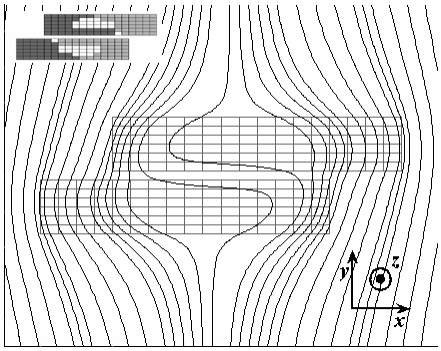

Fig. 2. Field distribution calculated for two filaments in external field along y. Inset shows the current distribution.

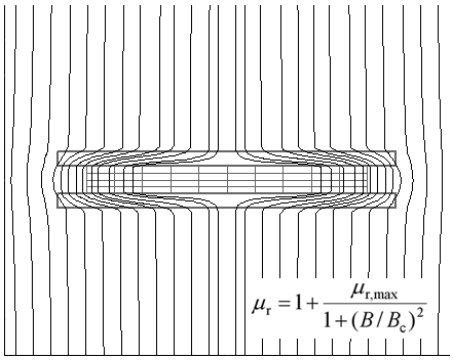

Fig. 3. Field distribution calculated for superconducting strip covered with two ferromagnetic strips.

[1] *Seiler, E., Gömöry, F., Fabbricatore, P., Greco, M., Perkins, G., and Caplin, A. D.: Supercond. Sci. Technol.* ***17*** *(2004) 549.*

[2] *Gömöry, F., Seiler, E., Šouc, J., Kováč, P., Hušek, I., Farinon, S., Fabbricatore, P., Perkins, G., Caplin, A. D., Pardo, E., Sanchez, A.,and Navau, C.: Supercond. Sci. Technol.* ***17*** *(2004) S150.*

[3] *Seiler, E. and Gömöry, F.: Czechoslovak J. Phys.* ***54*** *(2004) Supl. D D493.*

[4] *Pardo, E., Seiler, E., and Gömöry, F.: Czechoslovak J. Phys.* ***54*** *(2004) Supl. D D513.*

Voltage signal on superconducting wire at AC transport

B. Klinčok and F. Gömöry

Behavior of a superconductor with rectangular cross-section, transporting AC, is studied by means of the analysis of the accompanying voltage signal. In particular, we compare the electrical signal that would appear on a conductor with square cross-section, with the signals derived from the known models for a round wire and a thin strip, respectively.

We concentrate on the analysis of the 1st, 3rd and 5th harmonic components. The case when superconducting tape is carrying AC transport current is simulated. There, the voltage taken from a pair of taps soldered to the wire is analyzed with the help of a lock-in amplifier. We are using two basic approaches to evaluate voltage signal that would appear on such voltage taps. One is the minimum magnetic energy variation method [1,2] equivalent to the original critical state approach. Second is the Brandt's method [3] that is equivalent to smooth current-voltage curve. The second approach takes a flux creep into consideration. In our calculation we have used the power-law function linking the electrical field, E, with the local current density, J:

$$E(J) = E_c \left(J / J_c\right)^n$$

Figure 1 shows, how the voltage signals and AC losses are changed when considering flux creep in the superconductor. Significant feature is the shift of the zero value crossing with respect to the position of extreme actual values of transport current. Also, the characteristic knee is rounded with decreasing n. This is in correspondence with the expectation that by lowering the n one should find the behavior tending to that of a normal wire.

In the next step, the voltage signal is expanded into Fourier series to get harmonic components of the eletric field.

While the influence of n parameter on the higher harmonics is more significant than on the basic one , we could use harmonic analysis to describe better the behavior of superconductor during AC transport. Because AC losses are in general affected by many factors like inhomogeneity of superconductor or J_c (B) dependence we may use harmonic analysis to distinguish them by confrontation of their harmonic components.

[1] *Pardo, E., Sanchez, A., and Navau, C.: Phys. Rev.* ***B67*** *(2003) 104517.*
[2] *Klinčok, B., and Gömöry, F.: Czechoslovak Journal of Physics* ***54*** *(2004), Suppl.D 501*
[3] *Brandt, E., H.: Phys. Rev.* ***B54*** *(1996) 4264.*

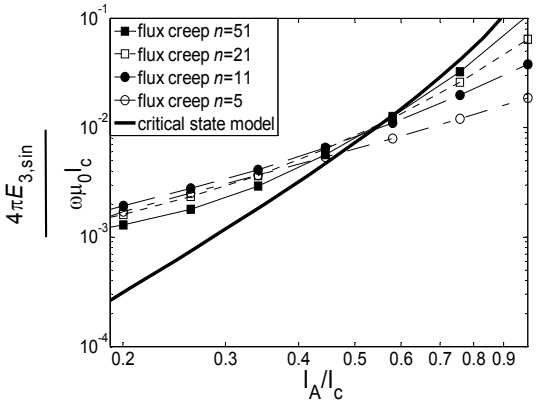

Fig. 2. Dependence of the 3rd sine component for different value of parameter n compared with criticla state model.

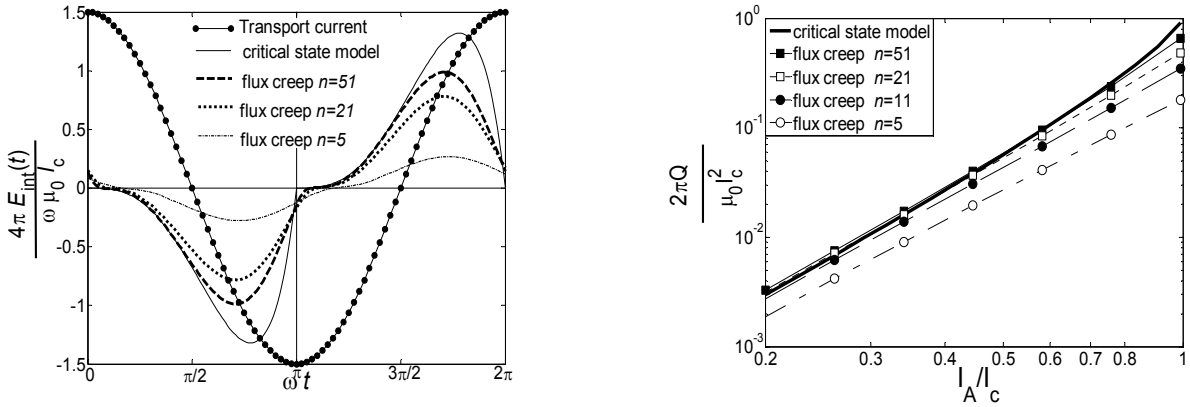

Fig. 1. Compensated voltage signal for superconductor with square cross-section for different value of parameter n on a left side. On the right side is corresponding normalized AC losses .Where I_A is current amplitude; I_C is critical current and E_{Int} electric field without inductive part due to transport current.

AC losses of superconducting flat cables due to edge currents and at additional magnetic field changes

S. Takács and F. Gömöry

The advanced superconductors for many applications (accelerators, fusion magnets, SMES, etc.) should carry large currents. Therefore, the conductors are produced in multistage process with individual parts being twisted, cabled or braided in order to reduce the *coupling losses* through different normal conducting regions. For practical reasons, the cables are usually flat. Due to the preparation conditions, the resistances between the strands are often lower at the edge regions. Therefore, the coupling losses of superconducting cables can be considerably enhanced.

Detailed results for coupling losses between *crossing* strands (*transverse coupling losses*), with additional normal conducting layer at the edges, were given previously [1]. Similar effects are expected for coupling losses between *adjacent* strands (*parallel coupling losses* – PCL), which are usually of little importance. However, if the inclusion of an insulating layer is desirable to decrease the coupling losses, the contribution of PCL to the total AC losses can become crucial.

The recent interest in YBCO *coated conductors* and the efforts to divide the surface of the superconducting layer, decreasing thus the *hysteresis* losses in these structures, is another reason for considering this problem more carefully.

Two concepts of the flat (Rutherford-type) cables are used: (1) strands soldered on a central layer (usually of stainless steel), without being in direct contact, (2) strands in direct contact, however, with some oxide layer in between. We calculate the coupling losses by including two contributions: (a) flux change between adjacent strands, (b) due to currents induced in a loop created by the same strand and the cable edge layer (until now, considered in [1] only).

The second contribution is larger than the second one, which is due to the currents between adjacent strands [2]. This result is true for any cable structures, both for strands soldered on the layer and embedded in a normal matrix, and even without better conducting region close to the edges. Of course, the situation is much worse when such an additional layer is present at the cable edges. Therefore, to maintain the coupling losses in coated conductors fragmented in tiny strips at reasonable level, the only effective way would be the inclusion of some insulating parts, segmenting the edge sheath in lengths not exceeding the cabling pitch l_0 [1,2].

Another problem connected with loss generation in cables may appear at using two or more magnets in a system. Namely, the change of the field at the position of the other ones may generate additional losses to those usually investigated. This can be caused by different reasons (redistribution of the current, relative mechanic movement of the magnets, etc.). This effect may be serious in complicated magnet designs, mainly due to the fact that the increased losses can influence the *stability* of the superconducting winding and cause eventually a premature quench of the magnet or the whole design. The typical case is the complicated magnetic system in the stellarator Wendelstein W7-X.* Therefore, we assumed that the applied field was increased up to the value of B_0 and calculated the influence of *additional field changes b* at the position of superconducting filaments, strands and cables, to the hysteresis and coupling losses.

To avoid any suspicions about the methods used and the results obtained, we performed always two different ways of the loss calculations.

The *hysteresis* losses were calculated in the Bean model with constant critical current density. As at low frequencies these losses do not depend on the special form of the field change, but only on the initial and final applied field values, we assumed for practical reasons a linear field change, τ_0 denoting the time interval for the field change. The losses are much smaller (approximately $\sim b^2$) for decreasing fields than for the increasing one (approximately $\sim bB_p$ or $\sim bB_0$ above and below the penetration field B_p, respectively). They are the highest above the penetration field and are given by $bB_p/2\mu_0$.

We solved the diffusion equation for the flux penetration to determine the *coupling* losses. We used the most realistic form of the temporal changes, namely an exponential function with τ_0 being the time constant for changing the applied field. The coupling losses are characterized by the field change b and the ratio of the time constants of the structure (τ) and of the changing field. The loss density q_c is always proportional to b^2 and for $\tau/\tau_0 < 10$ it can be approximated by a general formula

$$q_c = \frac{b^2}{2\mu_0}\frac{8}{\pi^2}\frac{\tau/\tau_0}{1+0.925\tau/\tau_0} \ .$$

Thus, for very short time constants of the structure (strand, subcable, cable), $\tau << \tau_0$, the loss density is proportional to τ, whereas for $\tau >> \tau_0$, we are close to the maximum energy ($b^2/2\mu_0$) which is transformed into AC losses. This value can be used always as the upper limit of the coupling loss density in any structure.

* We acknowledge the motivation and support for this study from the WENDELSTEIN W7-X project (Max-Planck-Institut für Plasmaphysik, Greifswald, Germany).

[1] *Takács, S.: Supercond. Sci. Technol.* ***14*** *(2001) 496.*
[2] *Takács, S.: Supercond. Sci. Technol.* ***18*** *(2005) 187.*
[3] *Takács, S. and Gömöry F.: Supercond. Sci. Technol.* ***18*** *(2005) 340.*

AC tests of short superconducting cable models

J. Šouc, F. Gömöry, and L. Frolek

Good current transport capability and low AC losses are required for the power transmission superconducting cables. With a proper design, significant improvement of these characteristics could be reached. A system for supplying of AC currents up to 2 kA at 20 – 200 Hz into short cable models was developed for this purpose. Its basic parts are cold toroidal core, Cu primary and superconducting secondary. With the help of a set of voltage taps, AC losses of the superconducting and the normal conducting parts of the secondary circuit have been determined.

Single layer cable model was explored as a load. It was constructed of 12 Bi-2223/Ag tapes situated parallel on the surface of the epoxy-fiberglass mandrel of diameter 2 cm. The critical current (77 K) of the cable model I_{cab} was 350 A and its length was 0.5 m. Brass tube was used as return conductor. The photo of the transformer and cable core is shown in Fig. 1.

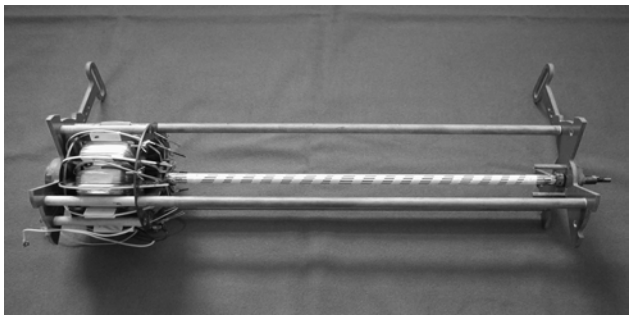

Fig. 1. Photo of the transformer and core of the superconducting cable.

In Fig. 2 the schematic set up for measurement of the AC losses is shown. As AC power source the 2.4 kW audio amplifier was used. The results presented here were obtained at 72 Hz. with help of a 7265 DSP lock-in amplifier. Current in secondary was measured by Rogowski coil (U_{rog}). Dissipation in the whole secondary circuit was evaluated as $P_{sys} = I_2 \times \mathrm{Re}(U_{sys})$, where I_2 represents the current in secondary and $\mathrm{Re}(U_{sys})$ the part of the voltage on the whole secondary in phase with I_2. This voltage was measured by contact-less loop embracing the transformer core [1].

The losses of brass tube and Cu terminals P_{tube} and dissipations on resistances P_{13} and P_{23} of the soldered connections were determined using an appropriate voltage taps. For determination of the AC loss of the superconducting cable model P_{cable} the procedure described in [2] was utilized.

Loss of the secondary winding P_{sec} was then acquired by subtracting of the P_{tube}, P_{cable}, P_{13} and P_{23} from dissipation P_{sys}, $P_{sec} = P_{sys} - P_{tube} - P_{cable} - P_{13} - P_{23}$.

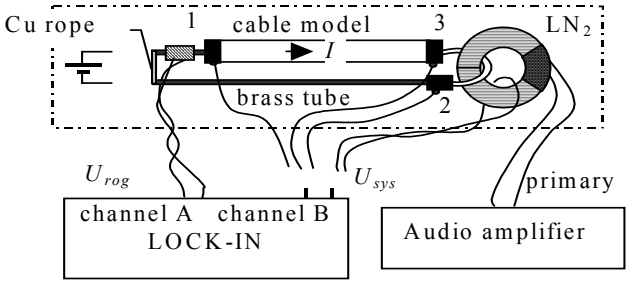

Fig. 2. Schematic measurement set up.

In Fig. 3 the losses on individual parts of the secondary in dependence on I_2 up to 700 A are shown. Loss on the metal parts P_{tube} represents substantial portion of the whole system losses P_{sys}. Only at currents $I_a = I_{rms} \times 2^{1/2} > I_{cab}$ difference between these two dependences is visible. Faster increase of P_{sys} comparing to P_{tube} is in this current region due to transition of the cable model to the normal state. Difference $P_{sys} - P_{tube}$ was calculated from difference of the analog signals U_{sys} - U_{tube}. Loss of the secondary winding P_{sec} was acquired by numerical subtracting of the P_{cable} and dissipations P_{13} and P_{23} from $P_{sys} - P_{tube}$,. In spite of higher critical current of secondary winding I_{sec} comparing to I_{cab} this loss is below I_{cab} higher thn loss of cable model. This discrepancy can be ascribed to the local AC magnetic field, in which the superconducting tapes of the secondary are situated.

[1] *Šouc, J. and Gömöry, F., Supercond. Sci & Techn.* ***15*** *(2002) 927.*

[2] *Gömöry, F., Frolek, L., Šouc, J., Colleta, G., Spreafico, S., and Tebano, R.: Proceedings of the 6th EUCAS 2003, Sorrento, Italy, 14-18 Sep. 2003, 149.*

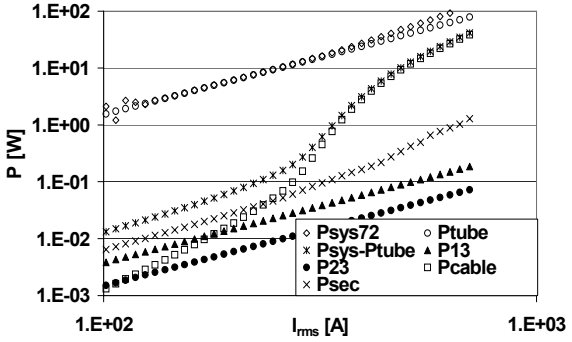

Fig. 3. Losses on individual parts of the secondary, f = 72 Hz.

Influence of non-uniform current distribution on the behavior of HTS cables for AC power transmission

F. Gömöry, L. Frolek, and J. Šouc

AC cables from high temperature superconductors (HTS) offer a solution for upgrading the existing power networks. Such cable consists of many parallel HTS tapes. It is expected that the non-uniformity in tape properties could degrade the cable performance.

Our investigation aimed on the consequences of an uneven current distribution on the cable's properties. As a model structure, short (1 meter) single layer cable with straight tapes have been manufactured – see Fig. 1 - and the properties of all its tapes determined in DC regime [1,2]. Additional factor influencing strongly the distribution of currents in such a short model is the spread in contact resistances. Different voltages appear on different tapes and the traditional definition of critical current becomes doubtful [3]. On the other hand, we have found both experimentally and with the help of a Finite Element simulation, that the spread of tape properties, typical for the state-of-the-art production, does not lead to a significant increase in the transport AC loss [4].

The most intriguing phenomenon documented in our AC experiments was the existence of phase shifts between the currents in the tapes. As a consequence, local magnetic fields could contain a component shifted in phase with respect to the total current in the cable. Then it is possible to understand the existence of false signals in electrical measurement of transport AC loss. Moreover, these signals can be used to deduce the phase shifts without necessity to place particular sensors – see Fig. 2. The correct value of AC loss can be extracted from the average of data taken on a set of voltage taps symmetrically placed on the cable – Fig. 3 [5].

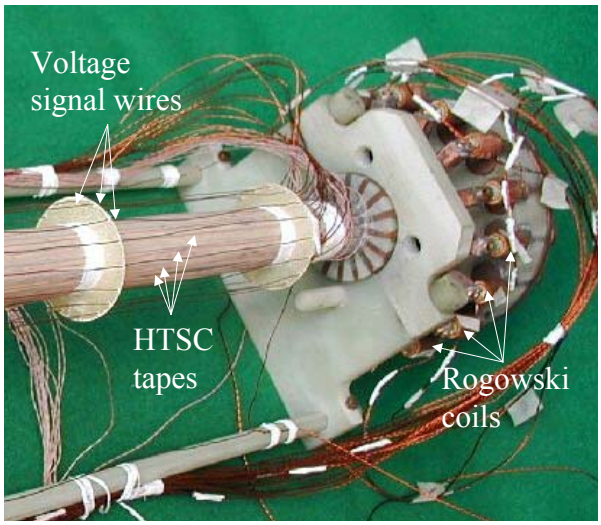

Fig. 1. Short model of superconducting power transmission cable manufactured on purpose to study the splitting of total cable current into individual tapes.

These activities have been carried out in collaboration with Pirelli Cables (Milan, Italy) and EPFL Lausanne (Switzerland).

[1] *Gömöry, F., Frolek, L., Šouc, J., Coletta, G., and Spreafico, S.: IEEE Trans. on Applied Supercond.* ***13*** *(2003) 1968.*
[2] *Frolek, L., Šouc, J., and Gömöry, F.:, Czechoslov. J. Phys.* ***54*** *(2004) Suppl. D497.*
[3] *Frolek, L. and Gömöry, F.: Physica C* ***401*** *(2004) 227.*
[4] *Grilli, F., Stavrev, S., Dutoit, B., Spreafico, S., Tebano, R., Gömöry, F., Frolek, L., and Šouc, J.: Physica C* ***401*** *(2004) 1761.*
[5] *Gömöry, F., Frolek, L., Šouc, J., and Grilli, F.: IEEE Trans. on Applied Supercond.* ***15*** *(2005) accepted.*

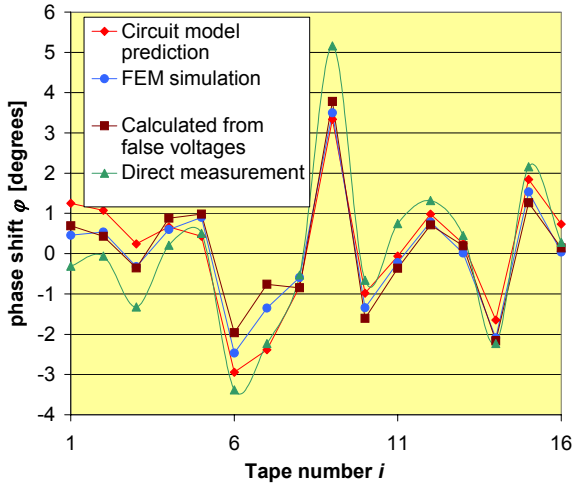

Fig. 2. Phase shifts of tape currents.

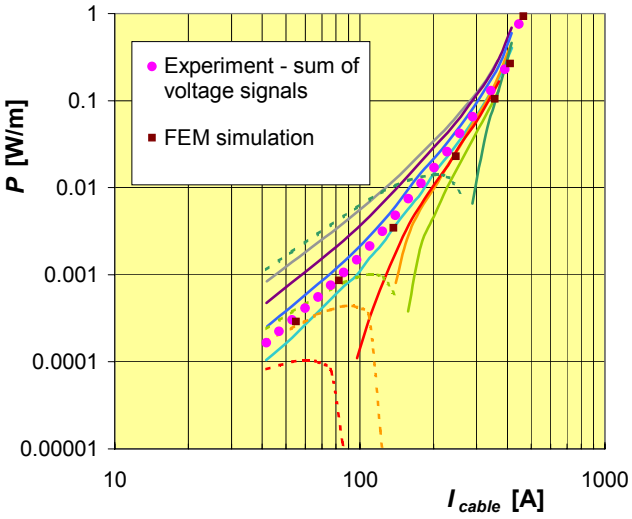

Fig. 3. AC loss determined from the sum of measured voltages, compared with FEM prediction. Raw experimental data (lines) exhibit spread due to non-uniformity of current distribution .

Department of Electrodynamics of Superconductors

Milan Polák

Research scientists
František Chovanec
Lubomil Janšák
Ludovít Krempaský
Elemír Ušák
Pavol Ušák

Technical staff
Dagmar Erbenová
Jozef Talapa
Jana Ryzá

Research Engineers
Jozef Kvitkovič
Pavol Mozola

PhD Student
Eduard Demenčík

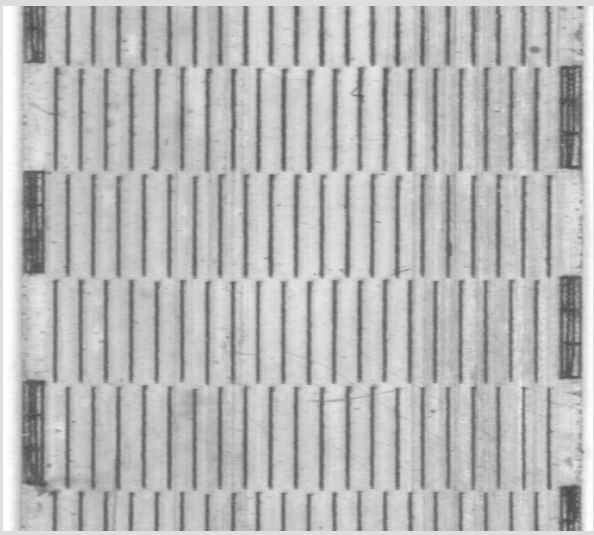

Our research was focused on four groups of problems: Study of electromagnetic properties of superconducting tapes $(Bi,Pb)_2Sr_2Ca_2Cu_3O_x$ (BSCCO), with emphasis on the use of contactless methods.

Study of electromagnetic properties of YBCO ($YBa_2Cu_3O_x$) coated conductors and development of an YBCO based conductor for AC use.

Development and testing of superconducting model transformers using BSCCO and YBCO tapes.

Experimental work associated with application of conventional superconductors (measurement system for current distribution measurement in bus-bar TFMC (Toroidal Field Magnet Coil), measurement of magnetization in LHC (Large Hadron Collider) cables, joining of Nb_3 Sn strands.

Projects:

*Transverse Resistivity of YBCO Coated Conductors for AC Use (*11/2003-10/2005), *Project FA 8655-03-1-3082*, European Office of Aerospace Research and Development (EOARD), US Air Force project

Measurement of the current distribution inside superconducting cable - supply and installation of Hall probe measuring system and joining of multifilamentary Nb_3Sn strands, 06/2003 – 06/2004, project number FU 06 – CT -2003 – 00041, EURATOM/EFDA

Applied Superconductivity Training and Research Advanced Center, ASTRA, 1/2003 až 12/2005, project number: ENK6-CT-2002-80658, EC project

Thanks to small active area Hall probes developed in our department we extended and improved contactless methods for characterization of superconducting samples. A great effort was paid to understanding of AC loss mechanisms in BSCCO tapes and in samples of second generation of HTC (High Critical Temperature tapes: coated conductors YBCO/Ni and YBCO/Hastelloy. We also developed and compared various experimental methods for the loss determination. Besides the classical method - analog integration of the pick-up coils voltage - we built and tested a measuring set-up based on Fourier analysis of the pick-up coil voltage and a set-up using lock-in nanovoltmeter. Hall probe method is based on measurement of sample magnetic field and its main advantage is the absence of signal drift. Determination of losses from the sample heating provides very reliable data in a limited interval of loss power.

YBCO coated conductors are prepared as a continuous YBCO layer on Ni or NiW substrates. They have very large AC losses if exposed to an external magnetic field oriented perpendicular to the tape plane. To reduce hysteresis losses, YBCO layer must be divided into narrow filaments with a small interfilamentary gap. In collaboration with University of Wuppertal, Cryoelectra Wuppertal and Department of Cryoelectronics in our Institute we prepared YBCO filamentary samples and studied their electromagnetic behavior. Mapping of sample magnetic field due to AC external magnetic field with frequencies up to ~ 500 Hz represents a powerful tool for sample diagnostic and shall be applied in experiments with YBCO coated conductors for AC use.

In the frame of NATO project and in collaboration with SKODA vyzkum sro and University of Wuppertal we developed and tested 2 models of 14 kVA transformer with superconducting winding made of Bi-2223/Ag tape. After tests at SKODA we rebuilt the transformer and prepare it for further studies.

The department is also involved in the Euratom/EFDA research activities. We participated in the current distribution measurements in large superconducting cables for BBIII (Bus Bar III), PFCI (Poloidal Field Coil Insert), and FSJS (Full Size Joined Sample).experiments.

International cooperation and informal scientific contacts with foreign Institutions contribute to the results of our department significantly. We collaborated with following Institutions: University of Wuppertal, Germany and Cryoelectra GmbH, Wuppertal, Germany (superconducting model transformers, YBCO coated conductors), Institut für Festkorperphysik, Technische Universität Wien, Austria (characterization of HTC tapes), Institut für Technische Physik, Germany (AC losses in HTC tapes), Tampere University of Technology, Laboratory of Electromagnetics, Finland (magnetic fields in the vicinity of HTC samples), Skoda výskum sro., Czech Republic, (superconducting transformers), Florida State University (Cobase) and Seconda Universita di Napoli (current distribution in cables for the fusion research).

Milan Polák

Magnetic fields in the vicinity of HTS superconductors Bi-2223/Ag and Y-123 exposed to AC magnetic fields

E. Demenčík and M. Polák

Magnetic field in the vicinity of Bi-2223/Ag and Y-123 filamentary tapes exposed to a time dependent magnetic field provides useful information about currents flowing in the sample. In Bi-2223/Ag and Y-123 stabilized with metallic layer all kinds of currents such as magnetization, coupling and eddy currents may be present, while in multifilament Y-123 tapes on $LaAlO_3$ substrates only intrafilament currents can flow. We measured magnetic field due to currents induced by AC external magnetic field applied perpendicularly to the tape face. The Hall probe technique is used to investigate the magnetic field in the vicinity of the measured sample. Cu magnet generates external AC magnetic field with amplitudes up to ~ 35 mT. Hall probes with active area 50 x 50 μm^2 and sensitivity ~ 170 mV.T^{-1} are used to get a signal proportional to the magnetic field of the sample current. The measuring probe provides signal from the sample, perpendicular component of magnetic flux density B_z is superimposed on the external field signal B_e. For external field signal compensation a compensation Hall probe is used. Moreover, the final signal suffers also from parasitic induction voltage originating in instrument leads. The induction voltage is not negligible and must also be compensated. Measuring cards National Instruments PCI - 6034E are used for data acquisition.

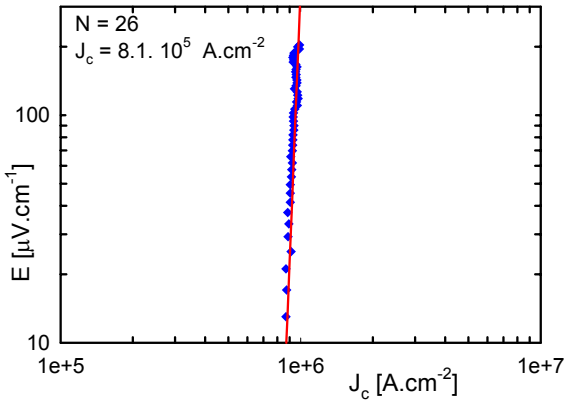

Fig. 1. E-J curve of the Y-123 sample with thin film layer 4.2x16 mm^2, non filamentary sample.

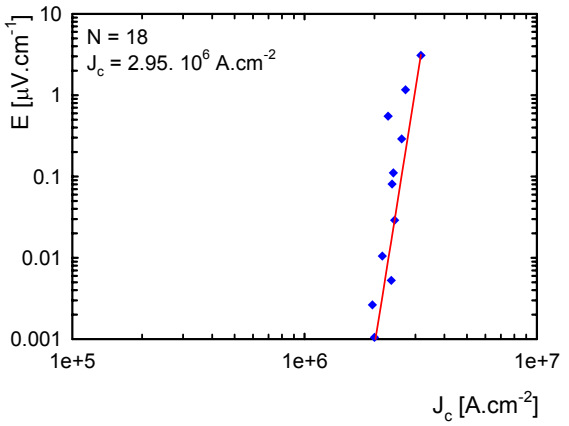

Fig. 2. E-J curve of the Y-123 multifilament sample 3.3x40 mm^2, 60 filaments 50 μm wide.

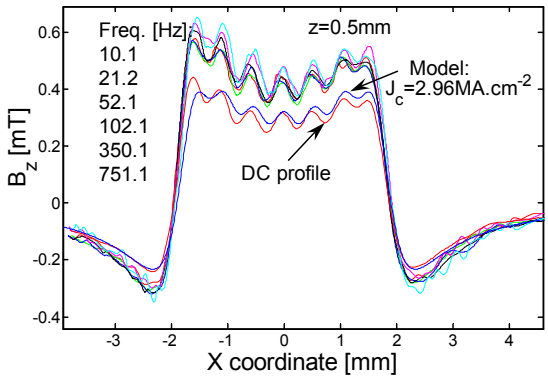

Fig. 3. AC magnetic profiles for various frequencies, sample with 7 filaments 0.5 mm wide.

By measuring hysteresis loops $B_z = f(B_e)$, above the central point of the sample, we measured the frequency response of the sample to the applied magnetic field. From the width of the hysteresis loop it is possible to determine the *E-J* curve in a non-destructive manner [1, 2]. In Fig. 1, 2 the respective *E-J* characteristics are shown. It can be noticed that the sample covered with continuous layer (Fig. 1) shows higher *N*-exponent, which indicates better homogeneity of the sample than it is in the case of striated sample.

Using the Hall probe technique it is possible to scan the magnetic field due to the currents in the sample generated by applied AC magnetic field. In Fig. 3, the magnetic profiles of the sample with 7 filament layout for various frequencies of applied magnetic field in the range 10 - 750 Hz can be seen. Also, the DC profile is shown to see the different sample response in AC field. The model assuming constant current distribution in the individual filament is compared with the measured data.

[1] *Demencik, E., Polak, M., Wehler, D., Moenter, B.: EUCAS 2003, Sorrento, Poster.*
[2] *Demenčík, E.: Workshop ASTRA, Bratislava, April 2004.*
[3] *Polák, M., Krempaský, L., Demenčík, E.: Workshop ASTRA, Bratislava, April 2004.*

AC losses in YBCO coated conductors - comparison of data, obtained by different measurement methods

L. Janšák

For YBCO tape AC loss measurement we used different measurement methods. All methods are described in detail in the AFOSR final report [1].

1. AC loss measurement using pick-up coils and analog integration.

For the measurement we used the dipole magnet. Three kinds of calibration samples were used: the first one was made using two 4.9 mm wide and 100 mm long copper foils connected at one end and supplied by a current, the second one was a loop made by copper wire with the same dimensions as the sample (10mm x 100 mm) and the third one was a copper foil with the same dimensions as the samples. This method is not suitable for frequency over 1 Hz.

2. Determination of AC loss from the sample heating.

AC losses due to currents induced by AC external magnetic field heat the sample. If the sample is well cooled (it is immersed in liquid nitrogen), its temperature slightly increases and the heat evaporates liquid nitrogen.

If the sample is thermally insulated, the losses give rise to measurable temperature increase of the sample. The sample temperature is proportional to the produced heat and can be used to determine the AC losses, as shown by Ashworth and Suenaga [2]. It was necessary to develop a new Cu coil for the measurements of samples 10 cm long and 1 cm wide. We designed and manufactured a dipole coil, which has the inner diameter 40 mm, length 120 mm and the field / current constant of 0.97 mT/A. The power supply KEPCO BOP 20-20M with maximal current of 20 A the dipole can produce magnetic field with amplitudes up to ~ 20 mT. Using two KEPCO power supplies connected in parallel it is possible to reach ~ 40 mT. The frequency interval is from 20 Hz up to 560 Hz. At frequencies above 100 Hz in series with the dipole we connected a battery of capacitors and modified the capacity to reach the series resonance. The sensitivity of this method is limited for low and high losses.

3. AC loss measurement using pick-up coils and evaluation using a Fourier analysis.

The principles of the measurement method and experimental equipment for the measurement of magnetization curves and evaluation of AC power losses was described in [3]. The measurement was made fully automatic. Magnetic field and magnetic moment vs. time waveforms are displayed on the computer screen. The calibration based on direct AC power loss measurements has been carried out. Two model samples with the power losses calculated from known sample dimensions and specific resistance were used. The first one was a sample made of single copper strip, in which the AC power losses correspond to eddy-current losses.

4. AC loss measurements in samples using 1ock - in nanovoltmeter.

The advantage of this technique is the high (6 orders) sensitivity of the measurements. However, the method is very sensitive to the deformation of the magnetic field. The measured frequency dependence of loss per cycle at small field amplitudes at which the hysteresis losses in the filaments are very small.

At 0.2 mT and 0.5 mT the losses increases proportional to frequency, which indicates that the losses have the character of the coupling losses.

The comparison of two methods (with possibility of frequency measurement and high sensitivity) for three YBCO samples B0, B3 and B5, (B0 – non striated with Ag layer, B3 – filament with bridges, B5 – non striated, Hastelloy substrate) at 20 Hz are shown in Fig. 1.

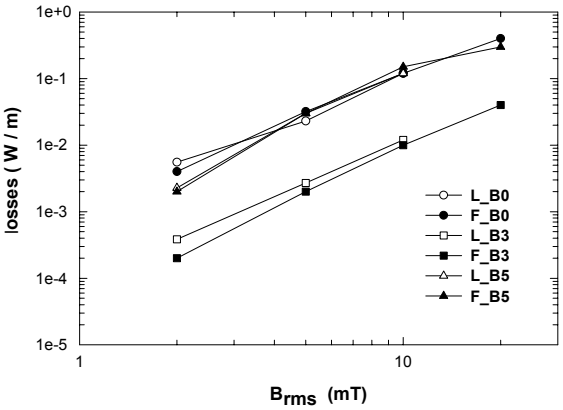

Fig. 1. Comparison of AC losses measurements by two different methods (L – lock-in, F – Fourier analysis).

The mean error of the AC loss measurements for the frequency of 20 Hz in the applied field 2 – 10 mT is ± 8% (B0), ±17.7% (B3) and ±8.7% (B5) sample.

Polák, M. at al.: AFOSR Final Report, IEE SAS, Bratislava, Oktober 2004.

[1] *Ashworth,S.P and Suenaga M.: Physica* ***C315*** *(1999) 79.*
[2] *Ušák, E., Janšák, L., Wehler, D., Mönter, B., and Polák, M.:Journal of Electrical Engineering* ***53*** *(2002) 161.*

Heating of Bi-2223/Ag tapes and coils

M. Polák, J. Kvitkovič, and P. Ušák

We studied experimentally current – voltage (*I-V*) curves and the temperature of homogeneous short samples of Bi-2223/Ag multifilamentary tapes immersed in liquid nitrogen and carrying a transport current in the resistive state [1, 2]. Current-voltage (*I-V*) characteristics of Bi-2223/Ag tapes cooled by liquid nitrogen measured with increasing and decreasing transport current under the self field conditions are not always identical. The curves measured with increasing and decreasing current were identical at low values of electric fields up to some microvolts per centimeter only. At electric fields above this value we observed hysteretic behavior of I-V curves. At a given value of the transport current the electric field is larger in the case of the increasing current than that measured at the decreasing current. The hysteretic behavior was observed in two interval of electric fields. The first one is between 10 and 100 μV/cm, in which the hysteresis can be removed by a small external magnetic field, as shown in Fig. 1. This behavior indicates that the hysteresis is an effect associated with magnetic fields and magnetization currents and it is not a thermal effect. To prove this assumption we studied the temperature of the measured samples carrying transport current in the resistive state. O heating effect which could cause such hysteresis was observed. At electric fields above ~ 1 mV/cm we observed a strong heating of the sample and a sudden drop of the measured voltage at increasing current and heat flux of about 0.4 to 1 W/cm^2, as illustrated in Fig. 2. The voltage drop was always accompanied by a sudden decrease of the sample temperature.

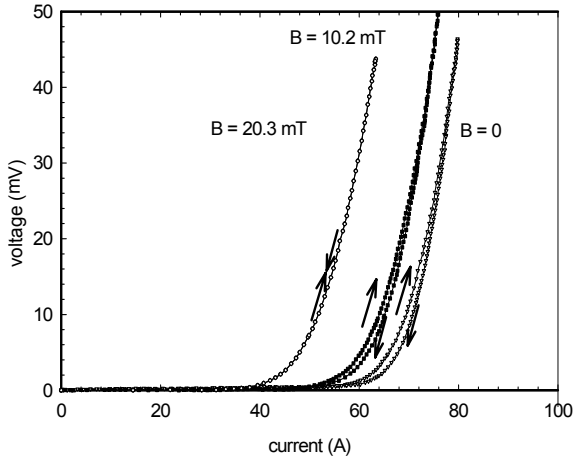

Fig. 1. I-V curves of Bi-2223/Ag sample measured at increasing and decreasing current. We clearly see the hysteretic behavior at zero external field and. External field of 20.3 mT completely removed the hysteresis.

In this case the drop can be seen also in the external magnetic field.

We also studied heat transfer characteristic using copper tape with dimensions similar to those of the superconducting samples. Finally, we measured a superconducting sample with an artificial inhomogeneity locally reducing the critical current.

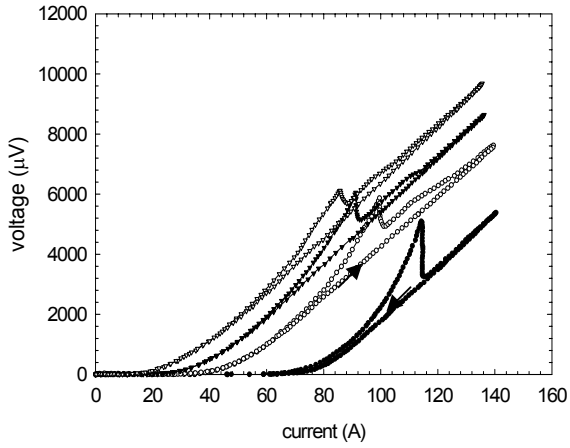

Fig. 2. I-V curves of Bi-2223 Ag sample for currents above I_c. Note the voltage jump observed at increasing current.

Studies of heating were also made with an experimental coil wound with Bi-2223/Ag multifilamentary tape. Heating was observed at currents above the critical current in DC regime. In AC regime the losses caused the coil heating at currents far below the critical current.

[1] *Polák, M., Kvitkovič, J., Demenčík, E., Janšák, L., and Mozola, P.:, Physica C* ***401*** *(2004) 160.*
[2] *Sastry, P., Nguyen, D., Usak, P., and Schwartz, J.: Superc. Sci. Ttechnol.* ***17*** *(2004) 314.*

Current-voltage characteristics of Bi-2223/Ag multifilamentary tapes exposed to inhomogeneous magnetic field

J. Kvitkovič

Bi-2223/Ag tapes in some winding sections of magnets, transformers, motors and generators are exposed to inhomogeneous magnetic fields. Current-voltage *(I-V)* curves and critical currents I_c are usually measured in homogeneous magnetic field and the determination of critical current in the case of inhomogeneous magnetic field is not a standard procedure.

We measured *I-V* curves of three different multifilamentary Bi-2223/Ag tapes in inhomogeneous and in homogeneous external magnetic fields with the aim to determine and compare the critical currents in both cases. In our simple model we supposed inhomogeneous field with constant field gradient across the tape width [1]. The main goal of our experiments was to find whether we could determine I_c of the tape in inhomogeneous magnetic field if we know *I-V* curves and I_c of the tape in homogeneous magnetic field.

In our experiments we used three multifilamentary tapes with different $I_c(B=0)$ values. Tapes 1, 2 and 3 had critical currents 24 A, 60 A and 138 A, respectively. The length of the measured samples was 30 mm. The *I-V* characteristics were measured with three pairs of potential taps located on both sample edges and in the sample center.

For generation of external field for the tapes we used special electromagnet with C-iron core with 8 mm air gap. The same magnet was used for tape measurements in homogeneous and inhomogeneous fields, only the position of the tape with respect to the iron core was different. The values of magnetic field B_{ce} in the center of the tape and corresponding magnetic field gradients were controlled by magnet current. The tape was placed on sample holder in air gap so that the magnetic field is perpendicular to the tape and the magnetic field gradient is oriented through width of the tape.

The Hall probe was mounted on the surface of the BSCCO tape to monitor the value B_{ce} during all measurements. Crucial point of the experiment is the precise position of the center of Hall probe active area on BSCCO tape longitudinal axis. Active area of the Hall probe must be placed very close (0.2 mm) to BSCCO tape to measure magnetic field on the tape surface, because in inhomogeneous magnetic fields the measurement error due to displacement could be very high. Hall probe center position on tape was checked by optical microscope. Also the active area of the Hall probe used for inhomogeneous magnetic field measurements should be very small (0.1 mm) in order to increase the space resolution of the measurement. Our Hall probe, produced at our department, had active area 0.1 x 0.1 mm^2 and sensitivity 182 mV/T at 77 K. At first we measured *I-V* curves in zero external field out of magnet, then in homogeneous magnetic field of B_{ce} and then the sample was moved to inhomogeneous magnetic field. The magnet current was set to the value at which the magnetic field in the sample center is also B_{ce}, then *I-V* curves were measured again. This procedure was repeated with all tapes. Critical currents were measured by standard four-point method. The criterion for I_c evaluation was 1 μV/cm. All measurements were done at 77 K in liquid nitrogen bath.

$I_c(B)$ characteristics of Tapes 1, 2 and 3 measured in homogeneous and inhomogeneous fields are presented in Fig. 1. We observed slightly higher I_c in inhomogeneous fields for tapes with higher I_c in $B = 0$, (Tapes 2 and 3) or critical currents were practically identical (Tape 1). Within 2% of measurement precision we can say that the critical currents of all our tapes measured in homogeneous magnetic field are the same as those determined in inhomogeneous magnetic field with the same mean value of magnetic field across the tape width.

According to our simple model and our measurements we can conclude that it is possible to estimate I_c of the tape in inhomogeneous magnetic field if *I-V* curves and I_c of the tape in homogeneous magnetic fields are known.

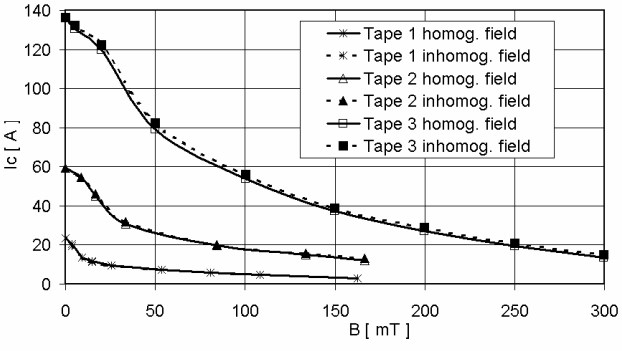

Fig. 1. Comparison of $I_c(B)$ characteristics of all tapes measured in homogeneous and inhomogeneous fields.

This work was supported by the Grant Agency of the Slovak Academy of Sciences VEGA No. 2/7197/20, NATO project SfP 974124 and OST Programme of BMBWK, Austria, GZ45.481/2-VIII/B/2a/2000.

[1] *Kvitkovič, J. and Polák, M.: Physica C* ***401*** *(2004) 146.*

Characterization of YBCO thin film samples using Hall probe contactless measurements

E. Demenčík, J. Kvitkovič, and M. Polák

Complex electromagnetic characterization of superconducting samples is a very important part of the technology developments. It is very important to study the sample response to various technology steps without affecting the sample by introducing contacts, changing sample shape, etc. Very often contact problems make the use of resistive methods impossible.

Since several years we develop and improve contactless methods for the characterization of superconducting samples at liquid nitrogen temperature, which allow determining several important electromagnetic properties of high temperature superconductors [1]. The method is based on the measurements of magnetic fields due to magnetization currents, in the vicinity of the sample. The measurements can be done in two regimes:

a) In the "static" regime, when persistent (frozen-in) currents flow in the sample. In this case we can determine the critical current, I_c, or critical current density, J_c, however, it is not easy to determine the electric field corresponding to these values of I_c and J_c. We can also determine I_c or J_c in magnetic field and $J_c(B)$ and $I_c(B)$, as well as, under circumstances, irreversibility field *Birr*. The measurements of the time dependence of magnetic field allows to determine J_c and the corresponding electric field, E, however, this is possible in very low electric field part of the *E-I* curve only. Further, by mapping the sample magnetic field we can obtain information on the sample homogeneity, localize "weak sections" of the sample and detect filament bridging [2]. It is also possible to determine the field of the full penetration, B_p.

b) In the dynamic regime, when AC external field is used and the magnetization currents are also changing. In this case we have to measure magnetic field in an appropriate point in the vicinity of the sample vs. external field for various frequencies of the external field. From these measurements we can determine *E-I* curves in various magnetic fields [3]. The electric fields are considerably larger than those in the relaxation experiment (static regime) and can be compared with those obtained by transport measurements. We can also measure hysteresis curves $B_{zs} = f(B_e)$ at various frequencies, determine the loss components and determine total losses vs. external field at the constant frequency [4]. To be able to study sample fields at higher frequencies, we have developed also measuring systems based on the use of data acquisition cards with sample rates up to 200 kS/sec [5]. Sometimes the differences between the critical currents determined by the magnetic measurements are quite different from those obtained by transport measurements. This is done by two main factors: differences in electric fields and the sample inhomogeneity. In the following we illustrate the method by comparing magnetic and transport measurements on the following YBCO sample dimensions: 4.3 x 28 mm^2, $LaAlO_3$ substrate, YBCO thickness 0.4 μm, covered by 0.5 μm Au layer. The frequencies of the external magnetic fields changed from 1 mHz to 100 mHz.

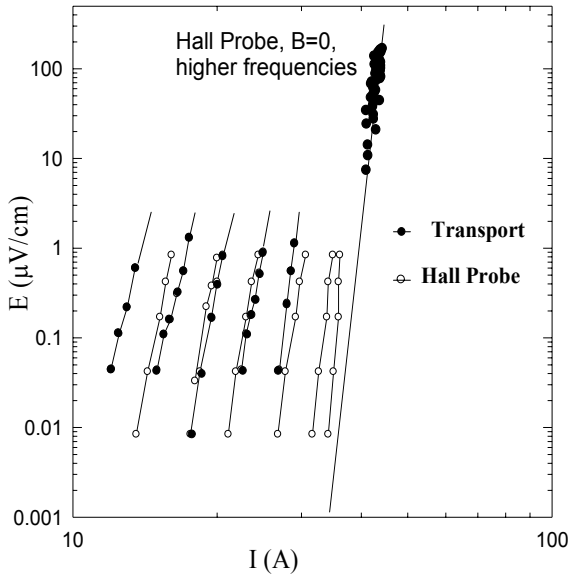

Fig. 1. Electric field – current characteristics of the sample, described in the text, obtained by magnetic field measurements with the Hall probe and transport measurements at 77 K in various magnetic fields. Transport measurements (from the right to the left): B_e = 9.3 mT, 18.6 mT, 37.2 mT and 93 mT. Magnetic measurements were done at the same fields. The first curve from the right was determined at frequencies of the order of 100 Hz, hence the corresponding electric fields are larger.

As seen, the *E-I* curves measured by transport and magnetic methods are very close one to the other and prove the usefulness of the magnetic method.

[1] *Polák, M., Windte, V., Schauer, W., Reiner, J., Maurer, W., and Wühl, H.: Proc. 6th Int. Symposium on Weak Superconductivity. Ed. Š.Beňačka. Singapore, World Sci. Publ. 1991. P. 43.*

[2] *Kvitkovič, J. and Polák, M.: Physica* ***C372-376*** *(2002) 1012.*

[3] *Polák, M., Windte, V., Schauer, W., Reiner, J., Gurevich, A., and Wühl, M.: Physica* ***C174*** *(1991) 14.*

[4] *Polák, M., Krempaský,L., Chromík, Š., Wehler, D., and Moenter, B.: Physica* ***C372-376*** *(2002)1830.*

[5] *Demenčík, E., Polák, M., Wehler, D., and Moenter, B.: Applied Superconductivity 2003. Proc. of the 6th EUCAS, Sorrento 2003. IoP Conf. Ser. No 181. Eds. A. Andreone et al. Bristol: IoP 2004. P. 2427.*

Current distribution in Nb_3Sn multiplets with joint measured at 4.2 K

P. Ušák, F. Chovanec, P. Mozola, and M. Polák

Large superconductors for fusion magnets consist of several hundreds of strands. The strands are assembled into the cable. The cabling loss, i.e. the percentage of superconducting strand lost during the manufacture of the cable has been found to vary between 4% and 15%, depending mainly on strand breakages during cabling and on the unit length of strand; the shorter the length, the larger the percentage lost. To avoid this strand loss the demand arose to solve the problem of strand joining during cabling.

We developed a method for strand joining. Joints of two types of Nb_3Sn conductors were prepared and tested, VAC strand and EM strand. Both strands have the diameter of 0.81 mm. The first one is a bronze Nb_3Sn strand manufactured by Vacuumschmelze (VAC), Germany, and the second one is internal tin Nb_3Sn strand produced by Europa Metalli (EM), Italy. The properties and applications of strands in cables are described in Ref. [1-4]. Nb_3Sn wires with and without joints were prepared and tested. Beside individual strands we tested also doublets and triplets of strands twisted together to check behavior of current-voltage characteristics and current distribution in doublets without joint and with one joint in multiplet. Measurement of *I-V* curves in different external magnetic fields and for different orientations of wires were made. The testing of samples of multiplets showed that the current is in general not uniformly distributed among the strands. The identification of reasons causing the non-uniform current distribution in these samples is of basic importance for the correct understanding of the behavior of multiplets in which also joined strands are used [5,6]. The reason is the inhomogeneity of resistance at soldered ends of strands in contact with current leads. The problem was solved by inserting sufficiently large resistances (copper wires) in series with the strands.

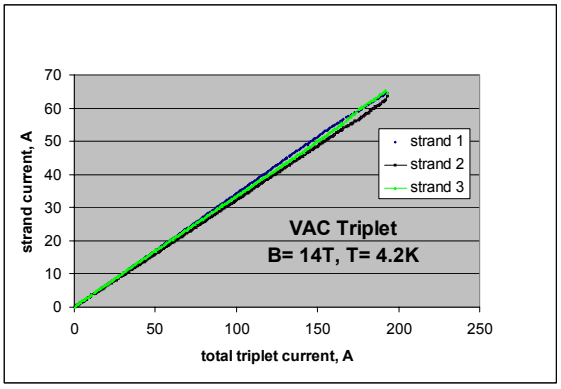

Fig. 1. Current distribution among strands of triplet (VAC-T0-1). Serial copper resistances are involved. Current differences are under 2%.

The equalization of current achieved by inserting serial shunts was observed also in multiplets with one joined strand. The heating in the joint is ~2 mW at 100 A (R = 0.2 μΩ). Joint resistance is approximately one order lower than the resistance of the shunt in series with the strand. As a result, the current distribution in the doublet or triplet with one joined strand is close to the uniform one.

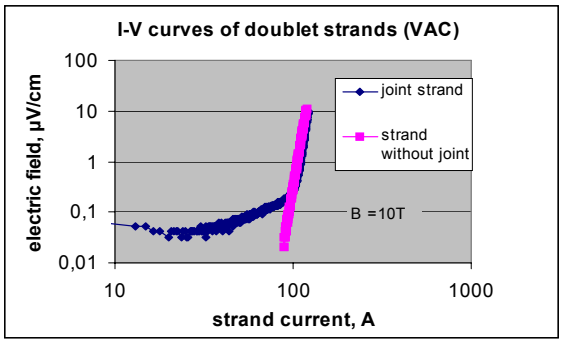

Fig. 2. Additional heat treatment of joined strand during joint creation resulted in somewhat higher critical current of the strand. Current distribution inhomogeneity in the region below I_c is less than 1%.

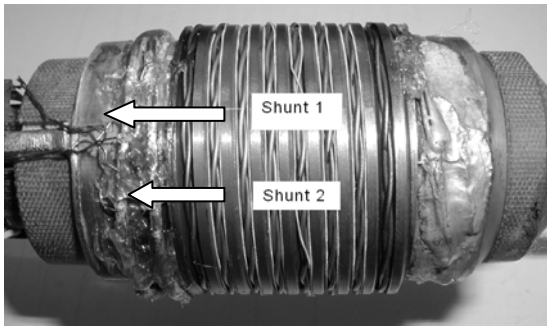

Fig. 3. Sample holder with resistive copper shunts in series with strands.

[1] *Duchateau, J.-L., Spadoni, M., Salpietro, E., Ciazynski, D., Ricci, M., Libeyre, P., and Della Corte, A.: Supercond. Sci. Technol.* ***15*** *(2002) R17.*
[2] *Mitchell, N. et al.: 1998 Proc. 15th Int. Conf. on Magnet Technology (Beijing: Science Press) p.347.*
[3] *Della Corte, A. et al.: 1998 Proc. 20th Symp. On Fusion Technology (Marseille, France) p. 841.*
[4] *Hense, K.:, EUCAS 2003, Sorrento, Italy.*
[5] *Chovanec, F., Muller, M., Kirchamay,r H., Fillunger, H., and Polak, M.: EUCAS 2003,, Sorrento, Italy.*
[6] *Mulle,r M., Schulz, H., Lackner, R., Kirchmayr H., Fillunger, H., Mai,x R., Polak, M., and Chovanec F.: EUCAS 2003, Sorrento, Italy.*

Hall probe measuring systems for current distribution measurements in FUSION related experiments

M. Polák and J. Kvitkovič

A number of research work investigate the behaviour of superconducting "Cable-in-Conduit Conductors" (CICC) for ITER (International Thermonuclear Experimental Reactor) magnets. Department of Electrodynamics of superconductors participated in experimental program focused on the current redistribution in CICC superconducting cables. Within the framework of the European FUSION Program Hall probe measuring heads have been designed, manufactured and tested.

High current superconducting cables consist of superconducting wires assembled in petals. Six petals are placed into a stainless steel jacket. Fig. 1 shows on CICC type of cable. The current redistribution in such cables depends on various factors. During current ramp up minor differences in inductive coupling between strands could produce large differences in individual currents. The resistance variation in individual strands at the cable terminations and within the cable will determine the current flowing in each strand.

In the strands themselves, the current flow is limited when the strand reaches critical conditions, locally somewhere along its length. The resultant voltage can lead to a current redistribution. Cables with some transverse conductivity can redistribute the current within the cable, with this redistribution eventually propagating back to the joint. In cables that do not permit an internal current redistribution, severe stability problems can occur, even in steady state conditions.

Current redistribution is very important issue as it may influence the total performance of a CICC cable. Unfortunately, the direct measurements of current redistribution inside a CICC are not possible. An indirect approach for the current profile estimate can be based on the measurement of the magnetic field around the CICC cable. The measuring systems are based on Hall Probe (HP) heads placed around the cable suitably located as near as possible to the surface of conductors.

In the period of 2002 - 2004 our department contributed to the following experiments:

TFMC - Toroidal Field Magnet Coil (experiment in Institute for Technical Physics (ITP) Karlsruhe)
BB III - Bus Bar III (experiment in ITP Karlsruhe)

FSJS - Full Size Joined Sample (experiment in Paul Scherrer Institute (PSI) Villigen)
PFCI - Polodial Field Coil Insert (experiment in ITER Naka)

TFMC:

For the 2002 test campaign on the toroidal field model coils (TFMC), two measuring heads, each provided with twelve Hall probes, were installed on one of the busbars at a distance of a quarter of a twist pitch [1]. The aim was to obtain the current redistribution at the location of the measuring heads. The magnetic field in the head location was also affected by the current flowing in the return conductor. These effects can be calculated on the basis of the known geometry. We tested the measuring heads with a resistive mock-up of the TFMC busbar. The mock-up had six petals, insulated one from another, of which one could be fed with a current independently from the other five. In one of the test cases, the five petals were fed with current of 600 A (120 A in each petal) while the sixth was unloaded.

BBIII:

The Bus Bar III (BBIII) experiment was located at the TOSKA facility at the ITP Karlsruhe, Germany. The BBIII consists of 7 m long NbTi superconductor with a thick square stainless steel jacket, cooled by supercritical He. It was energized with currents up to 80 kA and operates in its self magnetic field up to 0.8 T. The BBIII was instrumented by two Hall probe heads Fig. 2 with 12 HPs in each head and linear array with 16 HPs for magnetic field measurements, in order to get experimental data to be used for the validation of a hybrid thermal-hydraulic electro-magnetic code (THELMA), as well as for the assessment of the possibility of performing a reliable reconstruction of the current distribution on the conductor cross section under controlled conditions. In the tests, the current ramps at different rates were applied to characterize the conductor time constants. Two different resistive heaters were separately operated in order to approach forced current sharing in the conductor and to observe the related current redistribution. The magnetic measurements indicated a strong current redistribution several hundreds of seconds before the quench. These results could facilitate the protection of large coils [2].

FSJS:

FSJS has been designed and manufactured by European Industry using Polodial Field coil NbTi superconductor. In contrast to other samples, this FSJS uses the Central Solenoid Model Coil joint design with NbTi conductor and thick wall stainless steel square jacket. One leg of the FSJS has had both the conductor and subpetal stainless steel wraps removed at the time of jacketing and compaction, in order to assess the

difference in the superconducting cable performance between the two configurations.

In the FSJS experiment six measuring heads (Fig. 3) with ten HPs each have been placed around the two cable sections to be tested. During installation the Hall probe heads were precisely positioned in terms of angular orientation and fitted to the jacket.

The acquisition and signal conditioning system for the Hall probes was based on National Instruments devices, allowing to detect the field signals with an overall nominal accuracy better than 1%, the observed noise in the Hall probe signals was of the order of ± 0.1 mT [3]. This experiment showed that in the case of HP laying in large parallel magnetic field components the planar Hall effect could considerably affect measurement precision. Our experiments with planar Hall effect led to the change of the parameters of semiconducting material for HP for PFCI experiment.

PFCI:

The Poloidal Field Conductor Insert (PFCI) has been designed in the EU and is being manufactured at Tesla Engineering, UK. Completion of the PFCI is expected at the beginning of 2005. The PFCI consists of NbTi dual-channel conductor, 45 m long, with a 50 x 50 mm^2 square stainless steel jacket, wound in a single-layer solenoid. It should carry up to 50 kA in a field of 6 T, and it will be cooled by supercritical He at 4.5 K and 0.6 MPa. The PFCI will be instrumented with two measuring heads carrying HPs. They will be fixed to circular machined sections of the PFCI conductor [4]. Each circular head has 20 Hall probes distributed symmetrically around the cable 24.3 millimeters from the conductor axis. To minimize the effect of the background field, the voltage difference between the Hall voltage of each HP and that of the probe located on the other side of the cable axis in the radial direction will be measured. While the Hall voltage due to the cable current has the same sign for both HPs, the voltages due to the external field have opposite signs and they cancel mutually.

Hall probes with sensitivity of 40-65 mV/T at control current of 100 mA, with linearity error < 0.2 % in magnetic field interval ± 4 T were used. HPs (Fig.4.) for PFCI experiment were calibrated in superconducting magnet in magnetic field interval ± 4 T at 4.2 K with magnet hysteresis < ± 0.3 mT.

Several items of the test program, the current redistribution, the quench propagation and the DC characterization of the conductor should provide new results useful in bridging the extrapolation gap between cable and coil performance. The database for the validation of modern ITER-relevant computational tools will also be significantly extended, with particular emphasis on coupled thermal-hydraulic electromagnetic transients.

The tests of the superconducting ITER-type NbTi CICC cable have provided useful field data on the current distribution in this type of conductors during current and temperature transients, in particular approaching critical conditions, thanks to accurate Hall probe magnetic diagnostics.

This work was supported by EFDA EURATOM Contract: N^o FU06-CT-2003-00041.

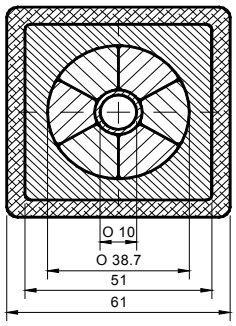

Fig. 1. CICC cable.

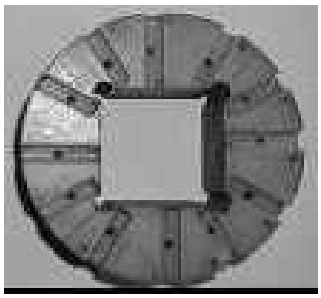

Fig. 2. Measuring head for BBIII experiment.

Fig. 3. Measuring head for FSJS experiment.

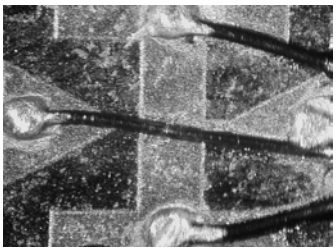

Fig. 4. *Photograph of the HP used in the experiments.*

[1] *Bellina, F. et al.: Fusion Engineering and Design **66-68** (2003) 1159.*
[2] *Zanino, R. et al.: presented at ASC 2004, Florida, to be published in IEEE Transactions on Appl. Superconductivity.*
[3] *Hurd, F. et al.:presented at ASC 2004, Florida, to be published in IEEE Transactions on Appl. Superconductivity.*
[4] *Zanino, R. et al.:presented at ASC 2004, Florida, to be published in IEEE Transactions on Appl. Superconductivity.*

Department of Cryoelectronics

Štefan Chromik

Research scientists
Štefan Beňačka
Vladimír Štrbík
Marianna Španková
Ondrej Vávra

Technical staff
Peter Drlička
Alexander Taldík

Research Engineers
Štefan Gaži

PhD Students
Zsolt Őszi
Jozef Vincenc Oboňa
Michaela Valeriánová

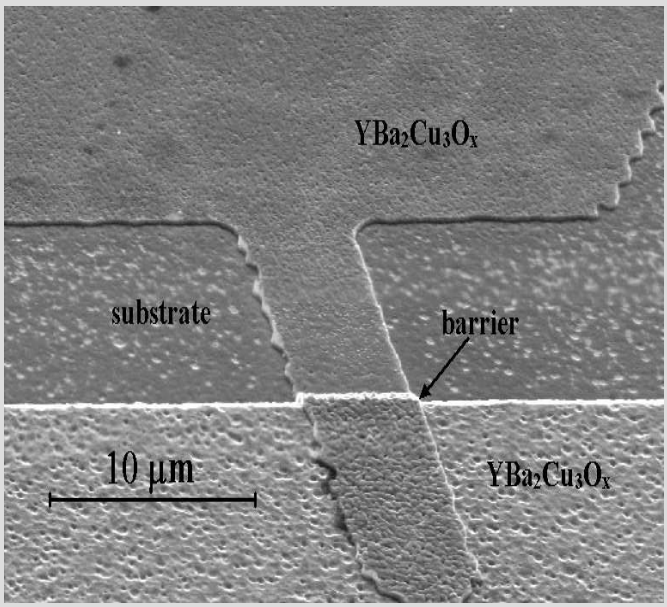

The main research activities of the Cryoelectronics Department in 2003-2004 is possible to divide into the following fields:

-Superconductor oxide thin films and weak link structures

-Superconductor MgB_2 films and weak link structures

-Dielectric oxide films for cryoelectronic structures

-Films and structures on the base of conventional superconductors

-Unconventional materials for cryoelectronics

Already optimised oxide $YBa_2Cu_3O_{7-\delta}$ (YBCO) thin films were applied for the preparation and study of properties of ramp type junctions formed by ions modified weak link interface. Prepared junctions have shown weak link behavior including almost periodic I_C-B dependences. YBCO films were patterned into superconducting microstrips by argon ion etching and studied their transport properties. These activities were supported mainly by two Slovak Grant Agencies for Science and Technology (VEGA 2/2068/22 "Thin films and microelectronics structures on the base of oxides ", VEGA 2/7199/20 "Josephson effects in high-T_C superconducting weak links", VEGA 2/3116/23 "Josephson effects in superconducting weak links and their application in cryoelektronics circuits" and APVT-51-0227 "Investigation of high temperature superconducting thin films detectors for superconducting quantum interference devices (SQUID)"). The Department also coordinates an international INTAS project entitled "Metal oxide thin film heterostructures on tilted-axes substrates". There are further bilateral agreements (Institute of Physics PAS, Poland, Institute of Electronics, Bulgaria, etc.). The national project "New materials and components in submicron technology“ supports mainly the attempts for cryoelectronic submicron structures. Further types of superconduting metal oxide films exhibiting the critical temperature above 100 K are films on the base of Hg and Tl. We prepare these films in cooperation with Laboratoire de Cristallographie CNRS, Grenoble. We study structural and electrical properties of these films. We found out that Hg (Re)-1212 films consist of epitaxial (aligned) grains. The films are interesting object for a study of femtosecond carrier dynamics in a frame of cooperation with the University of Rochester. This research is supported by the international mobility project ECONET ("Superconducting Tl and cuprate films") beside the national VEGA projects.

MgB_2 superconducting thin films are prepared by sequential evaporation of boron and magnesium followed by in–situ vacuum annealing. The nanogranular films deposited on NbN–buffered Si substrate have excellent electrical properties. We have obtained very promising first results on the SiC buffered substrate, too. The realised ramp-type $MgB_2/AlO_x/Al/Nb$ junctions demonstrated Josephson effect. We patterned our MgB_2 films into superconducting nanobridges up to 50 nm wide using focused ion beam in the frame of collaboration with the Twente University as the twinning Institute of the Centre of excellence (ASTRA project).

The preparation of oxide dielectric films has been an important part of our research activities for a long time. The films are applied as buffer layers, tunneling barriers and isolation layers to define of active areas of cryoelectonic structures. We have started to test Y_2O_3 oxide on the Si substrate as a potential buffer layer for the YBCO films. However, Y_2O_3 can be also attractive for potential applications including storage capacitors and gate insulators. We obtained first epitaxial MgO films on the top of the GaAs substrate. This is a promising step for the applications which exploit the combination of superconductor and semiconductor films. This research is supported by the international project THIOX (supported by ESF) and APVT -51-03-2902 "Integrated micromechanical sensors of elm. radiation on the base of manganite thin films"

The $Nb/Fe_xSi_{1-x}/Nb$ tunnel structures were studied due to a typical Andreev reflection and high transparency of S/F interface. NbN and AlN films were applied to create a nanogranular structure showing the effect of Coulomb blockade (at temperature above 4.2 K) and the influence of Josephson coupling on this effect..

Finally, we have studied the properties (especially the stability) and possible applications of fullerite films in cryoelectronics. Some properties of carbon nanotubes were examined, too.

Štefan Chromik

Problems of high-T_C superconductor Josephson junctions preparation

Š. Beňačka, Zs. Őszi, and M. Španková

Josephson coupling between two superconductors becomes possible when the bound quasiparticles carry the current without loosing phase coherence. The strength of the coupling is characterised by a critical current I_C of superconducting weak link (SIS, SNS, ScS junctions) and in the case of conventional superconductors (S) it depends on the *external phase* difference φ between the two superconductors ($I_C(\varphi) \sim \sin\varphi$). For unconventional high-T_C superconductors (HTS) with *d*-wave pairing (DID junctions) it was predicted [1] that *internal phases* (α, β) of the junction pair potential can be directly introduced into the Josephson relation ($I(\varphi,\alpha,\beta) \sim I(\varphi)\cos(2\alpha)\cos(2\beta)$). Angle α (β) is defined as the angle between the *a*-axis of the HTS crystal and normal to the junction interface. In HTS DID junctions zero energy bound states (ZES) are formed for the quasi-particles at the Fermi energy due to Andreev reflections and the sign change of the *d*-wave order parameter symmetry. At $\alpha, \beta = 0$ no ZES exist (as in the case of *c*-axis tunneling or in SIS junctions) for any angle Θ of the conducting electron wavevector incoming to the interface. On the other hand ZES are formed at the surface of the HTS at every Θ if $\alpha, \beta = \pi/4$. In this case low energy excitations significantly influence transport through DID junctions. As a result, the temperature dependence of the $I_C(T)$ is linear. A monotonically increasing $I_C(\alpha,\beta,T)$ with decreasing temperature confirm simulations [2], and besides linear dependence, the most significant increase of the $I_C(T)$ is for $\alpha, \beta = \pi/4$. In addition, for mirror-type junctions ($\alpha = -\beta$) unexpected non-monotonous $I_C(\alpha,-\alpha,T)$ appears in contrary to SR [1] prediction. The $I_C(T)$ minima are much more pronounced for increasing barrier potential or barrier thickness.

Our experimental results of $I_C(T)$ dependence on all HTS (YBCO) junctions, with barrier prepared by ion beam modification (IBM) [3], show the linear $I_C(T)$ with the exception of high temperature region ($T_C - T << T_C$) where thermal fluctuations are large ($I_C(T) \sim (T_C - T)^{1/2}$).

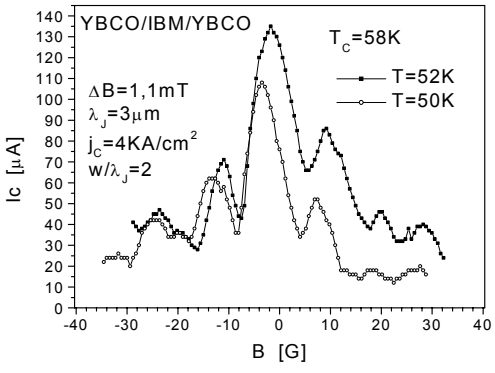

Fig. 1.

Our observation of non-monotonous $I_C(T)$ close to T_C will be discuss elsewhere [4].

The dependence of the critical current on magnetic field $I_C(B)$ of DID junctions is significantly different from the Fraunhofer diffraction pattern, typical for SIS small size junctions (width W of the junction is small in comparison to Josephson penetration depth λ_J). $I_C(B)$ strongly depends on the internal angles (α, β) of epitaxial HTS thin films, as well as on nonuniform critical current density distribution along boundaries of granular films [5]. $I_C(B)$ influence also flux trapping and flux focusing effects leading to inhomogeneous flux distribution along the junction. Our results on YBCO/IBM/YBCO ramp-type junctions show Fraunhofer-like dependence only close to the junction critical temperature (Fig. 1) with noticeable hysteresis. $I_C(B)$ periodicity corresponds to the junction area penetrating by external magnetic field. At lower temperature ($W/\lambda_J > 4$) properties of large junction appear and excess current reaches almost 50% of the total critical current. Because bottom YBCO electrode is deposited on lattice matched substrate ($LaAlO_3$) and the barrier direction is selected to have $\alpha \approx 0$ we suppose that the main contribution to the excess current can be ascribed to the counter electrode quality ($\beta > 0$). The counter electrode was deposited on relatively rough surface of the substrate surface, damaged after the ramp-edge preparation. This roughness influences the counter electrode growth and contributes to a depression of the specular charge reflection at the interface. About 50% amount of the excess current in I_C corresponds to $\beta \approx 30^o$ (allowing the existence of ZES at interface of the counter electrode and barrier).

HTS ramp-type junctions show much more complex dependence of the critical current with temperature and magnetic field, in comparison with conventional superconductors. The origin of these unusual properties may be attributed to the contribution of intrinsic angles (α, β) of the *d*-wave superconductors. Therefore, more sophisticated junction preparation is necessary to control and optimise the values of α, β, to be close to zero. As an alternative conception it appears transport in *c*-axis direction using high resistivity (e.g.$RBa_{2-x}Sr_xCu_2TaO_8$) tunneling barrier or barrier in the pseudogap state.

[1] *Sigrist, M. and Rice, T. M.:Rev. Mod. Phys.* ***67*** *(1995) 503.*
[2] *Kashiwaya, S. and Tanaka, Y.: Rep. Progr. Phys.* ***63*** *(2000) 1641.*
[3] *Őszi, Zs., Beňačka, Š., Španková, M., Chromik, Š., and Kostič, I.: Czechoslovak J. Phys.* ***54*** *(2004) D457.*
[4] *Beňačka Š. et al.: paper in preparation.*
[5] *Hilgenkamp, H. and Mannhart, J.: Rev. Mod. Phys.* ***74*** *(2002) 485.*

MgB_2 ramp-type superconducting thin film Josephson junctions

Š. Beňačka, Zs. Őszi, Š. Gaži, Š. Chromik, and V. Štrbík

Since the recent discovery of superconductivity in MgB_2 [1], with transition temperature $T_{C0} \approx 39$ K, there has been rapid progress in understanding both the basic physical properties and possible applications. From the point of view of weak superconductivity, MgB_2 may be more suitable superconductor for specific applications compared with high T_C superconductors because of lower material complexity, longer coherence length and therefore, smaller problems at the interface of MgB_2 and tunnel barrier. For reliable SIS tunnel junction fabrication it is necessary to prepare high quality superconducting (S) thin films and realize sharp interface with insulating (I) tunnel barrier. However, MgB_2 synthesis requires an annealing process at a relatively high temperature (~ 600 ^oC) and due to high reactivity of Mg with oxygen, residual O_2 greatly degrades the quality of the SIS junctions. Also, due to an excess of Mg on the film surface, more convenient for junction preparation occurs an edge-type junction preparation [2]. The MgB_2 thin films were prepared by sequential e-beam evaporation of boron and magnesium in high vacuum to create a double-layer synthesized by in-situ annealing. To suppress the reactivity of MgB_2 with the substrate, the magnesium and boron layers were deposited at the background pressure of 10^{-4} Pa on Si(100) substrate buffered by NbN [3]. The thickness of the boron film corresponds to about 200 nm stoichiometric final MgB_2 film. The best zero resistance critical temperature of the films was as a rule near 36 K.

For the preparation of ramp-type geometry we deposited in situ $SrTiO_3$ (STO) thin film (200 nm thick) on the MgB_2 film surface. The STO film provides insulation between the superconducting base MgB_2 layer and the counter electrode (Nb). For the flat ramp preparation the procedure was used we have developed for high temperature ramp-type junctions [4]. After the ramp preparation and removal of the photoresist mask the sample was transferred into a high vacuum sputtering chamber. After short rf cleaning of the MgB_2 ramp surface, thin film of Al (as follows oxidized to form a tunnel barrier) and Nb were in situ deposited by dc magnetron sputtering.

Below the Nb critical temperature, where the junction resistance R = 0, non zero critical current appears. At this temperature the junction current voltage characteristics (*IVC*) are qualitatively similar to proximity coupled S_1NIS_2 superconducting structures. The normal N layer is not completely oxidized Al film. The insulating I layer represents AlO_x resulting from the oxidation of Al film. Thicker Al layers (5-7 nm) give smaller spread of critical currents of the junctions (Fig. 1). The presence of Josephson coupling in the prepared junctions was confirmed by the registration of Shapiro current steps on *IVC* (ac Josephson effect) at irradiation of the junctions by microwaves (Fig. 2). The small dependence of the junction critical current on weak magnetic field is caused by self-field effect due to much larger junction dimensions in comparison with the Josephson penetration depth as well as by excess current present in the junction transport properties [5]. Investigation of a new barrier material for all MgB_2 junction preparation is in progress.

[1] *Nagamatsu, J., Nakagawa, N., Muranaka, T., Zenitani, Y., and Akimitsu, J.: Nature **410** (2001) 63.*

[2] *Beňačka, Š., Őszi, Zs.,Chromik, Š., Gaži, Š., Štrbík, V., and Kostič, I.: Proceedings of the 6th European Conference on Applied Superconductivity., Sorrento, Italy, 2003,1362.*

[3] *Chromik, Š., Beňačka, Š., Gaži, Š., Štrbík, V., Őszi, Zs., and Kostič, I.: Vacuum **69** (2003) 351.*

[4] *Őszi, Zs., Beňačka, Š., Španková, M., Chromik, Š., and Kostič, I.: Czechoslovak J. Phys. **54** (2004) D457.*

[5] *Beňačka, Š., Őszi, Zs., Gaži, Š., Štrbík, V., and Kostič, I.: Czechoslovak J. Phys. **54** (2004) D485.*

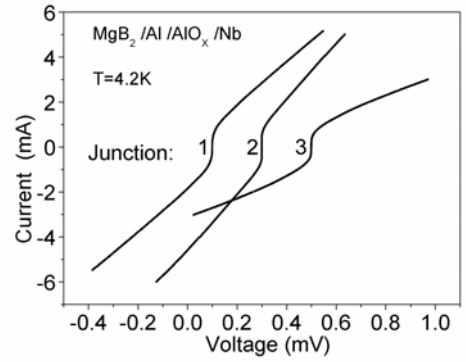

Fig. 1. Current voltage characteristics of different $MgB_2/Al/AlO_x/Nb$ junctions measured at temperature 4.2 K. Thickness of oxidized Al is 5nm.

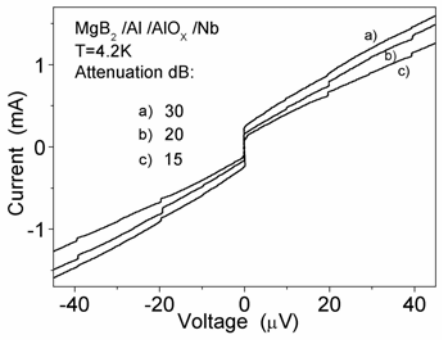

Fig. 2. IVC of the junction and Shapiro current steps of $MgB_2/Al/AlO_x/Nb$ junctions at 4.2 K. Applied microwave radiation at frequency $\nu = 9.66$ GHz and three different microwave power. levels.

High temperature supercoducting ramp-type Josephson junction

Zs. Őszi, Š. Beňačka, M. Španková, and Š. Chromik

All high temperature superconducting (HTS) ramp-type junctions, with tunneling barrier prepared by surface modification of a base superconducting electrode, are very attractive for applications in cryoelectronic circuits due to their high barrier homogeneity, chemical compatibility with superconducting electrodes and small spread of junction parameters [1]. HTS $YBa_2Cu_3O_x$ (YBCO) thin films (120 nm thick) were used to prepare YBCO/B/YBCO Josehpson ramp-type junctions with tunneling barrier (B) performed using Ar ion beam modification of the base electrode ramp area surface. The HTS surface modification process has been recently established [1] as the most reliable methods of the barrier formation for Josephson junctions, in comparison with an artificial barrier. A very thin (~2 nm) and uniform amorphous barrier is created by ion application followed by post-annealing and recrystallization during the deposition of the superconducting counter electrode [2]. The ramp-type geometry applied on *c*-axis oriented HTS films favours tunneling in the *ab*-direction, because the coherence length ξ_{ab} is much larger than the coherence length ξ_c in *c*-direction.

For preparation of YBCO/B/YBCO ramp-type geometry at first a bilayer of *c*-axis oriented YBCO and $SrTiO_3$ (STO) was deposited by an in-situ dc and rf magnetron sputtering on $LaAlO_3$ single crystal substrate. The STO layer about 200 nm thick provides insulation between the 120 nm thick superconductor layers. For flat ramp preparation (Fig. 1) we used photoresist mask and two angles ion beam etching system significantly improving smoothness of the ramp [3]. During the ramp fabrication the substrate was cooled by Peltier elements to about – 20 ºC at the Ar ion energy about 500 eV. After stripping the resist mask the sample was immediately transferred into a high vacuum sputtering system followed by cleaning and annealing steps applied just before the counter electrode deposition.

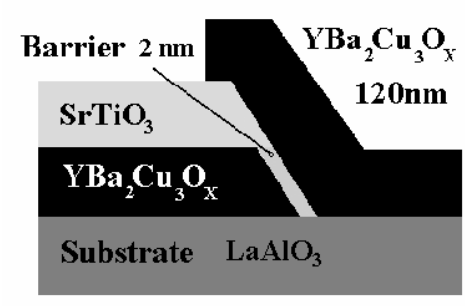

Fig. 1. Sketch of the ramp-type YBCO/B/YBCO junction.

For the most prepared YBCO/B/YBCO junctions the superconducting current appears below about 77 K. The typical current voltage characteristics (*IVC*), during irradiation of the junction by microwave (~ 10 GHz) are shown in Fig. 2 (clear Shapiro current steps are seen at different microwave powers). The average critical current $I_C \approx 1$ mA, critical current density $j_C \approx 30$ kA/cm^2 and the product of critical current I_C and the normal state resistance R_n $I_C R_n \approx 1$ mV, at the temperature $T \approx 4.2$ K. The temperature dependence of the *IVC* are more SNcNS like type (c-constriction) with low transmission probability through metallic channels [4]. Such situation may arise from the local barrier inhomogeneities due to a presence of some structures in the ramp region.

Typical characteristic of the prepared high-T_C weak link structures represents approximately linear temperature dependence of the junction critical current $I_C(T)$ over the entire temperature range below the junction critical temperature. A relatively weak magnetic field dependence of the critical current [5] is caused by self-field effects in large Josephson junction because of much larger junction dimensions $w = 10$ μm in comparison to the Josephson penetration depth $\lambda_J \approx 2$ μm.

[1] *Moeckly, B. H. and Char, K.: Appl. Phys. Lett.* ***71*** *(1997) 2526.*
[2] *Őszi, Zs., Beňačka, Š., Španková, M., Chromik, Š.: Proc. 6th European Conference on Applied Superconductivity, Sorrento, Italy,2003, 3093.*
[3] *Őszi, Zs., Beňačka, Š., Španková, M., Chromik, Š., and Kostič, I.: Czechoslovak J. Phys.* ***54*** *(2004) D457.*
[4] *Golubov, A., Kupriyanov, M. Y. and Ilichev, E.: Rev. Mod. Phys.* ***76*** *(2003) 411.*
[5] *Őszi, Zs., Beňačka, Š., Španková, M., Cigáň, A.: Proc. of International Conference, Measurement, 2005, in print.*

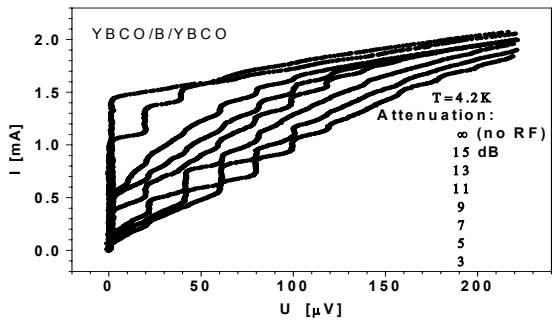

Fig. 2. Current voltage characteristics of microwave irradiated Josephson junction at different microwave powers. Temperature T = 4.2 K.

Influence of configuration on the mercuration and properties of Hg-based films

M. Valeriánová, Š. Chromik, and V. Štrbík

Mercury based superconductors $HgBa_2Ca_{n-1}Cu_nO_{2n+2+\delta}$ exhibit the highest critical temperature T_C at ambient conditions and under high pressure of all known superconductors [1, 2]. For cryoelectronic devices mainly thin films of mercury based superconductors are interesting. Because of high toxicity of mercury and decomposition of mercury oxide to mercury and oxygen at relatively low temperature, synthesis should be performed in closed vessels. Their preparation is very complicated and can be influenced by many parameters such as mercury and oxygen partial pressure, synthesis temperature etc. Therefore synthesis is often unreproducible. From the literature, the position of precursor film and mercury source is not clear. In some cases the precursor is a note that film is placed face to face to the mercury source but it is not clear whether there is physical contact between film and source. The physical contact can cause sticking of the part of the film on the mercury source or some rest of this source in the form of grains remains on the top of the film degrading the quality of final film. This was the reason why we decided to try mercuration with no physical contact between mercury source and precursor film.

Thin superconducting mercury based films were prepared by two step process involving deposition of an amorphous precursor and ex-situ mercuration in sealed quartz tube. Re-Ba-Ca-Cu-O precursor thin films were synthesized on top of the CeO_2 buffered R-sapphire substrate. Precursor films, 300 nm thick, with a nominal composition of $Re_{0.25}Ba_2Ca_2Cu_3O_x$ were deposited by RF magnetron sputtering from single target of the same stoichiometry. The precursor films were prepared in Ar atmosphere at room temperature at the pressure of 20 Pa. Mercuration was performed in sealed quartz tube using external source of mercury. This source was unreacted pellet with composition (Hg,Re)-1223. Precursor film was placed with or without physical contact with mercury source. Synthesis temperature was 800 °C / 5 h. We studied the influence of placing the film on the structural and electrical properties of final films. Prepared films were studied by X-ray diffraction (XRD) analysis, Scanning Electron Microscopy (SEM) and measurement of *R(T)* dependences.

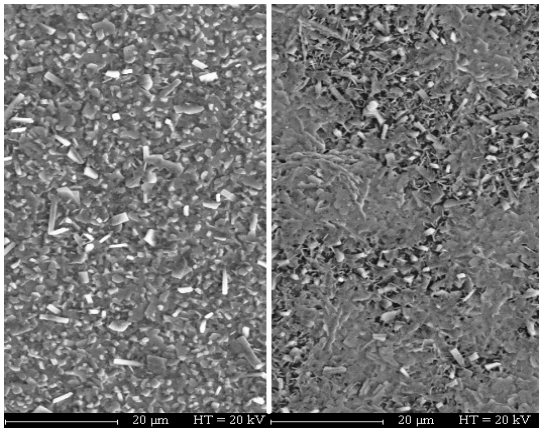

Fig. 1. SEM images (secondary electrons) of thin Hg-based films prepared by mercuration with (left) and without (right) physical contact.

In both cases of mercuration we obtained superconducting mercury based films. Films prepared by mercuration without physical contact were black, homogenous, without visible defects on the surface. On the other hand, films synthesized with physical contact with mercury source in majority had some holes on the surface. In some cases we obtained transparent but superconducting films with residuals of mercury source on the top. Using XRD analysis we identified c-axis oriented Hg-1212 phase with or without parasitic rhenium containing $Re_{2-x}Ba_4Ca_{1+y}O_{12}$ phase. Measurement of *R(T)* dependences confirmed presence of superconducting phase. Films prepared with physical contact had lower critical temperatures (T_{C0} = 98.5 K) as those prepared without contact (T_{C0} = 104 K). We suggest that that this difference can be due to larger amount of impurities in the films prepared with physical contact. Big influence of the way of preparation was sustained also by SEM analysis (Fig. 1). Films prepared with physical contact between precursor film and mercury source contained a lot of impurities on the top of the film. Films prepared without contact were completely distinct from the first ones. SEM images suggest that in some part of the film superconducting phase was formed. This can be due to low partial pressure of mercury during mercuration. These facts can explain by suppressed values of critical temperatures T_{C0}.

Thin superconducting films based on mercury were prepared by RF magnetron sputtering and ex-situ mercuration. Better superconducting properties showed films prepared without physical contact between precursor film and source of mercury. This method is suitable for the preparation of mercury based superconducting films. We can conclude that for the formation of superconducting film physical contact is not necessary and the creation of superconducting phase is performed by some vapour phase.

This work was performed in cooperation with Dr. P. Odier from the Laboratoire de Cristallographie, CNRS, Grenoble, France.

[1] *Chu, C. W., Gao, L., Chen, F., Huang, Z. J., Meng, R. L. and Xue, Y.Y.: Nature* ***365*** *(1993) 323.*

[2] *Nunez-Reguiero, M., Tholence, J. L., Antipov, E. V., Capponi, J. J., and Marezio, M.: Science* ***262*** *(1993) 97.*

MgB_2 nanogranular superconducting thin films on buffered Si substrates

Š. Chromik, Š. Gaži, M. Španková, V. Štrbík, I. Vávra, and J. Huran

Si substrates are very attractive for the preparation of MgB_2 films with zero resistance critical temperature T_{C0} below 30 K at present. We have observed an interaction of the Si substrate with the MgB_2 in the form of the Mg_2Si [1]. This is a reason why we were looking for a suitable buffer layer which will play the role of the effective diffusion barrier and allow the growth of the MgB_2 films with higher T_{C0}.

We investigated the properties of nanogranular MgB_2 films, prepared by sequential deposition of B and Mg on Si substrates, buffered by NbN, YSZ and SiC. The buffer layers significantly influence superconducting properties of the final MgB_2 films.

The presence of the unreacted Nb [2] on the top of the polycrystalline NbN buffer film, prepared in the Ar-N_2 mixture by magnetron sputtering, depresses the T_{C0} of the MgB_2 film by about 10 K. However, the in-situ preannealing of the Si substrate buffered by NbN (at a temperature of 730 ºC and a pressure of 10^{-4} Pa) avoids unreacted Nb. After this process, T_{C0} of the MgB_2 films is improved up to 36 K. The Selected Area Diffraction (SAD) pattern of the final films in this case consists of concentric rings that belong to the hexagonal MgB_2 phase (Fig. 1). In addition, the other diffraction rings correspond to the hexagonal NbN phase only. No rings belonging to the MgO particles were observed. Critical current density J_c of these films determined using the magneto-optical study [2] was 3×10^7 A / cm^2 at a temperature of 13.2 K. We observed almost field-independent J_c at the temperature of 13.2 K in the field range 0 – 300 G. The similar value of J_c was confirmed in [3], too. The analysis of the films using the method of temperature dependence of microwawe losses showed the presence of weak link type losses, present at the transition of the sample into the superconducting state only. This is in contrary to our previous results [4], where weak link losses were observed in a large temperature range below T_{C0}, too. This, together with fact that no MgO was observed in the bulk of the MgB_2 film are in agreement with the high value of J_c.

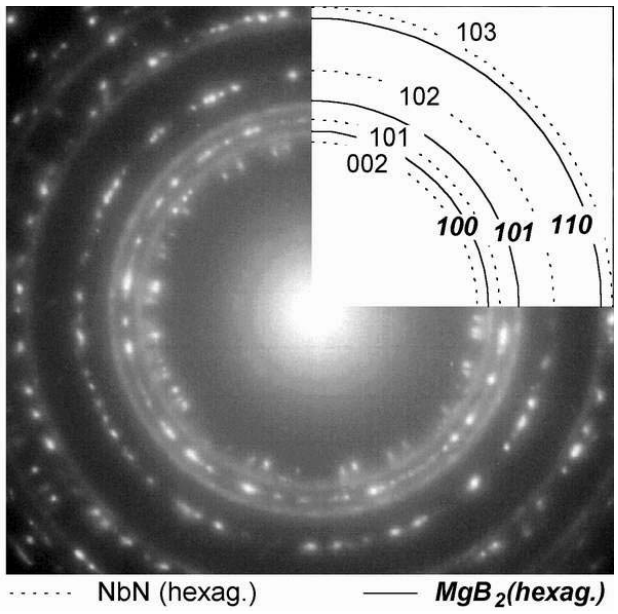

Fig. 1. SAD pattern of the MgB_2 / NbN interface in the preannealing step.

The development of other than NbN buffer layers is in progress. First, interesting results were obtained using SiC buffer layer [5]. The optimization of the preparation conditions, like the thickness, the growth temperature of the SiC layer and the in-situ annealing process of B - Mg bilayer increased T_{C0} of the MgB_2 films above 37 K. The temperature dependence of normalized resistance for different substrates and buffer layers is shown in Fig. 2.

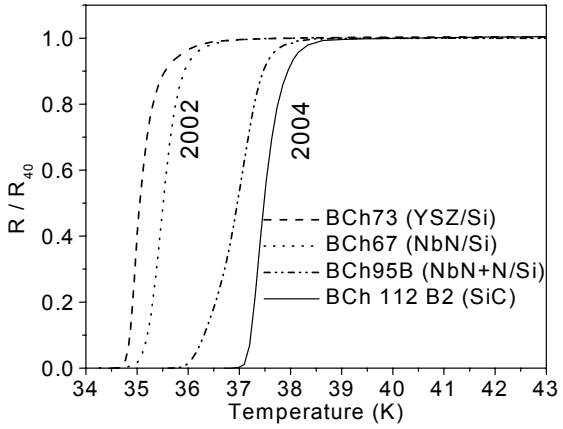

Fig. 2. The increase of critical temperature of the MgB_2 films in the period 2002-2004.

[1] *Andrade, E., Chromik, Š., Jergel, Mi., Falcony, C., Štrbík, V., and Rocha, M.F.: Thin Solid Films* ***433*** *(2003) 103.*

[2] *Chromik, Š., Gaži, Š., Štrbík, V., Španková, M., Vávra, I., Beňačka, Š., Van der Beek, C.J., and Gierlowski, P.: J. Appl. Phys.* ***96*** *(2004) 4668.*

[3] *Nishida, A., Taka, Ch., Chromik, Š., and Durný, R.: Physica C* ***412-414*** *(2004) 201.*

[4] *Chromik, Š., Beňačka, Š., Gaži, Š., Štrbík, V., Ōszi, Zs., and Kostič, I.: Vacuum* ***69*** *(2003) 351.*

[5] *Chromik, Š., et al: will be published.*

Superconducting and normal state properties of MgB_2 thin films and structures

V. Štrbík, Š. Chromik, and Š. Beňačka

In spite of a simple composition of a binary intermetallic MgB_2 superconductor, with a bulk critical temperature $T_C \approx 39 - 40$ K, the normal state properties (resistivity, resistivity vs. temperature dependence,…) show a wide dispersion in experimental values. It is difficult to find a correlation between the normal state and superconducting properties. Usually these effects are explained by a reduced cross-section for the current carrying area, by porosity, as well as by the properties of intergranular connections.

The MgB_2 thin films were prepared by a sequential evaporation of boron and magnesium, and synthesized by an in situ annealing. The B and Mg layers were deposited on various substrates (single crystalline SiC, Si, MgO, Al_2O_3, and NbN or SiC buffered Si). The MgB_2 films were created from B-Mg bilayer or B-Mg multilayer so that the total thickness of the films corresponded to the 200 - 600 nm of stoichiometric MgB_2 composition. An excess of about 100 % of Mg has been used if compared with stoichiometric composition. The B-Mg bilayer or multilayer was annealed in situ 10 min. at 630 - 850 °C in Ar atmosphere of 16 Pa pressure. The further details of in situ MgB_2 thin film processing are described elsewhere [1-8].

Our samples exhibit also a large variety of the normal state properties. The relation between the resistance ratio ($RR = R_{300K}/R_{40K}$) and the onset critical temperature T_{ON} which characterizes the beginning of the superconducting phase transition is shown in Fig. 1. The dashed line represents the bulk T_C value ≈ 40 K and the full line is the best fit to the experimental data. For samples with RR < 1 (the resistance increases with decreasing temperature) the onset of the superconducting transition T_{ON} is only slightly suppressed below 40 K. The samples with RR close to 1 mostly represent the intrinsic MgB_2 properties, T_{ON} is close to the bulk value. The samples with RR > 2 (metallic behavior) exhibit an unexpected but evident suppression of the superconducting transition to a lower temperature. The strong metallic behavior originates mainly from an excess of Mg in the sample. The critical current density (j_C) for three samples was estimated. In spite of three different methods, the difference in the j_C values is large enough; 10^8 A/cm^2 [3], 3×10^7A/cm^2 [2] and 10^6A/cm^2 [4] (all values at 13 K) for samples *jc1*, *jc2* and *jc3*, respectively. The resistance versus temperature (*R-T*) dependence displays again the various behavior. Instead of samples with RR < 1 (semiconductor-like behavior), the *R-T* dependence of the samples with RR > 1 can be described by the relation $R \sim T^n$, where n = 1 - 3, indicating various conducting mechanisms.

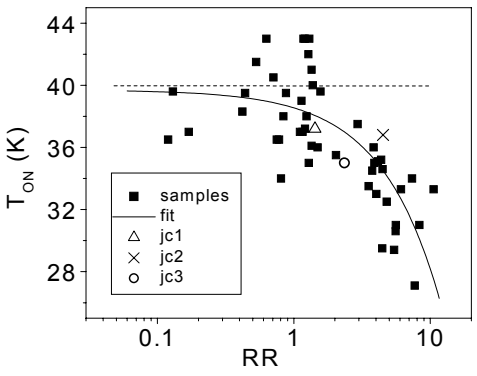

Fig. 1. Dependence of the onset critical temperature T_{ON} on resistance ratio RR for 50 samples.

To understand such properties of the MgB_2 thin films we carried out some microstructural [2], elemental composition analyses, depth concentration profiles of the prepared films [5-8]. The analyses showed that our films are nanogranular but polycrystalline, without MgO [2], but with Mg_2Si phase at the substrate - MgB_2 film interface [7,8]. MgB_2 films are rather inhomogeneous across the film thickness [7], indicating the existence of nonstoichiometric ($Mg_{1-x}B_2$) phases in the film, which may be the reason for such large dispersion in the normal state as well as in superconducting properties.

[1] *Chromik, Š., Gaži, Š., Štrbík, V., Španková, M., Vávra, I., Satrapinski, L., Beňačka, Š., van der Beek, C.J., and Gierlowski, P., arXiv:cond-mat/0401569 (2004).*

[2] *Chromik, Š., Gaži, Š., Štrbík, V., Španková, M., Vávra, I., Beňačka, Š., van der Beek, C.J., and Gierlowski, P.: J. Appl. Phys.* ***96*** *(2004) 4668.*

[3] *Nishida, A., Taka, C., Chromik, Š., and Durný, R.: Physica C* ***412-414*** *(2004) 201.*

[4] *Štrbík, V., Chromik, Š., Beňačka, Š., and Gaži, Š.: Czech. J. Phys.* ***54*** *(2004) D505.*

[5] *Chromik, Š., Kováč, P., Stanček, S., and Štrbík, V.: Acta Physica Slovaca* ***54*** *(2004) 169.*

[6] *Andrade, E., Chromik, Š., Jergel, Mi., Jergel, Ma., Falcony, C., Štrbík, V., and Rocha, M.F.: Nuclear Instruments and Methods in Physics Research, Section B* ***219-220*** *(2004) 768.*

[7] *Jergel, Mi., Andrade, E., Chromik, Š., Jergel, Ma., Falcony, C., Štrbík, V., Rocha M.F., and Zavala, E.P.:Physica C* ***383****(2003) 287.*

[8] *Andrade, E., Chromik, Š., Jergel, Mi., Jergel, Ma., Falcony C., Štrbík, V., Rocha, M.F., and Zavala E.P.: Thin Solid Films* ***433*** *(2003) 351.*

New type of Josephson junction of Nb/$Fe_{0.5}Si_{0.5}$/Nb structure

O. Vávra, Š. Gaži, J. Dérer, E. Kováčová, and I. Vávra

One of the results published in last year was the finding of the real structure of the Nb/$Fe_{0.5}Si_{0.5}$/Nb tunnel junction. It was described as the S/F/I/F/S junction. We found that at the barrier interfaces the Fe enrichment occurs as a consequence of outdiffusion.

The real structure of the Nb/$Fe_{0.5}Si_{0.5}$/Nb tunnel junction is considered as Nb/Fe/FeSi'/Fe/Nb [1]. The thickness of the Fe layers is about one or two monolayers, and the FeSi' layer is the rest of the $Fe_{0.5}Si_{0.5}$ alloy.

To investigate in more details above mentioned structure, a Nb/$Fe_{0.5}Si_{0.5}$/Si/Nb junctions [2] were prepared by the same technology as Nb/$Fe_{0.5}Si_{0.5}$/Nb junctions. This type of junctions contains only one S/F interface on the bottom double layer in the Nb/$Fe_{0.5}Si_{0.5}$/Nb junctions.

Current-voltage curve of the Nb/$Fe_{0.5}Si_{0.5}$/Si/Nb junction is shown in Fig. 1 and the experimental evidence of ac Josephson effect is clearly seen in the inset of Fig. 1. In the differential conductance *dI/dV* vs. bias voltage curve (Fig. 2) the double enhancement of G_n (arrow in Fig. 2) is observed (A ≈ 2). This enhancement is attributed to Andreev reflection at the bottom S/F interface. It is the same value of the Andreev reflection efficiency as it was observed in the case of the bottom interface, i.e. FeSi-on-Nb, of Nb/$Fe_{0.5}Si_{0.5}$/Nb junctions presented above. The peaks in the *dI/dV* curve with enhancement larger than two (A > 2) at the voltage $V < \Delta/e$ and the double enhancement (A = 2) at the voltage $V > \Delta/e$ are caused by the presence of the Si layer in the Nb/$Fe_{0.5}Si_{0.5}$/Si/Nb junctions.

Taking into account the Si outdiffusion from the $Fe_{0.5}Si_{0.5}$ layer, formation of only one S/F interface, and the observation of Andreev reflection at this S/F interface, the real structure of the Nb/$Fe_{0.5}Si_{0.5}$/Si/Nb junctions should be described as Nb/Fe/FeSi'/Si/Nb. The peak with enhancement A > 2 for the $V < 0.9$ mV is caused by the fact that low energy electrons coming from the Nb layer to the Fe layer can be reflected back at the Fe/FeSi' interface. After that reflection the electrons can be Andreev-reflected again and due to the fact that the differential conductance can be enhanced by the factor A > 2. This type of non-symmetric junctions consists of one Si barrier and one S/F interface connected in series. The voltage on the barrier is added to the voltage attributed to the S/F interface, thus the Andreev reflection occurs at the junction voltages $V > \Delta/e$, too.

[1] *Vávra, O., Gaži, Š., Vávra, I., Dérer, J., and Kováčová, E.: Physica C* ***404*** *(2004) 395.*

[2] *Vávra, O., Gaži, Š., Vávra, I., Radnóczi, G., Moshchalkov, V.V., Dérer, J., and Kováčová, E:, arXiv: cond-mat/0406242(2004).*

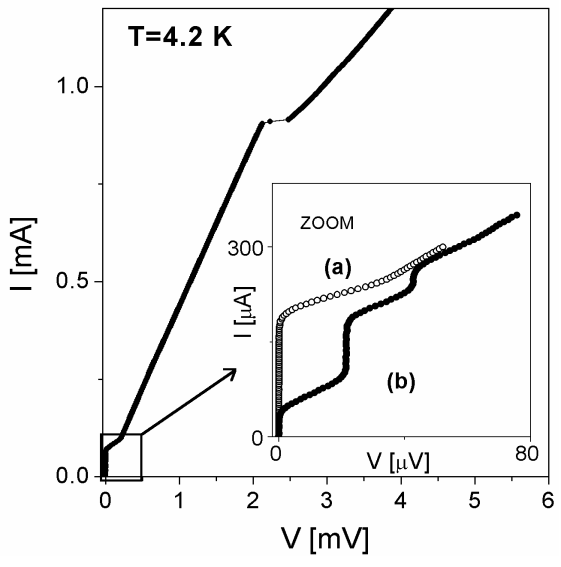

Fig. 1. Current-voltage characteristics of the Nb/$Fe_{0.5}Si_{0.5}$/Si/Nb superconducting tunnel junctions at 4.2 K. Inset: Zoom of current voltage characteristics of such junction (a) without microwave irradiation and (b) with irradiation by 10 GHz. The Shapiro steps confirm the presence of the ac Josephson effect.

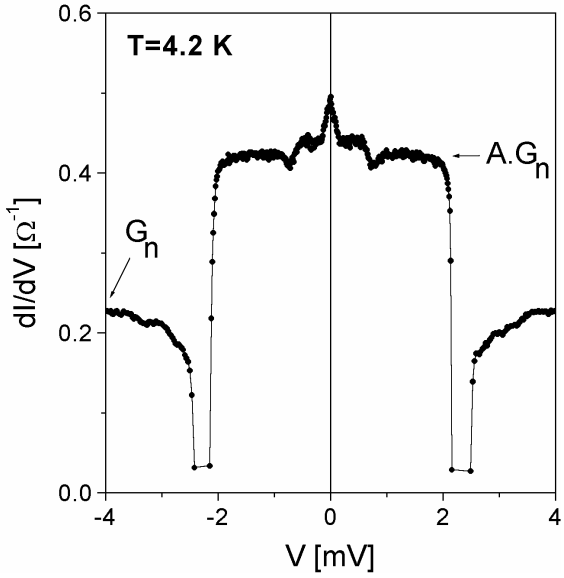

Fig. 2. Differential conductance vs. bias voltage of the Nb/$Fe_{0.5}Si_{0.5}$/Si/Nb junction at 4.2 K, showing a double enhancement of the conductance compared with that of the normal state.

Coulomb blockade and single charge tunneling observed in NbN nanograins

Š. Gaži

Capacitively coupled two pieces of conductors with a capacitance so small that the charging energy of such a junction $E_Q = e^2 / 2C$ exceeds k_BT make possible to control tunneling of the carriers by a Coulomb blockade. If such a system is coupled by a small capacity $C_0 << C$ to an external circuit with a battery at a voltage U_B the small variation ΔU_B induces a charge ΔQ_0 across the capacitors and the voltage across the junction $\Delta U = \Delta Q_0 / C$. If C is small ($C = 10^{-15}$- 10^{-17} F at the pieces of 100 × 100 mm^2 – 10 × 10 mm^2) an increasing of the voltage $\Delta U \geq U_T$ and the tunneling of the $\Delta Q = ne$ occurs. Followed voltage drop $\Delta U = ne / C$ evokes the Coulomb blockade, i.e. the next tunneling will proceed only after the increasing of the voltage on C by an induced charge ΔQ_0. So the voltage drop across the junction is periodic function of the induced charge with period e. If the two pieces are superconductors, the voltage drop across the junction is a periodic function of the induced charge with a period of $2e$, if only Cooper pairs are present. This system behaves like a quantum particle in a periodic potential where the potential is given by coupling energy $U(\varphi)$ of the junction. $Q_0(U_B)$ is a control parameter and charge imbalance Q is a dynamical variable. The total energy of the junction is the sum of the charging energy and coupling energy of the junction: $H = [(Q-Q_0)^2 / 2C] - E_j \cos\varphi$, $E_j = \hbar I_C / 2e$ in the case of Josephson coupling. Q is an operator and in the phase representation (the charge and φ are conjugate variables) $Q = (2e / i)(\partial/\partial\varphi)$. The eigenvalues of quantum equation are Bloch bands with periodicity $2e$, $E_n(q + 2e) = E_n(q)$ where q is quasicharge ($-e < q < e$) and measure of the induced charge Q_0 deviation from quantitized values $Q = n2e$. The periodicity of Bloch waves in this junction system gives picture of Brillouin zones, Fig. 1., in the case of Josephson energy $E_j < E_Q$ ($E_j / E_Q = 0.4$). In the first Brillouin zone ($|q| < e$) tunneling on the boundary of zone $|q| = e$ may happens after moving along axis q when the charging energy $E_Q = q^2 / 2C$ increases and exceeds

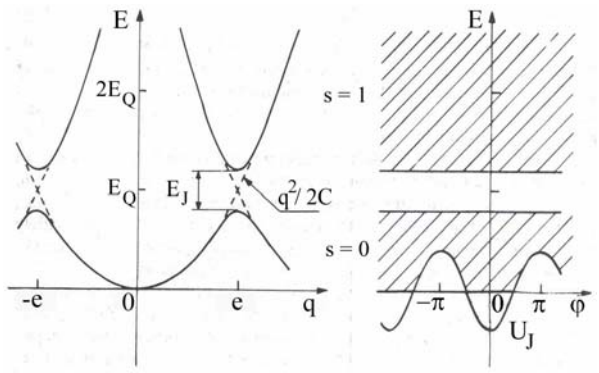

Fig. 1.

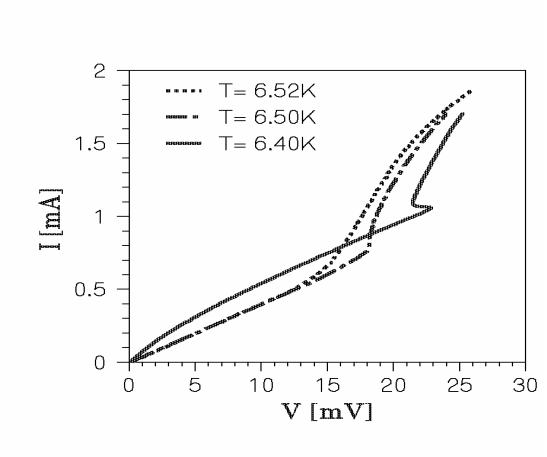

Fig. 2.

energy gap E_j [1]. If Q_0 is varied, actual charge Q and consequently junction voltage oscillate with a frequency $f_{BOT} = Q_0 / 2e$ [1]. These oscillations (BOT) are equivalent to the Bloch oscillations of crystal electron driven by an electric field. Averin [2] presents the another type of coherent oscillations as a single electron tunneling (SET) between metals, either superconducting or normal. In this type of oscillation Brillouin zone for q is $-e / 2 < q < e / 2$ and $f_{SET} = Q_0 / e$. When the voltage exceeds the value of Coulomb blockade voltage $U_Q = e / C$, the average current increases and a negative slope of the *I-V* characteristics arises as a consequence of coherent oscillations SET followed by BOT (Bloch nose). After this, Zener tunneling through the gap E_j to the second band follows. Requirement for observation of these effects is the presence of Coulomb blockade, i.e. shunt resistor $R_S >> R_q$ ($R_q = h / 4e^2 = 6.5$ kΩ for BOT and $R_q = h / e^2 = 26$ kΩ for SET) for holding of junction charge.

Coulomb blockade and single charge tunneling was observed in nanogranular NbN layers. The structure of NbN nanograins was isolated by amorphous AlN layers by sequential sputtering of NbN-AlN-NbN-AlN-NbN layers with a thicknesses of 15/4 nm and measured by four-contact method with special contact geometry. Such modifying grains at current contacts by annealing, the N parallel chains of grains was measured (Fig. 2.). Coulomb blockade $U_Q \div 20$ mV gives grain dimension ~10 nm (if $C = 10^{-17}$ F) at 1 mm wide strip $N \approx 5 \times 10^4$ chains. R_S for one chain is $R_S = 25\ \Omega \times 5.10^4 \Omega >> 26$ kΩ $= R_Q$. Single charge tunneling is manifested by negative slope branch of *I-V* characteristics in the temperature range 6.35 ÷ 6.5 K where E_j / E_Q grows with I_C.

[1] *Likharev, K.K. and Zorin, A.B.:J. Low. Temp. Phys.* ***59*** *(1985) 347.*
[2] *Averin, D.V. and Likharev, K.K.: SQUID'85, Ref.8, p .197.*

Structural properties of $SrTiO_3$ and Y_2O_3 thin films grown on Si substrates

M. Španková, I. Vávra, Š. Chromik, Š. Gaži, R. Lupták, J. Šoltýs, and K. Hušeková

Oxide thin films grown on the Si substrates have attracted much attention in the recent years due to important technological applications. Epitaxial insulator on the Si structures are key elements in silicon-on-insulator structures, three-dimensional integrated circuits, etc. Perovskite oxide - $SrTiO_3$ (STO) and fluorite-type oxide - Y_2O_3 films have been applied to the applications of memory devices. STO and Y_2O_3 are also considered to be the best buffer layers for $YBa_2Cu_3O_7$ growth on the Si substrates. Growth of the oxide films on the Si attracts special interest because the properties of the oxide can be combined with the recent microelectronics to create a new generation of the microelectronic and superconducting devices. The appropriate layer should have a low lattice mismatch, a high dielectric constant, a good chemical stability as well as blocking properties for chemical interdiffusion. STO and Y_2O_3 thin films meet the above requirements.

One of the key problems in growing the STO or Y_2O_3 films on the Si is the formation of an amorphous SiO_x at the interface preventing the intented oxide heteroepitaxy on the Si substrate. Prior to the deposition of the STO or Y_2O_3 films, a metallic Sr or Y intermediate layer was evaporated at a pressure of 2×10^{-4} Pa and substrate temperatures T_S of 750 - 800 °C. These metallic layers deoxidize the native oxide layer on the Si substrates [1,2].

The STO and Y_2O_3 were grown on the Si substrates using on-axis radio frequency magnetron sputtering [$p(Ar + O_2) = 12$ - 15 Pa, $T_S = 500$ - 800°C)] with a thickness of 100 - 130 nm.

The STO layers deposited on the Si(110) substrates exhibit an epitaxial character of the growth (Fig. 1) in spite of the fact that a silicide layer forms between the STO and the substrate. This polycrystalline interfacial layer does not prevent epitaxial growth of the STO films [1,2].

The Y_2O_3 layers deposited on the Si(100) and Si(111) are polycrystalline (Fig. 2) and do not contain any silicide layer. From the Transmission Electron Microscopy (TEM) analyses and ellipsometric measurements we can conclude that the Y_2O_3 layers prepared at higher substrate temperatures display higher density (less voids) due to their better crystallinity. The root-mean-square roughness value measured by the Atomic Force Microscopy is about 1.55 nm. The electrical properties of the Y_2O_3 layers were investigated by measuring the *C-V* characteristics that registered a decrease of the positive oxide charge value from 1.3×10^{12} to 3×10^{11} cm^{-2} due to annealing of the $Ru/Y_2O_3/Si$ in ambient O_2 [3].

Epitaxial STO and Y_2O_3 thin layers are expected to play an important role in silicon-on-insulator technology. Therefore it is necessary to investigate and further optimize the growth conditions of the layers.

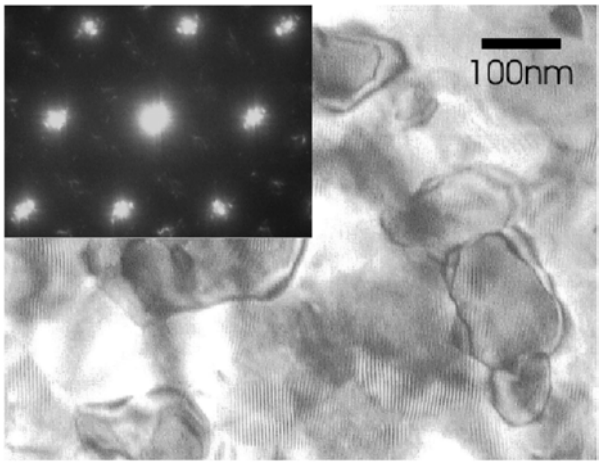

Fig. 1. TEM picture of the STO microstructure. In some parts of the layer Moiré fringes are present. The layer consists of blocks with a size ~100-150 nm. Selected Area Diffraction pattern in the inset shows the STO/Si interface and reveals double diffraction effect.

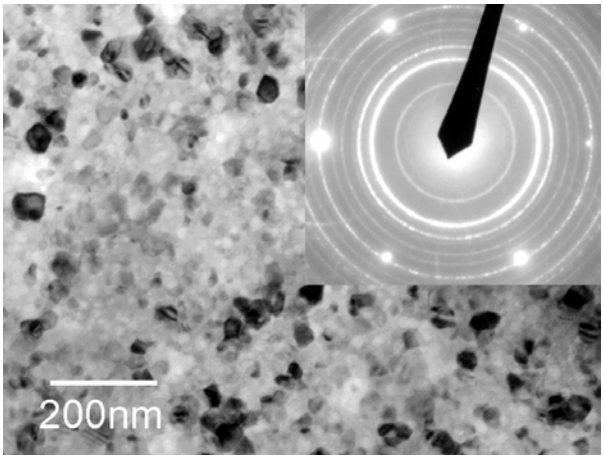

Fig. 2. TEM picture of the Y_2O_3 microstructure. The layer consists of randomly oriented grains with a maximum size ~30 nm. Voids, seen as white spots, are also observed in the layer. Selected Area Diffraction pattern taken from the Y_2O_3/Si interface (see the inset) reveals a polycrystalline growth of the Y_2O_3.

[1] *Španková, M., Chromik, Š., Vávra, I., Gaži, Š., and Kúš, P.: J. Phys. IV France* ***11*** *(2201) Pr11-169.*

[2] *Španková, M., Chromik, Š., Sedláčková, K., Vávra, I., Gaži, Š., and Kúš, P.: Solid State Phenomena* ***90-91*** *(2003) 589.*

[3] *Španková, M., Vávra, I., Chromik, Š., Harasek, S., Lupták, R., Šoltýs, J., and Hušeková, K.: Mat. Sci. and Eng. B* ***113*** *(2005) 30.*

Study of DC electrical properties of single-walled carbon nanotube layers

J. Vincenc Oboňa and V. Štrbík

The first carbon nanotubes were prepared by Iijima in 1991 in the process of arc discharge between two carbon electrodes [1]. Multi-walled nanotubes (MWNT) with a diameter higher than 1 nm and a length of several micrometers were obtained. Reproducible preparation of single-walled nanotubes (SWNT) was achieved later. We can imagine the structure of nanotubes (NT) as a graphitic plane rolled up to tube. According to the direction of rolling up the nanotubes show either metallic or semiconducting nature of conductivity (Fig. 1).

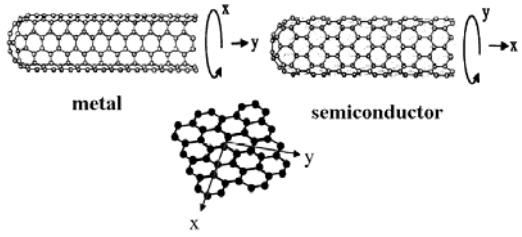

Fig. 1. The character of conductivity of nanotubes depends on rolling up direction.

In the SWNT with metallic conductivity of the electrons acts as the one-dimensional system (1D). Weak coulomb interaction in the 1D system (unlike in 2D and 3D systems) causes strong perturbations known as a Luttinger liquid (LL). 1D system behaves like a strong correlated. This fact is involved directly in the conductivity of 1D system. For example the tunneling into contacted SWNT exhibits a conductance of $G \sim T^{\alpha}$, where T is the temperature and $\alpha = 0.3$ - 0.6 in dependence of the contact preparation [2]. This dependence was observed in the range of 10 - 100 K and the NT conductivity sharply decreases in the temperature interval 4.2 - 30 K. The saturation of the NT conductivity phenomenon (the temperature independence) becomes above 100 K. The tunneling LL through the various barriers (for example the impurity in the one SWNT or crossing of two NT) can differ only in the value of α. Then we can observe the dependence of $G \sim T^{\alpha}$ for the one SWNT also for the bundle of nanotubes (ropes) [2], which are primarily created in the preparation process. The part of the bundle of NT contains also semiconducting ones. The semiconducting NT does not contribute to temperature dependence of the conductivity in the low temperature range of the measurement.

Purified SWNT produced by HiPCO method and obtained from CMI (Texas) were used in our experiments. The SWNT "paper" was produced from a suspension in 1 % solution of sodium dodecisulfat (SDS) in water and then filtrated through polymer membrane filter PTFE (polymer of Teflon). The SDS is eluted from the SWNT "paper" by the distilled water.

We realized DC conductivity measurements (Fig. 2) by a four-probe geometry. The silver paint contacts were made consecutively on the "paper". A considerable decrease of SWNT conductivity *σ(T)* becomes under 50 K. In the interval 4.2 - 100 K the temperature

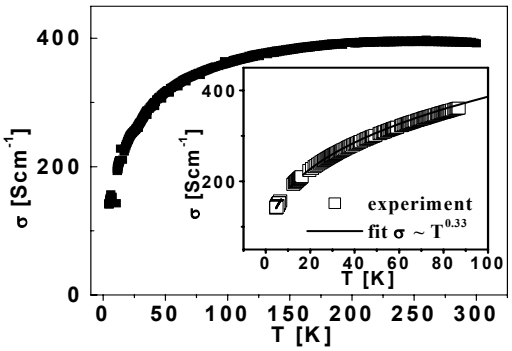

Fig. 2. Temperature dependence of conductivity for SWNT "paper". In the interval 4.2-100 K the temperature dependence of the conductivity follows the function of $\sigma \sim T^{\alpha}$ *(*α*=0.33).*

dependence of the conductivity follows the function of $\sigma \sim T^{\alpha}$ ($\alpha = 0.33$). We assume that in the case of DC measurements of SWNT "paper" the tunneling from the contacts between the nanotubes or tunnelling through the defects in the nanotubes contribute mainly for the *σ (T)* dependence.

The nanotubes have high ability to create hydrogen bonds with the other molecules. For example, the conductivity of semiconducting SWNTs greatly decreases in the presence of NH_3 [3]. The response time of the nanotube on the NH_3 concentration change takes a few minutes.

[1] *Iijima, S.: Nature* ***354*** *(1991) 56.*
[2] *Bockrath, M., Cobden, D. H., Lu, J., Rinzler, A. G., Smalley R. E., Balents, L., and McEuen, P. L.: Nature* ***397*** *(1999) 598.*
[3] *Kong, J., Franklin, N. R., Zhou, Ch., Chapline, M. G., Peng, S., Cho, K., and Dai, H.: Science* ***287*** *(2000) 622.*

III Cooperation

International projects

Project	Type	Agency	Responsible	Duration
Applied superconductivity training and research advanced centre – (ASTRA)	Centre of Excellence	EC, 5th Framework Programme	Dr. F. Gömöry	2003 - 2005
Quality monitoring of superconductors for the production of effecient, compact and reliable power transmission systems (Q-SECRETS)	RTD-project	EC, 5th Framework Programme	Dr. F. Gömöry	2000 - 2003
New gallium phosphide grown by vertical gradient freeze method for light emitting diodes (VGFGAPLED)	RTD-project	EC, 5th Framework Programme	Dr. J. Novák	2002 - 2006
Integration of very high-k dielectrics with silicon CMOS technology (INVEST)	RTD-project	EC, 5th Framework Programme	Dr. K. Frőhlich	2002 - 2004
Measurements of the current distribution inside superconducting cable - supply and installation of Hall probe measuring system and joining of multifilamentary Nb_3Sn strands	EURATOM RTD-project	EC, 5th Framework Programme	Dr. M. Polák	2003 - 2004
Metal oxide multilayers obtained by cost-effective new CVD technologies for magnetoelectronic microsystems and nanotechnologies (MULTIMETOX)	Network	EC, 5th Framework Programme	Dr. K. Frőhlich	2000 - 2003
Metal-oxide thin film heterostructures on tilted-axes substrates	INTAS - RTD-project	EC, 5th Framework Programme	Dr. Š. Beňačka	2002 - 2005
European network for superconductivity (SCENET-2)	Network	EC, 5th Framework Programme	Dr. F. Gömöry	2002 - 2006
One-dimensional transport in a semiconductor quantum wire with disorder, dephasing, and electron-electron interaction	Marie Curie fellowship	EC, 5th Framework Programme	Dr. P. Vágner	2001 - 2003
Superconducting coated conductor cable (SUPER3C)	RTD-project	EC, 6th Framework Programme	Dr. F. Gömöry	2004 - 2008
Nano-and micro-scale engineering of higher-performance MgB_2 composite superconductors for macro-scale applications (HIPERMAG)	RTD-project	EC, 6th Framework Programme	Dr. P. Kováč	2004 - 2008
Advanced Semiconductor Devices and Microsystems–ASDAM '04	Conference	EC, 6th Framework Programme	Dr. J. Osvald	2004 - 2005
Thin films for novel oxide devices (THIOX)	Network	ESF	Dr. K. Frőhlich	2003 - 2007
Arrays of quantum dots and Josephson junctions (AQDJJ)	Network	ESF	Dr. Š. Beňačka	2004 - 2009
Preparation of barriers, electrodes and oxide films for microelectronics	Network	COST	Dr. K. Frőhlich	2001 - 2006
Nanostructured materials	Network	COST	Dr. P. Lobotka	2002 - 2004
X-ray and neutron optics	Network	COST	Dr. D. Korytár	2002 - 2006

Project	Type	Agency	Responsible	Duration
One-dimensional electron transport in V-groove GaAs quantum wires: measurement and simulations for a broad temperature range	Network	COST	Dr. M. Moško	1999 - 2003
Microwave monolithic integrated transmitted power sensors and their industrial and metrological applications	RTD-project	NATO, Science for Peace	Dr. T. Lalinský	1999 - 2003
High temperature superconducting model transformers using BSCCO and YBCO tapes	RTD-project	NATO, Science for Peace	Dr. M. Polák	2000 - 2003
Electromagnetic properties of superconducting composites	Network	NATO	Dr. F. Gömöry	2003 - 2005
Transverse resistivity of YBCO coated conductors for AC use	RTD-project	European Office of Aerospace Research and Development (EOARD)	Dr. M. Polák	2003 - 2005

National projects

Project	Agency	Responsible	Duration
New materials and devices in sub-micrometer technology	Slovak Government	Dr. K. Frőhlich	2002 - 2005
Modular imaging X-ray system utilizing radiation detectors based on GaAs semiconductor compound	Slovak Ministry of Education	Dr. F. Dubecký	2001 - 2004
High power optocoupler	Slovak Ministry of Education	Dr. J. Novák	2002 - 2003
Transport of interacting electrons in a disordered one-dimensional conductor	VEGA	Dr. M. Moško	2003 - 2005
Mechanically reinforced composite Bi-2223 superconductors with optimised filament architecture	VEGA	Dr. P. Kováč	2002 - 2004
Investigation of technology, physical and detection performances of X- and gamma ray InP- based detectors	VEGA	Dr. F. Dubecký	2004 - 2006
Kvantové heteroštruktúry na III-N polovodičových materiáloch	VEGA	Dr. J. Kuzmík	2003 - 2005
Study of electro-physical and technological tasks of preparation of radiation detectors based on InP and GaAs	VEGA	Dr. F. Dubecký	2001 - 2003
Ternary and quaternary alloys in advanced semiconductor devices	VEGA	Dr. J. Novák	2003 – 2005
Flux penetration into superconductors of various shapes and configurations	VEGA	Dr. S. Takács	2003 - 2005
Josephson effects in superconducting weak links and their application in cryoelectronic circuits	VEGA	Dr. V. Štrbík	2003 - 2005
Thin films and microelectronic structures on the base of oxides	VEGA	Dr. Š. Chromik	2002 - 2004
Nanocrystalline thin film materials	VEGA	Dr. I. Vávra	2003 - 2005
Micromachined metal oxide gas microsensors	VEGA	Dr. J. Huran	2003 - 2005
Gas sensing microsystem based on GaAs microstructures	VEGA	Dr. J. Huran	2004 - 2007
Synthesis of poly-InP and its characterization	APVT	Dr. J. Novák	2002 - 2005
Non-traditional multiphase nanostructured materials with extraordinary physical properties	APVT	Dr. I. Vávra	2004 - 2006
Submicron Vector Hall Probe Microscope	APVT	Dr. V. Cambel	2002 - 2005
Epitaxial heterostructures high-brightness light emitting diodes based on GaP substrates	APVT	Dr. J. Novák	2004 – 2006
Electromagnetic properties of superconducting composite conductors	APVT	Dr. F. Gömöry	2002 - 2005
Investigation of high temperature superconducting thin film detectors for superconducting quantum nterference devices (SQUID)	APVT	Dr. Š. Beňačka	2002 - 2005
Composite superconductors for cryogen-free devices	APVT	Dr. P. Kováč	2004 – 2006
Strongly correlated and disordered electronic systems	APVT	Dr. M. Moško	2002 - 2005
Integrated MEMS senzors based on magnetoresistive thin films	APVT	Dr. P. Lobotka	2004 - 2006

IV Publications

2003

Tesař, R., Koláček, R., Kawate, E., **Beňačka**, **Š**., Gaži, Š., and Šimša, Z.: Far-infrared thermal spectroscopy of low-T_c and high-T_c superconductor films, Supercond. Sci Technol. **16** (2003) 916-120.

Serenyi, M., **Betko**, **J**., Nemcsics, Khahn N.Q., and **Morvic**, **M**.: Fabrication of a-SiGe structure by RF sputtering for solar cell purpose, Physica Stat. Solidi (c) **0** (2003) 857-861.

Cambel, **V**., **Gregušová, D**., and **Kúdela, R**.: Formation of GaAs three-dimensional objects using AlAs „facet-forming" sacrificial layer and H_3PO_4, H_2O_2, H_2O based solution, J. Applied Phys. **94** (2003) 4643-4648.

Jergel, Mi., Andrade, E., **Chromik, Š**., Jergel, Ma., Falcony, C., **Štrbik**, **V**., Rocha, M.F., and Zavala, E.P.: Composition depth profiles of superconducting MgB_2 thin films determined by ion beam analysis methods, Physica C **383** (2003) 287-294.

Hartmanová, M., Jergel, Ma., Thurzo, I., Kundracik, F., Gmucová, K., **Chromik**, **Š**., and Ortega, L.: Thin film electrolytes - yttria stabilized zirconia and ceria, Russian J. Electrochemistry **39** (2003) 478-485.

Chromik, **Š**., Plesch, G., **Štrbik**, **V**., Odier, P., and De Barros, D.: The influence of Re and fluorides based precursor thin film on morphology and microstructure of Hg-based cuprate films, Solid State Phenomena **90-91** (2003) 535-539.

Plesch, G., **Chromik**, **Š**., **Štrbik**, **V**., Kunc, M., Jergel, M., and Kostič, I.: The effect of (Ba/Sr) substitution on Tl-based superconducting thin films prepared from fluoride precursors, Solid State Phenomena **90-91** (2003) 571-575.

Andrade, E., **Chromik**, **Š**., Jergel. M., Jergel, M., Falcony, C, **Štrbík**, **V**., Rocha, M.F., and Zavala, E.P.: Study of the superconducting MgB_2 films by ion beam analysis methods, Thin Solid Films **433** (2003) 103-107.

Cheang-Wong, J.C., Jergel, Mi., Jergel, Ma., **Chromik**, **Š**., **Štrbik, V**., and Falcony, C.: RBS characterization of MgB_2 superconducting films annealed *ex situ* and *in situ*, Supercond. Sci Technol. **16** (2003) 879-884.

Fedor, **J**., **Cambel, V., Gregušová, D**., Hanzelka, P., **Dérer, J**., and **Volko**, **J**.: Scanning vector Hall probe microscope, Rev. Sci Instruments **74** (2003) 5105-5110.

Babonas, G-J., Reza, A., Szymczak, M., Baran, M., **Fröhlich**, **K**., Jasutis, V., and Diduszko, R.: Optical response of $La_{1-x}MnO_3/Al_2O_3$ films, Acta Physica Polonica A **103** (2003) 77-83.

De Santis, A., Bobba, F., Cristiani, G., Cucolo, A., **Fröhlich**, **K**., Habermeier, H.U., Salvato, M., and Vecchione, A.: Structural and electrical characterization of magnetoresistive $La_{0.7}Ca_{0.3}MnO_3$ thin films, J. Magnetism Magnetic Mat. **262** (2003) 150-153.

Gendiar, **A**., Maeshima, N., and Nishino, T.: Stable optimization of tensor product variational state, Progress of Theoretical Phys. **110** (2003) 691.

Kemper, A., **Gendiar**, **A**., Nishino, T., Schadschneider, A., and Zittartz, J.: Stochastic light-cone CTMRG: a new DMRG approach to stochastic models, J. Physics A **36** (2003) 29.

Zola, D., Polichetti, M., Senatore, C., Pace, S., and **Gömöry**, **F**.: Numerical calculation of the critical state in superconducting tapes above the full penetration field, Int. J. Modern Phys. B **17** (2003) 916-921.

Tebano, R., Mele, R., Boffa, V., **Gömöry**, **F**., **Strýček, F**., and **Seiler, E**.: Numerical investigation on AC properties in high T-c superconducting tapes, Int. J. Modern Phys. B **17** (2003) 528-533.

Gömöry, **F**., **Frolek, L., Šouc**, **J**., Coletta, G., and Spreafico, S.: Measurement od DC critical current in superconducting cable with non-uniformity, IEEE Trans. Applied Supercond. **13** (2003) 1968-1970.

Gömöry, **F**., Tebano, R., **Šouc, J**., and Farinon, S.: Generation of higher harmonics in the voltage on a superconducting wire carrying harmonic AC current, IEEE Trans. Applied Supercond. **13** (2003) 3622-3624.

Tebano, R. and **Gömöry**, **F**.: Higher harmonics in the voltage on a superconducting wire carrying AC electrical current, Central European J. Physics **1** (2003) 246-257.

Gregušová, **D**., **Cambel**, **V**., **Kúdela**, **R**., **Šoltýs**, **J**., Kostič, I., Attolini, G., and Pelosi, C.: Investigation of the GaAs-pyramids overgrowth using MOCVD, J. Crystal Growth **248** (2003) 417-420.

Gregušová, **D**., **Cambel**, **V**., **Fedor, J., Kúdela**, **R**., **Šoltýs**, **J**., **Lalinský, T.,** Kostič, I., and Bending, S. J.: Fabrication of a vector Hall sensor for magnetic microscopy, Applied Physics Lett. **82** (2003) 3704-3706.

Hasenöhrl, S., Novák J., Kúdela R., Betko, J., Morvic M., Fedor J.: Anisotropy in tran-sport properties of ordered strained InGaP, J. Crystal Growth **248** (2003) 369-374.

Jansak, **L**., Zizek, F., Jelinek, J., Timoransky, Z., Piel, H., and **Polak**, **M**.: Loss analysis of a model transformer winding, IEEE Trans. Applied Supercond. **13** (2003) 2352-2354.

Korytár, **D**., Mikulík, P., Ferrari, C., Hrdý, J., Baumbach, T., Freund, A., and Kuběna, A.: Two-dimensional x-ray magnification based on a monolithic beam conditioner, J. Phys. D **36** (2003) A65-A68.

Mikulík, P., Baumbach, T., **Korytár**, **D**., Lübbert, D., and Perrot, P.: Micrometer-resolved determination of 3D lattice misorientation for the semiconductor wafers inspection by synchrotron radiation area diffractometry, J. Phys. D **36** (2003) A74-A78.

Kováč, **P**., **Hušek, I**., Grovenor, Ch., and Salter, Ch.: Properties of as-deformed and post-annealed MgB_2/Fe(Fe-alloy) composite wires, Supercond. Sci Technol. **16** (2003) 292-296.

Pachla, W., **Kováč**, **P**., Diduszko, R., Mazur, A., **Hušek, I**., Morawski, A., and Presz, A.: Effects of the high-pressure treatment of *ex situ* MgB_2 superconductors, Supercond. Sci Technol. **16** (2003) 7-13.

Kováč, **P**., Dhalle, M., **Melišek, T**., van Eck, H.J.N., Wessel, W.A.J., ten Haken, B., and **Hušek, I**: Dependence of the critical current in *ex situ* multi- and mono-filamentary MgB_2/Fe wires on axial tension and compression, Supercond. Sci Technol. **16** (2003) 600-607.

Fabbricatore, P., Greco, M., Musenich, R., **Kováč**, **P**., **Hušek, I**., and **Gömöry, F**.: Influence of the sintering process on critical currents, irreversibility lines and pinning energies in multifilamentary MgB_2 wires, Supercond. Sci Technol. **16** (2003) 364-370.

Kováč, P., Ahoranta, M., **Melišek**, **T**., Lehtonen, J., and **Hušek, I**.: The effect of Fe-magnetization on I_c(B) and $I_c(\alpha)$ characteristics of iron-sheathed MgB_2 composite wires, Supercond. Sci Technol. **16** (2003) 793-798.

Kováč, **P**., Ahoranta, M., Lehtonen, J., and **Hušek**, **I**.: The behavior of MgB_2 composite with ferromagnetic sheath, Physica C **397** (2003) 14-18.

Kováč, **P**., **Hušek**, **I**., **Melišek**, **T**., Ahoranta, M., **Šouc**, **J**., Lehtonen, J., and **Gömöry**, **F**.: Magnetic interaction of iron sheath with superconductor, Supercond. Sci Technol. **16** (2003) 1195-1201.

Hense, K., Kirchmayr, H., **Kováč, P**., Lackner, R., Müller, M., Pachla, W., **Pitel, J., Polák, M**., and **Ušák**, **P**.: Preparation and characterization of Bi-2223 tapes, Physica C **392-396** (2003) 1007-1010.

Pinčík, E., Jergel, M., Falcony, C., Ortega, L., Ivančo, J., Brunner, R., and **Kučera**, **M**.: Low-energy particle treatment of GaAs surface, Thin Solid Films **433** (2003) 108-113.

Pinčík, E., Kobayashi, H., Glesková, H., **Kučera**, **M**., Ortega, L., Jergel, M., Falcony, C., Brunner, R., Shimizu, T., Nádaždy, V., Zeman, M., Mikula, M., Kumeda, M., and van Swaaijand, R.A.C.M.M.: Photoluminescence properties of a-Si:H based thin films and corresponding solar cells, Thin Solid Films **433** (2003) 344-351.

Pogany, D., Bychikhin, S., **Kuzmik**, **J**., Dubec, V., Jensen, N., Denison, M., Groos, G., Stecher, M., and Gornik, G.: Thermal distribution during destructive pulses in ESD protection devices using a single-shot, two-dimensional interferometric method, IEEE Trans. Device Mater. Reliability **3** (2003)197-201.

Javorka, P., Alam, A., Marso, M., Wolter, M., **Kuzmik**, **J**., Fox, A., Heuken, M., and Kordos, P.: Material and device issues of AlGaN/GaN HEMTs on silicon substrates, Microelectronics J. **34** (2003) 435-437.

Kuzmik, **J**., Pogany D., Gornik, E., Javorka, P., and Kordos, P.: Electrostatic discharge effects in AlGaN/GaN high-electron-mobility transistors, Applied Physics Lett. **83** (2003) 4655-4657.

Lalinský, T., **Haščík**, **Š**., **Mozolová, Ž**., Burian, E., **Krnáč, M**., Tomáška, M., Škriniarová, J., Držík, M., Kostič, I., and Matay, L.: Mechanically fixed and thermally insulated micromechanical structures for GaAs heterostructure based MEMS devices, Microelectronics Int. **20** (2003) 43-47.

Machajdík, **D**., Kobzev, A.P., **Fröhlich, K**., and **Cambel**, **V**.: RBS and ERD study of epitaxial RuO_2 films deposited on different single crystal substrates, Vacuum **70** (2003) 313-317.

Moško, **M**., **Vagner, P**., Bajdich, M., and Schaepers, Th.: Coherent "metallic" resistance and medium localization in a disordered one-dimensional insulator, Phys. Rev. Lett. **91** (2003) 136803.

Osvald, **J**.: New aspects of the temperature dependence of the current in inhomogeneous Schottky diodes, Semicond. Sci Technol. **18** (2003) L24-L26.

Osvald, J.: Numerical study of barrier height enhancement in n-$In_{0.35}Ga_{0.65}As$ Schottky diodes using a p-type near-interface layer, Physica Stat. Solidi (c) **0** (2003) 928-932.

Osvald, **J**.: C-V measurement of a doping profile of б-doped GaAs and its spatial resolution – numerical study, Acta Physica Slovaca **53** (2003) 129-133.

Öszi, **Zs**., **Beňačka**, **Š**., **Štrbík**, **V**., **Chromik**, **Š**., **Španková**, **M**., Kostič, I., and Kleja, P.: Properties of $YBa_2Cu_3O_x$ and $Bi_2Sr_2CaCu_2O$ thin films by ion beam analysis methods, Thin Solid Films **433** (2003) 359-362.

Jelinek, Z., Timoransky, Z., Zizek, F., Piel, H., **Polak, M., Chovanec, F., Mozola, P., Jansak**, **L**., **Kvitkovic, J**., and **Usak, P**.: Test results of 14 kVA superconducting transformer with Bi-2223/Ag windings, IEEE Trans. Applied Supercond. **13** (2003) 2310-2312.

Polak, **M**., **Krempasky, L., Demencik, E**., Wehler, D., Kreiskott, S., Moenter, B., Polyanskii, A., and Larbalestier, D.C.: Critical currents of narrow YBCO rings on Ni and $LaAlO_3$ substrates, IEEE Trans. Applied Supercond. **13** (2003) 2595-2598.

Bellina, F., Bonicelli, T., Breschi, M., Ciotti, M., Della Corte, A., Formisano, A., Ilvin, Y., Marchese, V., Martone, R., Nijhuis, A., **Polak**, **M**., Ribani, P., Salpietro, E., Savoldi, L., and Zanino, R.: Superconductive cables current distribution analysis, Fusion Engn. Design **66-68** (2003) 1159-1163.

Rosina, **M**., Audier, M., Dubourdieu, C., **Fröhlich**, **K**., and Weiss, F.: Defects in $(La_{0.7}Sr_{0.3}Mno_3/SrTiO_3)_{15}$ superlattices grown by pulsed injection MOCVD, J. Crystal Growth **259** (2003) 358-366.

Lebedev, O.I., Verbeeck, J., van Tendeloo, G., Dubordieu, C., **Rosina**, **M**., and Chaudouet, P.: Structure and properties of artificial $[(La_{0.7}Sr_{0.3}MnO_3)_m(SrTiO_3)_n]_{15}$ superlattices on (001)$SrTiO_3$, J. Applied Phys. **94** (2003) 7646-7656.

Xu, Y., Khafizov, M., L. **Satrapinsky**, **L**., Kúš, P., Plecenik, A., and Sobolewski, R.: Time-resolved photoexcitation of the superconducting two-gap state in MgB_2 thin films, Phys. Rev. Lett. **91** (2003) 197004.

Satrapinsky, **L**., Plecenik, A., Kúš, P., Jacko, V., Gregor, M., Halabica, A., Hain, M., Xu, Y., and Sobolewski, R.: Study of MgB_2 superconducting thin films properties by tunneling spectroscopy, Solid State Phenomena **90-91** (2003) 583-588.

Xu, Y., Khafizov, M., L. Plecenik, A., Kúš, P., **Satrapinsky**, **L**., and Sobolewski, R.: Femtosecond optical characterization of MgB_2 superconducting thin films, IEEE Trans. Applied Supercond. **13** (2003) 3316-3319.

Zelezny, V., Chvostova, D., Pajasova, L., Plecenik, A., Kus, P., and **Satrapinsky**, **L**.: Infrared studies of superconducting MgB_2 thin films, Physica C **388** (2003) 129-130.

Bárdošová, M., Hodge, P., Pach, L., Pemble, M.E., **Šmatko**, **V**., Tredgold, R.H., and Whitehead, D.: Syntetic opals made by the Langmuir-Blodgett method, Thin Solid Films **437** (2003) 276.

Pištora, J., Yamaguchi, T., Vlček, J., Mistrík, J., Horie, M., **Šmatko**, **V**., **Kováčová**, **E**., Postava, K., and Aoyama, M.: Spectral ellipsometry of binary optic gratings, Optica Applicata **33** (2003) 252.

Šoltýs, J., **Cambel**, **V**., and **Fedor, J**.: Study of tip-induced Ti-film oxidation in atomic force microscopy contact and non-contact mode, Acta Physica Polonica A **103** (2003) 553-558.

Španková, M., Chromik, Š., Sedláčková, K., Vávra, I., Gaži, Š., and Kúš, P.: The influence of $SrTiO_3$/Si interface treatment by Sr and Ti on structural properties of $SrTiO_3$ thin films, Solid State Phenomena **90-91** (2003) 589-593.

Takács, S.: Some parameters of superconductors with an extreme singularity in the density of state: (s+d) model, Solid State Comm. **128** (2003) 455-459.

Ušák, **P**.: Random instabilities of current-voltage curves of BSCCO-2223/Ag multifilamentary tapes in LN_2 at 77K, Supercond. Sci Technol. **16** (2003) 459-463.

Ušák, **P**.: The measurements of current distribution in superconducting tape. Comparison of destructive and non-descructive methods, Physica C **384** (2003) 93-101.

Vagner, P., Markoš, P., **Moško**, **M**., and Schäpers, Th.: Coherent resistance of a disordered one-dimensional wire: Expressions for all moments and evidence for non-Gaussian distribution , Phys. Rev. B **67** (2003) 165316.

Aliev, F.G., Schad, R., Volodin, A., Temst, K., Van Haesendonck, C., Bruynseraede, Y., **Vávra**, **I**., Dugaev, V.K., and Villar, R.: Electron interaction with domain walls in antiferromagnetically coupled multilayers, Europhysics Lett. **63** (2003) 888-894.

Vlček, J., Pištora, J., Ciprian, D., Yamaguchi, T., and **Vávra**, **I**.: Magnetooptical gratings with circular dots, Optica Applicata **33** (2003) 263.

2004

Beňačka, Š., Öszi, Zs., Chromik, Š., Gaži, Š., **Štrbík**, **V**., and Kostič, I.: MgB_2 ramp-type superconducting thin film Josephson junctions, Czechoslov. J. Phys. **54** (2004), Suppl. D485-88.

Cambel, V., Gregušová, D., Fedor, J., Kúdela, R., and Bending, S. J.: Scanning vector Hall probe microscopy, J. Magnetism Magnetic Mater. **272-276** (2004) 2141-2143.

Cambel, **V**., **Šoltýs, J., Moško, M.,** and **Kúdela, R**.: Two-dimensional electron transport through a barrier prepared by tip-induced oxidation, Superlatt. Microstruct. **36** (2004) 359-367.

Chromik, Š., Gaži, Š., Štrbík, V., Španková, M., Vávra, I., Beňačka, Š., van der Beek, C.J., and Gierlowski, P.: Electrical and structural properties of MgB_2 films prepared by sequential deposition of B and Mg on the NbN-buffered Si(100) substrate, J. Applied Phys. **96** (2004) 4668-4670.

Chromik, **Š**., Kováč, P., Stanček, S., and **Štrbík, V**.: The distribution of elements in MgB_2 superconducting films prepared by sequential e-beam evaporation, Acta Physica Slovaca **54** (2004) 169-173.

Nishiha, A., Taka, C., **Chromik**, **Š**., and Durný, R.: Investigation of magnetic properties of MgB_2, thin films on NbN/Si substrate, Physica C **412-414** (2004) 201-205.

Pinčík, E., Jergel, M., Müllerová, J., Falcony, C., Ortega, L., Buzynin, A.N., Lomonova, E., Brunner, R., **Chromik**, **Š**., and Hartmanová, M.: On structural properties of Si/Zr(Y)O_2 and Zr(Y)O_2/Si systems, Acta Physica Slovaca **54** (2004) 147-161.

Andrade, E., **Chromik**, **Š**., Jergel, M., Jergel, M., Cheang-Wong, J.C., Falcony, C., and **Štrbík, V**.: Elemental depth profiles of MgB_2/Si precursor and superconducting films, Nuclear Instr. and Methods in Phys. Res. B **219-220** (2004) 768-772.

Mosnáček, J., Lukáč, I., **Chromik**, **Š**., Kostič, I., and Hrdlovič, P.: Network formation of a phenyl vinyl ketone copolymer with 4-vinylbenzil and its photodetecrosslinking in films, J. Polymer Sci A **42** (2004) 765-771.

Perďochová, A., Nečas, V., Ly Anh, T., **Dubecký**, **F**., **Boháček, P., Sekáčová, M**., and Pavlicová, V.: Influence of top contact topology on detection properties of semi-insulating GaAs detectors, Nuclear Instr. and Methods in Phys. Res. A **531** (2004) 103-110.

Dubecký, F., Ščepko, P., Loukas, D., **Zaťko, B**., Sekerka, V., Nečas, V., Perďochová, A., **Sekáčová, M., Boháček, P**., Hudec, M., and **Huran**, **J**.: Application of monolithic strip line radiation detector based on semi-insulating GaAs in X-ray partable scanner, Nuclear Instr. and Methods in Phys. Res. A **531** (2004) 314-320.

Dubecký, F., **Boháček, P., Zaťko, B., Sekáčová, M., Huran, J., Šmatko, V**., Fornari, R., Gombia, E., Mosca, R., and Pelfer, P.G.: Role of electrode technology in radiation detector based on semi-insulating InP in development of detector array, Nuclear Instr. and Methods in Phys. Res. A **531** (2004) 181-191.

Kaminski, P., Pawlowski, M., Kozlowski, R., Surma, B., **Dubecký**, **F**., Yamada, M., and Fukuzawa, M.: Investigation of compensation defect centres in semi-insulating InP crystals, Eur. Phys. J. Applied Phys. **27** (2004) 171-175.

Eliáš, P., Kostič, I., **Šoltýs, J**., and **Hasenöhrl**, **S**.: Wet-etch bulk micromachining of (100) InP substrates, J. Micromech. Microengn. **14** (2004) 1205–1214.

Eliáš, **P**., **Šoltýs, J**., and Kostič, I.: Formation of micro- and nano-striations at (211)A facets during wet etching of InP in HCl, Superlatt. Microstruct. **36** (2004) 315-323.

Fröhlich, **K**., **Hušeková, K., Machajdík, D**., Hooker, J.C., Perez, N., Fanciulli, M., Ferrari, S., Wiemer, C., Dimoulas, A., Vellianitis, G., and Roozeboom, F.: Ru and RuO_2 gate electrodes for advanced CMOS technology, Materials Sci Engn. B **109** (2004) 117–121.

Fröhlich, **K**., **Hušeková, K., Machajdík, D., Lupták, R., Ťapajna, M**., Hooker, J.C., Roozeboom, F., Kobzev, A.P., Wiemer, C., Ferrari, C., Fanciulli, M., Rossel, C., and Cabral, C. Jr.: Preparation of $SrRuO_3$ films for advanced CMOS metal gates, Materials Sci Semicond. Process. **7** (2004) 265-269.

De Santis, A., Barucca, G., Bobba, F., Caciuffo, R., **Fröhlich**, **K**., **Pripko, M**., and Cucolo, A.M.: Effect of oxygen post-annealing on the magnetoresistance of highly epitaxial $La_{0.7}Ca_{0.3}MnO_3$ thin films, J. Magnetism Magnetic Mater. **272-276** (2004) e1501-1502.

Kallel, N., **Fröhlich**, **K**., Oumezzine, M., Ghedira, M., Vincent, H., and Pignard, S.: Magnetism and giant magnetoresistance in $La_{0.7}Sr_{0.3}Mn_{1-x}M_xO_3$ (M = Cr, Ti) systems, Physica Stat. Solidi (c) **1** (2004) 1649–1654.

Fröhlich, K., **Hušeková**, **K**., **Oszi, Z**., Hooker, J.C., Fanciulli, M., Wiemer, C., Dimoulas, A., Vellianitis, G., and Roozeboom, F.: Metal oxide gate electrodes for advanced CMOS technology, Annalen der Physik **13** (2004) 31.

Frolek, **L**. and **Gömöry**, **F**.: Influence of spread in tape properties on I-V characteristics measured on superconducting cables, Physica C **401** (2004) 227-230.

Frolek, L. and **Gömöry**, **F**.: Measurement of E(I) characteristic of superconducting cable, Czechoslov. J. Phys. **54** (2004) Suppl. D497-500.

Gömöry, F., Seiler, E., Šouc, J., Kováč, P., Hušek, I., Farinon, S., Fabbricatore, P., Perkins, G., Caplin, A.D., Pardo, E., Sanchez, A., and Navau, C.: Influence of filament arrangement on current distribution and AC loss in Bi-2223/Ag tapes, Supercond. Sci Technol. **17** (2004) S150-S154.

Grilli, F., Stavrev, S., Dutoit, B., Spreafico, S., Tebano, R., **Gömöry, F., Frolek, L**. , and **Šouc**, **J**.: Numerical modelling of a HTS cable in AC regime, Physica C **401** (2004) 176-181.

Zola, D., **Gömöry, F**., Polichetti, M., **Strýček, F**., **Seiler**, **E**., **Hušek, I., Kováč, P**., and Pace, S.: A study of coupling loss on bi-columnar BSCCO/Ag tapes through ac susceptibility measurements, Supercond. Sci Technol. **17** (2004) 501-511.

Hasenöhrl, **S**., Betko, J**., Morvic M., Novák J., and Fedor J**.: Resistivity and mobility in ordered InGaP grown by MOVPE, Physica Stat. Solidi (c) **1** (2004) 382-387.

Hasenöhrl, S., Novák, J., **Vávra**, **I**., and Šatka, A.: Material properties of graded composition $InxGa_{1-x}P$ buffer layers grown on GaP by organometallic vapor phase epitaxy, J. Crystal Growth **272** (2004) 633-641.

Haščík, **Š**., **Lalinský, T.,** Krnáč, M**., Mozolová, Ž**., Matay, L., Hrkút, P., and Hotový, I.: Polyimide-fixed GaAs island structure prepared using plasma etching technique, Czechoslov. J. Phys. **54** (2004) Suppl. C1001-1005.

Hrkút, P., Držík, M., Mozolík, M., Kováč, P., **Haščík**, **Š**., Piller, W., Platzgumer, E., and Loeschner, H.: The influence of ion beam bombardment on the stress of carbon layers prepared by RF magnetron sputtering, Vacuum **76** (2004) 329-333.

Hotový, I., **Huran**, **J**., and Spiess, L.: Characterization of sputtered NiO films using XRD and AFM, J. Materials Sci **39** (2004) 2609-2612.

Huran, **J**., Hotový, I., Kobzev, A.P., and Balalykin, N.I.: Further studies of N doped a-SiC:H films deposited by PECVD and annealed by pulse electron beam, Thin Solid Films **459** (2004) 149-151.

Huran, **J**., Hotový, I., Kobzev, A.P., and Balalykin, N.I.: RBS study of amorphous silicon carbide films deposited by PECVD, Czechosl. J. Phys. **54** (2004) Suppl. C C1006-C1010.

Hotový, I., **Huran**, **J**., and McPhail, D.S.: Study of enhanced magnetron sputtering process of NiO by using flow modulation of oxygen, Czechosl. J. Phys. **54** (2004) Suppl. C C976-C983.

Hotový, I., **Huran**, **J**., Siciliano, P., Capone, S., Spiess, L., and Rehacek, V.: Enhancement of H_2 sensing properties of NiO-based thin films with a Pt surface modification, Sensors & Actuators B **103** (2004) 300-311.

Hušek, I., **Kováč**, **P**., Grovenor, C.R.M., and Goodsir, L.: Microhardness as a tool for the filament density and metal sheath analysis in MgB_2/Fe/(Cu) wires, Supercond. Sci Technol. **17** (2004) 971-976.

Janíková, E., Gömöry, F., and **Šouc**, **J**.: Higher harmonics in voltage on superconductor carrying AC current due to non-linear I-V curve, Physica C **401** (2004) 191-195.

Janíková, E. and **Gömöry**, **F**.: Waveform of resistive voltage on superconducting wire at AC current overload, Supercond. Sci Technol. **17** (2004) 1395-1400.

Klinčok, B. and **Gömöry**, **F**.: Study of AC transport in superconducting wire with the help of pick-up coils, Czechoslov. J. Phys. **54** (2004) Suppl. D501-505.

Ahoranta, M., Lehtonen, J., and **Kováč**, **P**.: Feasibility of iron-sheathed MgB_2 wires for magnet applications, Physica C **400** (2004) 89-96.

Grovenor, C.R.M., Goodsir, L., Salter, C.J., **Kováč, P.,** and **Hušek**, **I**.: Interfacial reactions and oxygen distribution in MgB_2 wires in Fe, stainless steel and Nb sheaths, Supercond. Sci Technol. **17** (2004) 479-484.

Kováč, **P**.: Torsion tests of filamentary Nb/CuSn and BSCCO/Ag composite wires, Supercond. Sci Technol. **17** (2004) 630-635.

Kováč, **P**., **Hušek, I., and Melišek, T**.: The effect of used deformation, metal sheath and heat treatment on the I-V curve of ex situ MgB_2 composite, Physica C **401** (2004) 282-285.

Ahoranta, M., Lehtonen, J., **Kováč**, **P**., **Hušek, I**., and **Melišek, T**.: Effect of bending and tension on the voltage-current relation of Bi-2223/Ag, Physica C **401** (2004) 241-245.

Lehtonen, J., Korpela, A., Nah, W., Kang, J., **Kováč, P**., and **Melišek**, **T**.: Influence of self-field on the critical current of Bi-2223/Ag tapes, Physica C **403** (2004) 257-262.

Kováč, **P**., **Hušek, I., Melišek, T**., Grivel, J.C., Pachla, W., **Štrbík, V**., Diduszko, R., Homeyer, J., and Andersen, N.H..: The role of MgO content in ex situ MgB_2 wires, Supercond. Sci Technol. **17** (2004) L41-L46.

Kováč, **P**., **Hušek, I., Melišek, T**., Grovenor, C.R.M., Haigh, S., and Jones, H.: Improvement of the current carrying capability of ex situ MgB_2 wires by normal particle additions, Supercond. Sci Technol. **17** (2004) 1225-1230.

Pachla, W., Presz, A., **Kováč**, **P**., **Hušek, I.,** and Diduszko, R.: Structural characterization of multifilament heat treated ex situ MgB_2 superconducting wires with Cu and Fe sheaths, Supercond. Sci Technol. **17** (2004) 1289-1294.

Kováč, **P**., **Hušek, I.,** and Jones, H.: Tensile stress applied to NbTi, Nb_3Sn, Bi-2223 and MgB_2 composite superconductors at room temperature, Supercond. Sci Technol. **17** (2004) 1411-1414.

Pachla, W., Diduszko, R., Presz, A., **Kováč, P.,** and **Hušek**, **I**.: Effect of texture on J_c in Bi-2223 tapes, Supercond. Sci Technol. **17** (2004) 1426-1429.

Pinčík, E., Kobayashi, H., Takahashi, M., Fujiwara, N., Brunner, R., Glesková, H., Jergel, M., Müllerová, J., **Kučera**, **M**., Falcony, C., Ortega, L., Rusnák, J., Mikula, M., Zahoran, M., Juráni, R., and Král, M.: Photoluminescence, structural and electrical properties of passivated a-Si:H based thin films and corresponding solar cells, Applied Surface Sci **235** (2004) 351-363.

Kicin, S., Kromka, A., **Kúdela R., Hasenöhrl, S**., Schwarz, A., and **Nov**ák J.: Micro-Raman study of InGaP composition grown on V-grooved substrates, Materials Sci Engn. B **113** (2004) 111-116.

Pelosi, C., Attolini, G., Frigeri, C., Bersani, M., Giubertoni, D., Vanzetti, L., and **Kúdela**, **R**.: In-depth analysis of the interfaces in InGaP/GaAs heterosystems, European Physical J. – Applied Phys. **27** (2004) 379-383.

Kuzmik, **J**., Pogany D., Gornik E., Javorka, P., Kordoš, P.: Electrical overstress in AlGaN/GaN HEMTs: study of degradation processes, Solid-State Electronics **48** (2004) 271-276.

Kuzmík, **J**., Konstantinidis, G., Harasek, S., **Haščík, Š**., Bertagnolli, E., Georgakila, A., and Pogany, D.: ZrO_2/(Al)GaN metal-oxide-semiconductor structures characterization and application, Semicond. Sci Technol. **19** (2004) 1364-1368.

Kvitkovič, J. and **Polák**, **M**.: Current-voltage characteristics of Bi-2223/Ag multifilamentary tapes exposed to inhomogeneous magnetic field, Physica C **401** (2004) 146-150.

Jakovenko, J., Husak, M., and **Lalinský**, **T**.: Design and simulation of micromechanical thermal convertor for RF power sensor microsystem, Microelectr. Reliability **44** (2004) 141-148.

Lobotka, **P**., **Vávra, I**., Fendrych, F., and Chayka, O.: Structural and electrical manifestation of ageing in thin-film Fe-Ta-O nanocomposite prepared by plasma jet technique, Physica Status Solidi A **201** (2004) 1493-1499.

Baláž, P., Godočíková, E., Kriľová, L., **Lobotka**, **P**., and Gock, E.: Preparation of nanocrystalline materials by high-energy milling, Mater. Sci Engn. A **386** (2004) 442-446.

Novák, **J**., **Hasenöhrl, S., Kučera, M., and Šoltýs, J**.: Nano-patterning surfaces by the self-organized growth of ordered and strained epitaxial layers, Superlatt. Microstruct. **36** (2004) 123-131.

Osvald, J.: Self-consistent analysis of Si δ-doped layer placed in a non-central position in GaAs structure, Physica E **23** (2004) 147-151.

Osvald, J. and Horváth, Zs.J.: Theoretical study of the temperature dependence of electrical characteristics of Schottky diodes with an inverse near-surface layer, Applied Surface Sci **234** (2004) 349-354.

Osvald, **J**.: Comment on „Negative Schottky barrier berween titanium and n-type Si(001) for low-resistance ohmic contacts, Solid-State Electronics **48** (2004) 2347-2349.

Osvald, **J**.: Electronic properties of a near surface Si δ-doped GaAs under an applied electric field, J. Phys. D: Applied Phys. **37** (2004) 2655-2659.

Öszi, Zs., Beňačka, Š., Španková, M., **Chromik**, **Š**., and Kostič, I.: High temperature superconducting thin film Josephson junctions, Czechoslov. J. Phys. **54** (2004), Suppl. D457-60.

Pardo, E., **Seiler, E**., and **Gömöry**, **F**.: A comparison of numerical methods for superconducting tapes in the critical state with transverse applied field, Czechoslov. J. Phys. **54** (2004) Suppl. D513-516.

Písečný, P., Hušeková, K., **Fröhlich**, **K**., Harmatha, L., **Šoltýs**, **J**., **Machajdík**, **D**., Espinos, J.P., Jergel, M., and Jakabovič, J.: Growth of lanthanium oxide films for application as a gate dielectrics in CMOS technology, Materials Sci Semicond. Process. **7** (2004) 231-236.

Lehtonen, J., Korpela, A., **Pitel, J**., and **Kováč**, **P**.: Local extreme values in critical current on anisotropic Bi-2223/Ag tapes, Physica C **403** (2004) 139-144.

Polák, **M**., **Kvitkovič, J., Demenčík, E., Janšák, L., and Mozola, P**.: Temperature of Bi-2223/Ag samples in the resistive section of I-V curves, Physica C **401** (2004) 160-164.

Abilio, C.C., **Rosina, M**., Dubourdieu, C., Weiss, K., **Fröhlich**, **K**., and Godinho, M.: Effect of magnetic field orientation on magnetization of $(La_{0.7}Sr_{0.3}MnO_3/SrTiO_3)_{15}$ superlattices, J. Magnetism Magnetic Mater. **272–276** (2004) 1260–1262.

Chvostová, D., Železný, V., Pajasová, L., Tarasenko, A., Plecenik, A., Kúš, P., and **Satrapinskij**, **L**.: Optical properties study of MgB_2, Thin Solid Films **455-456** (2004) 213-216.

Xu, Y., Khafizov, M.L., **Satrapinskij**, **L**., Kúš, P., Plecenik, A., Karpinski, J., Jun, J., Kazakov, S.M., and Sobolewski, R.: Picosecond dynamics of the superconducting state in MgB_2, Physica C **408-410** (2004) 90-92.

Seiler, E., Gömöry, F., Fabbricatore, P., Greco, M., Perkins, G., and Caplin, A.D.: Contactless j_c determination and magnetic coupling in multifilament Bi-2223/Ag tapes, Supercond. Sci Technol. **17** (2004) 549-554.

Seiler, E. and **Gömöry**, **F**.: Modelling of magnetic-flux penetration into multifilamentary superconducting wire with the help of magnetic-energy minimization Czechoslov. J. Phys. **54** (2004) Suppl. D493-6.

Bárdošová, M., Hodge, P., **Šmatko**, **V**., Tredgold, R.H., and Whitehead, D.: A new method of forming synthetic opals, Acta Physica Slovaca **54** (2004) 409-415.

Šouc, **J**., **Gömöry, F., and Janíková, E**.: I-V curve of Bi-2223/Ag tapes in overload conditions determined from AC transport data, Physica C **401** (2004) 75-79.

Šouc, J., Frolek, L., and **Gömöry**, **F**.: Cold core transformer system for AC tests of short superconducting cable models, Czechoslov. J. Phys. **54** (2004) Suppl. D509-512.

Španková, **M**., **Vávra, I., Chromik, Š**., Harasek, S., **Lupták, R., Šoltýs, J**., and **Hušeková, K**.: Structural properties of Y_2O_3 thin films grown on Si(100) and Si(111) substrates, Materials Sci Engn. B **16** (2004) 30-33.

Štrbík, **V**., **Chromik, Š., Beňačka, Š**., and **Gaži, Š**.: Superconducting MgB_2 microstrips, Czechoslov. J. Phys. **54** (2004) Suppl. D505-8.

Takács, **S**.: Basic and higher harmonics of superconducting cylinder at applying the current below and above the critical current, Physica C **401** (2004) 187-190.

Ťapajna, M., Písečný, P., Lupták, R., Hušeková, K., **Fröhlich**, **K**., Harmatha, L., Hooker, J.C., Roozeboom, F., and Jergel, M.: Application of Ru-based gate materials for CMOS technology, Materials Sci Semicond. Process. **7** (2004)271-276.

Sastry, P.V.P.S., Nguyen, D.N., **Ušák**, **P**., and Schwartz, J.: Verification of thermal interpretation of BSCCO-2223/Ag current-volatge hysteresis, Supercond. Sci Technol. **17** (2004) 314-319.

Vávra, O., Gaži, Š., Vávra, I., Dérer, J., and **Kováčová**, **E**.: High efficiency Andrew reflection observed in $Nb/Fe_{0.5}Si_{0.5}/Nb$ Josephson junctions, Physica C **404** (2004) 395-399.

Zaťko, B., Dubecký, F., Boháček, P., Gombia, E., Frigeri, P., Mosca, R., Franchi, S., **Huran**, **J**., Nečas, V., Sekáčová, M., Förster, A., and Kordoš, P.: On the spectrometric performance limit of radiation detectors based on semi-insulating GaAs, Nuclear Instr. and Methods in Phys. Res. A **531** (2004) 111-120.

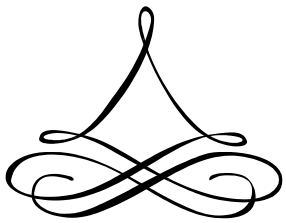

Printed in Slovakia by K&S, Reklamná produkcia s.r.o., Bratislava, 2005

INSTITUTE OF ELECTRICAL ENGINEERING

Slovak Academy of Sciences
Dúbravská cesta 9
841 04 Bratislava
Slovak Republic

Phone: (421 2) 54 77 58 06
Fax: (421 2) 54 77 58 16
http://www.elu.sav.sk